Íris de Brito Soares

Licenciatura em Bioquímica

Multifunctional coatings of polymeric films for biofilm-mediated infections

Dissertação para obtenção do Grau de Mestre em Biotecnologia

Orientador: Ana Catarina Bernardino Baptista, Investigadora, Departamento de Ciências dos Materiais, FCT-UNL

Co-orientadores: Ana Bettencourt, Professora Auxiliar, Faculdade de Farmácia, Universidade de Lisboa

Júri:

Presidente: Isabel Sá Nogueira, Professora Catedrática, Departamento de Ciências da Vida, FCT UNL

Arguentes: Ana Rita C. Duarte, Professora Associada, Departamento de Química, FCT-UNL

Vogais: Ana Catarina Bernardino Baptista, Investigadora, Departamento de Ciências dos Materiais, FCT-UNL

Dezembro, 2020

FACULDADE DE CIÊNCIAS E TECNOLOGIA
UNIVERSIDADE NOVA DE LISBOA

Science my lad, is made of mistakes, but they are mistakes which it is useful to make, because they lead little by little to the truth

Jules Verne

A Journey to the Centre of the Earth

Acknowledgements

Primeiramente, gostaria de agradecer às minhas orientadoras, Ana Baptista e Ana Bettencourt por me darem a oportunidade de trabalhar com elas e me ajudarem sempre que necessário, guiando-me neste projeto. Seguidamente agradeço ao Professor João Paulo Borges e à Professora Isabel Ferreira pela oportunidade de trabalhar no DCM bem como a todo o material e ajuda fornecidos. Agradeço ainda ao Iván Lamela-Gómez e à Prof. Lídia Gonçalves pela ajuda na produção e análise das micropartículas.

Jaime, que me aturou no laboratório, sendo o "baby-sitter". Obrigada por me deixares fazer parte deste trabalho, mas mais que isso por me aturares e responderes a todas as perguntas, mesmo as mais absurdas, e por partilhares todos os momentos de desespero onde nada funcionava e tudo o resto falhava e só apetecia desistir. Sem qualquer dúvida esta tese não seria a mesma sem o "bullying" ou a partilha de receitas ou canções aleatórias no laboratório (maioritariamente o diabo do burrito). Felizmente o dia da explosão do laboratório ainda não chegou, mas também estou a escrever isto cedo, por isso ainda há tempo.

Passando ao resto do pessoal, primeiro, aos que "abandonaram", obrigada à Patrícia, ao Lima e à Ana Gaspar, quer pelos momentos sérios de trabalho ou pelos de avacalhar, ambos igualmente necessários (obrigada também pela comida) e mesmo ao António, que me ensinou um bocadinho de "electro-coisas", quem diria que seria útil um dia. Ainda nas pessoas do laboratório, agora as que ainda lá estão, obrigada primeiro à Ana Pinheiro, a minha companhia matinal de cusquice ou mostra de música/vídeos que eu não necessitava de ver. Depois, à Ana Marques, à Catarina, ao David, à Joana e ao Joãozinho, novamente, pelos tempos de trabalho e partilha de conhecimento, e por responderem aos meus mil "o que estás a fazer, e para quê e porquê e como funciona", mas também pelas conversas parvas, em especial, à Ana Marques pelas horas dedicadas a Raman e AFM.
Aos alunos de tese, Bruno, que és mais "parceiro de tese" porque partilhas um pouco o tema, à Sofia, pelos cafés cervejas e horas de espera partilhadas, e os dias até às 8 da noite (aleluia conseguimos). À Andreia, que mais partilhou as "madrugadas e noitadas", e por todas as discussões mais ou menos relevantes de séries comidas filmes e a estupidez da raça humana.

Ao pessoal do lab de polímeros, obrigada por não me estrangularem de nenhuma das vezes que ia chatear, obrigada pelos momentos de relaxar a meio do dia. Adriana fofinha, Catarina e Henrique que acabaram por aturar mais, têm direito a carinho especial.
André Manuel, que apesar de te integrares no último grupo tens direito a separação, (o teu eu antissocial agradece certamente) obrigada. Obrigada pelas cervejas ao final do dia, as sestas ao sol e cafés infinitos no mini. Obrigada pelos momentos de bolinho da sorte e por teres razão mesmo quando detestava que tivesses, obrigada por me dares na cabeça e me manteres na linha. Obrigada por seres um enorme idiota. Foi divertido ter-te por aqui, foste um daqueles rebuçados que a vida manda no meio dos limões.
Agradeço ainda ao Prof. João Canejo pela explicação da tração, e por estar sempre disponível para ajudar em todos os "momentos" do sistema.

Aos que não trabalham no laboratório, e só para não amuares por não seres o primeiro, obrigada querido padrinho, onde quer que estejas no vasto espaço/tempo, aquele que é uma besta, mas que é na mesma o meu melhor padrinho (apenas por ser o único) pelos aninhos de faculdade e por me ensinares as mil coisas de materiais e teres paciência para a minha lentidão de aprendizagem. Obrigada pelo resto também, um abraço em modo enguia da tua melhor e mais adorada afilhada. Hey, obrigada por me obrigares a levantar o cu e ir falar com o Borges e com a Ana.
Chica, como és adulta e não amuas podes vir em segundo (em primeiro no meu coração) obrigada por seres a minha pessoa, que Krishna nos apoie.
Smeagol, tu, que partiste para o outro lado do mundo para um frio horrível e bebidas caras e bicicletas (às quais ainda não acredito que sobreviveste até agora). Epá, val val, c'mon, palavras. Tu sabes koala mamma, por tudo, que mais hei de agradecer sem ser por tu seres tu e estares aqui? Obrigada por existires, e por me deixares pertencer à tua existência. Por me arrastares de casa e me tornares neste ser quase social. Pelas idas ao kapa, sermões e agressões. Obrigada por seres a lógica no caos e por me

veres deambular e me apanhares no último momento umas vezes e esfregares bem a cara no chão das outras, conforme necessário e possivelmente bastante recomendado. Ao resto do pessoal, com especial carinho ao Huguinho, à Debbie, e Dini e Rita por associação, thank you, arigato bakka.

Para terminar, obrigada à minha família, por serem eles, o mau e o bom. (sim Diana Maria só tens direito a uma frase no fim) (Djiaaaaannaaaaaa)

The author thanks Fundação para a Ciência e Tecnologia (FCT) for the financial support under Projects UIDB/04138/2020 and UIDP/04138/2020 (iMed.ULisboa)

Abstract

Implant related infections, mainly caused by Staphylococcus aureus, are a public health concern. Treatment is challenging due to multi-resistant strains, and S. aureus ability to adhere and form biofilm on bone and implant surfaces, as well as to invade and persist in osteoblast cells. The present work consisted in the preparation and evaluation of novel dual polymeric film coatings in stainless steel that provide local and controlled antibiotic delivery for the treatment of implant-related infections. Multilayers of chitosan, polymethylmethacrylate (PMMA) and polycaprolactone (PCL) loaded with microspheres containing vancomycin or daptomycin were produced using the dip-coating technique. To enhance polymeric film adhesion on the surface of the metallic substrate, different surface treatments were evaluated such as chemical etching, electrochemical etching, and mechanical abrasion. From this study, it was possible to conclude that the mechanical abrasion showed the best results.

After films production optimization, morphological, chemical, and mechanical properties were evaluated in detail for the several film combinations. Finally, the drug-release studies of daptomycin and vancomycin were carried out for drug and microsphere loaded films. It was possible to conclude that the release is mainly diffusion dependent.

In summary, this work has shown that the films obtained exhibit promising characteristics to be used in the context of implant-related infection treatment.

Keywords: Implant-related infection; Dip-coating; Polymeric films; Vancomycin; Daptomycin; Controlled drug release.

Resumo

As infeções associadas a implantes, maioritariamente causadas por *Staphylococcus aureus*, são um problema grave de saúde pública. O seu tratamento apresenta um desafio devido a estirpes multirresistentes e à capacidade de *S. aureus* de aderir à superfície de implantes formando biofilmes, bem como a sua capacidade de invasão e permanência em osteoblastos.
O presente trabalho consistiu na preparação e avaliação de novos filmes poliméricos em aço inoxidável para a libertação local controlada de antibióticos para o tratamento de infeções relacionadas com implantes.
Multicamadas de chitosano, polimetilmetacrilato (PMMA) e policaprolactona (PCL) com microesferas com vancomicina ou daptomicina foram produzidos utilizando a técnica de dip-coating.
Para melhorar a adesão dos filmes poliméricos, diferentes tratamentos de superfície foram avaliados, tais como erosão química, erosão eletroquímica e abrasão mecânica. Deste estudo foi possível concluir que a abrasão mecânica mostrou os melhores resultados.
Após a otimização da produção de filmes, as propriedades mecânicas, químicas e morfológicas foram avaliadas em detalhe para os vários filmes. Finalmente, estudos de libertação de daptomicina e vancomicina foram realizados para filmes com os fármacos e filmes com as microesferas. Foi possível concluir que a libertação ocorre maioritariamente por difusão.
Em suma, este trabalho demonstrou que os filmes obtidos mostram potencial para a sua utilização no tratamento de infeções relacionadas com implantes.

Palavras-chave: Infeções associadas a implantes; *Dip-coating*; filmes poliméricos; Vancomicina; Daptomicina; Libertação controlada de fármacos.

Table of Contents

List of Figures

List Of Tables

Abbreviations and symbols

Ti-6Al-4V – Grade 5 titanium
316L-SS - stainless steel 316L
Chi - Chitosan
PMMA - Polymethylmethacrylate
PCL – Polycaprolactone
Dap – Daptomycin
Van – Vancomycin
S. Aureus - *Staphylococcus aureus*
S. epidermidis - *Staphylococcus epidermidis*
PEB-b-PTBAEMA - poly(ethylene-co-butylene)-b-poly[2-(tert-butylamino) ethyl metHAcrylate]
HA – Hydroxyapatite
DNA – Deoxiribonucleic acid
PHAs – polyhydroxyalkanoates
PVA – polyvinyl alcohol
EVA – ethylene vinyl acetate
PLGA – poly lactic-co-glycolic acid
POE – poly ortho esters
CVD – chemical vapour deposition
PVD – physical vapour deposition
PECVD – plasma enhanced chemical vapour deposition
LbL – Layer-by-layer
PEG – polyethylene glycol
PEI – poly(ethyleneimine)
PAH – poly(allylamine)
PAA – poly(acrylic acid)
EUD - Eudragit®
MRSA - Methicillin-resistant *Staphylococcus aureus*
MRSE - Methicillin-resistant *Staphylococcus Epidermidis*
BJI – bone and joint infections
PJI – prosthesis joint infections
VRSE - vancomycin-resistant *enterococci*
GISA - glycopeptide-intermediate *S. aureus*
DCM – Dichloromethane
SEM - Scattering Electron Microscopy
APTES – Aminopropyltriethoxysilane
TEOS - tetraethyl orthosilicate
MMA - methyl methacrylate
DMAc – Dimethylacetamide
DD – Deacetylation degree
HAc – Acetic acid
PMMA-Van - PMMA microspheres loaded with vancomycin
PMMA-EUD-Dap - PMMA-EUD daptomycin loaded microspheres
AFM – Atomic force microscopy
EDS - Energy-dispersive X-ray spectroscopy
Au-Pd – gold/palladium
SBF – simulated body fluid
EE – Encapsulation efficiency
DL – Drug loading
µS – Microsphere
OM – Optical microscopy

1 Introduction

1.1 Motivation

A current estimate of the total of hip replacements in the world is nearly one million a year, and of knee replacements more than 250,000. Over 30 % of hospitalized patients have vascular catheters in place and 10 % of hospitalized patients have urinary catheters [1].
Bacterial infection is a potential complication for patients receiving implanted devices. Infection arises from the presence of pathogens in the implant. These pathogens adhere to and grow in the biomaterial, sometimes forming a biofilm in the implant in the peri-operative (before the operation) period. Once the implant is placed in the recipient, these organisms grow, and infection sets in the implanted site, potentially leading to implant failure [2]. Infections of implants used in orthopaedic fractures and reconstructive devices occur in 5 % of the surgeries. For primary total hip replacement, the infection rate varies from 0.2 % to 2.2 % [3]. Infections in spine surgery occur in 2 % -5 % of the cases and prosthetic joint replacement procedures infection rates are of approximately 1 % – 2 % of all replacements [4]. These implant infections are not only a consequence of patient related factors and surgical technique, but also of the implant itself, including size, shape, material and topography [3].
Regularly infections are treated with long course of systemic antibiotics [5]. Systemic administration of antibiotics, however, has many disadvantages including possible systemic or organ specific toxicity and low drug concentration at the target site, which combined with drug resistance from the bacteria leads to the failure of antibiotics as a method to fight infections[6]. The concentration of drug in the body is derived from its administration, distribution and metabolism, which is characterized by wave like distribution curves (Figure 1.1). At each dosage the patient receives, drug concentration increases, as the drug is absorbed. Then, as the drug is distributed, the concentration reaches the maximum drug concentration, meanwhile, the drug is metabolized, and the concentration decreases until a new dose is administered and the pattern repeats[7].

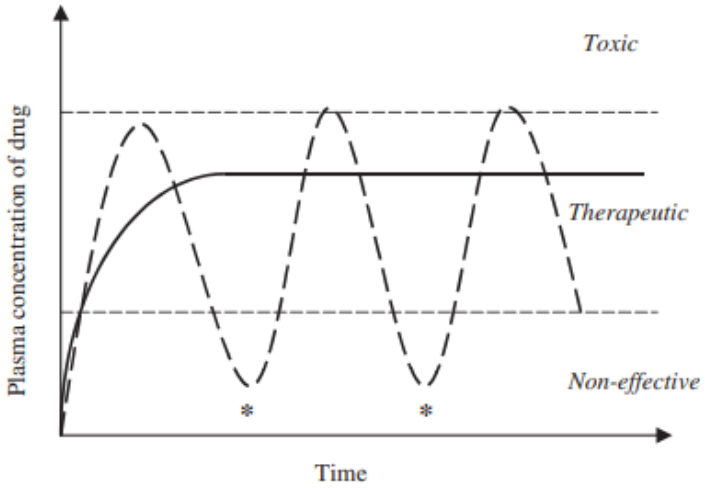

Figure 1.1: Drug concentration in plasma over time showing traditional administration (dotted line) and ideal administration (solid line) as well as therapeutic, toxic and non-effective dose range [7].

For the drug to take effect, however, the dosage must be high enough that the local concentration at the target location is in its therapeutically dose range [7]. Because of the distribution of the drug in the body and the metabolization between the administration and target site, to be in the therapeutical interval at the target, the drug concentration may need to be higher than the maximum of the therapeutic interval

and be toxic. When the concentration drops, it sometimes reaches concentrations below the therapeutic interval, and is therefore ineffective on the patient[6] [8].
When antibiotics fail, prosthesis removal and replacement, or even joint fusion, are often the only solutions to definitively eradicate severe infections[9]. Because of this, infection of a device can cause significant morbidity, extended hospital stays, and even mortality, being that costs associated with implant infection average between $ 25,000-32,000 per patient [10]. In Portugal for example, the cost of infection in primary arthroplasties of the hips and knees increased from approximately 3,000 € (corresponding to a lack of infection) up to approximately 14,000 €, depending on the type of treatment required. The cost of aseptic revision was 6,089 € for a hip implant and 7,985 € in the knees. If the infection were treated with debridement and implant retention the cost was 5,528 € in the hips, and 4,009 € in the knees and in cases of infections treated with a two-stage revision the cost was 11,415 € and 13,793 € for hips and knees, respectively [11]. Due to the high costs associated to implant failure as well as the well-being of the patient, it is essential to have strategies that inhibit the settling of infection and/or mitigates infection after its settlement.
The objective of this work is the development of one of these strategies, in the shape of a novel multifunctional polymeric-based coating for metallic implants capable of responding to existing bacteria, releasing pharmaceuticals at the infection site to kill those bacteria, stopping the infection.

1.2 Objectives and structure

The objective of this work is to produce an antibacterial polymeric coating suitable for local controlled drug release using the dip-coating technique. For this, two metal alloys commonly used in biomedical devices, grade 5 titanium (Ti-6Al-4V) and stainless steel 316L (316L-SS) were chosen as substrates for coating deposition[12]–[15]. These were coated with films made of multilayers of chitosan (Chi), polymethyl methacrylate (PMMA) and polycaprolactone (PCL), that are known biocompatible materials, often used as part of implants, whether in their main structure, or in a portion of the device[16]–[18]. The polymer layers should contain one of two antibiotics, daptomycin (Dap) or vancomycin (Van) encapsulated on acrylic microspheres. These antibiotics are often used to fight implant site bone-infections, with daptomycin being the most recent, and therefore the one that does not yet result in antibiotic resistance[19]. Vancomycin is a bit older than daptomycin, being a model drug in drug release studies, but several bacterial strains already present resistance to this antibiotic [20].
Because when infection occurs the pH at the infection site changes, lowering from 7.4 to 5.5[14], this property will be used, and the films produced should be pH responsive, this is, the drug release should depend on the pH at the implant site. For a pH of 7.4, that corresponds to the physiological pH, very little or even no drug release should be observed, and for pH values lower than this, corresponding to the occurrence of infection, the drugs incorporated in the films should be released from the coating via degradation of the polymer layers and diffusion from microspheres, leading to a burst release phase and a slow-release phase respectively, since this behaviour results in higher antibiotic efficacy. The film should also be anti-adhesive, due to the inclusion of chitosan, that is known for this property, and the surface morphology itself [21].
To reach such goals, several milestones should be attained:

1) Production of microspheres loaded with both selected drugs.
2) Production of a uniform multilayer polymeric coating.
3) Production of a uniform multilayer film incorporating drug-loaded microspheres.

The film produced should also display appropriate mechanical properties that would allow it to sustain the physical stress present in the implant site and the suitable chemical properties that allow it to endure the implant site environment.
This work will be divided into 4 chapters:

Chapter 1 – Introduction
In the Introduction, a brief context of implant related bone infection is presented. It will describe the microorganisms responsible for these infections and the mechanisms and problems associated with their biofilm assembly ability and capacity to invade and persist within osteoblast cells. Then, it will proceed

to the challenge of the conventional antibiotic treatment, indicating novel local drug delivery systems as a new therapeutic strategy and listing some systems that have been developed. Finally, the system developed in this study will be introduced.

Chapter 2 – Materials and Methods

This chapter will describe both materials and methods used. Starting by describing the materials, it will then go over the preparation of the drug delivery system, with details on microsphere and film preparation, as well as substrate treatment, and characterization of all, microspheres, films and substrate treatments. The experimental procedure for the several processes are detailed, encompassing for instance etching of steel substrates, microsphere production and dip-coating solutions and setup parameters. Then, the characterization techniques, will be shortly detailed. It will also explain how swelling, degradation and drug release studies were performed.

Chapter 3 – Results and Discussion

Here all results obtained from the experiments performed throughout this study and subsequent discussion are presented. It concerns the production of microparticles and their characterization, substrate treatment and subsequent characterization, and film optimization, culminating with the description and characterization of the optimized system obtained.

Chapter 4 – Conclusion and Future Work

The last part of this thesis contains the main conclusions drawn from this work and possible alterations and improvements that can be made to the methodologies used and the potential impact they may provide.

1.3 Contextualization

Infection is defined as a homeostatic imbalance between the host tissue and the presence of microorganisms. Infections occur when pathogens invade the host and begin to reproduce [5]. Among others, infections involving bone are very difficult to control, being a significant cause of morbidity and mortality. Furthermore, they can result in prolonged hospital stays, long courses of systemic antibiotics and frequently require new surgical intervention in the case of bone infections associated with implants [5].

Bone infection related to the use of orthopaedic implants is associated with complications following surgery and device implantation, leading to implant failure, and resulting in diseases such as osteomyelitis, and septic arthritis.

This type of infection leads to necrosis and destruction of bone. It may affect any bone, being limited to one or several portions of the bone, and the surrounding soft tissue [22]. This infection can be acquired after bone surgery, joint replacement, or as consequence of a trauma, being that immunosuppressed people face a higher risk of infection.

Nowadays, with sterility within the operating room and protocols of peri-operative antibiotic prophylaxis, there is a decrease of the incidence of infections associated with orthopaedic implants. Nevertheless, surgical implant procedures have become extremely common to restore the function of affected joints, fractured bones and impaired limbs. The enormous population of patients with orthopaedic implants estimates only about 0.5 % - 5 % of risk of infection, however, implant related infections are still the number one cause of the failure of implants and a potential complication for patients receiving them[9]. These devices are predispose to infection by damaging or invading epithelial or mucosal barriers and by supporting growth of microorganisms that adhere to and grow in the biomaterial, sometimes forming a biofilm in the implant in the peri-operative (before the operation) period or postoperatively, e.g. via haematogenous seeding from infections elsewhere in the body[23]. Once the implant is placed in the recipient, these organisms grow, and infection sets in the implanted site [2].

The presence of an implanted material alone increases the risk of infection, e.g. it has been demonstrated that 10^4 times fewer bacteria are necessary to infect patients with sutures compared to those suture-free [23].

When an infection is diagnosed several therapeutic approaches may be adopted. There have been several studies focused on different strategies to fight implant infection, whether before surgery, or after it. Pre-operative procedures involve antibiotic prophylaxis [24], [25] or sonication of the implant to remove

any adhered biofilm [26]. Post-operative procedures include systemic antibiotics for a prolonged period of time and wound debridement and lavage [24]. However, both the simple debridement procedures with retention of prosthesis and antibiotic therapy treatments are not always effective on infections that have already established. Often, prosthesis removal and replacement, when not even joint fusion, it is the only solution to definitively eradicate severe infections [9].
Another inherent problem is that antibiotic therapy takes long periods of time. By intravenous route, the antibiotics are prescribed for three weeks, followed by three more weeks of oral antibiotics. Furthermore, to achieve effective therapeutic drug concentration at the site of infection a high parenteral dose of antibiotic is needed. These facts can lead to systemic toxicity of the antibiotic [6].
The therapeutic success in bone infections is also determined by the rate and extent of antibiotic penetration in bone tissues. Penetration of an antibiotic into infected bone tissue depends on its pharmacological and physico-chemical characteristics, degree of vascularization, good conditions of soft tissues, and presence of foreign bodies. When there is a clinical treatment failure of bacterial infectious disease, it is usually associated with low bioavailability of antibiotics and their side effects, biofilm-related infections and the emergence of resistant bacteria.
The microorganisms most frequently associated with infection caused by the presence of implants are staphylococci (Figure 1.2), being their capability to adhere to materials and to promote the formation of biofilms is the key feature of their pathogenicity [9].

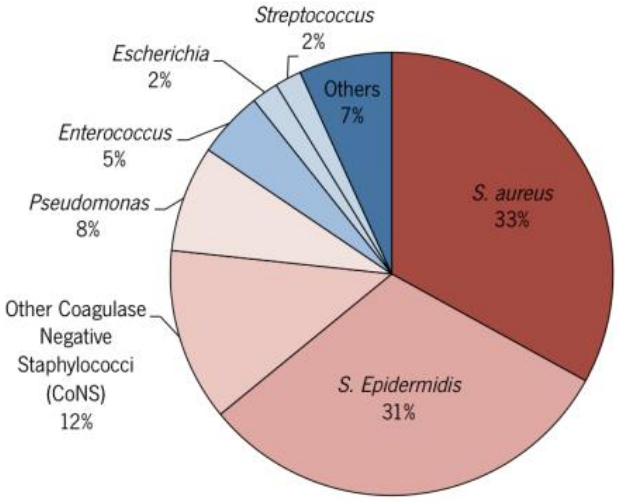

Figure 1.2: Bacteria associated with implant infection [27].

The most commonly found bacteria in implant infection is *Staphylococcus aureus* (*S. aureus)*, that has multiple mechanisms to promote immune evasion, including biofilm formation, and the ability to persist in necrotic bone [28]. This leads to reinfection after surgical intervention, which occurs in 10-30% of cases [10]. Apart from *S. aureus*, *Staphylococcus epidermidis (S. epidermidis)* is also a common cause of implant-associated infections, being that *S. aureus* is associated to metal-biomaterial, bone-joint, and soft-tissue infections, whereas *S. epidermidis* is related with polymer-associated implant infections [28]. Both species produce biofilms in a process that requires bacterial adhesion, followed bacteria-bacteria adhesion, film maturation (Figure 1.3). The biofilm contains multiple layers of bacteria and can be very difficult to treat since bacteria on the interior of the biofilm are protected from phagocytosis and antibiotics [28].

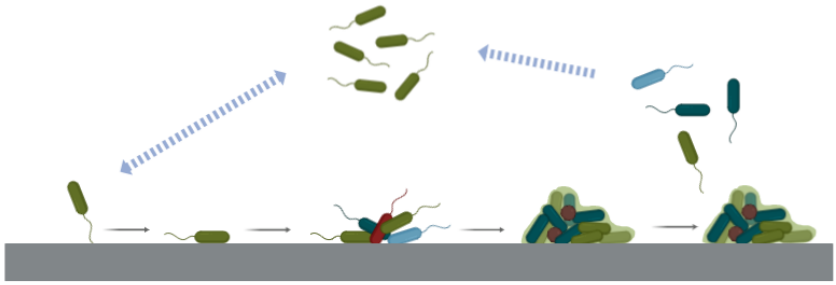

Figure 1.3: Biofilm formation showing from left to right reversible bacterial adhesion, irreversible bacterial adhesion, bacteria- bacteria adhesion, film maturation, and dispersion of bacteria from the film (adapted from [28]).

Considering the pathogenicity of bacterial strains, there is an urgent need to develop novel therapeutically approaches to fight implant-associated infections [29]. To prevent biofilm formation on implants several anti-microbial surfaces have been. They can be divided in 3 classes: 1) Structured; 2) Permanent antimicrobial surfaces and 3) Elution systems [30].

- Structured Surfaces

These are surfaces where topography has been tailored, often at the nanoscale, to decrease bacterial adhesion. Structures that decrease bacteria adhesion include nanoparticle- and nanotube-modified surfaces [31][32], molecular structures and engineered metal topographies such as alterations in charge, hydrophobicity, roughness, and porosity [33][34]. Studies focused on heat treatment and anodization of titanium (Ti), for instance, have shown to reduce bacterial adhesion 10 to 100 times [30].

- Permanent Antimicrobial Surfaces

Permanent antimicrobial surfaces contain permanently bonded agents that generate antimicrobial surfaces that prevent long-term bacterial adhesion[35]. Antimicrobial molecules include chitosan and amines, antimicrobial peptides, and antibiotics. Commonly, antibiotics are coupled directly to metals, but hydrogels, for example, can also be bound to metal surfaces. Despite the more fragile bond between hydrogels and metal (when compared to that of antibiotics) their chemistry can be tailored to display antimicrobial agents [30]. Some studies have been done in theses surfaces, for example, Lenoir et al. [36] showed a dispersion of a poly(ethylene-co-butylene)-b-poly[2-(tert-butylamino) ethyl methacrylate] (PEB-b-PTBAEMA) that has antimicrobial properties against *Escherichia coli*. Fighting the same bacteria, Lian et al. [37] developed a method to functionalize polymeric and cellulosic materials with pyridinium groups that possess antibacterial properties.

- Elution Systems

Elution systems are a strategy of local drug delivery that consist in surfaces that actively release antimicrobials to inhibit bacterial adhesion and/or promote bacterial cell death in both the implant and adjacent tissues [30]. This sort of systems relies on the release of antimicrobials in the infection site, allowing for high concentrations of the active substance to be achieved without systemic toxicity associated with the body availability of the antimicrobials. Buchholz et al. first introduced the incorporation of antibiotics into PMMA bone cement for local antibiotic delivery in total joint arthroplasty, and since then, several studies have shown that antibiotic loaded bone cements can decrease infection rates of cemented total hip arthroplasties [3]. Another common bone cement coating in implants is hydroxyapatite (HA). HA has been used for delivery of growth factors, deoxyribonucleic acid (DNA), antibiotics and others. These applications have been used for example in titanium implants [3][38]. With the increasing use of cementless implants worldwide, however, the use of antibiotic loaded bone cement has reduced, leading to the development of new delivery systems.
With the emergence of cementless implants, drug delivery turned to new materials such as natural and synthetic polymers and other porous and non-porous materials as base for the delivery systems.

These new systems keep the same function as the bone cements with new materials including cancellous bone, collagen sponges [39], and polymeric coatings. These materials are loaded with antibiotics, e.g. amoxicillin, tobramycin, and vancomycin and have been used, for example, in coatings of orthopaedic implants [3]. Polymeric coatings made from polylactic acid and its copolymers with glycolic acid have also been produced [5].
In recent years, studies have focused on biodegradable materials including natural rosin-based biopolymers and polyhydroxyalkanoates (PHAs). PHAs incorporated with cefoperazone and ampicillin for instance have shown promising results in treating implant-related osteomyelitis in rabbits [5] and rosin's use has been confirmed by Fulzele et al. [5] who encapsulated ciprofloxacin in this polymer. Rossi et al. [5] have reported the coating of discs from a femoral hip implant with PHAs loaded with gentamicin. This coating exhibited an initial burst release followed by continuous release of gentamicin with bacterial eradication within 24–48 h in vitro. Hans et al. [40] produced a low molecular weight biodegradable poly (D,L-lactic acid) coating with integrated gentamicin and teicoplanin for ocular implants. This coating showed a continuous release over a period of 96 h, achieving a higher attachment of non-viable microorganisms, but a lower number of viable bacteria. Other drug eluting coatings include polymers such as polyvinyl alcohol (PVA), ethylene vinyl acetate (EVA), poly lactic-co-glycolic acid (PLGA), polycaprolactones (PCL), polyanhydrides and poly ortho esters (POE), being that each polymer has a specific feature that makes them appropriate to a certain drug eluting profile, being than possible to adapt the use of the polymer to the function needed [41].
These antimicrobial systems, when applied in implants, reduce the incidence of infections at the implant site, therefore, reducing the risk of implant failure, and also reducing the costs of hospitalizations due to treatments subsequent to implant surgery [9].
To produce any antibacterial system numerous parameters, and their interdependence, need to be considered. For elution systems, the drug selected, the delivery route, drug release mechanism, drug release kinetics, and system and implant materials for instance have to be taken into account simultaneously[42].

The approach studied in this thesis consists in the incorporation of drug containing microparticles into a robust coating. The strategy to produce drug containing microparticles has been developed before, leading to the successful incorporation of vancomycin and daptomycin in PMMA and PMMA-Eudragit® microparticles respectively as a controlled-release antibacterial agents against *S. aureus*[16], [43], [44]. These particles allowed a localized treatment and overcome the initial burst release showed by biodegradable bone cements[45].
Coatings found in literature are majorly produced by expensive techniques, such as plasma spray [46] and radiofrequency magnetron sputtering[47]. Dip-coating technique allows layer-by-layer films production of high purity material and homogeneity in complex geometries [48][49], and can be used to form films at low temperature, atmospheric conditions, and in a simple and cost-effective process. With this technique the multilayers of drug and polymer or drug microparticles and polymer are easy to produce and good osteointegration of coatings produced by this technique has been reported, being attributed to hydroxyl groups that promote calcium and phosphate's nucleation[12]. Regarding the coating's polymeric components, chitosan stands out due to its charge and biological properties. Since chitosan is positively charged at physiological pH, multilayer coatings can be produced with alternating positive and negative charge polymers[13] such as PCL and PMMA that will be used to form the negatively charged layer of the LbL system, since both have been reported as biocompatible, and used commonly in implant coatings[16], [18]. Moreover chitosan, whose biocompatibility and biodegradability is well established, improved PMMA bone cements antibacterial activity, wound healing and bone regeneration. Furthermore, the use of chitosan as coating would add antifouling and anticoagulant properties to the implant's surface, which would be a major advantage for the prevention of biofilm formation.
Additionally, these coatings take advantage of the *S. aureus* biofilm structure to produce the antiadhesion/antibacterial coatings. Since chitosan is pH sensitive, degrading at low pH values, bellow 6.5[17]. Because the surrounding media's pH changes during biofilm formation [14], the proposed coatings should be pH sensitive and would first release the drugs via burst release – degradation of the film/membrane – and then via diffusion mechanism particles would release the drug with the increase/decrease of pH by dissolution of the capping polymer throughout time.

All together, these coatings entitle for 4 major breakthroughs:

- ability to efficiently coat different materials.
- controlled drug release by pH response for two pharmaceuticals.
- coatings produced from biocompatible and/or bioabsorbable polymers.
- cost effective process and materials.

A major aspect of the coating to be produced is the ability to release drug in a controlled manner. Controlled drug delivery occurs when a biopolymer is combined with an active agent in such a way that the active agent is released from the material in a predesigned manner. The release may be constant, cyclic, or triggered by external events (Figure 1.4).

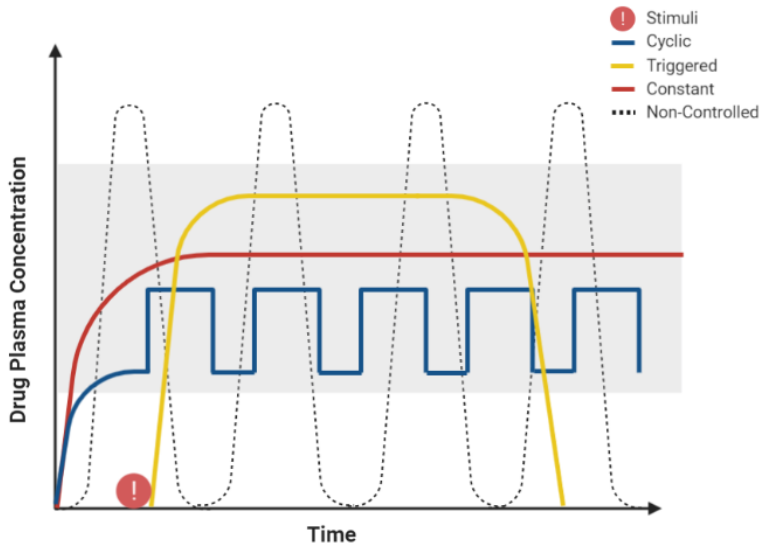

Figure 1.4: Controlled release systems showing: blue) cyclic, yellow) triggered; red) constant; black) non-controlled release and the therapeutic interval (grey) (adapted from[7]).

The purpose behind controlling drug delivery is to achieve effective therapies while eliminating both under- and overdosing. Other advantages include maintaining drug levels within a desired range, fewer administrations, optimal use of the drug, and increased patient compliance. Providing control over the delivery of a drug can be the most important factor on occasions when traditional administration cannot be used:

- situations requiring the slow release of water-soluble drugs,
- situations requiring the fast release of low-solubility drugs,
- drug delivery to specific sites,
- delivery of two or more agents with the same formulation,
- systems based on carriers that can dissolve or degrade and be readily eliminated.

The ideal system should be inert, biocompatible, mechanically appropriated, comfortable for the patient, have high drug loading, safe from accidental release, simple to administer and remove, and easy to fabricate and sterilize[7].

1.4 Film Production - Dip-coating

Films are systems used in many applications since they bring additional functions to any kind of materials. They can be prepared by several methods that can be divided into two main groups, dry and wet processes. Dry processes such as chemical vapour deposition (CVD) physical vapour deposition (PVD) and plasma enhanced chemical vapour deposition (PECVD) require, as the name indicates, the

evaporation of precursor or material, with no need for a liquid solution or dispersion of the deposited material. Wet processes such as spray coating, brush casting, spin coating and dip-coating consist in spreading a solution or suspension of the material to be deposited. These wet methods are well adapted for the preparation of multiphase materials since any non-volatile compound that is dispersed or dissolved into the solution will be homogeneously distributed or organized into the final films, and with a good control of the thickness. For instance, hybrid organic/ inorganic, or composite, layers are easily obtained by evaporation of solutions containing metal oxide precursors, organic functions, monomers, polymers, or various kinds of nanoparticles. Wet processes are also appropriate for the preparation of materials with controlled porosity since porogenic species can easily be embedded and eliminated from the final material.

Among the various methods available to perform liquid deposition, dip-coating has always been the most attractive one because of its simplicity. However, some drawbacks are associated to this technique. First, one faces the difficulty to homogeneously wet the substrate, especially when high surface tension solvents, such as water, are used. The thickness becomes difficult to control when ultra-thin (1 µm) layers need to be prepared from highly diluted or highly viscous solutions. Another challenge concerns the deposition onto porous substrates, or onto porous layers, within which the solubilized precursors may infiltrate and modify their initial properties. Another important obstacle resides in the formation of cracks often resulting from the presence of lateral tensile stress occurring during drying, and/or consolidation.

Compared with conventional thin film forming processes such as chemical vapor deposition, evaporation, or sputtering, dip-coating is an ideal method to prepare thin layers from chemical solutions since it is a low cost and waste-free process that is easy to scale up and offers a good control on thickness. For such reasons, it is becoming more and more popular not only in research and development laboratories, but also in industrial production, as testified by the increasing number of annual publications [50].

Dip-coating consists in the deposition of a film by dip and withdrawal of a substrate from a liquid medium. In summary, the process of film formation includes several stages (Figure 1.5). The film starts with the immersion of a substrate on the coating fluid, followed by its withdrawal. With this, a liquid film is formed on the substrate, which will then dry and consolidate. A final step, called curing or sintering step, is a post-treatment that may also be necessary to obtain the final coating material [51].

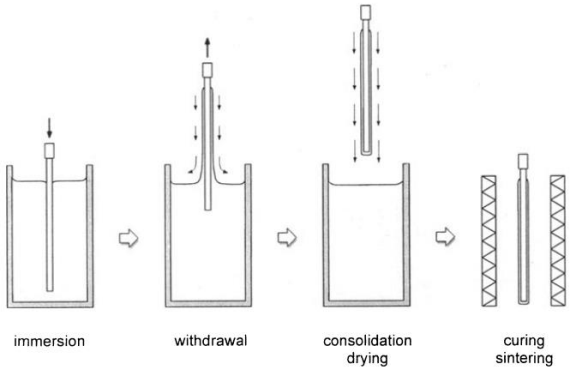

Figure 1.5: Dip-coating process, showing from left to right the immersion and withdrawal of the substrate, film drying and curing with arrows indicating the direction of forces at play [51].

In further detail the steps are:

- Immersion: The substrate is submerged into the coating solution at a constant speed followed by a certain dwell time for interaction of the substrate with the solution for complete wetting.
- Withdrawal: The pulling of the substrate upward at a constant speed forms a thin layer of coating solution (film deposition). Excess liquid drain from the surface thorough gravitational forces.
- Drying: The solution solvent evaporates, forming the as-deposited thin film [52].

This technique has been used in medicine to make coatings of several natures and purposes. As early as 1996, Li et al. reported the coating of titanium rods with HA by a dip-coating method for bone replacement applications[53]. Studies of HA coatings have continued, for instance, in 2007, Aksakal and Hanyaloglu studied coatings of ceramics in on Ti–6Al–4V and 316L-SS implant materials[54]. In 2013, Khalid et al. proposed a method for dip-coating of nano-HA on a titanium alloy using a plasma assisted γ-Alumina layer between HA and the titanium [55]. Bulk polymer systems like polylactic acids or polycaprolactones, however, are not easily coated onto complex medical devices and are typically prepared in harsh solvents or at high temperatures, which destroy antibiotics during the synthesis. To solve this, layer-by-Layer (LbL) assembly was created.
In this method, a substrate is alternately dipped in differently charged polymer baths, building a coating of nanolayered thin films (Figure 1.6 A). LbL systems can also be used in particles (Figure 1.6 B) that can be used to form coatings or as drug carriers, not being then fixed to a surface [56].

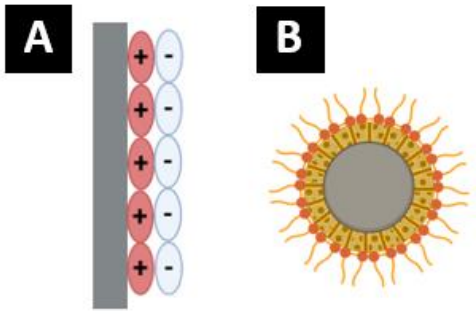

Figure 1.6: LbL deposition on A) surface with: red) positively and blue) negatively charged monolayers, and B) sphere showing: grey) core; yellow) first layer and orange) second layer.

In some coatings fabricated by LbL assembly, cell-resistant polymeric materials such as polyethylene glycol (PEG) and dextran have been developed to reduce adsorption of serum and cell-borne proteins [57]. Several other polymers have been used, namely natural and synthetic polymers, being the natural polymers of increasing interest since they are naturally available, nontoxic, and biocompatible. Some examples of these polymers are albumin, collagen, and gelatine, polylysine and poly(aspartic acid), and hyaluronic acid and chitosan. Synthetic polymers have also been used such as poly(ethyleneimine) (PEI), and poly(allylamine) (PAH), poly(vinylsulfate), and poly(acrylic acid) (PAA) [57].
LbL assembly also allows the use of multiple drugs in the same coating and the control of the architecture of the film, providing compartmentalization of the different components and thus their sequential release [58][59]. With this last property, one can build systems of controlled or responsive release, in which layers only elute the molecules in response to a stimulus such as pH, ions and so on. Several studies have focused on responsive release properties, for instance, Sukhishvili et al. demonstrated the release of fluorescent dyes from films containing weak poly(acids), which dissolve in response to changes in pH while Schuler and co-workers studied the NaCl-induced degradation of LbL thin films with calf thymus DNA incorporated as a functional component [59].
In recent years, the properties of responsive and antibacterial coatings have been brought together to make coatings that will only release the antibacterial agents in specific conditions, acting as an active attack surface, that can be activated at any time. These active attack surfaces, however, still have issues such as the accumulation of dead bacteria and debris, that shield the surface, reducing the bactericidal effect and also provide nutrients for subsequent bacterial adhesion. To avoid these issues, studies have focused on surfaces with different parts, called units, one responsible for killing bacteria, and one responsible for releasing the dead bacteria from the surface. To do such, responsive systems are often incorporated in the coatings [60].

The study presented uses this technique to produce antibacterial polymeric coatings for local controlled drug release. The coatings are to be deposited in two metal alloys commonly used in biomedical devices,

Ti-6Al-4V and 316L-SS that are used in orthopaedic and dentistry implants as well as integrated fixtures, sutures and staples [12]–[15]. These will be coated with films made of multilayers of Chi, PMMA and PCL, that are known biocompatible materials, often used as part of implants, whether in their main structure, or in a portion of the device[16]–[18]. The polymer layers are to be loaded with Dap or Van encapsulated on acrylic/Eudragit® (EUD) and acrylic microspheres respectively. These antibiotics are often used to fight implant site infections, with daptomycin being the most recent, and therefore the one that does not yet result in antibiotic resistance[19]. Vancomycin is older than daptomycin, being a model drug in drug release studies, but several bacterial strains already present resistance to this antibiotic [20]. The two drugs have been previously encapsulated in the spheres, and it was concluded that for daptomycin encapsulation the addition of Eudragit® led to higher encapsulation efficiencies, so the compound was added to the structures [44].

2 Materials and methods

This chapter will provide details about the processes and materials used in the work. Starting with the materials used it will then go through the production and analysis of polymeric microspheres, and then moves to the treatment of the metallic substrates. Then film production and optimization will be described, and finally the methods used to analyse and characterize the several film properties are presented.

2.1 Materials

For this work, two metal alloys, Ti-6Al-4V and 316L-stainess steel, three polymers, PMMA, Chi and PCL, and two drugs, vancomycin and daptomycin were used.

- **Metal alloys**

Titanium alloys, specially Ti-6Al-4V are widely used in orthopaedic and dentistry (Figure 2.1) due to its corrosion resistance, mechanical strength and biocompatibility. They are, however, prone to protein adsorption and infection, especially in dentistry implants, for being exposed to natural bacteria of the mouth [61].

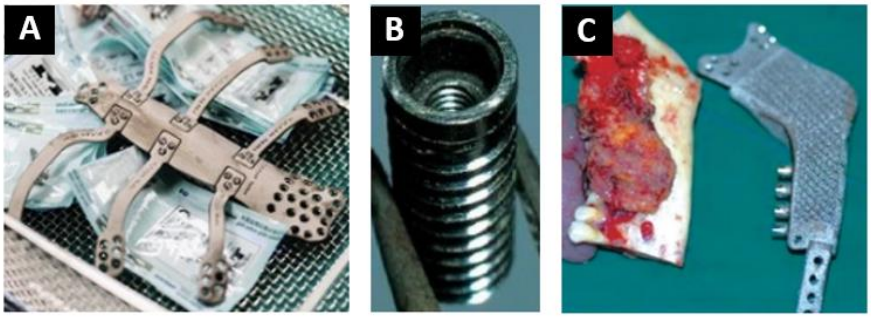

Figure 2.1: Titanium implants showing: A) thoracic wall implant [35], B) orthodontal screw insert[36] C) Mandibular implant [37].

Steel alloys date back to the 1800's, having since then replaced for stainless steels, that have nickel, chromium, and molybdenum as alloying elements. The most common medical steels are 316, 316L, and 304L, being mostly used for fracture fixation plates, stabilization rods, screws, and other integrated fixtures tied to primarily orthopaedic structures, as well as sutures and staples (Figure 2.2) [15]. Because the use of stainless-steel implants occurs often near open wounds, this kind of implant is prone to infection.

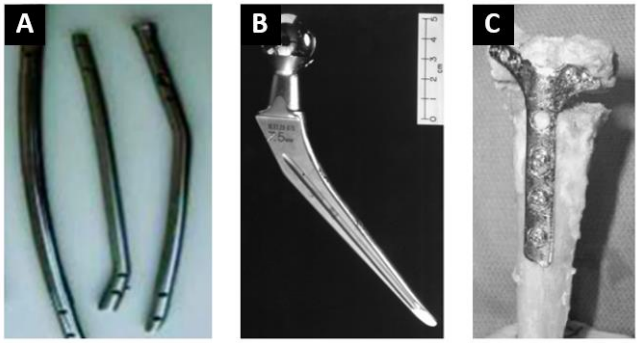

Figure 2.2: Stainless steel implants showing: A) intramedullary nails [62] B) Müller straight stem hip implant [63] C) dorsal nonlocking plate (Wright Medical Technology) [64].

- **Polymers**

PMMA is a synthetic polymer from the methyl methacrylate monomer (MMA) (Figure 2.3).

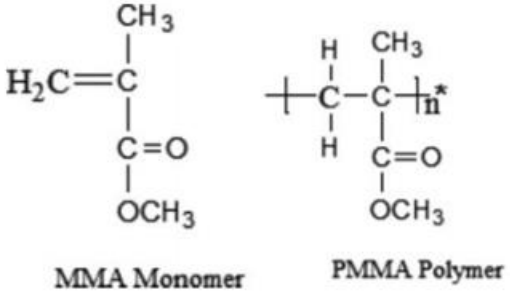

Figure 2.3: Chemical structure of PMMA (right) and its monomer MMA (left)[65].

Its use extends from the ophthalmological field, dentistry, and to the orthopedy [66]. PMMA is a widely explored biomedical material, and recent publications have shown an increasing interest in its applications as a drug carrier [16]. PMMA has been coupled with several agents such as antibiotics [67][68][69], fungicidal molecules [70], and biomolecules [71] for local drug delivery as well as radiopaque agents so the polymer can be visualized on x-rays[72].
The properties that allow the use of this polymer include its low cost, easy processability, resistance to acidic and alkaline solutions, non-polar solvents and aliphatic hydrocarbons, minimal inflammatory reactions with tissues, and great fracture resistance [65].

Chitosan is a natural cationic, and highly basic, linear polymer (polysaccharide) prepared by N-deacetylation of chitin (Figure 2.4). Chitosan is formed by units of glucosamine e N-acetyl-D-glucosamine with β(1→4) bonds between them. It is the ratio between these two units that distinguishes chitosan from chitin, being that chitosan chains have a content of N-acetyl-D-glucosamine lower than 50 % - 60 %. The ratio between the two constituent units is called the deacetylation degree (DD)[73].

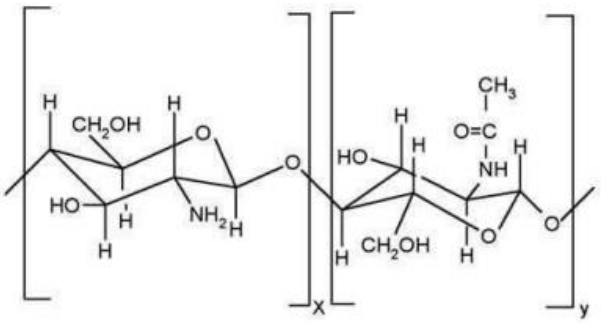

Figure 2.4: Structure of chitosan with glucosamine (left) and N-acetyl-D-glucosamine (right) [73].

Chitosan has unique solubility, and chemical and biological activity, such as biodegradability and non-toxicity as well as haemostatic, bacteriostatic, fungistatic, spermicidal, anticancerogenic and anticholesteremic properties that have attracted attention for uses in biomedicine. Other important characteristics of chitosan are its molecular weight, viscosity, DD, crystallinity index and water retention value [74][17][75]. This polymer is soluble in acidic solutions with pH<6.5 [17], [74], forming gels with several multivalent anions and has a high charge density which allows it to interact strongly with negative surfaces [17]. Chitosan can be made into films, fibres and beads as well as powders and solutions, having many commercial applications. This versatility made chitosan highly researched, with increasing interest [17]. The cationic nature of the polymer attracts negatively charged cytokines and

growth factors and is believed to help protect and concentrate cytokines and growth factors secreted by local cells and lead to accelerated healing [76]. The coating of chitosan onto metal and metal alloy implants has been achieved via several methods such as chemical reactions, electrodeposition, dip-coating and LbL assembly among others [76].

PCL (Figure 2.5) is a bioresorbable semicrystalline poly(α-hydroxyester). PCL is degraded by hydrolysis of its ester linkages in physiological conditions, being this hydrolysis slow due to its high crystallinity and hydrophobic nature. The polymer has therefore received a great deal of attention for use in long-term implantable devices [18].

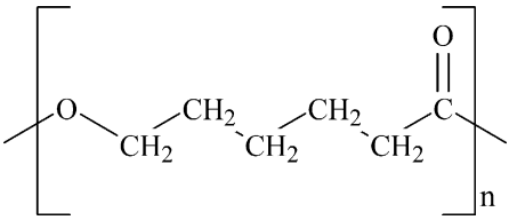

Figure 2.5: Chemical structure of polycaprolactone [18].

In addition, PCL is biocompatible, easily processable and does not elicit immune responses which add to its potential to be used in bone regeneration applications. The application of PCL and its composites in bone tissue engineering has been studied with a variety of PCL products being investigated including scaffolds, electrospun and solvent-extracted PCL, loaded PCL scaffolds as well as PCL composites[48], [77], [78].

- **Drugs**

Vancomycin (Figure 2.6) is a tricyclic glycopeptide antibiotic produced by the actinobacteria *Amycolatopsis orientalis* discovered in the 1950's and in clinical use since 1958 [79]. This antibiotic is indicated in infections caused by Gram-positive bacteria, especially Methicillin-resistant *Staphylococcus aureus* (MRSA), Methicillin-resistant *Staphylococcus epidermidis* (MRSE) and penicillin-resistant pneumococci [20].

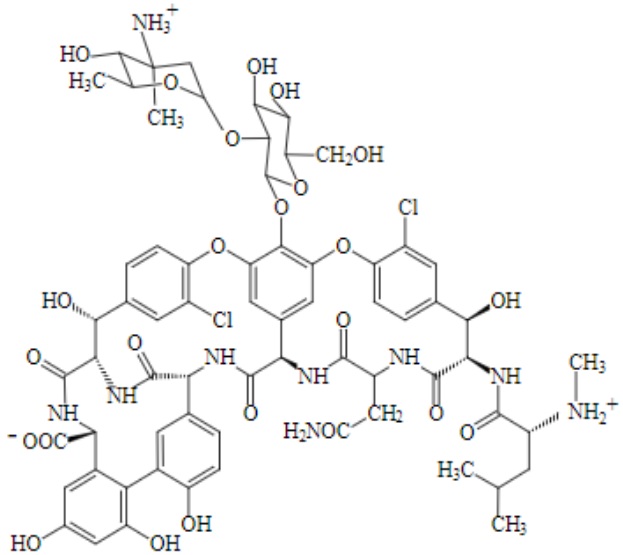

Figure 2.6: Chemical structure of vancomycin [80].

Vancomycin is a first-line treatment for many bone and joint infections caused by organisms like MRSA. However, *S. aureus* has reduced susceptibility to vancomycin due to its ability to produce

biofilms. Furthermore, vancomycin has poor bone penetration[19], [81]. Furthermore, the increased use of vancomycin has led to the development of isolates with reduced susceptibility. Therefore, the need for new potent antimicrobial agents with MRSA activity is essential[82].
Daptomycin (Figure 2.7) is a lipopeptides and a novel antimicrobial agent used for the treatment of gram-positive infections [82]. It has been used in bone and joint infections and prosthesis joint infections considering spectrum of activity and biofilm penetration [81].

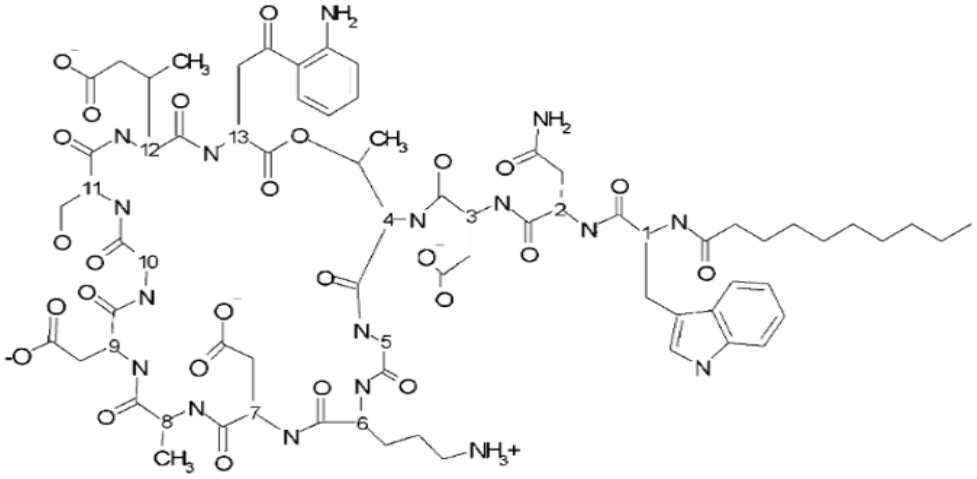

Figure 2.7: Chemical structure of daptomycin [83].

The agent has activity against multidrug-resistant, gram-positive bacteria such as MRSA, vancomycin-resistant enterococci (VRE), glycopeptide-intermediate *S. aureus* (GISA) and penicillin-resistant *Streptococcus pneumoniae*[84]

2.2 Methods

2.2.1 Microparticle production

Microparticles of PMMA and PMMA together with Eudragit® loaded with Dap and Van were prepared using a previously described double-emulsion w1/o/w2-solvent evaporation method [43]. For this, solutions were obtained by dissolving PMMA (350 kDa, Sigma Aldrich, USA) or PMMA and Eudragit® RL 100 (Evonik Degussa International AG, Spain) in dichloromethane (Fisher Scientific, USA). EUD is reported to help encapsulating daptomycin since its addition results in a more positive charge of the particle and reduces Dap/PMMA repulsion, increasing the encapsulation efficiency[44].
Daptomycin (Cubicin®, 350 mg, Novartis Pharma AG, Switzerland) and vancomycin hydro-chloride (Vancomicina Generis 1000 mg, Generis Farmacêutica, S.A., Portugal) were added to a 10 % wt/v PVA (13 kDa–23 kDa, 87–89% hydrolysed) solution. All components of the solutions were weighed according to Table 2.1.

Table 2.1: Composition of microparticles produced.

Microsphere type	PMMA (mg)	EUD (mg)	Van (mg)	Dap (mg)	DCM (mL)	PVA (10 % wt/v) (mL)
Vancomycin loaded	125	-	18.75	-	5	1
Daptomycin loaded	87.5	37.5	-	18.75	5	1
PMMA drug-free	125	-	-	-	5	1
PMMA-EUD drug-free	87.5	37.5	-	-	5	1

For all formulations, the PVA solution was added to the PMMA or PMMA/EUD solution and homogenized for 3 min using an Ultra-Turrax T10 basic (IKA, Staufen, Germany) at maximum speed

(level 6). Afterwards, this solution was added to 30 mL of 1.25 % (wt/v) PVA solution in a 200 mL glass beaker and homogenized with a Silverson Laboratory Mixer Emulsifier L5 M (Silverson Machines Inc., Chesham, UK) at 9999 rpm for 10 min. This mixture was then left in magnetic agitation at 350 rpm for 4 h for solvent evaporation.
After the total evaporation of the solvent the particles were purified. To do so, 1 mL of sucrose solution 10 % (wt/v) was added to the polymer suspension and the resulting mix centrifuged (Allegra 64R High Speed Centrifuge, Beckman Coulter Inc., Fullerton, USA), for 10 min at 4 ºC and 7500 rpm (5723 g). The supernatant was discarded, and the pellet resuspended in 1 mL sucrose 10 % (wt/v) and 20 mL filtered sterilized water and centrifuged again with the same parameters.
The pellet was then resuspended in 5 mL sucrose 0.5 % wt/v and subsequently freeze-dried (Christ Alpha 1–4, B. Braun Biotech International, Melsungen, Germany).

2.2.2 Production Yield

Particle production yield was obtained by calculating the mass of particles produced after freeze drying and comparing it to the initial polymer plus drug mass used for the spheres.

2.2.3 Encapsulation Efficiency and Drug Loading

To measure the encapsulation efficiency and drug loading an indirect method was used[44]. This method relies in the quantification of the antibiotics in the supernatant (i.e., non-encapsulated antibiotic) obtained during particle preparation. This quantification was made by UV-Vis spectroscopy (Spectrophotometer U-2001, Hitachi Instruments Inc., Tokyo, Japan) for 3 replicas of each microparticle solution: PMMA, PMMA with vancomycin, PMMA+EUD and PMMA+EUD with daptomycin. For quantification, calibration curves were made for both drugs at concentrations of 1000 µg/mL, 500 µg/mL, 250 µg/mL, 62.5 µg/mL, 31.25 µg/mL, 15.63 µg/mL, 7.812 µg/mL, 3.906 µg/mL, 1.953 µg/mL, 0.9766 µg/mL and 0 µg/ml.

2.2.4 Particle size

Particle size was measured after the first centrifugation of the particle cleaning step and before and after lyophilization. This was done to both ensure that no microparticles were being lost during the centrifugation process and to study the effect of the lyophilization step in particle size.
The measurements before lyophilisation were made by laser diffraction in a Malvern Mastersizer 2000 – Hydro SM (Malvern Instruments, Malvern, UK) using ultrapure water as dispersion medium. For this, samples were loaded to the sample dispersion unit under constant agitation. The size distribution measurements were performed using at least three replicate samples. Size distribution of microparticles was characterized using the volume mean diameter.
After lyophilization the size of the particles was measured by Scattering Electron Microscopy (SEM) in a Hitachi 82400 model. For these measurements, a small amount of particles was suspended in ethanol and the suspension was dispersed directly over the carbon tape.

2.3 Substrate treatment

For all substrates produced in this work, titanium alloy was Grade 5- ASTM B365 (Ti90/Al6V4) and the stainless steel was AISI 316L (Fe/Cr18/Ni10/Mo3) in foil form with a thickness of 0.1 mm from Goodfellow, England were used.
First, the substrates were cleaned of any impurities. Stainless steel substrates were cleaned in ultrasound baths of water and acetone for 5 min each. Afterwards, they were placed in an oven at 300 ºC for 10 minutes. Next, they were transferred into ultrasound baths of acetone and water for 10 minutes each. Finally, the substrates were submerged in a 0.75 M solution of sodium hydroxide (NaOH) (Labchem, Portugal) for 4 min and then rinsed with water and storage for further treatment.

For titanium substrates, the metal was placed in an ultrasound bath of ethanol 96 % v/v for 10 minutes and then air dried. After the cleaning process, the stainless-steel substrates underwent an electropolishing step.

2.3.1 Electropolishing

Non-treated cleaned 316L-SS substrates were submerged in a solution of sulfuric acid 98 % (H_2SO_4) (Honeywell, Germany); phosphoric acid (H_2PO_4) (85 % wt/v,Honeywell, Germany) and ultrapure water in a proportion of 2:2:1 v/v and connected to a power source (AIM-TTI Instruments model PL303), forming an electrode, being distanced from another electrode, a palladium wire submerged in the same solution, by 2.5 cm (Figure 2.8). Using a dip-coater (Silar Dip-coating System with stirrer model HO-TH-03A), the substrates were dipped 6 times running a cycle that included a dip in the acid solution at 70 ºC for 60 seconds at 6 V, followed by a dip in ultrapure water at room temperature for 5 seconds (protocol adapted from [85]). The substrates were then cleaned in ultrapure water and acetone, and then air dried and stored for future treatment.

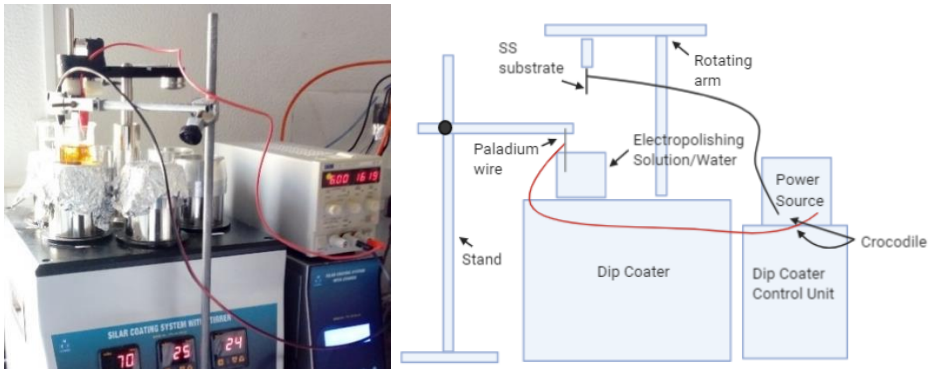

Figure 2.8: Setup used for electropolishing showing: dip coater, power source, electropolishing solution with a substrate in it and crocodiles connecting the substrate and power source (red and black wires).

2.3.2 Electrochemical etching

For all electrochemical etchings, 316L-SS substrates and a palladium wire were connected to a power source, serving as electrodes, and kept at 2.5 cm (Figure 2.9). The two electrodes were then dipped into one of the several etching solutions and the power source was turned on. The power source (AIM-TTI Instruments model PL303) was set at 0.5 A, and the etching process ran for 12 minutes (adapted from [86]).
The etching solutions used were: 1) Piranha solution, with a ratio of 2:1 (v/v) of hydrogen peroxide 130 volume (H_2O_2) Labchem, Portugal) and sulfuric acid 37 % (v/v) (Labchem, Portugal); 2) HCL 18.5 % (v/v) (Honeywell, Austria); 3) H_2SO_4 32.3 % (v/v) (Honeywell, Germany).
The etching solutions were placed in an ice bath during the etching process to avoid overheating and boiling, reducing bubble formation and resultant overflow.

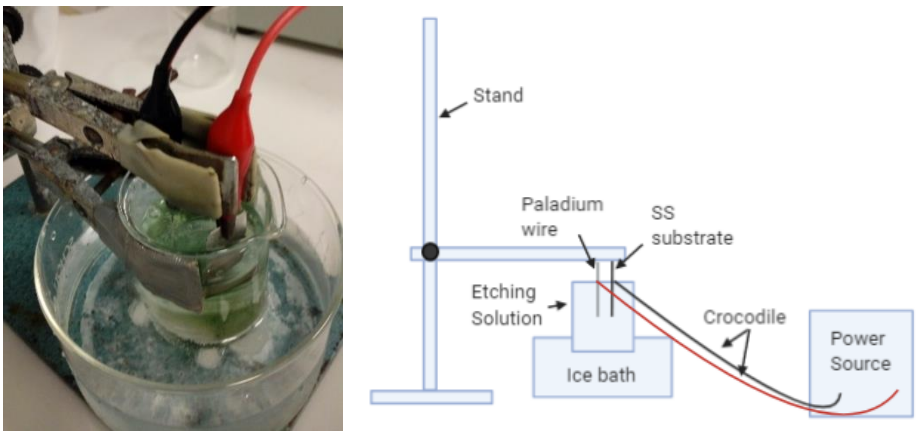

Figure 2.9: Setup used for electrochemical etching showing the etching solution in an ice bath, a 316L-SS substrate and palladium wire submerged in it and connected to a power source (not shown in the picture) by crocodiles (red and black wire).

2.3.3 Acid Etching

Acid etching is another process for chemical surface treatment of metals in which metallic contaminations on the surface are removed using an aqueous solution of an acid. Hence, acid etching can be used for natural oxide layer removal and formation of a new, thin and homogenous layer[87]. The etching of the stainless-steel substrates was made using a method of immersion in a HCl 37% v/v (10 N) and 18.5 % v/v (5 N) solutions (adapted from [86]). For this, the substrate was first washed, as previously described, and then submerged in the acid for 2 h, 1 h and 30 min, 1 h, 45 minutes and 30 minutes. After removal from the acid the substrates were cleaned with ultrapure water.

2.3.4 Mechanical abrasion

For mechanical abrasion, the substrates were treated with sandpaper (1000 grit, Dexter). The sandpaper was passed in the surface 100 times in vertical, horizontal and circular directions (Figure 2.10). The same process was employed in Ti-6Al-4V substrates that then proceeded to a salinization process.

Figure 2.10: Diagram of mechanical abrasion showing horizontal, vertical and circular motions (from left to right).

After the several treatments the 316L-SS substrates were cleaned for 15 minutes in sequential ultrasound baths of ultrapure water, ethanol (96 % v/v) and toluene (Carlo Erba, France). Afterwards all substrates were placed in a vacuum chamber at 70 ºC and -1 bar for 90 minutes, being then the temperature lowered to room temperature and the samples removed from vacuum and stored for further use.

2.3.5 Silanization

Silanization is a low-cost methodology to modify surfaces that are rich in hydroxyl groups (-OH), such as metal oxide surfaces. The binding of silicon-based molecules to metals occurs because the -OH can form a stable bond to silicon (Si) atoms. Silane compounds are used in the modification of biomedical implant surfaces because titanium, stainless steel, and cobalt–chromium alloys readily form oxide surfaces that are naturally rich in hydroxyl groups, for instance, an amine-ending silane, aminopropyltriethoxysilane (APTES), has been investigated as a way to attach many different compounds, including enzymes, proteins, and chitosan to medical implant alloys [76].
Ti-6Al-4V was cut to pieces of with sizes of 1 cm by 1.2 cm, cleaned and treated with mechanical abrasion as previously described. The substrates were then taped to a glass crystallizer with tape. The crystallizer was inverted and placed over two petri dishes containing 2 mL of ammonium (25 % v/v, Labchem, Portugal), and 2 mL of tetraethyl orthosilicate (TEOS) (98 % v/v, Aldrich, China) (Figure 2.11).

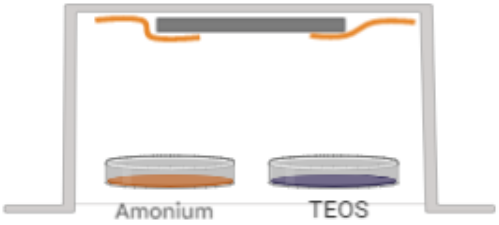

Figure 2.11: Silanization setup showing ammonium, TEOS and substrate position.

The substrates were left in the crystallizer for 24 hours and then stored for further examination and use. The same procedure was repeated inside an argon (Ar) filled container (Figure 2.12). The reaction was left to occur for 24 hours.

Figure 2.12: Recipient used for silanization in Ar atmosphere with detail on TEOS and amonium recipients on the right.

The procedure in Ar atmosphere was repeated with 2 mL of APTES (Millipore, Germany) instead of TEOS. In a different process, the substrate was dipped in TEOS or APTES and then placed in the Ar chamber that contained the ammonium.
In another method, Ti substrates were placed for 5 min in sequential ultrasound baths of ultrapure water, ethanol (96 % v/v) and acetone (99 % v/v). After this, the samples were placed in piranha solution (1:3 v/v H_2O_2/H_2SO_4) for one hour, in a passivation step, and then proceeded to one of the silanization methods described above.

2.4 Polymeric Solutions

2.4.1 PMMA

To produce the polymeric solutions, PMMA (Sigma Aldrich, Germany, 350 kDa) was dissolved in a solvent solution of acetone (≥99.5% Honeywell, Germany) and dimethylacetamide (DMAc) (Carlo Erba, France), in a ratio of 2:1 v/v to obtain a solution of PMMA 12 % (wt/v). The solution was kept under magnetic agitation at 35 ºC overnight. This solution was diluted to concentrations of 6 % (wt/v) and 3 % (wt/v). Another PMMA solution was obtained by dissolving the polymer in DCM (Carlo Erba, France) in ratios of 1:5 (wt/v), 1:20 (wt/v) and 1:40 (wt/v) being the solutions agitated overnight at room temperature.
For the drug and microparticle loaded films, to the solutions above of the lowest concentrations (3 % wt/v and 1:40 wt/v), the drugs and particles produced were added in a ratio of 2.5 % wt to the polymer mass.

2.4.2 Chitosan

For different chitosan solutions (Table 2.2), low molecular weight chitosan (Aldrich, Iceland) was dissolved in the respective solvent and stirred with magnetic agitation until the solution was homogeneous.
The solvents used were ethanol (Honeywell, Germany, ≥99.8 %), acetic acid (HAc) (Sigma-Aldrich, Germany, ≥99.7 %) and ultrapure water. All solutions were kept under magnetic agitation overnight and then kept in a flask sealed with parafilm.

Table 2.2: Chitosan solutions used throughout the study.

Solution	Concentration (% wt/v)	Solvent
A	3	HAc 90 % v/v
B	0.5	HAc 1 % v/v
C	0.5	50 % HAc 1 % v/v and 50 % Ethanol
E	0.04	50 % HAc 1 % v/v and 50 % Ethanol

2.4.3 PCL

Several PCL solutions (Table 2.3) were produced by the addition of PCL (Sigma-Aldrich, UK, 80 kDa) to different solvent systems composed of acetone (Honeywell, Germany, ≥99.5 %), DMAc (Carlo Erba, France) and dichloromethane (Carlo Erba, France). For this the desired quantity of polymer was added to the solvent and then stirred overnight under magnetic agitation at 35º C for solvent systems composed of acetone and DMAc and at room temperature for systems with DCM.

Table 2.3: PCL solutions used throughout the study.

Solution	Concentration (% wt/v)	Solvent
A	3	Acetone
B	6	2:1 (v/v) Acetone/DMAc
C	13	DCM

Solutions B was diluted to concentrations of, 0.75 % (wt/v), 1.5 % (wt/v) and 3 % (wt/v). Solution C was diluted to concentrations of 1.95 % (wt/v) and 0.1 % (wt/v).

2.5 Film deposition - Dip-coating

For all dip-coating procedures a Silar Dip-coating System with Stirrer model HO-TH-03A was used (Figure 2.13).

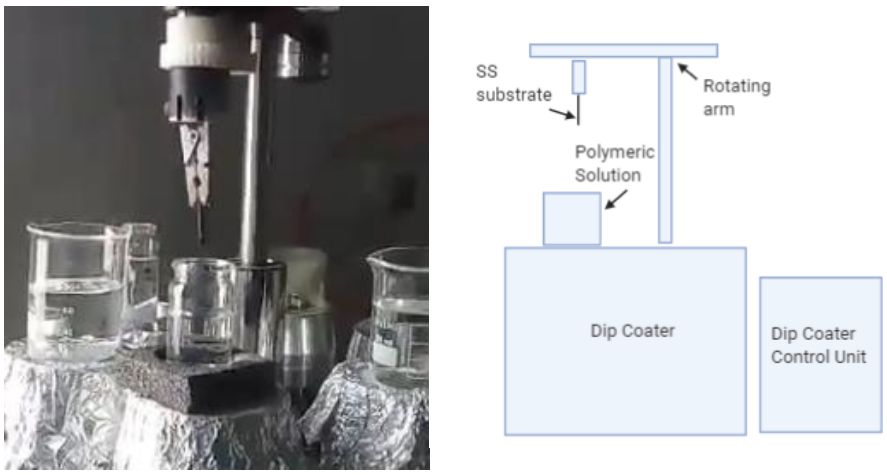

Figure 2.13: Dip-coating setup used for film deposition showing polymeric solutions and a 316L-SS substrate with a representative diagram to the right.

PMMA, chitosan and PCL solutions were used, and polymer concentration and solvent were changed. Dip-coating parameters, such as retrieval speed, dip duration, drying time between depositions, and washing steps between depositions were also altered. Films were produced with single layers, deposition of alternating polymer layers, and superimposing layers of the same polymer.

2.6 Characterization techniques

2.6.1 Optical microscopy

Optical microscopy (OM) is one of the oldest techniques used in biomedicine to study specimens or samples. Optical microscopes consist of a set of lenses that focus the image of a sample and a light source to illuminate the sample, that is usually placed on a glass slide, between the illumination source and the lenses[88]. Several adaptations can be made to a microscope to improve their qualities giving space for a better resolution of the image obtained, that can either be observed directly, or through a computer connected to the microscope[88].
For this analysis, the samples were placed directly in the slide support of a Leica DMi8 inverted microscope and the images were obtained in reflective mode. This technique was used in preliminary analysis of substrate surface and film depositions.

2.6.2 Micrometre measurements

Thickness of the films produced were measured using a digital micrometre (Mitutoyo, Japan). For this the sample was placed between two acetate sheet pieces and thickness measured (Figure 2.14). The acetate and metal thicknesses were measured and subtracted to obtain film thickness.

Figure 2.14: Setup used to measure film thickness showing the placement of micrometre clamps, acetate sheet and sample.

2.6.3 Atomic Force Microscopy (AFM)

AFM is a technique that produces topographic images of a surface by the movement of a tip in the surface of a sample. images are obtained by measurement of the force on a sharp tip created by the proximity to the surface of the sample. This force is kept small and at a constant level with a feedback mechanism, then, as the tip is moved sideways it will follow the surface contours[89].
Characterization of the surface morphology of the stainless steel before and after the several treatments was performed with the Atomic Force Microscope of WITec Alpha 300 RAS confocal spectrometer. The cantilever was operated with an WITec Arrow Al coated probe in tapping mode at 75 kHz and constant load of 2.8 N/m. Sections of 30 μm^2 were analysed to acquire values of average roughness and morphological and 3D maps of the samples.

2.6.4 SEM and EDS

SEM is an electronic microscopy that allows us to obtain a topological image and relative composition of a sample. This is made by way of a focused electron beam which will interact with the sample. When they interact with the sample, electrons will scatter, and a detector will receive the signals corresponding to this interaction and an image is formed on a computer [90]. Samples of the steel after the several treatments as well as samples of the Ti after several silanization processes were analysed using SEM (Hitachi model 2400) and Energy-dispersive X-ray spectroscopy (EDS) (Hitachi model 2400) to obtain images of the surface of the samples and to verify the presence of chemical groups at the surface of the metals provided by the several treatments. For the Ti substrates the Si content was observed to verify which of the several treatments was more effective.
Films of chitosan and PCL prior to and after peel-off studies were also analysed, namely, 6 bilayer films of chitosan/PCL loaded with the microparticles produced, Dap or Van as well as unloaded, 1 bilayer film of chitosan and PCL and 6 bilayer films of chitosan and PCL loaded with Dap, Dap loaded microparticles and unloaded after peel-off studies. For these, small sections of the samples were cut and placed on a SEM disk using carbon tape and then another stripe of carbon tape was placed over the film samples to allow electron flow from the top of the samples partially to the disk and thus improve image quality (Figure 2.15).
Samples of the produced microparticles, PMMA were also analysed. For these samples, a small amount of microparticles was suspended in ethanol (96%) and then the suspension placed directly atop the carbon tape (Figure 2.15) The samples were then covered in a gold/palladium (Au-Pd) coating before analysis.

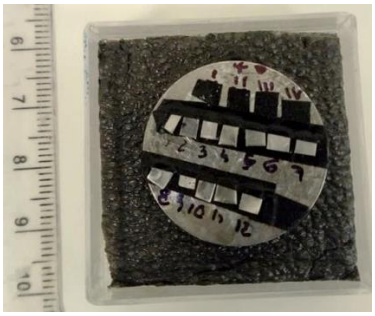

Figure 2.15: SEM disk with samples on carbon tape (black stripes) showing microparticle (I to IV) and film (1 to 12) samples.

2.6.5 Raman spectroscopy

Raman spectroscopy is a non-destructive chemical analysis technique that provides information about vibrational energy and molecular structures. For this, Raman uses a monochromatic light source to strike a sample, this light will be scattered by the sample and generates light of either the same (elastic scattering) or a different (inelastic scattering) energy from the incident one. From the inelastic scattering it's possible to have information about the chemical composition of the sample[91].
Raman spectroscopy was used to analyse access the presence of daptomycin and vancomycin in the microspheres and films obtained. The films analysed were those of 6 bilayers of chitosan/PCl loaded with the microparticles produced, with Dap and with Van as well as unloaded. Analysis of chitosan, PCL, PMMA, Dap and Van were also performed to use as comparison for the spectra of the films.
Maps of the distribution of the compounds in an area of 5 μm^2 for the microsphere loaded films were also made. All analysis was performed in a Confocal Raman spectrophotometer (Witec Alpha 300 RAS) using a laser of 532 nm and a power of 30 mW.

2.6.6 Peel-off

Film adhesion was tested by the peel-off method[92] (Figure 2.16). For a first analysis, a 90º peel-off test was preformed manually, verifying the existence of detachment of the film from the substrate. A later analysis was made at 180º.

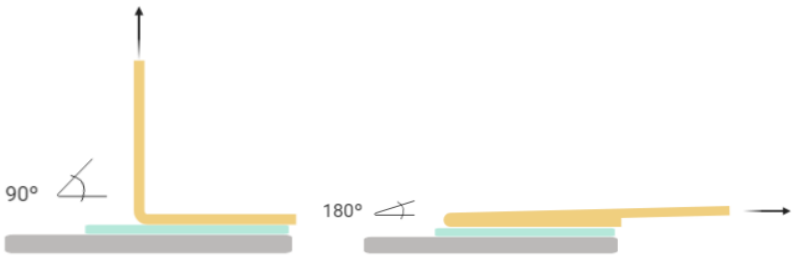

Figure 2.16: 90º (left) and 180º (right) peel-off test diagram showing: grey) substrate; blue) film and yellow) tape with peel direction indicated by black arrows.

For 180º test, the film was covered with tape and the tape pulled off at a constant force using a traction machine (20 N load cell Rheometric Scientific uniaxial machine operable with the "Minimat" software (Minimat Control Software Version 1.60 February 1994 (c) P.L. Thermal Science 1984-94 Rheometric Scientific Ltd.). For all peel-off tests, the tape used was Tesa® Basic Packaging Tape-58572 and was fixed to the moving claw (Figure 2.17).

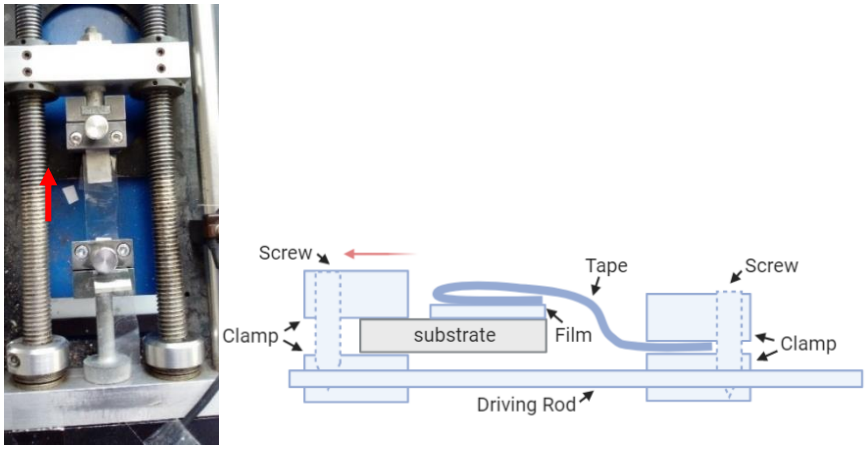

Figure 2.17: System used for 180º peel-off tests showing a substrate and tape clamped to the machine as it moves (direction of the red arrow) and representative diagram in the right.

Peel-off forces are given by the interception of the linear fit with a slope of 0 of the linear part of the load vs. extension plot that is parallel to the x axis (Figure 2.18 B)[93].

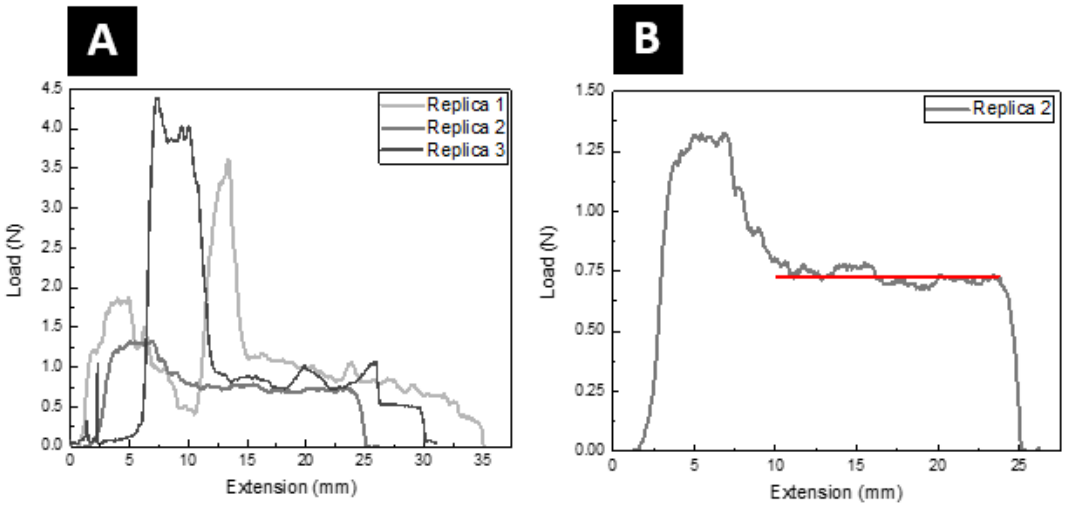

Figure 2.18: Peel-off curves for three replicas of films made with chitosan 0.5% wt/v in 50 % (v/v) ethanol and 50 % (v/v) HAc 1 % (v/v) (A) and representative linear fit of the second replica (B).

2.6.7 Degradation

For degradation studies, films of chitosan and PCL were made by a casting method[94]. For this, approximately 200 mL of a chitosan solution with a polymer concentration of 0.1 % wt/v in a solvent system composed of 50 % v/v absolute ethanol and 50 % v/v HAc 1 % v/v, and a PCL solution with a polymer concentration of 0.1 % and DCM as solvent were poured into plastic and glass petri dishes respectively and then left uncovered in a fume hood overnight so the solvent would evaporate. The films obtained were then cut in pieces with similar areas that were then placed in a falcon tube and submerged in 10 mL of simulated body fluid (SBF) at 37 ºC adjusted to pH values of 8, 7.4, 7, 6.5, 6, 5.5, and 5. 3 replicas were made for each pH value. After submersion, the films were cleaned in ultrapure water to remove any salt residues and then dried in an incubator at 40 ºC until completely dry

(protocol adapted from [95]). The films were then weighted, and the mass compared to that obtained before submersion to ascertain mass variation.

2.6.8 Swelling

For swelling studies, a similar procedure to that of degradation was done, with only the surface of the samples being dried with paper before weighing them. The swelling studies occurred at 37 ºC under orbital agitation in a Comecta Optic Ivymen® S2000 system for a total period of 1 week. Samples were weighed before and after the swelling process as to assess the mass variation (protocol adapted from [96]).

2.7 Drug release

2.7.1 Calibration curve

To do the drug release study first there were made several solutions of daptomycin and vancomycin in SBF to produce calibration curves for 3 pH values: 7.4, correspondent to the normal physiological pH value, 5.5 correspondent the value of pH existent in a stage of infection and 6.5, a pH value between the two to verify if the changes in drug release occurred in a linear fashion. For both drugs the concentrations studied were of 0.666 mg/mL, 0.5 mg/mL 0.333 mg/mL, 0.25 mg/mL, 0.1665 mg/mL, 0.125 mg/mL, 0.08325 mg/mL, 0.0625 mg/mL, 0.03125 mg/mL, 0.01563 mg/mL, 0.00781 mg/mL, and 0.00391 mg/mL.
The solutions were analysed with UV-Vis spectroscopy in photometry mode and calibration curves were made to study the dependence of the absorbance in function of the drug concentration for the peaks observed in the spectra of a sample of drug release for both drugs: 225 nm, 236 nm and 282 nm for vancomycin and 225 nm, 261 nm, 282 nm, 289 nm, and 362 nm for daptomycin.

- **Simulated body fluid (SBF)**

The SBF solution was made following a protocol[97] that consisted upon the addition of several compounds (Table 2.4) into ultrapure water at room temperature in a 1 L glass flask under magnetic agitation creating a vortex. After the addition of the several compounds, the solution's pH was adjusted to 7.4 (or other needed pH values) with a HCl 1 M. The SBF was then stored in a refrigerator.

Table 2.4: Simulated body fluid composition in order of addition (from top to bottom).

Compound	Formula	Mass (g)
Sodium chloride (Sigma-Aldrich, Germany)	NaCl	6.547
Sodium carbonate (PanReacAppliChem, Germany)	$NaHCO_3$	2.268
Potassium chloride (Scharlau, Spain)	KCl	0.373
Sodium phosphate dibasic dihydrate (Fluka Analytical)	$Na_2HPO_4 \cdot H_2O$	0.178
Magnesium chloride hexahydrate (PanReacAppliChem, Germany)	$MgCl_2 \cdot 6H_2O$	0.305
Hydrochloridric acid (1 M)	HCL	15 mL
Calcium chloride dihydrate (Sigma-Aldrich, Germany)	$CaCl_2 \cdot 2H_2O$	0.368
Sodium sulphate (Sigma-Aldrich, Germany)	Na_2SO_4	0.071
Tris(hydromethyl)aminomethane (Sigma-Aldrich, USA)	$(CH_2OH)_3CNH_2$	6.057

2.7.2 Drug Release profile

For the drug release profile studies, substrates coated with Chi/PCL films produced placed inside 4 mL screw cap plastic vials and submerged in 500 µL of SBF at a pH of 7.4, 6.5 and 5.5 at room temperature for determined periods of time. The absorbance of the release medium was analysed by UV-VIS spectroscopy (T90+ UV/VIS Spectrometer from PGInstruments Ltd. with a Rotilabo® quartz cuvette with a path length of 1 cm and a maximum volume of 0.7 µL). New SBF was added to the vials each

time the SBF with the released drug was removed, to avoid the saturation of the release medium with the drug (Figure 2.19). This analysis was made for 5 replicas of several film: 6 bilayers of chitosan/PCL loaded with Dap, Van or the microspheres produced. The study was conducted for a total period of 96 hours (protocol adapted from [78]).

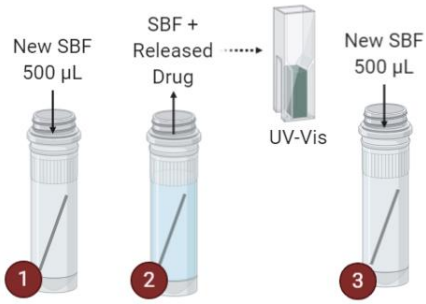

Figure 2.19: Steps for drug release studies showing the substrate inside a vial and: 1) addition of new SBF; 2) the removal of SBF and subsequent UV-Vis analysis and 3) addition of new SBF in the same vial.

The UV-Vis spectroscopy analysis was made in the photometry mode at the same wavelengths used to build the calibration curves mentioned above.

3 Results and discussion

In this chapter the results of particle and film production and analysis will be presented. First it will go over microsphere production and analysis, referring to morphological aspects and drug encapsulation and release. From there it will overview the preparation and analysis of metal surfaces for film deposition, first for stainless steel, and then for titanium. Subsequently, it will discuss film deposition optimization, providing information on film morphology, chemical composition, and physical properties such as swelling and degradation rates. Apart from showing the results obtained this chapter also tries to provide the reader with the logic used to make the several choices that culminated in the final object.

3.1 Production of PMMA microspheres

During microsphere production, encapsulation efficiency, drug loading and particle size were analysed. For the first two, firstly, solutions at specific concentrations of Dap and Van were analysed by UV-Vis spectroscopy. The absorbances obtained (Appendix A) were used to calculate the drug concentration by use of a calibration curve (Figure 6.1 in Appendix B).
The several linear fits obtained (Table 3.1) show that the quantification of vancomycin cannot be done at a wavelength of 365 nm since at this wavelength, no concentration has a significant absorbance value. This drug should be quantified at a wavelength of 230 nm where the slope is larger and therefore, the absorbance changes the most for different concentrations. By using this wavelength, even if the change in concentration is very small, a shift in the absorbance should be noted. As for daptomycin, all wavelengths could be used. Because for 365 nm vancomycin has no notable absorbances, this wavelength should be used, as to make sure the absorbances measured correspond to the drug being analysed.

Table 3.1: Equation and R^2 values for calibration curves of Dap and Van at several wavelengths.

	Vancomycin		Daptomycin	
Wavelength (nm)	Equation	R^2	Equation	R^2
230	y=0.02746x+0.0771	0.99338	y=0.01716x+0.05425	0.99738
260	y=0.00108x+0.02587	0.99267	y=0.00659x+0.02397	0.99179
280	y=0.00394x+0.03407	0.99427	y=0.0042x+0.00572	0.99577
365	y =5.05113E-6x+0 .00281	0.02	y= 0.0031x+ 0.01061	0.99451

3.1.1 Encapsulation Efficiency

Encapsulation efficiency (EE) and drug loading (DL) were calculated from the supernatant obtained during the washing step of sphere production, composed from sequential centrifugations of the microsphere solutions. To calculate the amount of drug contained in the supernatant, samples of 200 µL of it were analysed with UV-Vis spectrometry (Appendix A) and drug quantification of these samples was done using the above-described calibration curves.
Encapsulation efficiency refers to the amount of drug present in the particles and is expressed as the percentage of encapsulated drug compared to the initial amount used for particle preparation (Equation 3.1). This amount was calculated by analysing the supernatant from the cleaning step of particle production (Table 6.2 and Table 6.5 in Appendix A) and quantification of drugs present in this supernatant (ie, non-encapsulated antibiotic). It was assumed that the drug encapsulated corresponded to the total drug minus the drug left in the supernatant (Equation 3.2)

$$Encapsulated\ drug\ = initial\ drug\ mass - supernatant\ drug\ mass \quad (3.1)$$

$$\frac{Encapsulated\ Drug}{Initial\ Drug} * 100 \quad (3.2)$$

Taking the concentrations of daptomycin at a wavelength of 365 nm and of vancomycin at a wavelength of 230 nm (Table 6.6 and Table 6.9 in Appendix A), and making the average from the several replicas, it is possible to conclude over the approximate encapsulation efficiency (Table 3.2).

Table 3.2: Drug mass added to the particle formulations and concentration found in supernatant as well as EE values obtained for Dap and Van loaded microparticles.

	Drug Concentration (mg/ml)	**Vol. (mL)**	**Supernatant drug (mg)**	**Initial drug (mg)**	**Supernatant drug (%)**	**Encapsulation Efficiency (%)**
Dap	0.16 ± 0.07	32	0.52 ± 0.23	18.75	2.80 ± 1.20	97.20 ± 1.20
Van	0.12 ± 0.07	32	0.39 ± 0.007	18.75	2.11 ± 0.04	97.89 ± 0.04

These values are in accordance to the literature, where Van loaded microparticles (PMMA-Van) have a EE of 91.1 ± 0.7 % and Dap loaded microparticles (PMMA-EUD-Dap) of 95.6 ± 1.2 %.

3.1.2 Drug Loading

For the loaded microparticles, values of EE, particle mass and initial drug mass were used to calculate the DL (Formula 3.3)

$$Drug\ loading = \frac{EE * initial\ drug\ mass}{particle\ mass} * 100 \quad (3.3)$$

The DL values obtained (Table 3.3) are of 21.64 ± 0.67 for Dap and of 22.55 ± 2.73 for Van which are almost double of those reported for this process that are of 12.4 ± 0.3 and of 11.9 ± 0.1 respectively[44].

Table 3.3: DL values obtained for microparticle production.

Drug	**Vial**	**Initial drug mass (mg)**	**Microparticle mass (mg)**	**EE (%)**	**Drug Loading (%)**
Van	4	18.75	88	99.6228	21.2264
	5	18.75	89	99.6228	20.9879
	6	18.75	83	99.6228	22.5052
Dap	10	18.75	94	99.9078	19.9284
	11	18.75	87	99.9078	21.5332
	12	18.75	71	99.9078	26.3841

3.1.3 Particle production yield

Particle production yield was obtained by calculating the mass of particles produced and comparing it to the initial polymers and drug mass used (Formula 3.4) for the unloaded spheres.

$$\frac{microsphere\ mass}{initial\ polymer\ mass + initial\ drug\ mass} * 100 \quad (3.4)$$

Taking this formula and applying it to the microparticles produced one can see that the yields are mostly consistent with values between 49 % and 65 % except for vial 3 (Table 3.4).

Table 3.4: Values of drug and particle mass as well as particle production yield.

Vial	IP mass (mg)	Dr mass (mg)	µS mass (mg)	Yield (%)
1	125	0	76	60.80
2	125	0	76	60.80
3	125	0	11	88.00
4	125	18.75	88	61.22
5	125	18.75	89	61.91
6	125	18.75	83	57.74
7	125	0	446	356.80
8	125	0	76	60.80
9	125	0	77	61.60
10	125	18.75	94	65.39
11	125	18.75	87	60.52
12	125	18.75	71	49.39

Vials 1-3) unloaded PMMA microspheres; Vials 4-6) PMMA-Van microspheres; Vials 7-9) Unloaded PMMA-EUD microspheres; Vials 10-12) PMMA-EUD-Dap microspheres; IP-initial polymer; Dr-drug added; µS-microspheres

3.1.4 Particle size

Particle size was measured at several stages of the particle production process: after the first centrifugation, after both centrifugations, and after lyophilization. This was done to both ensure that no microparticles were being lost during the centrifugation process and to study the effect of the lyophilization step in particle size.

Observing the drug free PMMA particle size distribution before and after one centrifugation (Figure 3.1), it is possible to note an absence of particles in the micrometric range after the centrifugation process (Figure 3.1 B). Being that the solution analysed is the supernatant of the particle suspension, one can then conclude that no microparticles are being lost in the centrifugation process, since they are all in the pellet that is later resuspended for lyophilization and not in the supernatant which is discarded. It is also possible to see a significant concentration of particles in the nanometric range in the suspension (Figure 3.1 A), indicating a loss of polymer, and possibly a loss of drug during this process.

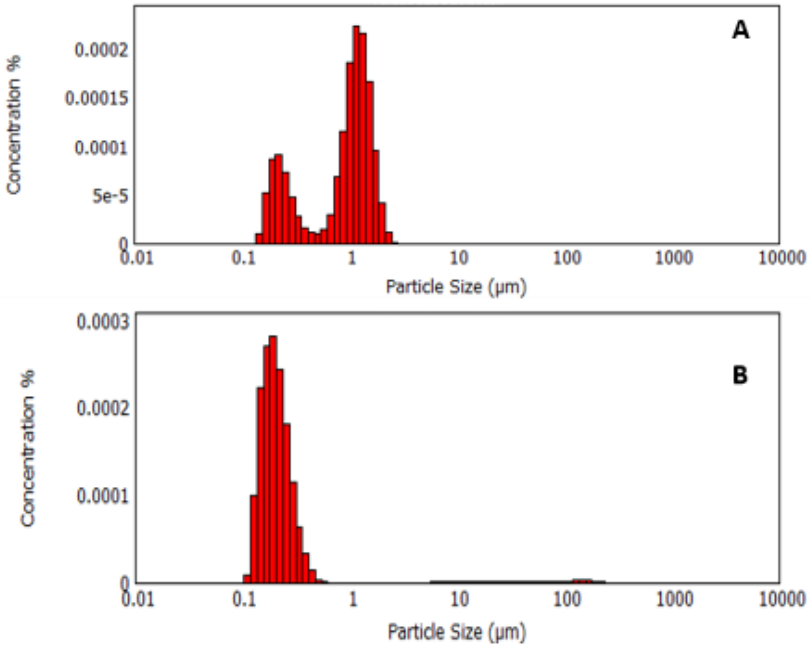

Figure 3.1: Particle size distribution of a sample of drug-free PMMA particle suspension before (A) and after (B) a centrifugation step at 7500 rpm for 10 minutes.

When looking at the unloaded PMMA/EUD (PMMA-EUD) particles before lyophilization (Figure 3.2), it is possible to note an aggregation of the particles occurring during the time between measurements (during a period of 34 minutes), indicating that the suspension is not very stable. This is observed by the appearance of two populations in plot B, which show an increase of the concentration of particles with sizes of about 1 µm and the decrease of the concentration of particles with sizes of around 100 nm when compared to plot A. In plot C this aggregation is further accentuated by the addition of a third population, with particle sizes of approximately 100 µm.

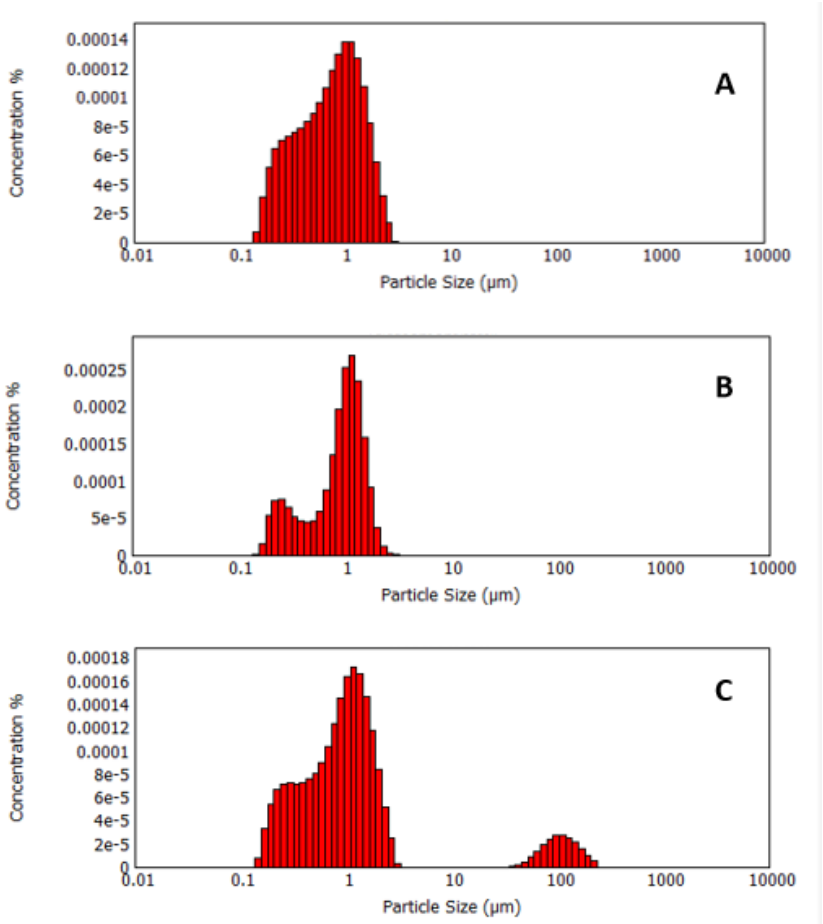

Figure 3.2: Particle size distribution of 3 replicas of PMMA-EUD particles in order of time of measurement from top to bottom with a 34 minute gap between first and last measurements.

Aggregation is also visible in the PMMA-EUD-Dap particles (Figure 3.3), indicating that the probable cause for this aggregation is the EUD, and that Dap does not seem to stabilize the particles. It is however important to note that two replicas were joined as to obtain the minimum laser obscurity needed for analysis and aggregation can be present only in one replica due to an error in the particle production.

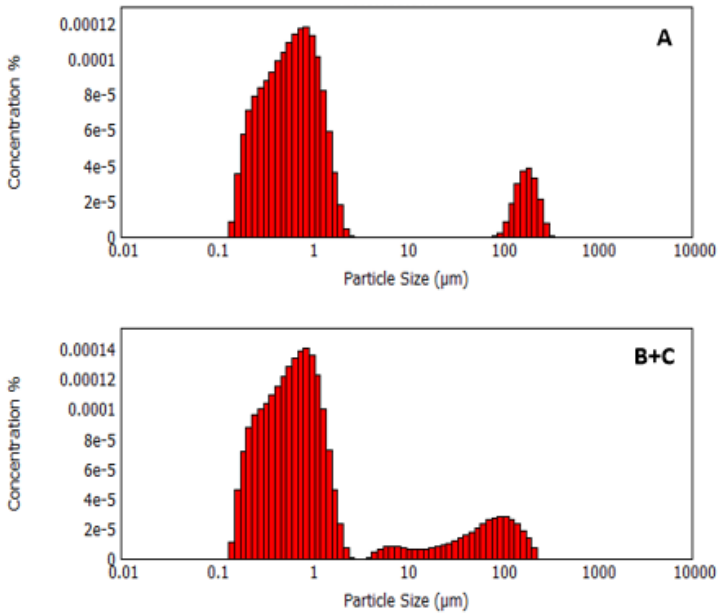

Figure 3.3: Particle size distribution for three replicas of PMMA-EUD-Dap particles with a 35 minutes gap between the first (A) and last (B+C) measurement. Samples B and C have been joined to reach the minimum laser obscurity needed.

When looking at PMMA-Van microparticles (Figure 3.4), aggregation is not seen for the same time lapse between measurements. Instead, the nanometric and micrometric populations stay mostly unchanged, showing a higher stability of these particles when compared to their EUD containing counterparts.

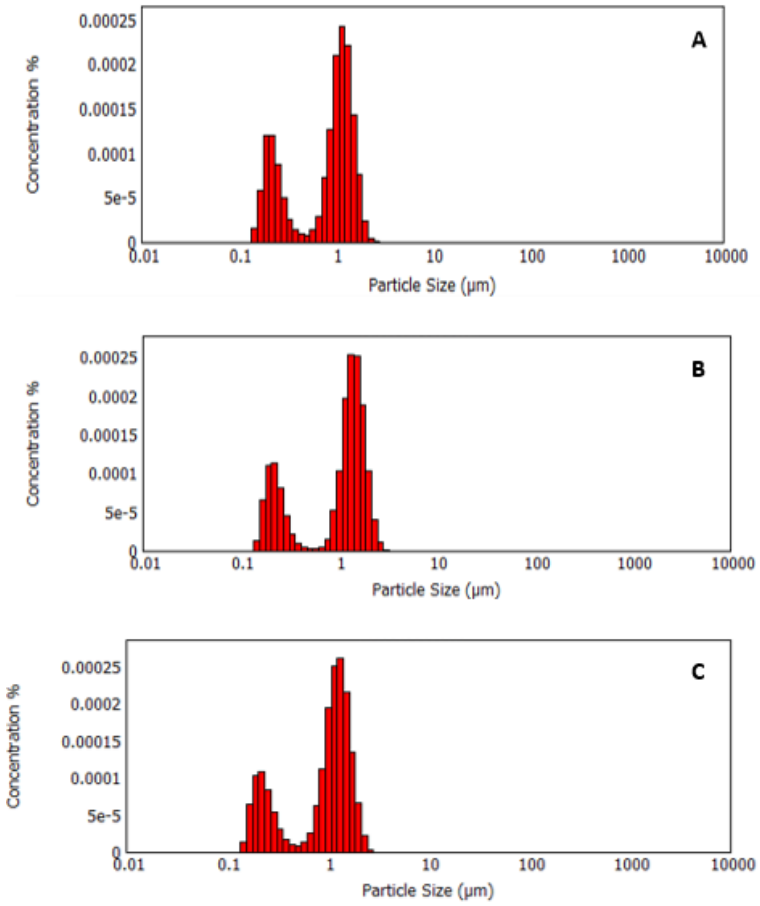

Figure 3.4: Particle size distribution of three replica of PMMA-Van particles with a 37 minute gap between the first (A) and the last (C) measurement.

After lyophilisation, the particle size was measured by SEM (Figure 3.5).

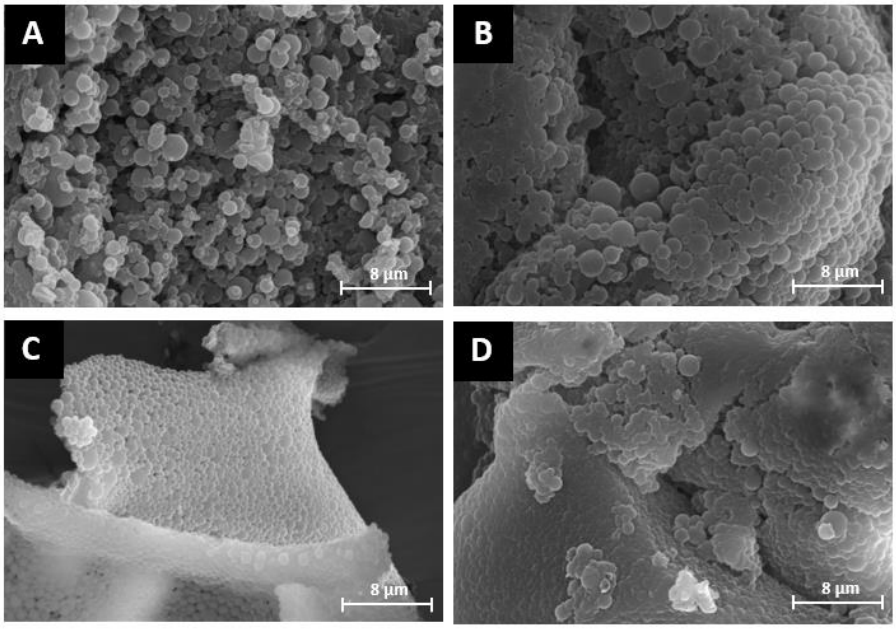

Figure 3.5: SEM micrographs of the microspheres obtained showing: A) PMMA, B) PMMA-Van, C) PMMA-EUD, D) PMMA-EUD-Dap microspheres.

Using ImageJ software, the particle size was measured (Table 3.5), and an average diameter obtained for 30 measurements of each kind of sphere (Figure 6.2 in Appendix 0).

Table 3.5: Microparticle size obtained after lyophilization (mean ± SD; *n*=30) comparing both experimental and literature values.

	Diameter (µm)	
Particle	**Experimental**	**Literature** [44]
PMMA	1.29 ± 0.13	1.69 ± 0.04
PMMA-Van	1.15 ± 0.28	1.50 ± 0.21
PMMA-EUD	0.96 ± 0.25	1.23 ± 0.09
PMMA-EUD-Dap	0.68 ± 0.11	1.34 ± 0.3

The sizes obtained show that while PMMA, PMMA-Van and PMMA-EUD values are in accordance to those reported, the PMMA-EUD-Dap spheres have a lower diameter than expected. It is also possible to note that the particles produced show a higher diameter dispersion than those of the literature [44].

3.2 Film optimization - 316L-SS Treatment

Starting with stainless steel, the sheet purchased was cut into rectangles and then washed, to remove oils and other residues from the surface. Afterwards, put through an electropolishing step, smoothing and cleaning the metal surface. The polished steel did not allow film deposition, therefore, several treatments to the surface were made. For this, the steel was treated with acid etching, by submersion in HCl, electrochemical etching, with HCl, H_2SO_4 and piranha solution, and mechanical abrasion, to see which treatment led to the best film adhesion and was therefore the most appropriate for film deposition.

3.2.1 Electropolishing

OM and SEM were used to observe the surface of the 316L-SS after electropolishing (Figure 3.6).

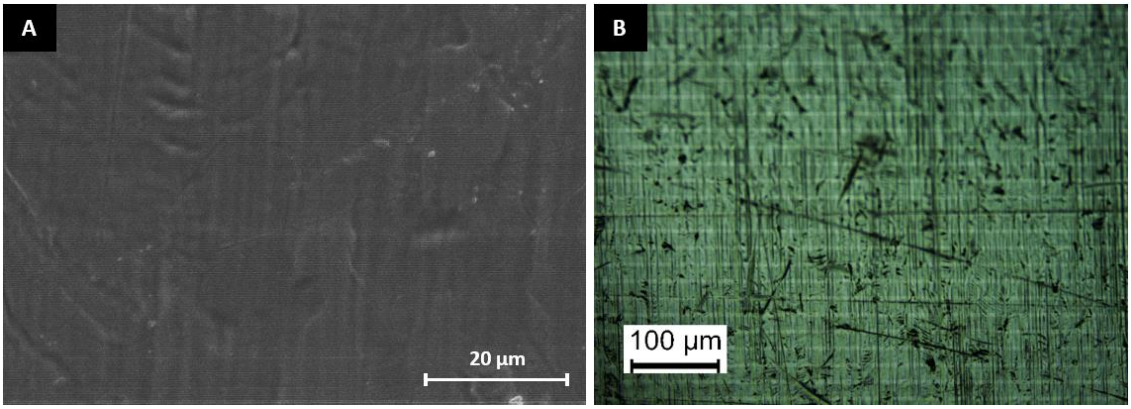

Figure 3.6: SEM micrograph (A) and OM image (B) of a 316L-SS substrate after an electropolish step as described above.

In both analysis it can be seen that the surface presents as very smooth, as it is to be expected, since the purpose of electropolishing is to both smoothen out the metal and remove any contaminants in the metal surface [98]. The sample of polished steel was also analysed by AFM technique (Figure 3.7 and Figure 6.3 in Appendix D) to obtain a value of the roughness of the steel surface after the treatment and verify its effectiveness.

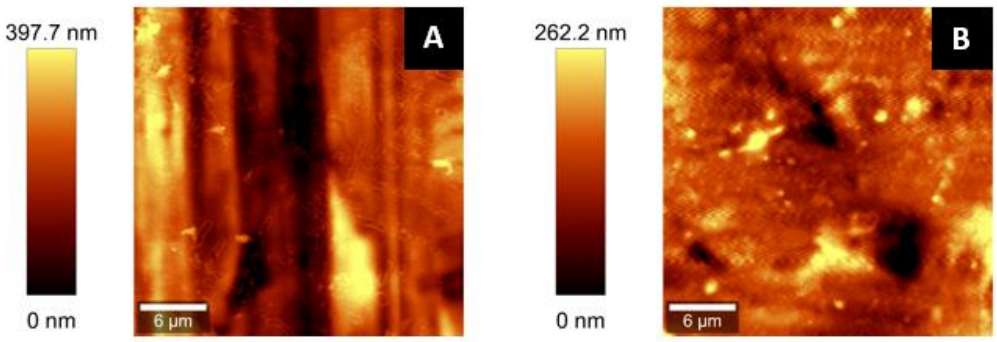

Figure 3.7: AFM images of 316L-SS sample A) before and B) after an electropolishing step.

The average value of roughness obtained after the electropolishing of the metal is of 46.4 nm, which lies within the range of roughness values obtained for different electropolishing treatments, albeit, being slightly high [85]. This value shows a decrease of average roughness, that changes from 93.9 nm before the electropolishing step to 46.4 nm after it, corresponding to a roughness decrease of 51.6 %, indicating that the treatment used is effective in the smoothing of the metal surface. This phenomenon is denominated anodic levelling and results from difference in the dissolution rate of metal ions released from erosion between peaks and valleys on the surface (Figure 3.8), that leads to different current distribution and corrosion rates.

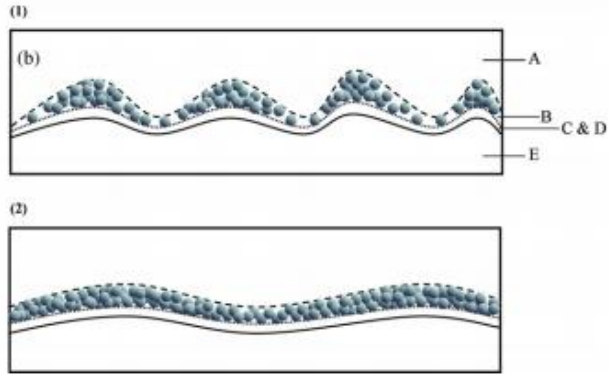

Figure 3.8: Schematic of anodic dissolution showing: A) bulk solution, B) adsorbed shielding molecules, C) Salt-Solution layer, D) metal ion layer and E) metal surface (taken from [99])

The decreases of roughness observed are smaller than the micrometre scale and attributed to an effect called anodic brightening. This effect requires the metal dissolution to be mass-transport-controlled and the formation of a precipitated salt layer at the electrode surface. The salt layer is needed to suppress the influence of crystallographic orientation and surface defects on the dissolution process. Usually, a fine electropolished surface of metals, results from a combination of levelling (changes of roughness within the micrometre scale) and brightening [99].
Since after the electropolishing step the polymeric solutions did not adhere to the metal, several surface treatments were studied.

3.2.2 Acid Etching

A first treatment consisted in acid etching with HCl. For this, the substrates were submerged in HCl at concentrations of 37 % v/v or 18.5 % v/v for times from 30 minutes to 2 hours.
From the acid etching process in the 316L-SS substrates (Figure 3.9) it can be noted that by using a concentration of 37 % the grain boundaries are exposed from 45 minutes up to 2 hours, being that the acid appears to corrode the metal from these areas, since the lines that define grain boundaries become thicker with longer immersion times. By using HCl 18.5 % v/v the same assessment cannot be made since grain boundaries are not as clearly shown. Instead, the surface seems to be more evenly eroded, without a clear area or zone where corrosion seems more intense.

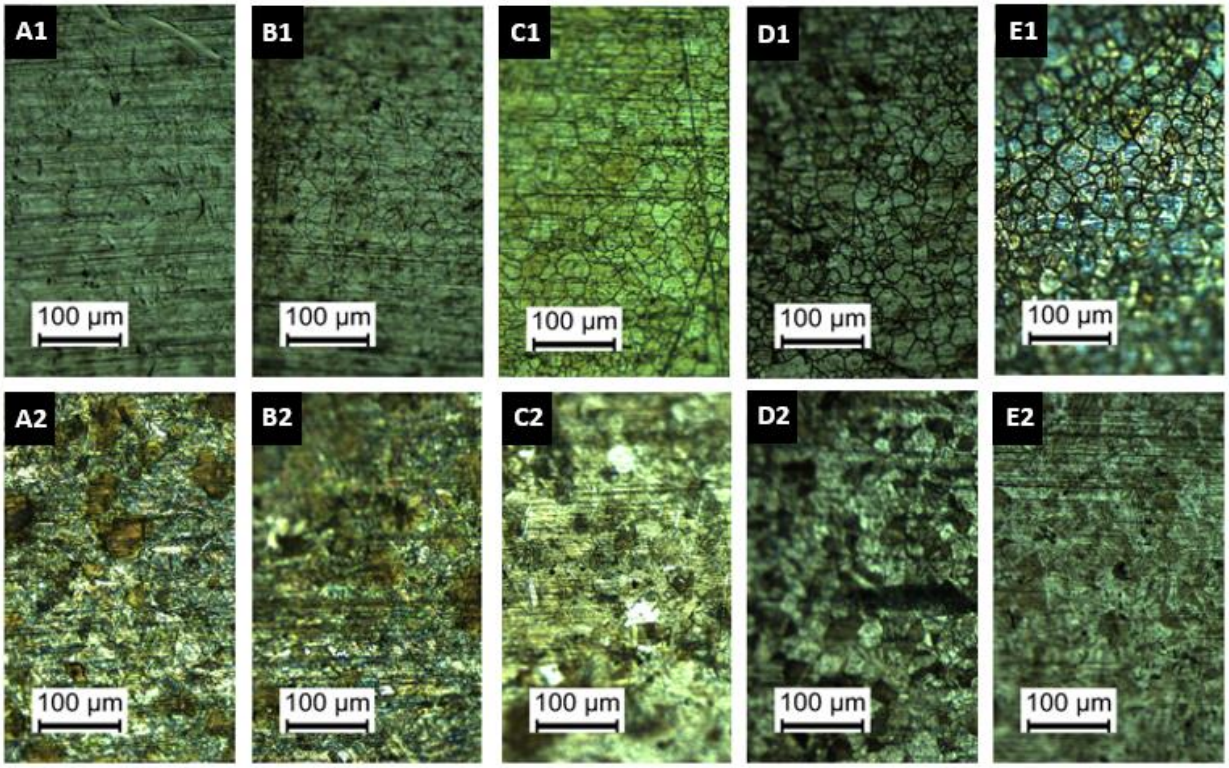

Figure 3.9: 316L-SS surface after acid etching with 1) HCl 37 % v/v and 2) HCl 18.5 % v/v, for A) 30 min, B) 45 min, C) 1 h, D) 1 h and 30 min and E) 2 h.

Analysing the samples with AFM (Figure 3.10 and Figure 6.5 in Appendix D) one can conclude on the average roughness of the samples. Starting with the immersion in HCl 37 % v/v, it can be confirmed that the corrosion occurs at a higher degree in the grain boundaries. As immersion time increases the roughness increases and the grains become more defined, as was visible in the OM images. The grain surface becomes smoother as time increases which shows that the corrosion is happening in both the grain boundaries and the grain surface. When looking at the treatment done with HCl 18.5 % v/v the grain boundaries do not change as much, instead, the surface seems to be smoothened out, with the whole surface appearing to be etched equally.

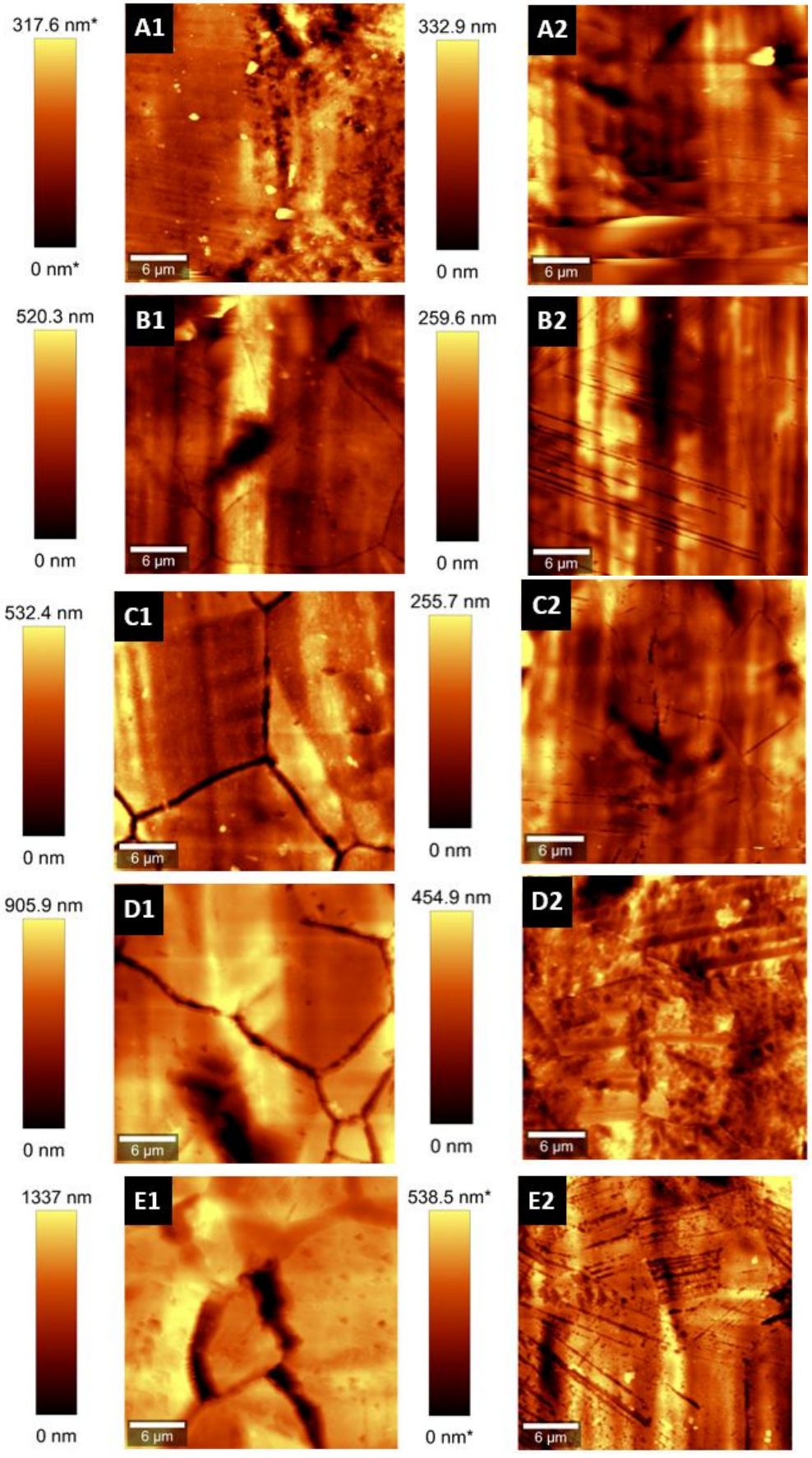

Figure 3.10: AFM image of a section of a sample of 316L-SS submerged in: 1) HCl 37 % v/v 2) 18.5 % for A) 30 min, B) 45 min, C) 1 h, D)1 h and 30 min, E) 2 h.

Taking the average roughness values and plotting them versus the immersion times (Figure 3.11) it is possible to observe that time affects roughness more for higher acid concentrations. At a concentration of 37 % v/v, the roughness increases by 400 % within 2 hours, whereas for an acid concentration of 18.5 % v/v the increase is only of 160 %.

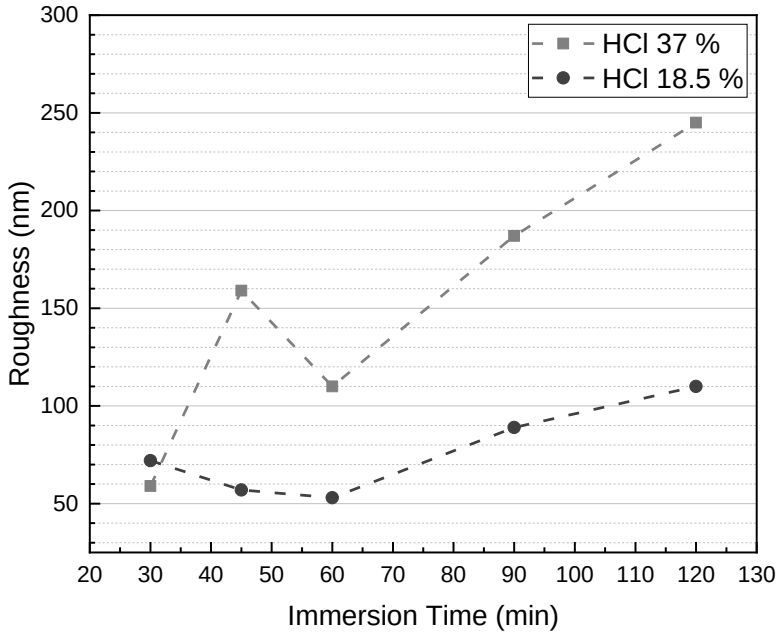

Figure 3.11: Plot of roughness vs immersion time in HCl 37 % v/v and HCl 18.5 % v/v.

As for the thickness of the obtained substrates (Figure 3.12 and Figure 6.7 and in Appendix D), one can conclude that immersion time seems to affect very little the thickness obtained for both acid concentrations used.

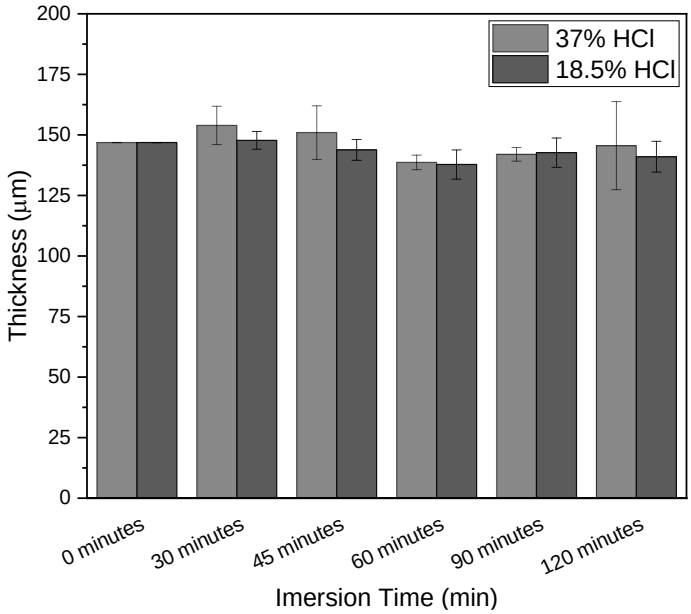

Figure 3.12: Thicknesses obtained for the several immersion times of 316L-SS in HCl 37 % v/v and HCl 18.5 % v/v.

When comparing the results for both concentrations, it is possible to observe that the average thicknesses are very similar. From the standard deviations, it is also possible to note that a higher concentration of acid leads to less homogeneous surface and that the acid treatment leads to a decrease of substrate uniformity when compared to the non-treated steel, which is to be expected since acid increases surface rugosity. To conclude, the acid concentration affects the rugosity more than the immersion time, and it leads to different corrosion patterns. As such, to change surface rugosity it would be better to alter acid concentration.

3.2.3 Electrochemical etching

- **Hydrochloric acid**

Electrochemical etching step done with HCl solutions (Figure 3.13) shows to increase the roughness in the substrate, affecting both the submerged portion of the substrate and the surface above the solution, which meets acid vapour.

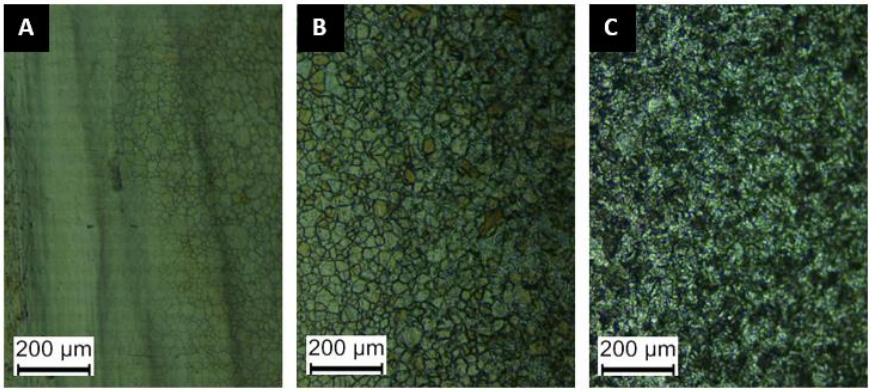

Figure 3.13: Effects of electrochemical etching with HCl 18.5 % v/v showing: A) non-treated area, B) area affected by acid vapours and C) submerged area.

The electrochemical etching with HCl 18.5 % v/v at 0.5 A (Figure 3.14 A) resulted in a rough surface. This same process performed after a polishing step resulted in a similar result, indicating that the polishing step does not significantly change the corrosion of the surface. This shows that the polish step can be absent from the substrate treatment, thus simplifying the process. Comparing these results to those of acid etching, in the surface of the substrate submerged in HCl 37 % v/v for one hour (Figure 3.14 B), the grain limits are seen but no cavities are present, showing a smoother surface.

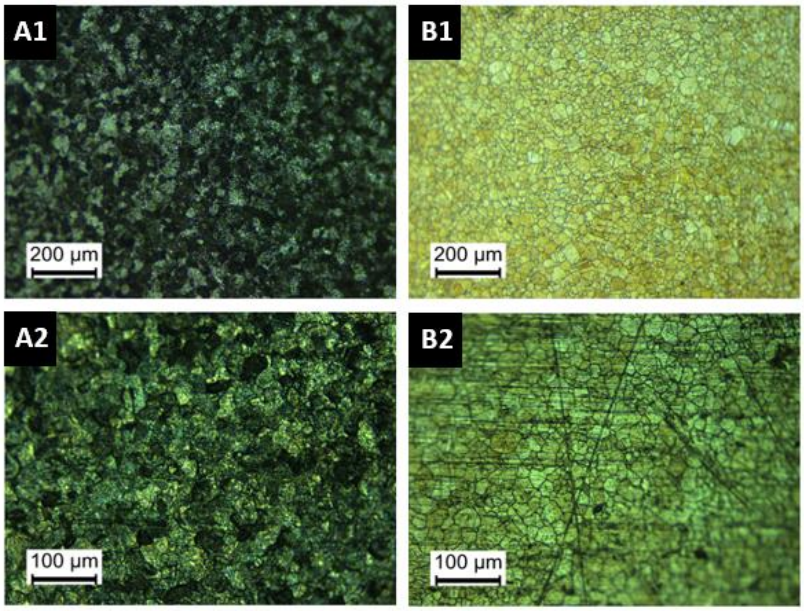

Figure 3.14: OM image of the surface of 316L-SS substrates after: **A)** electrochemical etching in HCl 18.5 % **B)** Immersion in HCl 37% v/v for 1 h **1**) after a polishing and **2)** without a previous polishing step.

The obtained SEM and AFM results for these samples (Figure 3.15 and Figure 6.5 in Appendix D), it is possible to see a general corrosion of the surface. In this process a roughness of 334 nm was obtained.

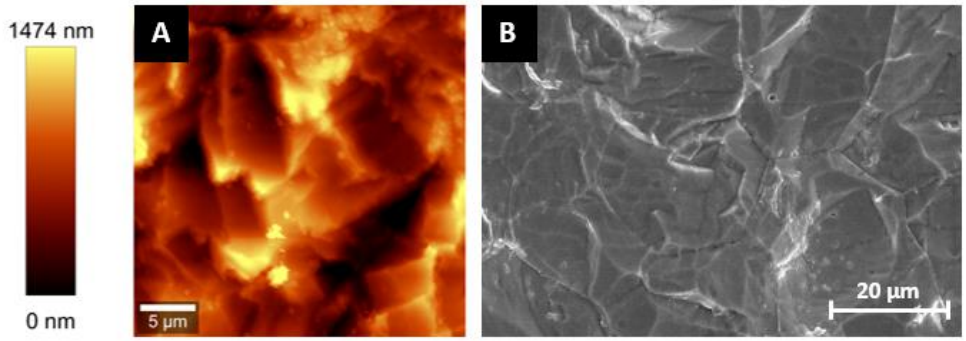

Figure 3.15: AFM image (A) and SEM micrograph (B) of 316L-SS electrochemical etched by HCl 18.5 % v/v.

The same sample was also analysed by SEM-EDS technique (Figure 3.16) to assert if the treatment left any chemical groups in the surface that could influence film adhesion.

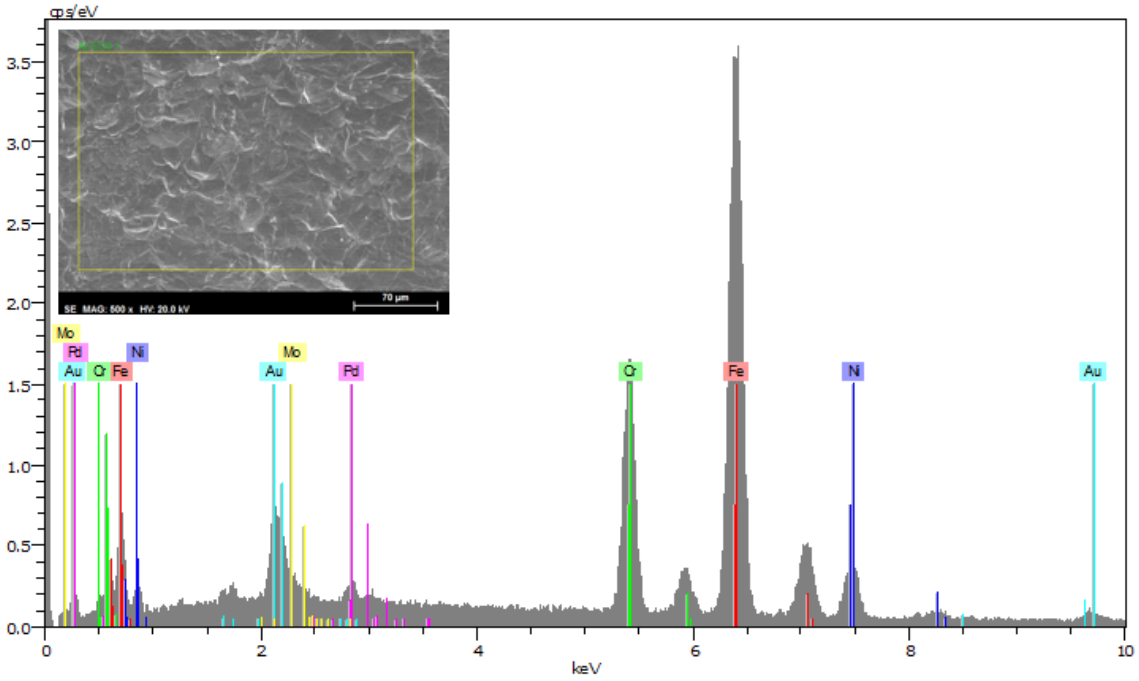

Figure 3.16: EDS with the several elements and relative intensities of a sample of 316L-SS after electrochemical etching by HCl at 18.5 % v/v.

Several peaks can be found correspondent to the metal from the substrate, such as Fe, Cr, Ni and Mo, and some from the coating used, Au and Pd. There are no visible chlorine peaks. This shows that the effect of HCl treatment in film adhesion will be by physical properties, such as surface rugosity, and not by specific chemical bonding.

- **Piranha solution**

After an electrochemical etching step using piranha solution at a ratio of 2:1 sulphuric acid and hydrogen peroxide at 0.5 A for 12 minutes, in the OM image (Figure 3.17) the surface seems to be eroded by the grain boundaries.

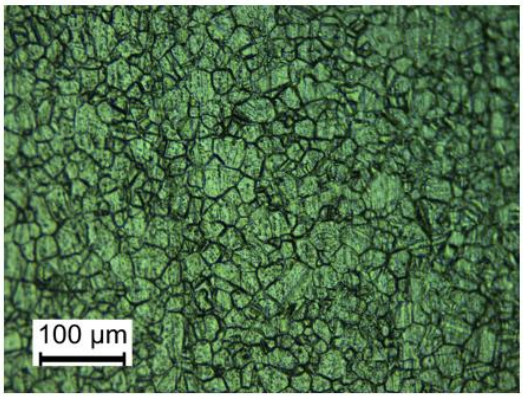

Figure 3.17: OM image of a 316L-SS substrate after electrochemical etching in piranha solution.

In the SEM analysis (Figure 3.18 and Figure 6.5 in appendix D), it is possible to observe that the erosion occurred in a more organised fashion, with deep valleys being observed in what seem to be grain boundaries. The roughness obtained by this method is of 337 nm, which is very similar to that obtained using the same process with HCl.

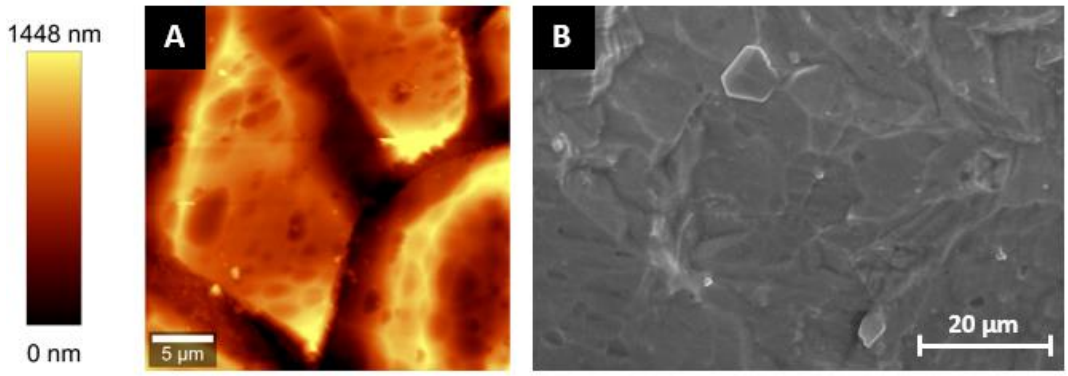

Figure 3.18: AFM image (A) and SEM micrograph (B) of 316L-SS after electrochemical etching in piranha solution.

As for the SEM-EDS analysis (Figure 3.19), in this sample there are peaks correspondent to sulphur, that seems to be from chemical groups formed at the surface by the treatment since the piranha solution is made with sulphuric acid.

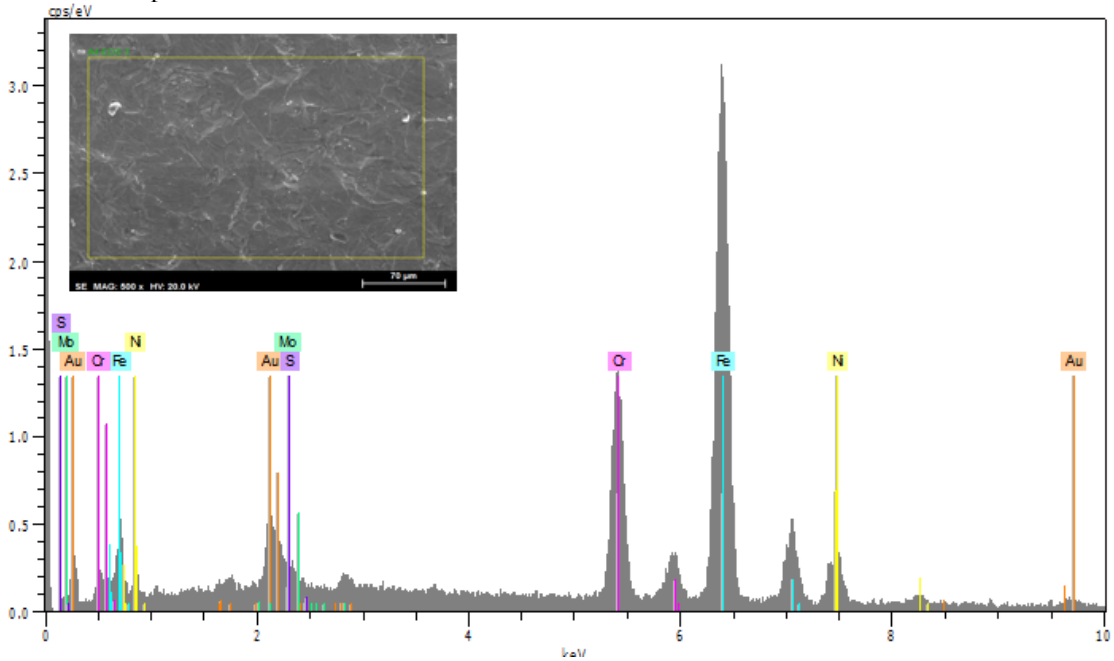

Figure 3.19: EDS report of a 316L-SS treated by electrochemical etching with piranha solution.

- **Sulphuric Acid**

Electrochemical etching with H_2SO_4 37 % v/v at 0.5 A for 12 minutes (Figure 3.20 A) shows the grain borders, much like it happened with the piranha solution. It is possible to note that the surface treated with H_2SO_4 appears more angular than the one treated with piranha, and yet, the roughness of both surfaces seems similar.

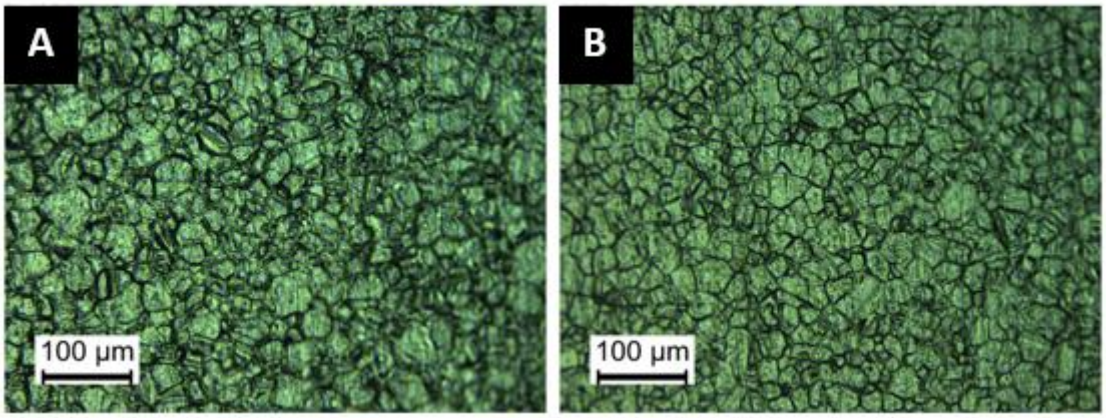

Figure 3.20: OM image of the surface of a 316L-SS substrate after electrochemical etching in A) H_2SO_4 37 % v/v and B) piranha solution.

AFM and SEM analysis (Figure 3.21 and Figure 6.5 in Appendix D) of the sample of 316L-SS treated with H_2SO_4 indicates that the pattern of erosion is very similar in morphology to that encountered in the samples treated by the same method with HCl. The roughness obtained however is of 1103 nm, which is much higher than for the same treatment done with piranha solution or HCl.

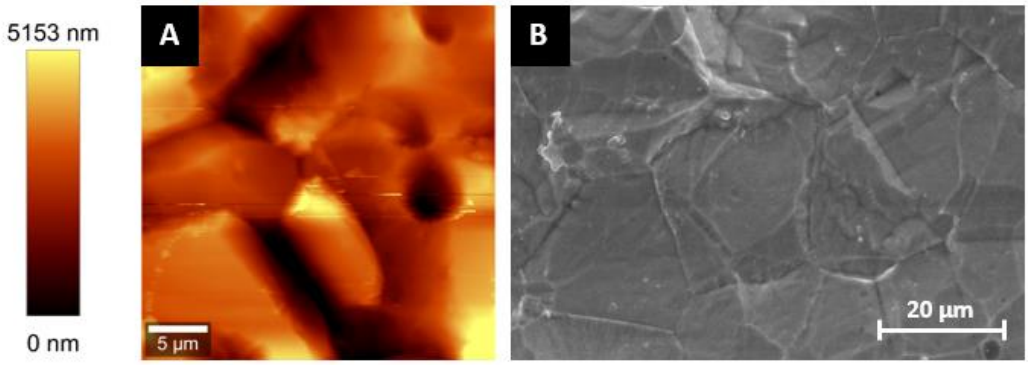

Figure 3.21: AFM image (A) and SEM micrograph (B) of 316L-SS electrochemical etched H_2SO_4.

The EDS results for this sample (Figure 3.22) shows peaks corresponding to sulphur indicating that treatment with sulphuric acid also leads to the deposition of chemical groups in the surface that may influence film adhesion.

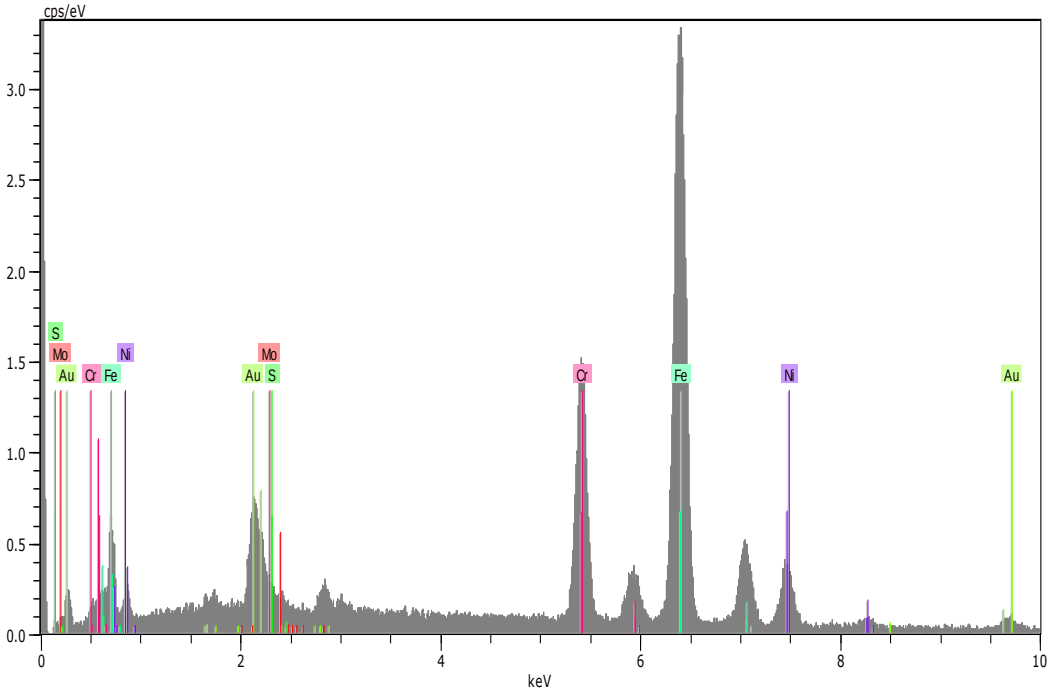

Figure 3.22: EDS report for a sample of 316L-SS treated by electrochemical etching with H_2SO_4.

3.2.4 Mechanical abrasion

To treat the steel surface with mechanical abrasion (Figure 3.23) the substrates were abraded with a 1000 grit sandpaper 100 times in each direction (vertical, horizontal and circular) on both sides of the substrate.

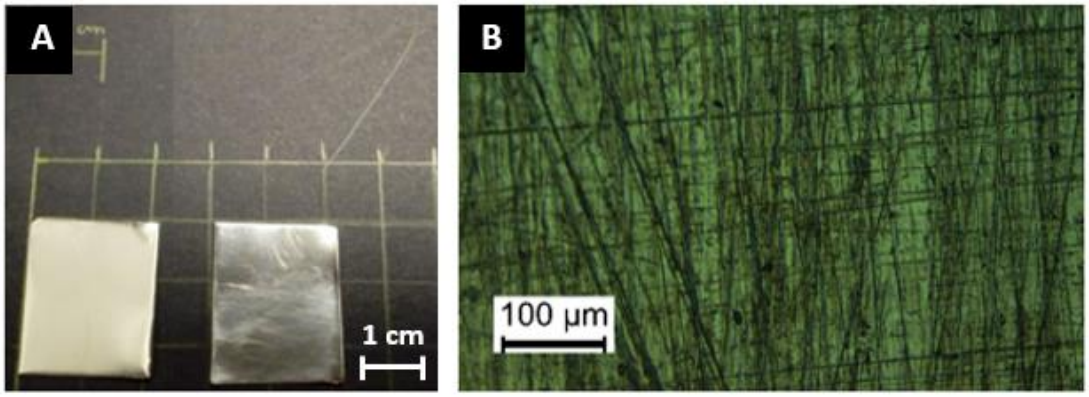

Figure 3.23: A) 316L-SS treated by mechanical abrasion, before (left) and after the treatment (right), and B) OM image of the substrate treated by mechanical abrasion.

Comparing several treatments, it is possible to see the differences between the substrates (Figure 3.24) even at the naked eye.

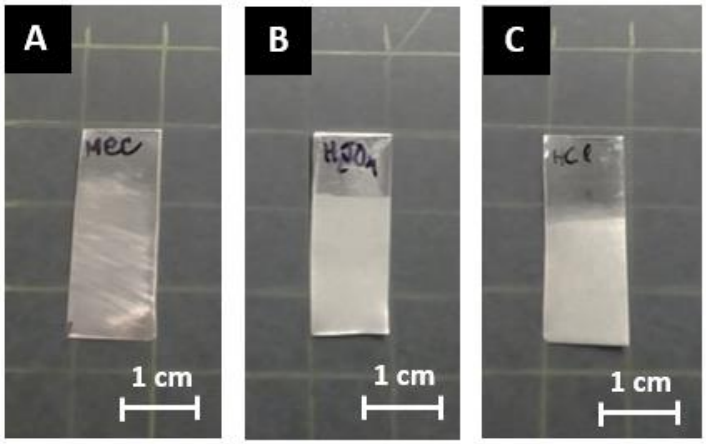

Figure 3.24: 316L-SS treated by: A) mechanical abrasion, B) electrochemical etching with H_2SO_4 48.5 % v/v and C) electrochemical etching with HCl 18.5 % v/v.

Because this treatment is mechanical, no EDS analysis was made. In the SEM analysis (Figure 3.25 B) a lack of a generalized erosion of the surface can be noted, unlike what happened with the acid treatments. AFM analysis (Figure 3.25 A and Figure 6.6 in Appendix D) shows that this treatment does not expose grain boundaries. The treatment also lacks the smoothing of grain surface seen in the chemical treatments, being that the whole surface has some roughness, and the places where the sandpaper scratched the metal are deeper valleys. Overall, this treatment leads to a roughness of 88 nm.

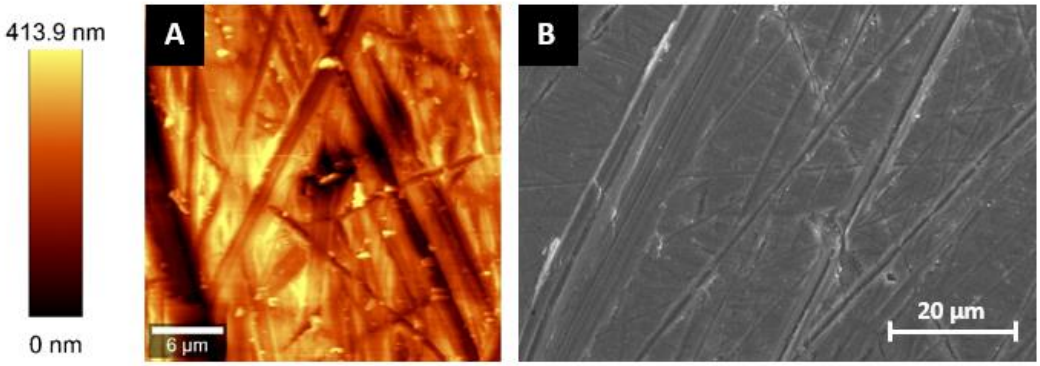

Figure 3.25: AFM image (A) and SEM micrograph (B) of 316L-SS after mechanical abrasion.

The comparison done for the substrates treated by acid etching, electrochemical etching, and mechanical abrasion (Figure 3.26) shows the different surfaces obtained. Steel treated with acid show grain boundaries, being the erosion more notorious in the electrochemical etching processes. Mechanical treatment does not expose grain boundaries, or a generalized erosion of the surface.

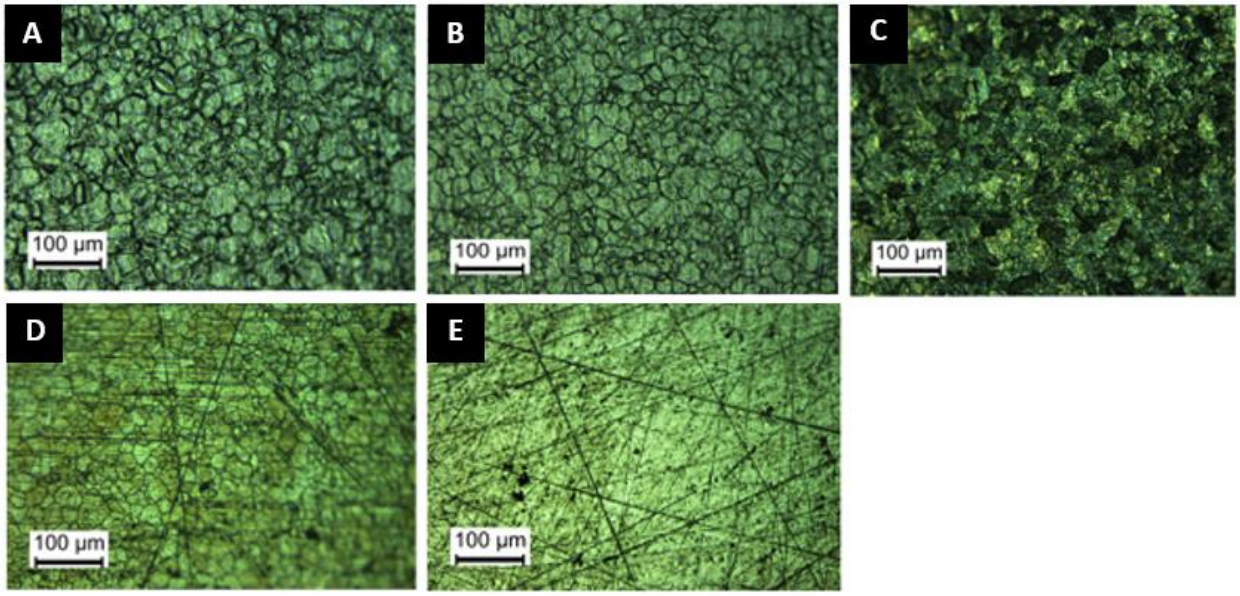

Figure 3.26: OM image of 316L-SS treated by electrochemical etching with A) H_2SO_4 32.5 % v/v, B) piranha solution and C) HCl 18.5 % v/v, and by D) submersion in HCl 37 % v/v for 1 h and E) mechanical abrasion.

The roughness obtained for the several processes is, in crescent order, lower in the mechanical treatment (88 nm), then in immersion in HCl (110 nm for 1 h in HCl 37 % v/v), afterwards in electrochemical etching with HCl 18.5 % v/v (334 nm), then with piranha solution (337 nm) and lastly with sulphuric H_2SO_4 32.3 % v/v (1103 nm). From the results presented, it is concluded that mechanical abrasion led to the smoothest surface, not exposing the grain limit. Because this treatment is manual, however, also shows the least reproducibility.
As for the chemical properties of the surface, only the treatments performed with piranha and sulphuric acid lead to the addition of chemical groups in the metal surface.

3.3 Film optimization – Ti-6Al-4V Treatment

Titanium substrates underwent several silanization processes and were analysed by SEM (Figure 6.9 in Appendix F), that showed heterogenous depositions in the metal. Only the Ti treated by immersion in APTES after a piranha passivation and Ti treated with TEOS vapour in Ar atmosphere without previous passivation in piranha solution result in Si deposition in the metal according to EDS reports (Figure 6.10 and Figure 6.11 in Appendix F).

3.4 Film optimization – Film Deposition

For film deposition, different processes were used. Films of PMMA, PCL and chitosan were made, as well as films with a combination of these polymers, namely chitosan/PMMA and chitosan/PCL. Films were deposited in 316L-SS treated and washed in different ways. The several treatments mentioned were used, and the final step of the washing process, an ultrasound bath in toluene was sometimes omitted to verify the effect of such changes in the deposition.
Polymer concentration and solvent used were altered. Several coating parameters were also tried, such as retrieval speed of the substrate from the solution, number of layers, drying time between layers, immersion time, and washing steps between layers. A crosslinking step in PMMA films, done by exposure of the films to UV light for 1 h was also added or not, to verify the effect of such treatment in adhesion (Table 3.6 and Table 3.7).
Films were considered optimal when they presented with a homogenous surface and no detachment from the steel, even when submerged in SBF or water.

Table 3.6: Dip-coating Parameters used for several polymer solutions for depositions of only one layer.

Total number of layers	Intercalation of layers	Chitosan Layers	PMMA layers	PCL layers	Washing step	Washing Solvent	Dry time	Dip Duration (s)	Retrieval Speed (mm/s)	Polymer Concentration (% wt/v)	Solvent
1	No	0	1	0	No	NA	NA	0, 1	10	2.5, 3	DMAc/Acetone, DCM
2	No	0	2	0	No	NA	3.6 s, 15 min	0, 1	10	2.5, 3	DMAc/Acetone, DCM
3	No	0	3	0	No	NA	3.6 s, 15 min	0, 1	10	2.5, 3	DMAc/Acetone, DCM
1	No	1	0	0	No	NA	NA	0	10	3, 0.5	HAc 1% v/v + Ethanol, HAc 1% v/v; HAc 90 % v/v
2	No	2	0	0	No	NA	12 h, 15 min, 7.2 s	0	10	0.5	HAc 1% v/v + Ethanol, HAc 1% v/v
3	No	3	0	0	No	NA	12 h, 15 min, 7.2 s	0	10	2.5, 0.5	HAc 1% v/v + Ethanol, HAc 1% v/v
6	No	6	0	0	No	NA	3 s	0	10	0.5	HAc 1% v/v + Ethanol, HAc 1% v/v
12	No	12	0	0	No	NA	3 s	0	10	0.5	HAc 1% v/v + Ethanol, HAc 1% v/v
16	No	16	0	0	No	NA	3 s	0	10	0.5	HAc 1% v/v + Ethanol, HAc 1% v/v
20	No	20	0	0	No	NA	3 s	0	10	0.5	HAc 1% v/v + Ethanol, HAc 1% v/v
1	No	0	0	1	No	NA	NA	0, 15, 30, 60	10	6, 3, 1.5, 0.75	DMAc/Acetone
1	No	0	0	1	No	NA	NA	10	10	13, 1.95	DCM

Table 3.7: Dip-coating Parameters used for several polymer solutions for depositions of alternating layers.

Total number of layers	Intercalation of layers	Chitosan Layers	PMMA layers	PCL layers	Washing step	Washing Solvent	Dry time	Dip Duration (s)	Retrieval Speed (mm/s)	Polymer Concentration (% wt/v)	Solvent
2	Yes	1	1	0	No, Yes	H_2O; Ethanol; Acetone	12 h, 15 min, 36 s, 18 s, 3.6 s	0	10	0.5; 2.5	HAc 1% v/v; DMAc/Acetone, DCM
4	Yes	2	2	0	No, Yes	H_2O; Ethanol; Acetone	15 min, 36 s, 18 s, 3.6 s	0	10	0.5; 2.5	HAc 1% v/v; DMAc/Acetone, DCM
6	Yes	3	3	0	No, Yes	H_2O; Ethanol; Acetone	15 min, 36 s, 18 s, 3.6 s	0	10	0.5; 2.5	HAc 1% v/v; DMAc/Acetone, DCM
12	Yes	6	6	0	No, Yes	H_2O; Ethanol; Acetone	36 s, 18 s, 3.6 s	0	10	0.5; 2.5	HAc 1% v/v; DMAc/Acetone, DCM
20	Yes	10	10	0	No, Yes	H_2O; Ethanol; Acetone	36 s, 18 s, 3.6 s	0	10	0.5; 2.5	HAc 1% v/v; DMAc/Acetone, DCM
40	Yes	20	20	0	No, Yes	H_2O; Ethanol; Acetone	36 s, 18 s, 3.6 s	0	10	0.5; 2.5	HAc 1% v/v; DMAc/Acetone, DCM
2	No	0	1	1	No	NA	NA	0	10	0.5; 1.95	HAc 1% v/v + Ethanol; DCM
6	Yes	0	3	3	No	NA	NA	0	10	0.5; 1.95	HAc 1% v/v + Ethanol; DCM
12	Yes	0	6	6	No	NA	NA	0	10	0.5; 1.95	HAc 1% v/v + Ethanol; DCM
2	No	0	1	1	No	NA	60 s	0	10	0.04; 0.1	HAc 1% v/v + Ethanol; DCM
6	Yes	0	3	3	No	NA	60 s	0	10	0.04; 0.1	HAc 1% v/v + Ethanol; DCM
12	Yes	0	6	6	No	NA	60 s	0	10	0.04; 0.1	HAc 1% v/v + Ethanol; DCM

3.4.1 Depositions with PMMA

The deposition of PMMA films was done in several substrates to study the effect of the surface structure in the film adhesion. Several other variables were considered such as the number of dips made, the presence or absence of a toluene bath in the washing process, the existence or not of a crosslinking step, when the crosslinking step occurred (after all the dips were made, or after each dip) and the solvent and polymer concentrations used. Adhesion of the film to the substrate was observed at two points: after drying, and after submersion in water (Table 6.10 and Table 6.11 in Appendix G).
First, films of PMMA in DMAc/acetone and PMMA in DCM at concentrations of 12 % wt/v and 20 % wt/v respectively were made. These films showed an immediate detachment of the substrates for all dip-coating parameters used. The films also showed shrinking, which seemed to be the cause for the film detachment (Figure 3.27).

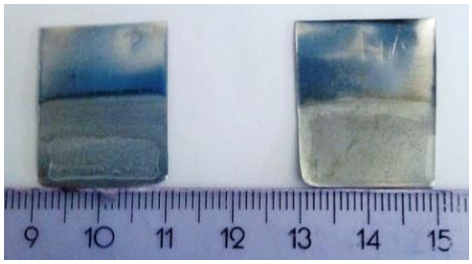

Figure 3.27: Film of PMMA 12 % wt/v in DMAc/Acetone deposited in 316L-SS treated with electrochemical etching with Piranha solution (left) and HCl 18 % v/v (right) showing the relative size between substrate and deposited film with scale in cm.

Because of the poor adhesion of the films, the solutions were diluted to PMMA concentrations of 6 % wt/v and 10 % wt/v in DMAc/acetone and PMMA in DCM respectively and the problems observed persisted, so these solutions were again diluted to half. The solution with DCM as solvent was further diluted to a concentration of 2.5 % wt/v. Depositions with polymer concentrations of 2.5 % and 3 % resulted in films without shrinkage and overall improvement of film adhesion. Consequently, only 3 % wt/v and 2.5 % wt/v solutions were used for further work. With these solutions, films were deposited in 316L-SS substrates with different washing processes (with or without a step of an ultrasound bath in toluene), treatments, and post-treatments (crosslinking under UV light) (

Table 6.12 in Appendix G). The films produced with PMMA in DCM show to be detached from the 316L-SS in some areas, demonstrating a poor adhesion of the films in the substrates treated with HCl and H_2SO_4. The mechanical treatment appears to be the best one, with only the substrate not washed in toluene in which a non-crosslinked film was deposited shows film detachment (Figure 3.28).

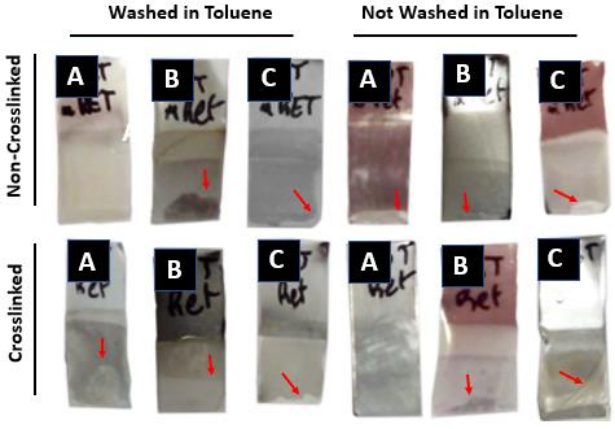

Figure 3.28: Films of PMMA 3 % wt/v in DCM deposited in 316L-SS substrates treated by: A) mechanical abrasion, B) electrochemical etching with H_2SO_4 and C) electrochemical etching with HCl, with detachment areas marked with red arrows.

Preliminary peel-off tests performed in films deposited in 316L-SS that underwent electrochemical etching show a partial film detachment upon drying, and the full detachment after peel-off tests (Figure 3.29).

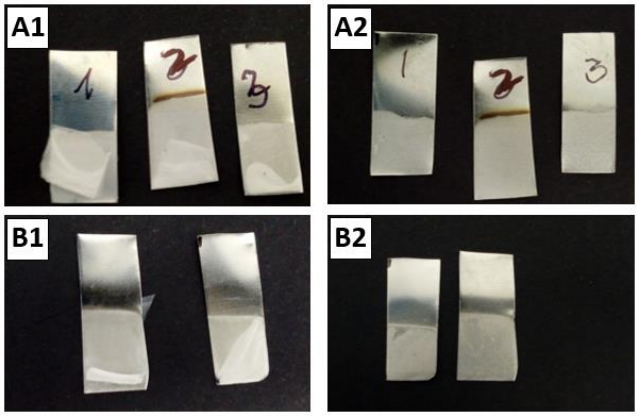

Figure 3.29: Films of PMMA in DCM deposited in 316L-SS treated by electrochemical etching using A) H_2SO_4 and B) HCl, before (1) and after (2) peel-off tests.

From this, it was concluded that the mechanical treatment was to be used for the deposition of films made with this solution, and that there was no apparent need for a crosslinking step.
The films made with DMAc/Acetone a solvent system show detachment from the 316L-SS treated with chemical and electrochemical etching and a lack of detachment from the 316L-SS treated mechanically. The crosslinking process and the addition of a toluene bath before film deposition do not cause any clear improvement of film adhesion. Because the PMMA films showed adherence to mechanically treated substrates, these were used for the deposition of drug loaded PMMA films. For these films, solutions of PMMA in DMAc/acetone and in DCM at concentrations of 3 % wt/v and 2.5 % wt/v with addition of daptomycin and vancomycin in a ratio of 2.5 % of the polymer weight were used and the same parameters were changed. As for the films made with the solution of PMMA in DCM and in DMAc/Acetone (Figure 3.30), the addition of both drugs does not seem to affect film deposition, with all films maintaining a lack of detachment from the substrate.

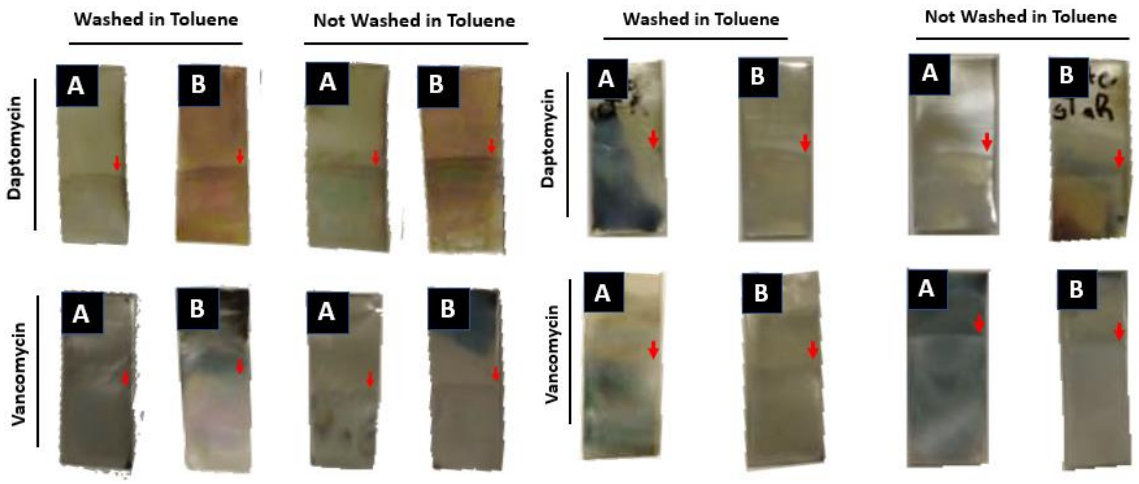

Figure 3.30: Films of PMMA in DCM (left) and in DMAc/Acetone (right) in 316L-SS with addition of Dap and Van being A) crosslinked B) non-crosslinked with film limits marked by red arrows.

Apart from detachment there seems to be no macroscopic difference between the several films except for a whiter colour of the Van loaded ones. Preliminary peel-off tests were performed in these films and it was verified that the film showed no detachment from the mechanically treated 316L-SS (Figure 3.31).

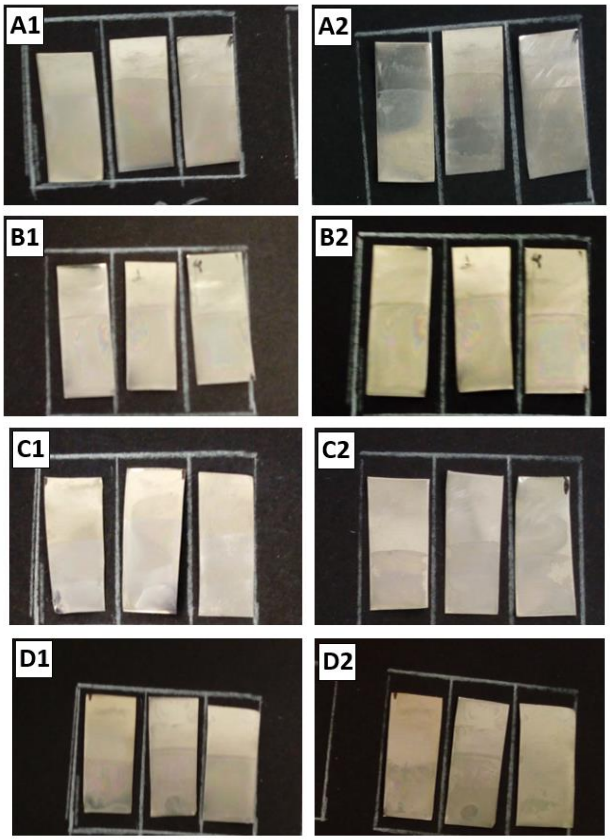

Figure 3.31: Films made with PMMA in DCM (B and D) and in DMAc/Acetone (A and C) with Van (A and B) and with Dap (C and D) before (1) and after (2) preliminary peel-off tests.

Because the step of washing the 316L-SS substrate in toluene did not seem to affect film adhesion and it was a lengthy process, this step was skipped from this point forward.
Thicknesses of the films was obtained for films made with both solvent systems and with the addition or not of Van or Dap and with or without a crosslinking step. The thickness of these films (Figure 3.32 and Figure 6.14 in Appendix H) shows to be very heterogeneous for almost all the films made with the vancomycin loaded films being the most homogenous.

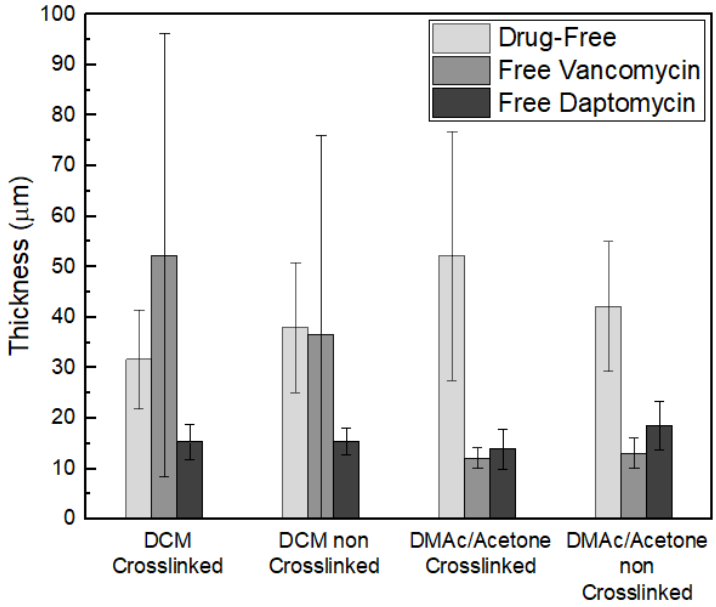

Figure 3.32: Average thickness (*n*=30) of PMMA films in two solvent systems, without drugs (light grey) with Van (grey) and with Dap (dark grey).

The addition of both Dap and Van seems to decrease film thickness in both solvent systems, with the change being more notorious in films with DMAc and acetone as solvents. Crosslinking process does not seem to affect film thickness. When comparing both solvents, it is possible to conclude that DCM leads to more heterogenous films. From the combination of the studies performed, it was concluded that the better parameter combination was a mechanical treatment, with DMAc/Acetone as solvent system, and, for process simplicity, the addition of toluene bath or crosslinking step were dropped.

3.4.2 Depositions with Chitosan

Chitosan films were deposited in 316L-SS treated as described before and several deposition parameters and solutions were tested to obtain the combination that resulted in higher film adhesion and homogeneity. First a solution of chitosan at a concentration of 3 % wt/v in HAc 90% v/v (Solution A) was tested. Films were deposited in 316L-SS treated with electrochemical etching using HCl at a concentration of 18.5 %. Films were made with 1 layer, up to 5 layers to verify the effect of this parameter in film adhesion and morphology (Figure 3.33).

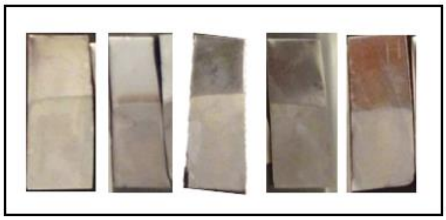

Figure 3.33: Chitosan films deposited in 316L-SS treated by electrochemical etching with HCl 18.5 % v/v with 1 (left) to 5 (right) layers using solution A.

The films obtained appear very heterogenous both within the same film and within replicas, indicating a low reproducibility of the process. The adhesion of these films was measured, and peel-off force values were obtained for 3 replicas of each film (Figure 3.34 and Appendix J). The peel-off forces show that the number of layers does not affect adhesion.

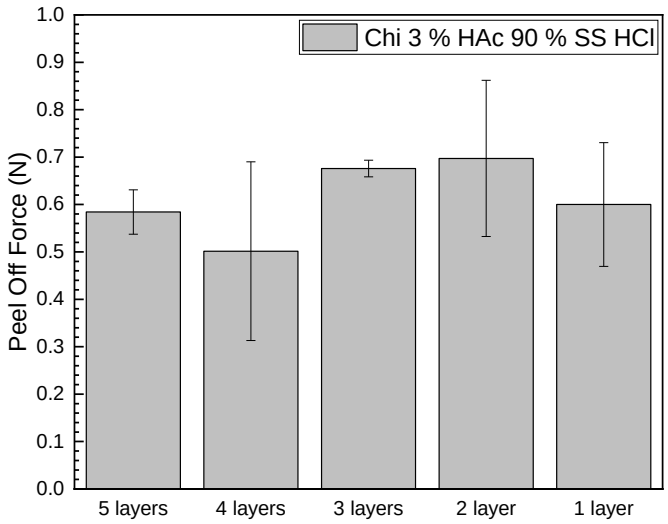

Figure 3.34: Peel-off forces of 1 to 5-layer films deposited in 316L-SS treated by electrochemical etching with HCl obtained with solution A.

Because the concentration of acetic acid in this solution was very high, the solution was changed for one of chitosan 0.5 % wt/v in HAc 1% v/v (Solution B). This solution was used to make several films where several substrate treatments and dip parameters were studied to obtain the best combination. Films with this solution with 1, 3, 6 and 12 layers were obtained in mechanically treated 316L-SS, and the drying time in between layers was set at either 1 minute or no time at all. Peel-off forces measured for 3 replicas of each film (Figure 3.35 and Figure 6.17 in Appendix J).

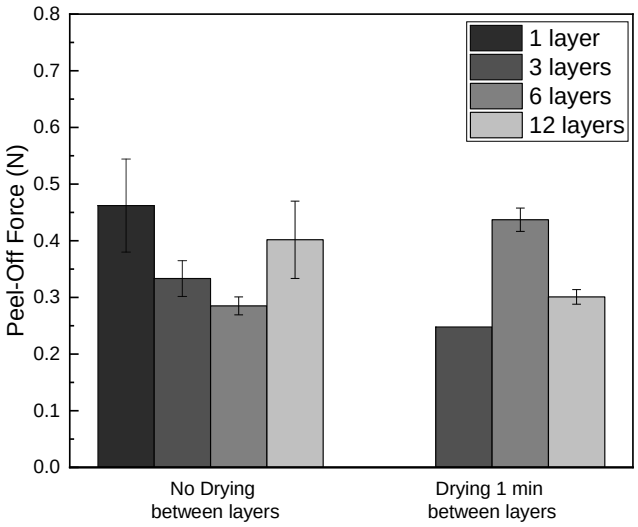

Figure 3.35: Peel-Off forces obtained for chitosan films of 1 to 12 layers made with solution B.

From the peel-off forces it is possible to conclude that neither the number of layers nor the drying time between layers changes film adhesion, with the peeling occurring in an adhesive fashion for all films.
To improve the adhesion of chitosan films obtained with the two solutions tested, a process of electrodeposition was performed. For these depositions, a new solution was made that consisted on chitosan at a concentration of 0.5 % wt/v in a solvent system composed of 50 % HAc 1 % v/v and 50 % absolute ethanol (Solution C). Electrophoretic deposition was done at several current values and for

different periods of time. The films obtained could not be visualized at the naked eye or even in the optical microscope (Figure 6.16 in Appendix I). Peel-off studies were made on all films obtained by electrophoretic deposition (Figure 3.36 and Figure 6.17 in Appendix J), but because the films obtained were very thin, the results of deposition and peel-off could not be visualised, thus the processes were dropped and the same solution used for dip-coating.

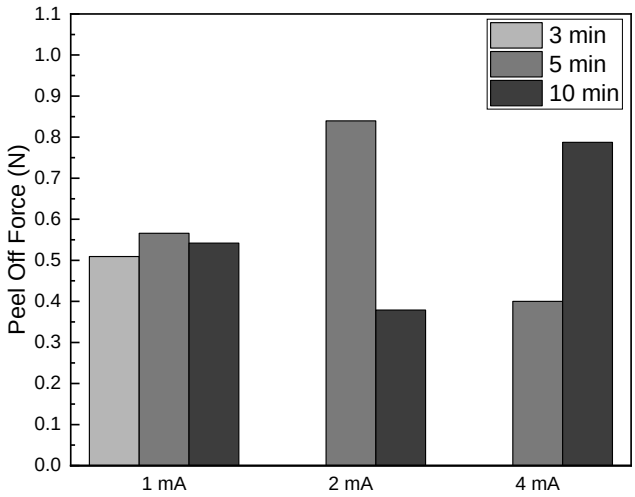

Figure 3.36: Peel-off forces obtained for electrodeposited chitosan films.

The films obtained with the chitosan solutions B and C were visually similar (Figure 3.37) with all films being transparent and showing some birefringence even with different number of deposited layers.

Figure 3.37: Chitosan films of 4 layers made with solutions B (left) and C (right).

The thickness of the several films produced was studied (Figure 3.38 and Figure 6.15 in Appendix H). For films made with solution C there seems to be an increase of film thickness until the deposition of 6 layers. As for films made with solution B thickness seems to drop from 1 to 4 layers, and then increase as the number of layer increases. Solution C seems to make thicker, more homogenous films.

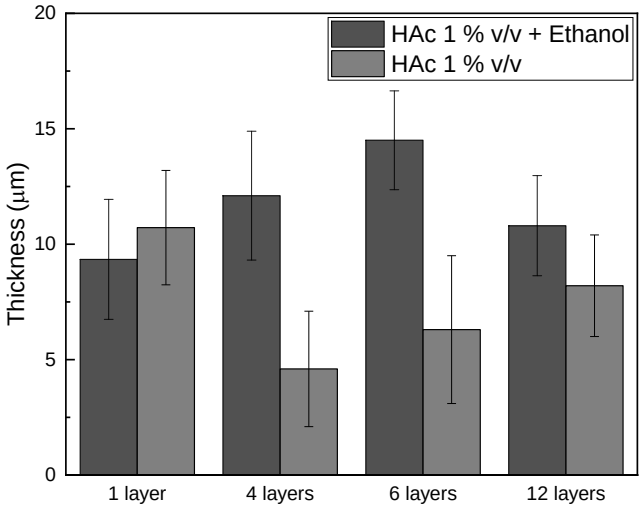

Figure 3.38: Thickness of 1-, 4-, 6- and 12-layers chitosan films made with solutions B and C.

Different dipping times were studied reaching from 0 to 60 seconds to ascertain if film homogeneity changed. From the film thickness (Figure 3.39 and Figure 6.15 in Appendix H) it is noted that dip duration does not change film homogeneity.

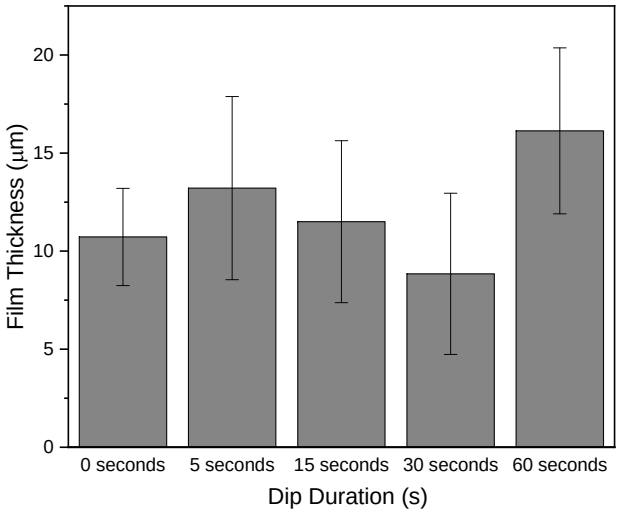

Figure 3.39: Thickness of chitosan films using solution C and dip durations from 0 s to 60 s.

The same solution was used to make films with 1, 3, 6 and 12 layers, and with drying times between layers of 0 min and 1 min and the peel-off force of these films obtained (Figure 3.40 and Figure 6.17 in Appendix J). It was shown that peel-off force does not change for a drying time of 0 min, and yet seems to increase with the increase of the number of layers for a drying time of 1 min.

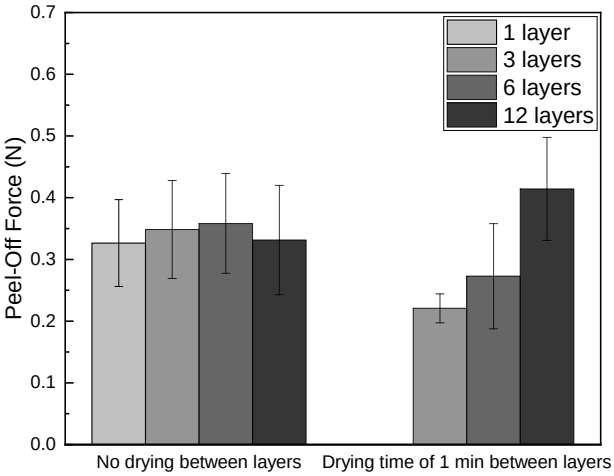

Figure 3.40 Peel-off forces for chitosan films made with solution C without and with 1 min of drying between layers.

A drying time of 1 min seems to lead to lower peel-off forces than no drying, so drying time was set at 0s for chitosan deposition. Along with this, from the results obtained, the solution selected as the best for deposition is solution C, chitosan at a concentration of 0.5 % wt/v in 50 % v/v HAc 1% v/v and 50 % v/v absolute ethanol.

3.4.3 Depositions with PMMA and Chi

Because of their better results, the solutions chosen for the deposition of chitosan/PMMA multi-layered films were those of chitosan solution C and of PMMA at a concentration of 3 % wt/v in a solvent system of DMAc/Acetone. The substrate treatment chosen was mechanical abrasion. Starting off with a system of one bilayer, i.e., a layer of one polymer superimposed by a layer of the other polymer, films were made with chitosan or PMMA as first layer to verify which polymer worked best at the metal/film interface.
The films obtained by a combination of both polymers, however, showed detachment from the substrate upon drying. The substrates used and several dip-coating parameters were changed with no success (Table 3.7). Adding a washing step between layers by dipping the substrate in ultrapure water, ethanol and even acetone made adhesion even worse (Figure 3.41), and the addition of microspheres or drugs to the films did not improve film adhesion either.

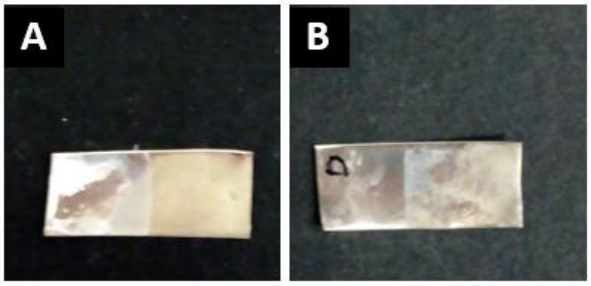

Figure 3.41: PMMA/Chitosan films obtained with 1 bilayer, with a washing step between layers with A) Millipore water and B) ethanol.

Because of this persisting problem, PMMA was replaced by PCL, a polymer that also carries a negative charge and has slow biodegradation while maintaining biocompatibility.

3.4.4 Depositions with PCL

As done for the other polymers, the polymer solution was first optimized so that a PCL film could be deposited in the metal. For this, 316L-SS that underwent mechanical abrasion was used and several solutions and dipping parameters were tested (Table 3.6).
One of the tested solutions was of PCL 6 % wt/v, 3 % wt/v, 1.5 % wt/v and 0.5 % wt/v. in a solvent system of DMAc/Acetone. The films obtained showed detachment from the metal (Figure 3.42) and the polymer only dissolved at temperatures of about 30º, complicating the dip-coating process.

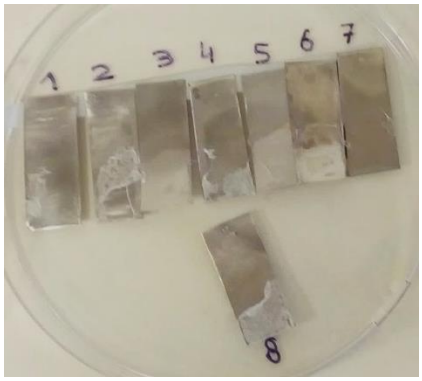

Figure 3.42: Films of PCL 1.5 % wt/v in DMAc/Acetone deposited at retrieval speeds of 1) 2 mm/s, 2) 5 mm/s, 3) 10 mm/s, 4) 15 mm/s with a dip duration of 0s and at 5) 2 mm/s, 6) 5 mm/S, 7) 10 mm/s, 8)15 mm/s with a dip duration of 60 s.

Due to the poor solubility of the polymer and the poor adhesion of the films the DMAc/Acetone system was replaced by dichloromethane. Starting off with a concentration of 13 % wt/v, immediate solvent evaporation occurred when the substrate was removed from the solution, making film deposition impossible. Because off this the solution was diluted to a concentration of 1.95 % wt/v.
Using a retrieval speed of 10 mm/s, and a dip duration of 0s with this polymer concentration, clear homogeneous films were obtained (Figure 3.43). Thus, the solution was used for deposition of PCL/chitosan multi-layered films.

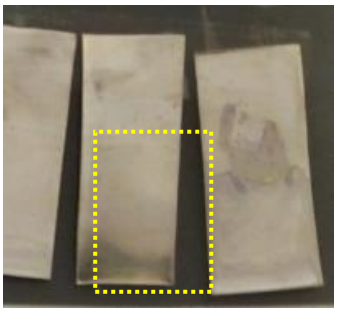

Figure 3.43: Films deposited with a solution of PCL 1.95 % wt/v in DCM with the film covered area detailed in yellow.

3.4.5 Depositions with PCL and Chitosan

Films of 6 and 3 bilayers of chitosan and PCL were deposited in 316L-SS using a retrieval speed of 10 mm/s and a dip duration of 0s, with no washing or drying step between layers. Upon the addition of Dap at a concentration of 1 mg/mL to these films, however, a poor film adhesion was observed (Figure 3.44).

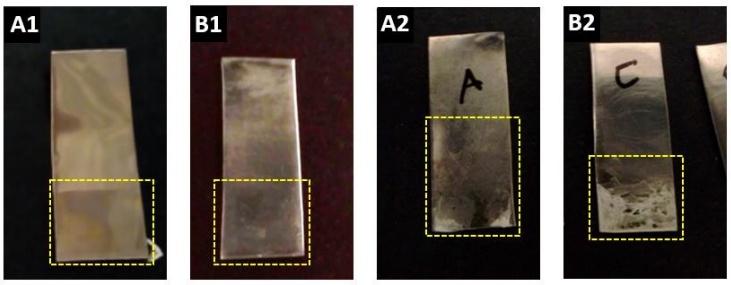

Figure 3.44: PCL/Chitosan films with A) 6 bilayers and B) 3 bilayers 1) without and 2) with daptomycin at a concentration of 1 mg/mL.

Because of this, the concentrations of both PCL and chitosan were altered. For a chitosan concentration of 0.04 % wt/v and a PCL concentration of 0.1 % wt/v films with seemingly good adhesion and acceptable uniformity were produced. These films kept their properties even after the addition of Dap and Van, at a concentration of 0.8 mg/mL and the microspheres produced at a concentration of 4 mg/mL (Figure 3.45).

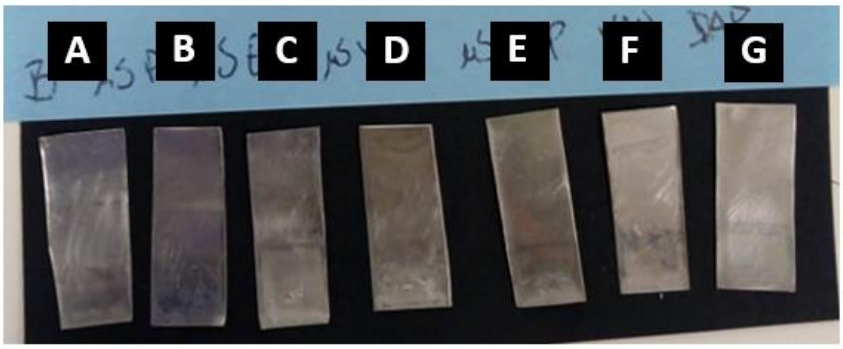

Figure 3.45: Chitosan/PCL films with A) no drugs or microspheres, B) PMMA microspheres, C) PMMA-EUD microspheres, D) PMMA-Van microspheres, E) PMMA-EUD-Dap microspheres, F) vancomycin and G) daptomycin

These films were considered the optimal films and were used as the drug delivery systems studied.

3.5 Optimal Films

After the optimization process, the films chosen for further analysis were the ones made with 6 bilayers of alternating films of chitosan 0.04 % in 50 % ethanol and 50 % of HAc 1 % v/v and PCL at a concentration of 0.1 % in DCM. To these films Dap and Van at a concentration of 0.8 mg/mL and PMMA-EUD and PMMA microspheres loaded with Dap or Van respectively and unloaded at a concentration of 4 mg/mL were added to chitosan solutions to make loaded films (Figure 3.46).

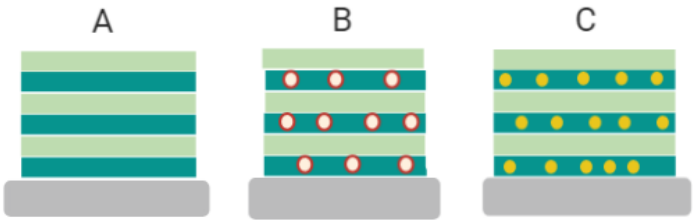

Figure 3.46: Schematic design of the final films showing: green) chitosan layers, light green) PCL layers, red) microspheres and yellow) drug.

The concentration of drugs was selected considering the range of the calibration curves and the approximate film volume. Microsphere concentration was made so it was 5 times that of the drug, since considering that the spheres have a drug loading of approximately 20 % this was the ratio needed to obtain the same drug mass in the films. For all films, the same dip-coating parameters were used (Table 3.8), changing solutions accordingly. A different PCL solution was used for each kind of film to avoid cross contamination between samples.

Table 3.8: Parameters used for the dip-coating process of optimized Chit/PCL films.

Parametre	**Value**
Retrieval speed	10 mm/s
Dip Duration	0 s
Rotation speed in solution	0 degree/s
[1]Arm rotation speed	10 degree/s
[2]Dry time between solutions	1 min
Temperature	20 ºC - 25 ºC
Humidity	20 % - 40 %
Time Elapsed per film	15 min
1 – Solutions distanced by 60º, 2 – excludes time elapsed from arm rotation	

From here on these films were denominated as mentioned in Table 3.9.

Table 3.9: Denomination of optimized films.

Compound added	**Film denomination**
None	Chi/PCL
Daptomycin	Chi/PCL-Dap
Vancomycin	Chi/PCL-Van
PMMA-EUD microspheres	Chi/PCL-PMMA-EUD
Daptomycin loaded PMMA-EUD microspheres	Chi/PCL-PMMA-EUD-Dap
PMMA microspheres	Chi/PCL-PMMA
Vancomycin loaded PMMA microspheres	Chi/PCL-PMMA-Van

3.5.1 Film Thickness

The average thickness (n=30) with the standard deviation were calculated (Figure 6.18 in Appendix K) for each sample (Figure 3.47).

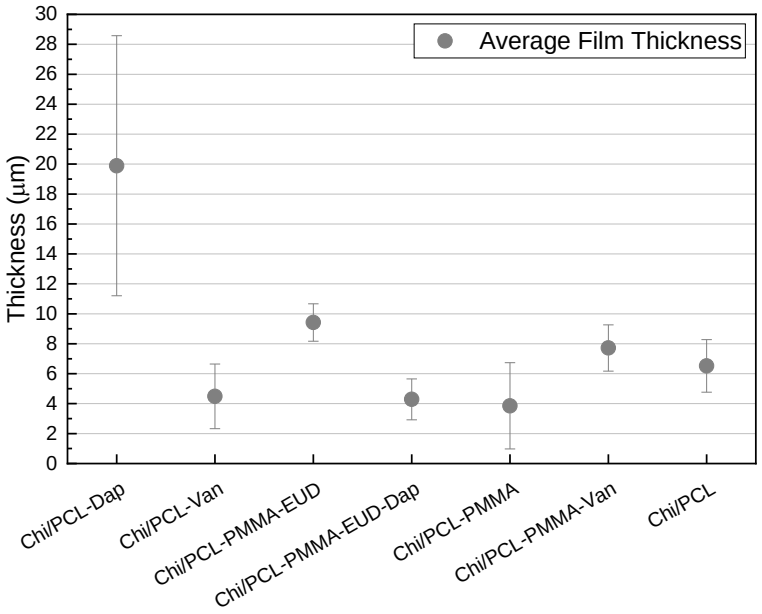

Figure 3.47: Average film thickness of the several optimized films.

From these values it is possible to note that there is a large heterogeneity of thickness throughout the films, with highlight on the Chi/PCL-Dap film that shows the highest standard deviation and thus higher heterogeneity of the film. Visually, the Chi/PCL-Dap film appears however to be homogeneous, thus, the thickness variation may be due to the variation of substrate thickness, and not the film. It must also be taken into account that several parts of the film were measured and therefore standard deviations may be due to a different thickness of different areas in the same film, due to the accumulation of polymeric solution in one area upon drying.

3.5.2 Peel-Off force

Peel-Off tests were performed as mentioned for 15 replicas of all films obtained (Figure 6.19 and Table 6.13 in Appendix L).
The kind of peel-off obtained for all samples showed a cohesive failure, meaning that the detachment occurred between the film layers, and not adhesive failure i.e. detachment between the sample and the metal (Figure 3.48). This indicates that the adhesion force between film and metal are stronger than those between film layers.

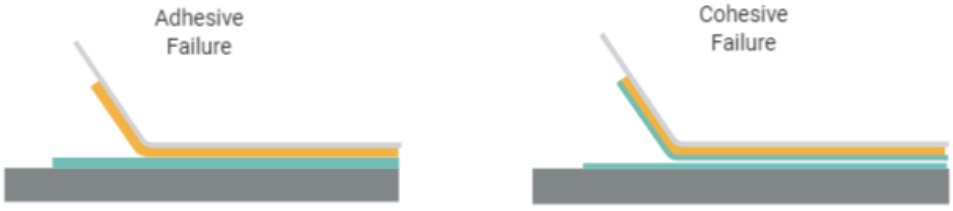

Figure 3.48: Schematic of the types of failure present in the peeling-off of the films produced showing both adhesive (left) and cohesive failures (right) [100].

As can be seen from the average peel-off forces (Figure 3.49), all films show peel-off forces between 0.6 N and 0.95 N (Table 3.10), albeit, with high standard deviation values. These inconsistency in the values obtained may be due to both the heterogeneity of the samples, or the technique itself, since it is impossible to verify that the tape is glued the same way and with the same force in all samples.

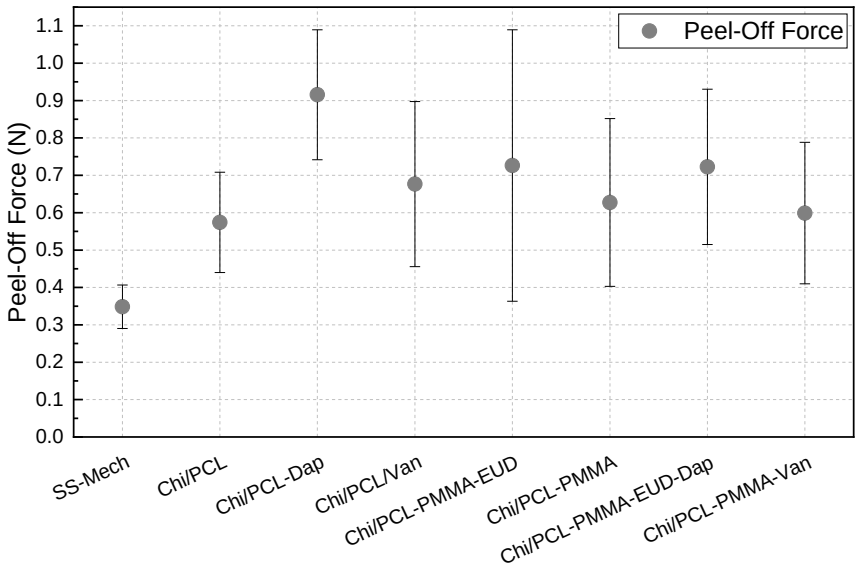

Figure 3.49: Average peel-off forces (*n*=15) for optimized films and 316L-SS treated by mechanical abrasion.

Table 3.10: Peel-off forces obtained for the optimized films.

Film	**Average ± SD**
Chi/PCL	0.574 ± 0.134
Chi/PCL-Dap	0.916 ± 0.174
Chi/PCL/Van	0.677 ± 0.221
Chi/PCL-PMMA-EUD	0.726 ± 0.363
Chi/PCL-PMMA	0.627 ± 0.224
Chi/PCL-PMMA-EUD-Dap	0.723 ± 0.208
Chi/PCL-PMMA-Van	0.599 ± 0.189

From the forces obtained, it can be concluded that no component seems to decrease film adhesion, and the addition of Dap specially seems to increase film adhesion. The addition of Van loaded spheres does not seem to affect film adhesion and the addition of Van, PMMA spheres and PMMA-EUD speres, both loaded and unloaded seem to slightly increase adhesion. From this, one may conclude that the addition of drugs and drug loaded spheres does not compromise this film properties, and instead, even seems to improve it.

When comparing the values obtained to the adhesion to stainless steel one can see that the adhesion of the films is much higher, with adhesion to metal being of 0.349 ± 0.0581 N corresponding to almost half the lowest adhesion for films that is of 0.474 ± 0.134 N.

The peel-off curves obtained are like those found in the literature with areas of the curve showing the peeling of the film and tape and of the film alone or just the peeling of the film, with no discerning the two areas of the curve (Figure 3.50)

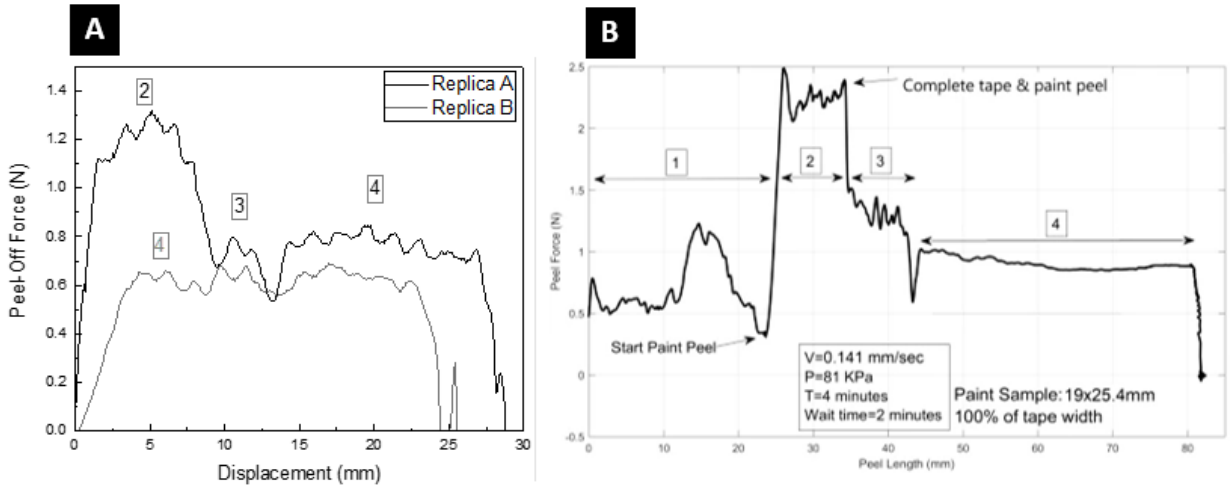

Figure 3.50: Peel-off curves obtained for A) Chi/PCL-PMMA films compared to B) curves found in the literature showing 1) just tape peeling, 2) partial tape and film peeling, 3) complete tape and film peeling and 4) just film peeling.

3.5.3 Polymer Degradation

The film degradation studies for PCL and chitosan were performed for a period of 35 days for both polymers. PCL mass was accessed weekly, and the mass of chitosan films was measured at first every other day, and then weekly, as the degradation rate stabilized. Plots of the mass loss vs time (Figure 6.20 and Figure 6.21 in Appendix M) were obtained to access the degradation rates observed for both polymers at pH values between 5 and 8.

In the case of chitosan (Figure 3.51), the mass loss seems to be dependent in the pH values, being that for a pH of 7.4 almost no mass loss is observed and at a pH value of 5.5 a mass loss of approximately 75 % is obtained after 35 days of submersion in SBF. For a pH of 6.5 the degradation rate lies in between those of pH 5.5 and of pH 7.4. More pH values were studied (Figure 6.20 in Appendix M) and it was confirmed that the degradation increases as pH decreases, as is reported in the literature for this polymer [17], [74].

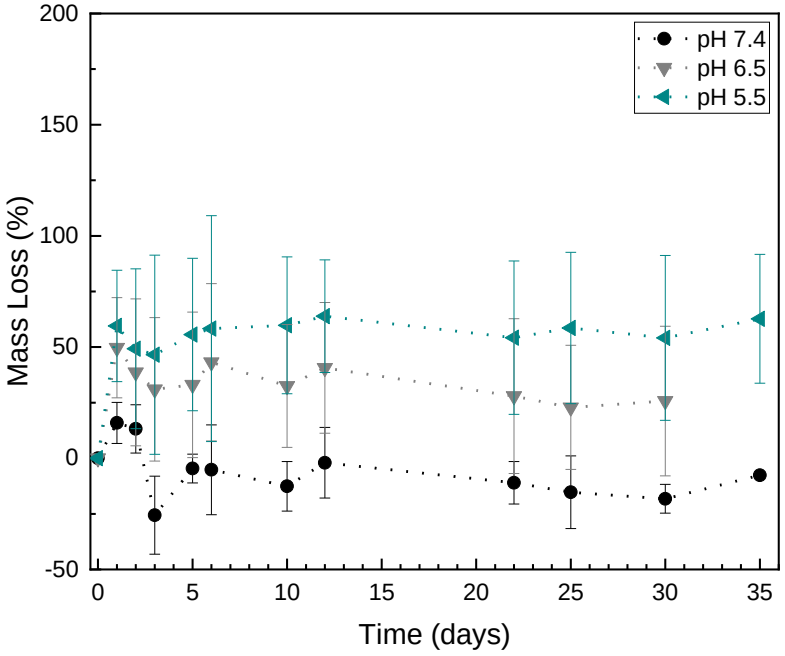

Figure 3.51: Plot of the mass loss vs. time for chitosan films during a period of 35 days at pH values of: black) 7.4, grey) 6.5 and blue) 5.5.

As for PCL (Figure 3.52), degradation rate does not change with differences in pH. Instead, for all 3 pH values presented there seems to be no noticeable degradation occurring even after 4 weeks of submersion in SBF for all cases. This is in accordance to the literature where it is stated that only at extreme pH values, of under 3 and over 11 a significant change in degradation rate can be seen for this polymer [101].

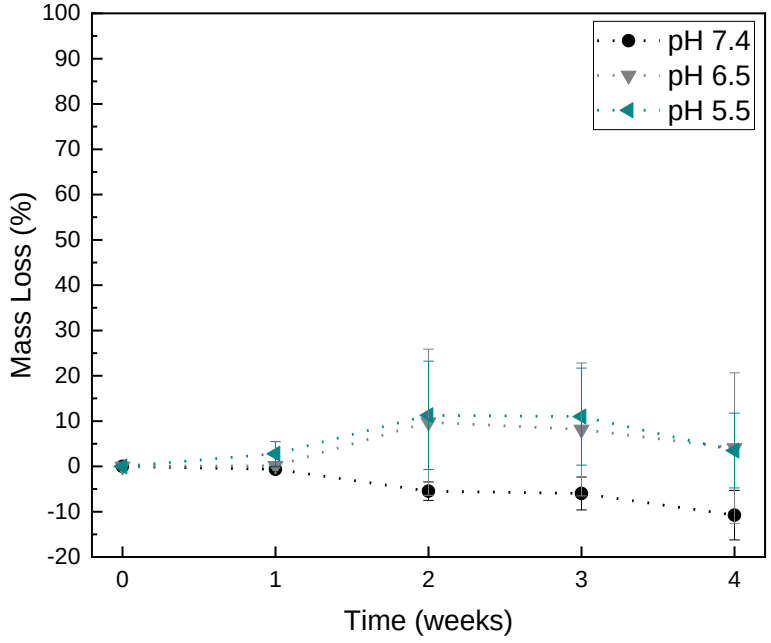

Figure 3.52: Plot of the mass loss vs. time for PCL films over a period of 4 weeks at a pH of: black) 7.4, grey) 6.5 and blue) 5.5.

3.5.4 Polymer Swelling

The swelling ratio of the 3 replicas used was calculated by weighing the samples before and after immersion (Formula 3.5). The average of all samples was used to form the plot presented that describes the swelling behaviour of PCL and Chitosan.

$$Swelling\ ratio = \frac{initial\ mass - final\ mass}{initial\ mass} \times 100 \quad (3.5)$$

The plot of the swelling ratio vs. time was obtained for both polymers over a period of 1 week for several pH values (Figure 6.22 and Figure 6.23 in Appendix M). The swelling ratio of chitosan (Figure 3.53) hits the equilibrium at a swelling of 150 % after 30 minutes for a pH value of 7.4 and at 400 % after 15 minutes for pH values of 6.5 and at 700 % for a pH of 5.5 after 15 minutes of submersion.

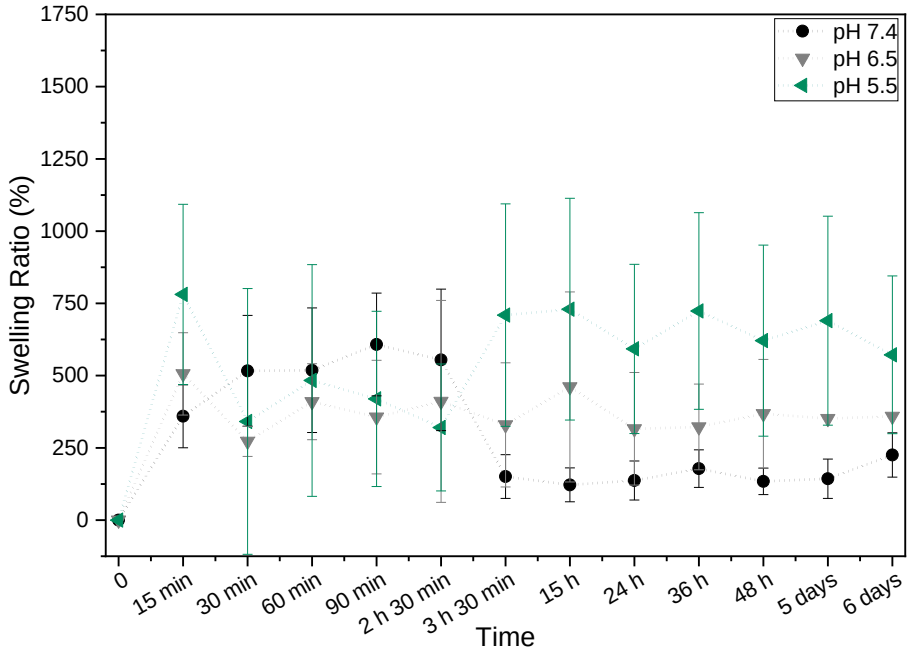

Figure 3.53: Plot of the swelling ratio vs. time for chitosan films obtained at 3 different pH values: black) 7.4, grey) 6.5 and blue) 5.5 obtained for a period of one week.

These results indicate that the swelling ratio depends of the pH value, being higher for lower pH. This is in accordance with the tendence observed in degradation since a higher swelling ratio means higher diffusion of acid and water into the polymer and therefore higher hydrolysis rate.

For PCL (Figure 3.54) a very low swelling ratio is noted, which is to be expected since the polymer is reported as being hydrophobic [101]. Apart from this, there does not seem to be a relation between swelling ratio and pH values for this polymer. For all three pH values presented, the swelling ratio of PCL at equilibrium if of 20 % and observed after 36 hours of submersion in SBF.

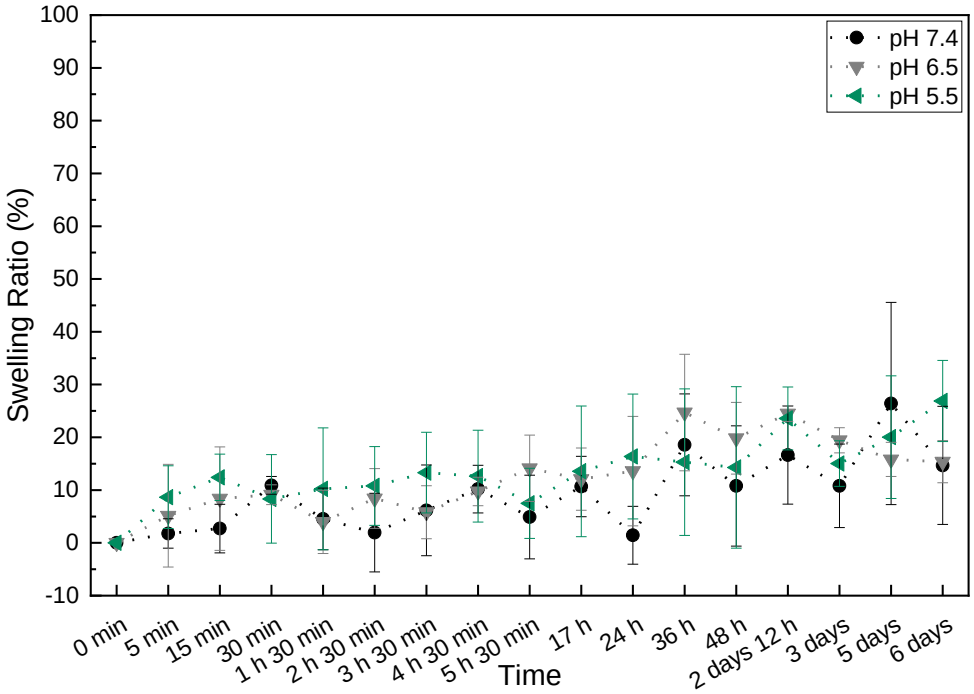

Figure 3.54: Plot of the swelling ratio vs. time for PCL films obtained at 3 different pH values: black) 7.4, grey) 6.5 and blue) 5.5 for a period of one week.

The swelling behaviour observed is also in accordance with the degradation of the polymers, since low swelling ratios reflect low degradation rates, and there is no pH dependence in both swelling and degradation as is to be expected[101].
In chitosan films it is possible to note that the standard deviations obtained are very high. This comes from the fact that when submerged the chitosan films form a gel like structure, specially at low pH values (Figure 3.55) that makes it hard to remove only the surface water of the films effectively.

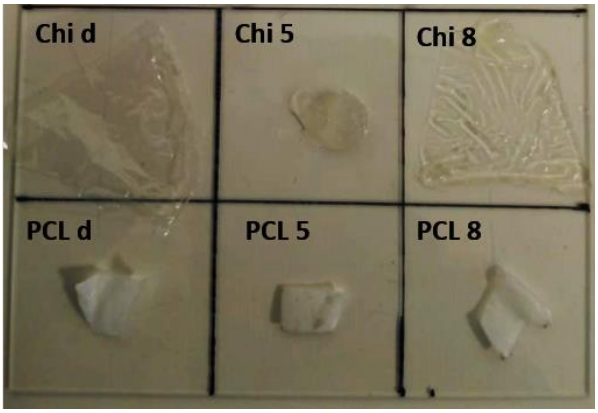

Figure 3.55: Chitosan ad PCL films before (Chi d and PCL d), and after submerged in SBF for 24 h at a pH value of 5 (Chi 5 and PCL 5) and 8 (Chi 8 and PCL 8).

3.5.5 Raman Spectroscopy

Raman spectra were taken of the polymers and drugs used as well as of the microspheres produce to access the presence and distribution of each component in the films produced. Spectra of the several

films were also measured for single point and areas of the films (Appendix N). The spectra of the components used to produce the films (Figure 3.56) show several characteristic peaks for all polymers, with the spectra of the two drugs and of chitosan having lower peak intensities than PMMA and PCL (Figure 6.24 in Appendix N)

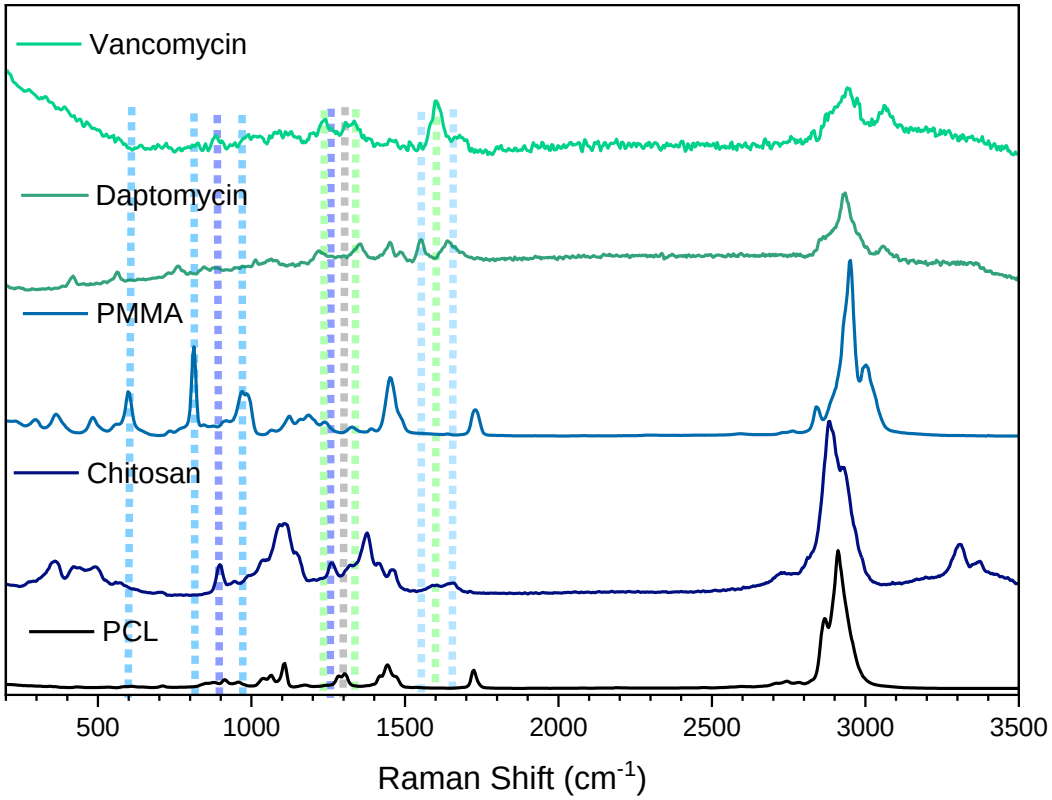

Figure 3.56: Raman spectra of the 2 drugs 3 polymers used for film and particle production.

As for the correspondence to the spectra found in the literature, all compounds show peaks correspondent to those found in literature (Table 6.14 in Appendix N). For PCL, peaks correspondent to both the crystalline and amorphous phase can be found, as can be seen by the low intensity of the broad peak correspondent to the amorphous phase at 865 cm^{-1} contrasting to the high intensity of peaks correspondent to the crystalline phase at 913 cm^{-1}, 1003-1110 cm^{-1}, 1270-1320 cm^{-1}, 1405-1470 cm^{-1} and 2800-3200 cm^{-1} that relate to skeletal stretching, ω(CH2), δ(CH2) and υ(CH) vibrational modes respectively[102].
For Chitosan, several carbon-hydrogen and carbon-oxygen bonds correspondent to the main structure of the polymer can be found, as well as the NH_2 bond at 1603 cm^{-1} and the C=O bond correspondent to the acetyl group at 558 cm^{-1}[103]. For the PMMA spectra, out of the observed bands, the most prominent is the one at 2949 cm^{-1} that corresponds to a C-H stretching vibration. A peak at 362 cm-1 is also observed corresponding to the C=O symmetric in plane bending bond vibration[104], [105]. For vancomycin, ν(C-C) skeletal mode bond, ν (C-N) of amide III, δ(C-H) of CH2 and CH3, ν(C=O) of amide I and ν(C=C) can be found at 990 cm^{-1}, 1242 cm^{-1}, 1334 cm^{-1}, 1602 cm^{-1} and 1678 cm^{-1} respectively[106]. The Raman spectrum of daptomycin was not found, so the peaks obtained for this drug were compared to the peaks of the amino acids that compose it[107]. Peaks for arginine, threonine, aspartic acid, alanine, glycine and serine were found at several wavelengths, namely 420 cm^{-1}, 562 cm^{-1}, 759 cm^{-1}, 844 cm^{-1}, 1013 cm^{-1}, 1063 cm^{-1}, 1218 cm^{-1}, 1353 cm^{-1}, 1433 cm^{-1}, 1553 cm^{-1} and 1638 cm^{-1} with only alanine having a characteristic peak at 852 cm^{-1}[108].

- **PMMA-EUD and PMMA-EUD-Dap microspheres**

From the spectra of the microspheres with and without Dap (Figure 3.57) it is possible to observe that both are like that of PMMA, which is to be expected since the polymer is in higher concentrations and its peak intensities are higher than those of the drug.

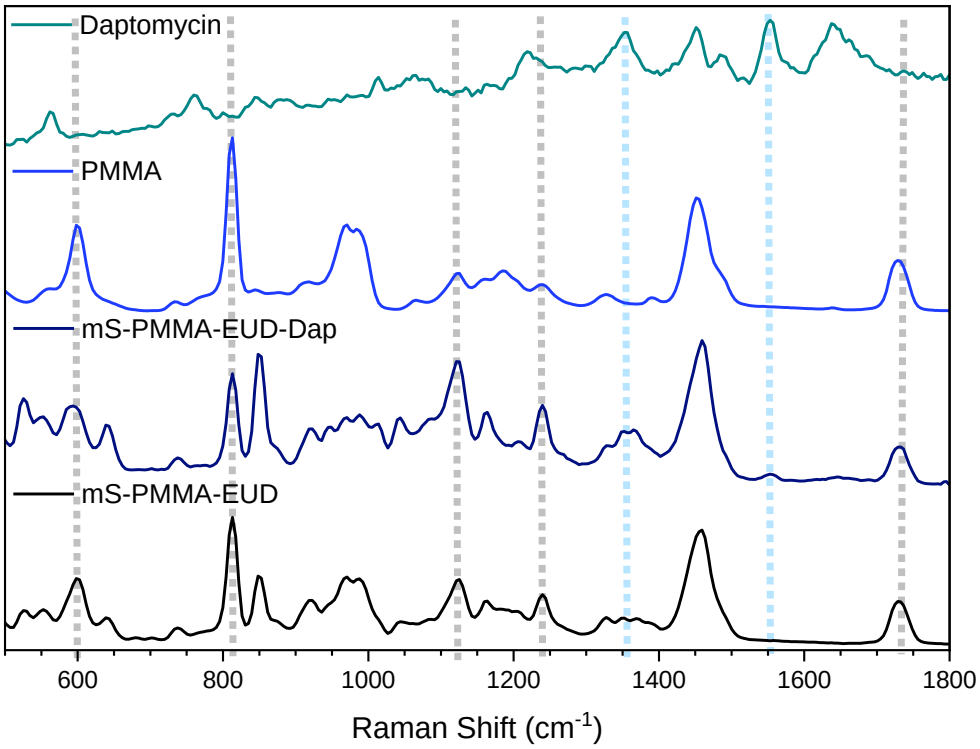

Figure 3.57: Raman spectra of: black) PMMA-EUD and dark blue) PMMA-EUD-Dap microspheres, blue) PMMA and green) Dap, with dotted lines detailing characteristic peaks from: blue) Dap and grey) PMMA.

It is noted that the PMMA-EUD-Dap microsphere spectrum (Figure 6.25 in Appendix N) contains two peaks with Raman shifts of 1553.5 cm^{-1} and 1646 cm^{-1} that correspond to Dap peaks at 1553.5 cm^{-1} and 1638.4 cm^{-1}. It is possible to conclude that the peaks are from the drug since they do not superimpose any PMMA peaks. With these two peaks it is possible to conclude that the drug is present in the microspheres.

- **Dap loaded films**

Raman spectra of the several films (Chi/PCL, Chi/PCL-PMMA-EUD, Chi/PCL-PMMA-EUD-Dap and Chi/PCL-Dap) (Figure 6.26 in Appendix M) was taken and the results compared to verify if all components could be found in the films produced (Figure 3.58).

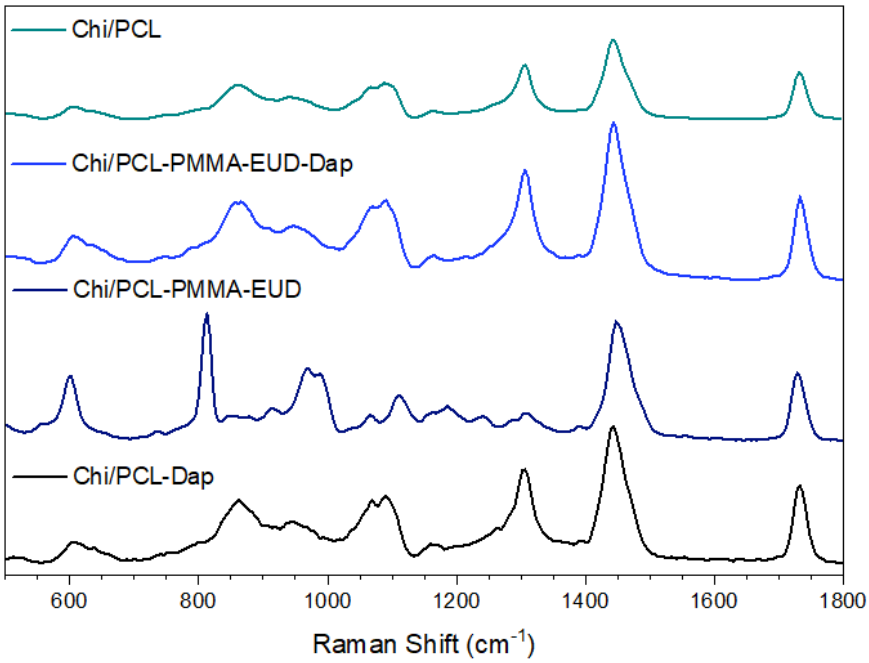

Figure 3.58: Raman spectrum of: green) Chi/PCL, blue) Chi/PCL-PMMA-EUD-Dap, dark blue) Chi/PCL-PMMA-EUD and black) Chi/PCL–Dap films.

As can be seen from the spectra above, the four films show similar compositions, which is expected since the main components of the films, PCL and Chitosan are the same in all constructs. The differences that one would expect to see are the presence of PMMA peaks in the films with microspheres, or daptomycin peaks in the films that contain it.
While the PMMA showed high peak intensities in its powder form, because in the films this polymer is in low concentrations, any peaks corresponding to it would be expected to have low intensities when compared to those of PCL, that also has high peak intensities and is at much higher concentrations. The peaks corresponding to the drug would be expected to appear in the film where the drug is incorporated directly in the chitosan, albeit with very low intensity peaks due to both a low concentration when compared to PCL and Chi the low intensity of the peaks even in the powder form. In the films with Dap loaded microspheres the drug is not expected to be noticeable, because of both what was said above and because the addition of PMMA which also has high intensity peaks and is in higher quantities than the drug, masking Dap peaks even more.
As can be seen from the Raman spectra from both films that contain Dap, when compared to a PCL/Chi film and the spectra of the drug (Figure 3.59), it is possible to note a lack of clear peaks belonging to Dap in either film. In the PCL/Chi-Dap film, possible Dap peaks, at 1553 cm^{-1} and 1637 cm^{-1}, may indicate the presence of the drug.

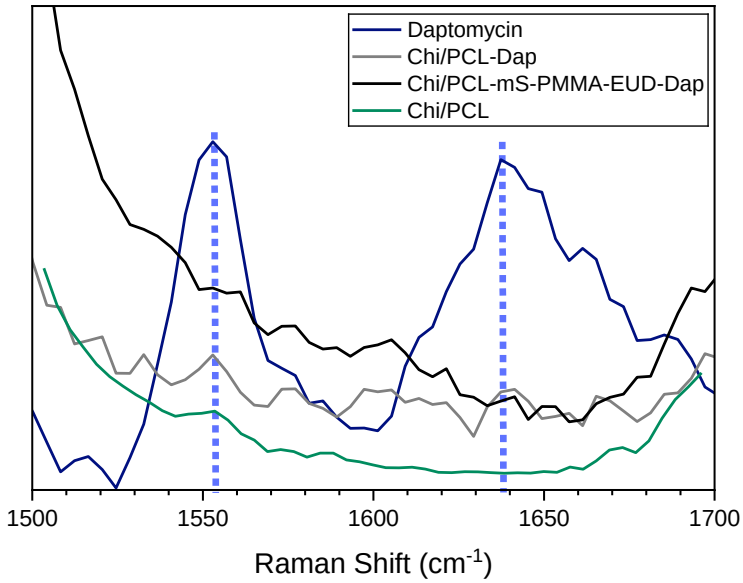

Figure 3.59: Raman spectra of: green) Chi/PCL grey) Chi/PCL-Dap, black) Chi/PCL-PMMA-EUD-Dap and blue) Dap between 1500 cm^{-1} and 1700 cm^{-1}.

Using Raman technique, maps of an area of 5 μm^2 of Chi/PCL-PMMA-EUD-Dap film was obtained (Figure 3.60), measuring the intensity of different peaks, allowing to understand the distribution of the several components in the film. The peaks used were the characteristic peaks found: 1810 cm^{-1} for PCL, 475 cm^{-1} for chitosan, 813 cm^{-1} for PMMA and 1350 cm^{-1} for Dap.

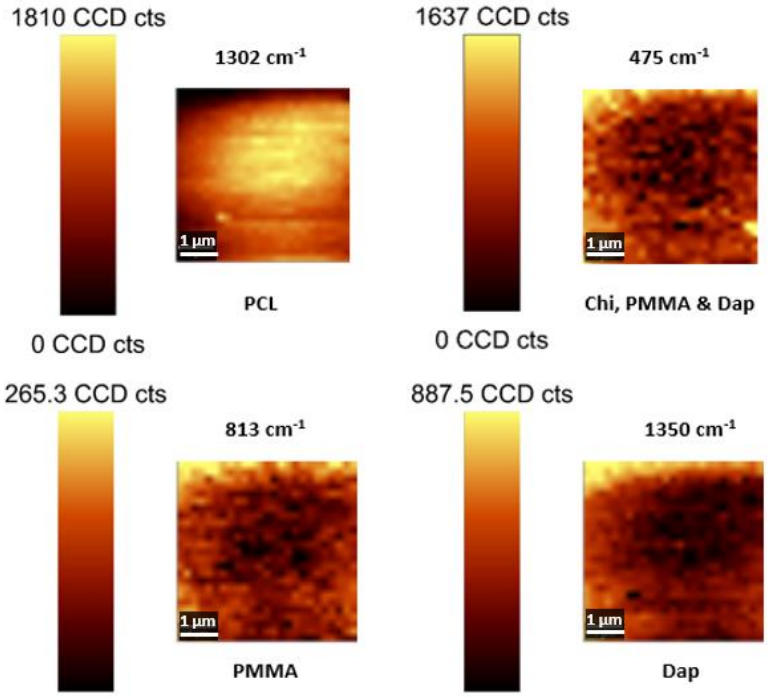

Figure 3.60: Raman maps made at 1302 cm^{-1}, 1080 cm-1, 813 cm^{-1} and 1350 cm^{-1} for the analysis of distribution of PCL, Chitosan, PMMA and Dap respectively.

In the maps obtained, it is possible to observe that at 1080 cm^{-1} the intensity is higher than at the other three analysed wavelengths. It may be also noted that the distribution of PCL has a complementary distribution to the other three components, and that the peaks correspondent to Chi, PMMA and Dap

that have similar distributions amongst themselves. This is to be expected because the construction of the film implies that both PCL and Chi are distributed throughout the whole film in overlapping layers and Dap loaded microspheres are in the chitosan layer.
From the Raman spectra of the Dap loaded microspheres it was possible to observe that the Dap was inside or in the surface of the spheres. Then, it would be expected that both PMMA and Dap would be found in the same place, and should be present where Chi is present, which is confirmed by the similar distribution of the three compounds. It is however important to note that no peak belonging solely to chitosan was found and thus the intensity observed at 475 cm^{-1} cannot be attributed to chitosan alone. Because the intensity of PMMA and Dap in these wavenumbers are low, however, it is possible to conclude that the map observed corresponds mostly to Chi.

- **PMMA and PMMA-VAN microspheres**

From the Raman spectra of the PMMA and PMMA-Van microspheres (Figure 3.61) it is possible to conclude that there are two peaks, at 882 cm^{-1} and at 1306 cm^{-1} that correspond to Van, showing the presence of the drug in the microspheres.

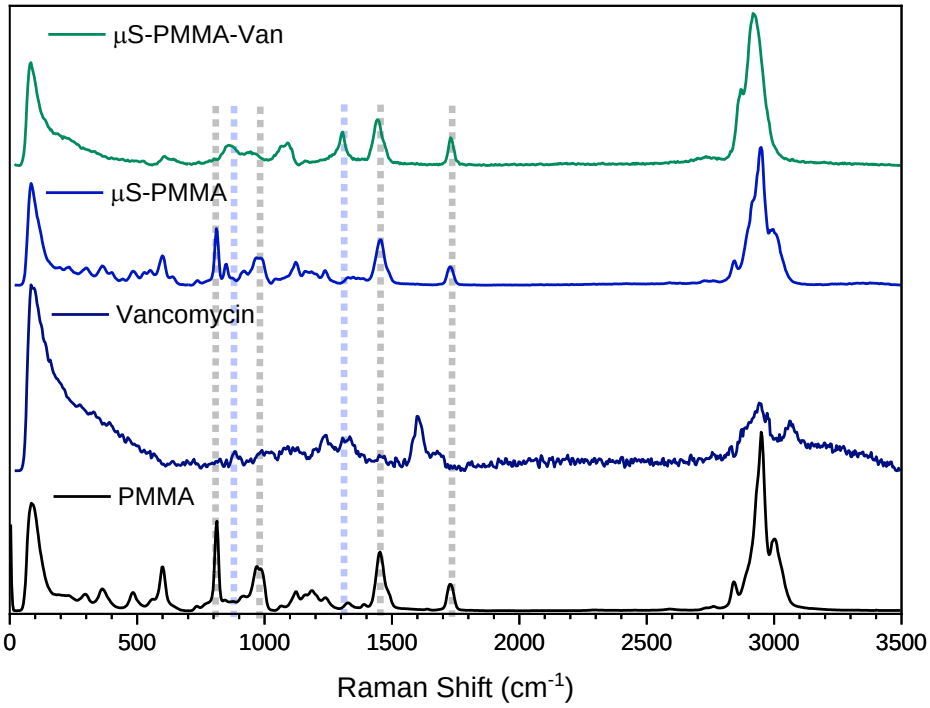

Figure 3.61: Raman spectra of PMMA (black), vancomycin (deep blue), PMMA microspheres (blue) and PMMA-Van microspheres (green) with dotted lines detailing peaks corresponding to PMMA (grey) and vancomycin (blue).

- **Van loaded films**

When observing the films loaded with Van and with PMMA-Van microspheres (Figure 3.62) two peaks, at 1606 cm^{-1} and at 1334 $cm^{-1,}$ that are not present in the PCL/Chi film, are common to the spectrum of Van, indicating its presence in these films.

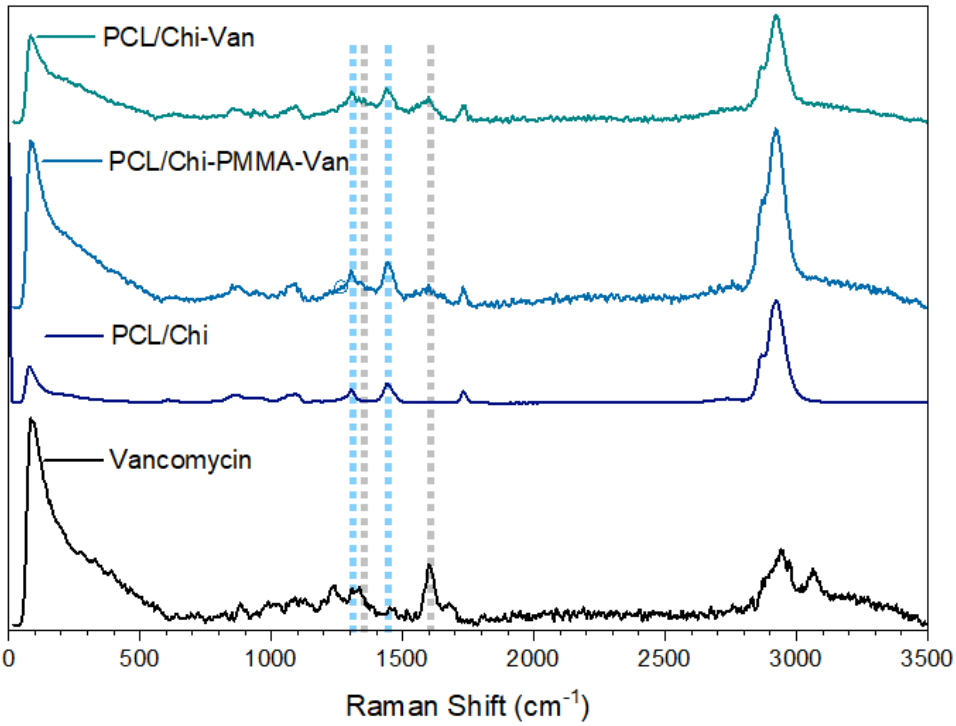

Figure 3.62: Raman spectra of: green) Chi/PCL-Van, blue) Chi/PCL-PMMA-Van, dark blue) Chi/PCL, and black) Van with dotted lines detailing peaks corresponding to vancomycin (grey) and to PCL or chitosan (blue).

Raman distribution maps were obtained for Chi/PCL-PMMA-Van and Chi/ PCL -Van films. In the map obtained for the first film (Figure 3.63), it is possible to note that the map of the polymers seems to be complementary to that of the drug. Because, as mentioned previously, PCL has much higher intensities than Chi, one can infer that the map of the polymers consists mostly of PCL. Because in these films separate maps for Chi and PCL were not possible to obtain, it is impossible to determine if the drug is located in the chitosan layer. The maps also show that Van is evenly distributed throughout the film. The spheres cannot be seen clearly, and, since no map of the distribution of PMMA alone was made, the presence of the polymer cannot be ascertained and therefore it is impossible to conclude if the drug and PMMA have similar distributions.

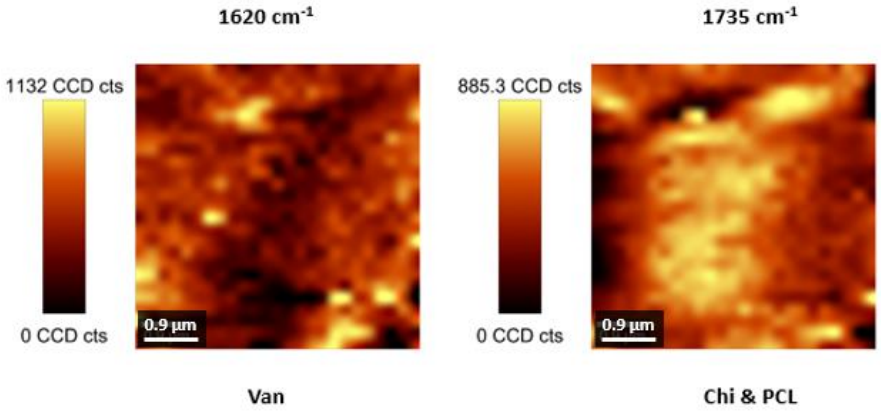

Figure 3.63: Raman distribution maps obtained for Van, PCL, and chitosan in a 5 μm^2 area of a Chi/PCL-PMMA-Van film.

In the maps obtained for Chi/PCL-Van film (Figure 3.64) the same assessment can be made. Both maps complement each other, indicating that the Van is not in the PCL layer. In these films as well, the drug seems to be evenly distributed through the film.

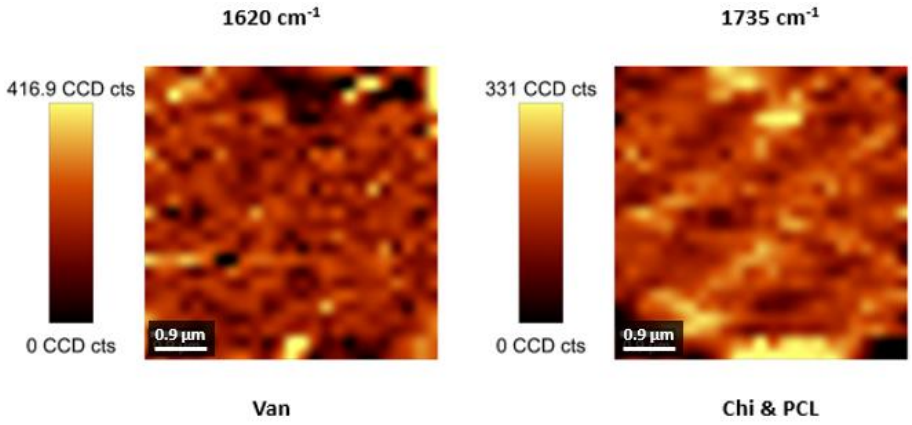

Figure 3.64: Raman distribution maps obtained for Van, PCL, and Chi in a 5 µm^2 area of a Chi/PCL-Van film.

3.5.6 Drug Release

To do the drug release study first there were made several solutions of daptomycin and vancomycin to produce a calibration curve for each of the pH values used for drug release, this is, 7.4, 6.5 and 5.5 correspondent to the normal physiological pH value (7.4), the value of pH existent in a stage of infection (5.5) and a pH value between the two to verify if the changes in drug release occurred in a linear fashion. The solutions were analysed with UV-Vis spectroscopy and calibration curves were made to study the dependence of the absorbance in function of the drug concentration for the calculations of drug in the drug release solutions (Figure 3.65).
For both drugs the solutions studied were of 0.666 mg/mL, 0.5 mg/mL 0.333 mg/mL, 0.25 mg/mL, 0.1665 mg/mL, 0.125 mg/mL, 0.08325 mg/mL, 0.0625 mg/mL, 0.03125 mg/mL, 0.01563 mg/mL, 0.00781 mg/mL and 0.00391 mg/mL. The wavelengths used to construct the several calibration curves (Figure 6.27 in Appendix O) correspond to the peaks observed in the spectra of the drugs, being only one wavelength chosen for each drug for drug release studies. For Dap the wavelength chosen was of 262 nm and for Van of 280 nm since they show a linear tendency for a broader range of concentrations and no peak shift.

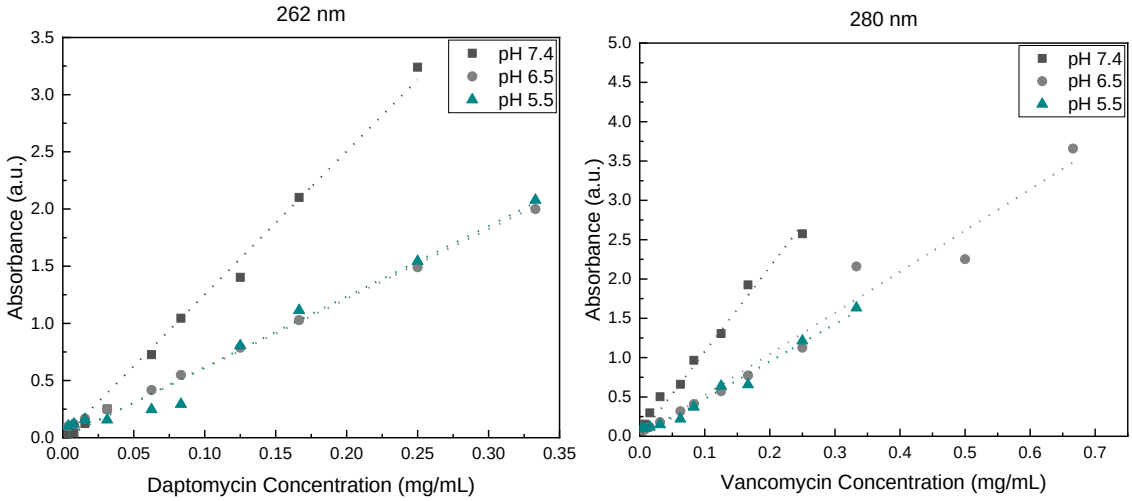

Figure 3.65: Calibration curves for Dap and Van in SBF at 262 nm and 280 nm respectively.

Samples of the several films were then submerged in SBF at a pH of 5.5, 6.5 or 7.4 and the drug contained in this SBF quantified for 5 replicas of each film. Plots of the drug concentration versus release time were obtained, and the release mechanism was studied by comparing several known mathematical models of drug release. For the drug free samples, the quantification was not done, being these samples only used as reference, to ensure that the peaks observed belonged to the drugs and not to any other component of the films.

- **Unloaded films**

The absorbances obtained for the unloaded films (Figure 3.66 and Figure 6.28 to Figure 6.30 in Appendix O) show that some polymer is being eroded. Because of this, an off-set value is observed in the spectra, that was visible in all Chi/PCL, Chi/PCL-PMMA and Chi/PCL-EUD films. These values show high standard deviations, thus, the amount of drug released cannot be calculated because the absorbances measured will always be due to partially the drug concentration, and partially to the polymer concentration. Instead, only a qualitative analysis between the several samples can be made.

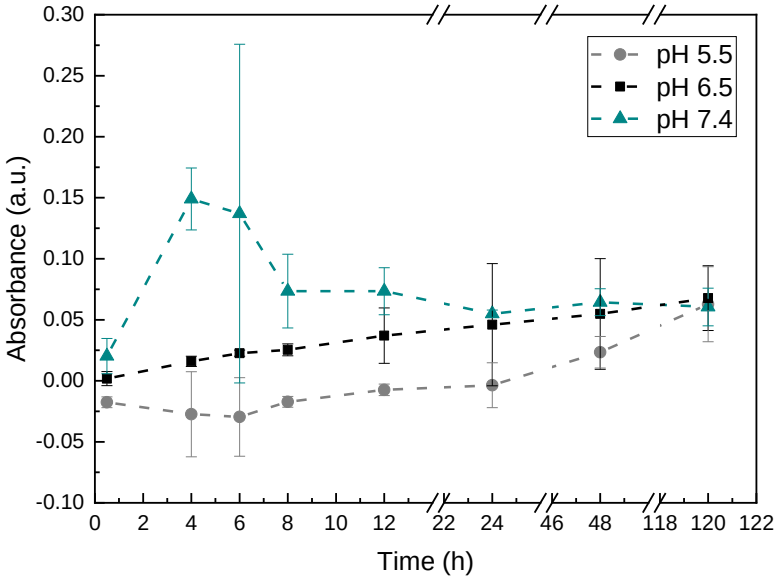

Figure 3.66: Average absorbances measured for drug release of Chi/PCL-PMMA-EUD films (n=5).

- **Chi/PCL-Dap**

For Chi/PCL-Dap films it is possible to note that the changes in pH do not seem to alter the drug release profile greatly. For all 3 pH values 90 % drug release is only achieved after 48 h of release, and 50 % release is achieved between 2 and a half hours and 4 h of release (Figure 6.31 in Appendix O). Apart from this, concentrations of 19.53 ± 19.58 µg/mL, 13.13 ± 4.53 µg/mL and 33.25 ± 26.37 µg/mL are achieved for pH values of 5.5, 6.5 and 7.4 respectively, showing that the amount of drug released for all pH values is also similar.

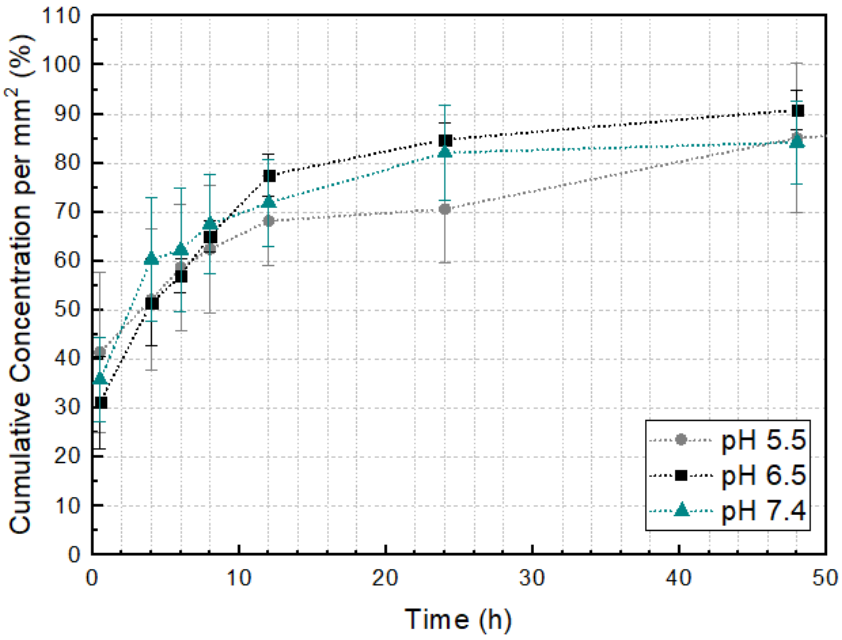

Figure 3.67: Cumulative daptomycin release from Chi/PCL-Dap films plotted versus the release time for the first 48 hours of drug release.

Comparing the drug release profile with several models (Figure 6.32 in Appendix O) it is possible to note that the most appropriated release model is the Korsmeyer-Peppas model[109] since this model is the one whose graphical representation leads to a higher R^2 value of the linear regression (Table 3.11).

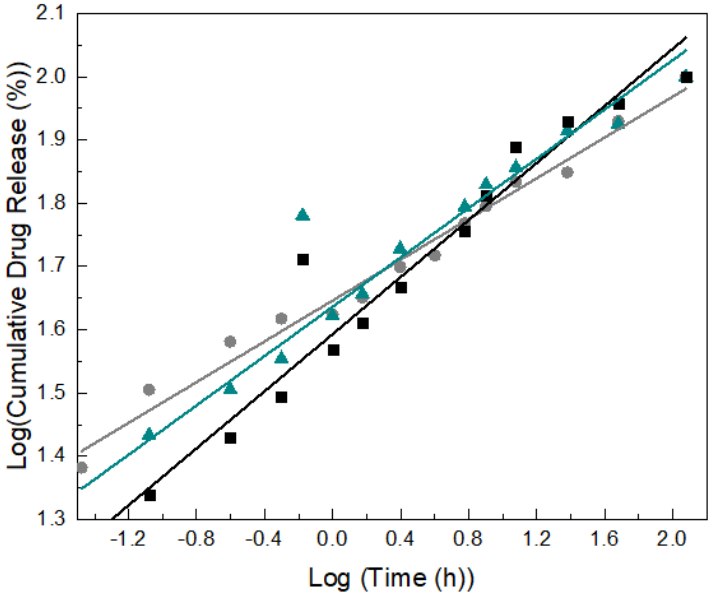

Figure 3.68: Korsmeyer-Peppas model representation for release of Dap from Chi/PCL-Dap films at pH values of 5.5, 6.5 and 7.4.

Table 3.11: Values of R^2 obtained for the linear fit of the several mathematical models that describe drug release profiles.

	R^2 Value		
Model	**pH 5.5**	**pH 6.5**	**pH 7.4**
Zero Order	0.6712	0.51567	0.51463
First Order	0.47	0.33378	0.31399
Higuchi	0.90407	0.79288	0.76642
Hixon-Crowell	0.53944	0.39585	0.38015
Korsmeyer-Peppas	0.98121	0.94587	0.91322

Taking the equation that describes the Korsmeyer-Peppas model (Formula 3.6)

$$log\left(\frac{M_i}{M_\infty}\right) = \log(K) + n\log(t) \quad (3.6)$$

Where M_∞ is the amount of drug at the equilibrium state, M_i is the amount of drug released over time *t*, *K* is the constant of incorporation of structural modifications and geometrical characteristics of the system (also considered the release velocity constant) and *n* is the exponent of release (related to the drug release mechanism) in function of time, one has that, by the graphical representation of the model, n represents the slope of the linear fit obtained.

Depending on the value of n that better adjusts to the release profile, it is possible to classify the kind of release that corresponds the type of observed behaviour [110]. These types can be divided into 3:

- Quasi-Fickian
- Fickian model (Case I)
- Non-Fickian models (Case II, Anomalous Case and Super Case II)

In the Quasi-Fickian model, n<0.5 release mechanism is ruled by diffusion, that occurs partially in the swollen matrix and partially in the solvent filled pores[111].

In the Fickian model, n=0.5 and the drug release mechanisms are governed by diffusion because the diffusion is much greater than the polymeric chain relaxation[110].

When 0.5<n<1 the model is Non-Fickian or anomalous transport, and drug release is governed by diffusion and swelling that have comparable rates. In this case, the combination of the rearrangement of polymeric chains that happens slowly and diffusion that occurs at the same time results in anomalous effects[110].

When n=1, the model is non-Fickian (Case II), the drug release corresponds to a zero-order release kinetics and the mechanism driving the drug release is the swelling or relaxation of polymeric chains[110].

At the end of Case II transport, a fast increase of the swelling ratio may be observed. In this situation, the mechanism becomes Super Case II, where n > 1, due to the expansion of forces exercised by swollen gel in the vitreous nucleus. For studies related to the value of n, only values of drug release percentage up to 60 % are used (Figure 3.69).

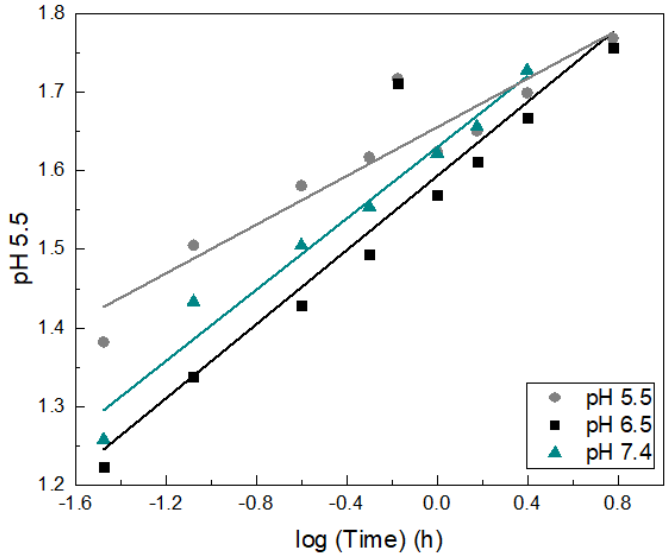

Figure 3.69: Korsmeyer-Peppas model applied to drug release values <60 % for the calculation of n value for Chi/PCL-Dap films.

From the Korsmeyer-Peppas model equation, one has that the value of n represents the slope of the linear fit obtained (Table 3.12).

Table 3.12: Linear Fits obtained for the calculation of n value for Dap in Chi/PCL-Dap films at ph values of 5.5, 6.5 and 7.4.

Release medium	Linear Fit equation
pH 5.5	Y= 0.15485 x + 1.65554
pH 6.5	Y= 0.23573 x + 1.59352
pH 7.4	Y= 0.22658 x + 1.63008

For this value of n, as described above the value of n for all pH studied is lower than 0.5 and therefore the mechanism of release is Quasi-Fickian, with release mechanism being ruled by diffusion, that occurs in both the swollen matrix and solvent filled pores.

- **Chi/PCL-PMMA-EUD-Dap**

For Chi/PCL-Dap films (Figure 3.70) the drug release shows to be more affected by the pH of the release medium. For a pH of 5.5 50 % of the drug is released within 1 and an half hours and 2 and an half hours (Figure 6.33 in Appendix O), however for a pH of 6.5 this same percentage of release occurs only within 8 h and at a pH of 7.4 within 8 h. The same trend maintains itself for a drug release percentage of 90 % that occurs at 12 h for a pH of 5.5 and yet only at about 48 h for pH values of 6.5 and 7.4. This indicates that the lower pH results in a faster drug release, although similar concentrations of drug released are achieved for all pH values being of 6.24 ± 1.38 µg/mL, 16.22 ± 9.93 µg/mL and 6.33 ± 0.91 µg/mL for a pH of 5.5, 6.5 and 7.4 respectively.

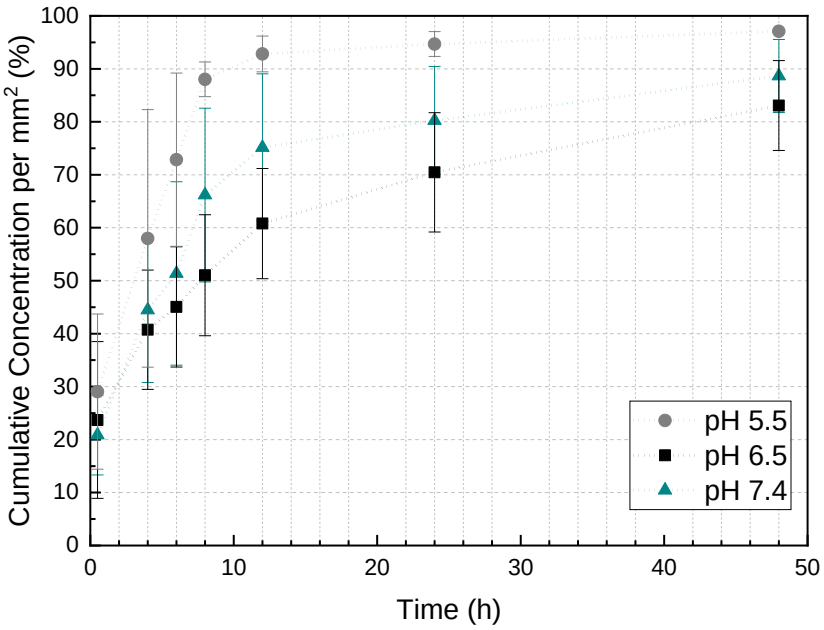

Figure 3.70: Cumulative Dap release from Chi/PCL-PMMA-EUD-Dap films plotted versus release time for the first 48 hours of drug release.

Doing as before and comparing the drug release profile obtained for the Chi/PCL-PMMA-EUD-Dap films with several models (Figure 6.34 in Appendix O) it is possible to note that the most appropriated release model is again the Korsmeyer-Peppas model (Figure 3.71) since it is the one that leads to the linear fit with the highest R^2 value (Table 3.13).

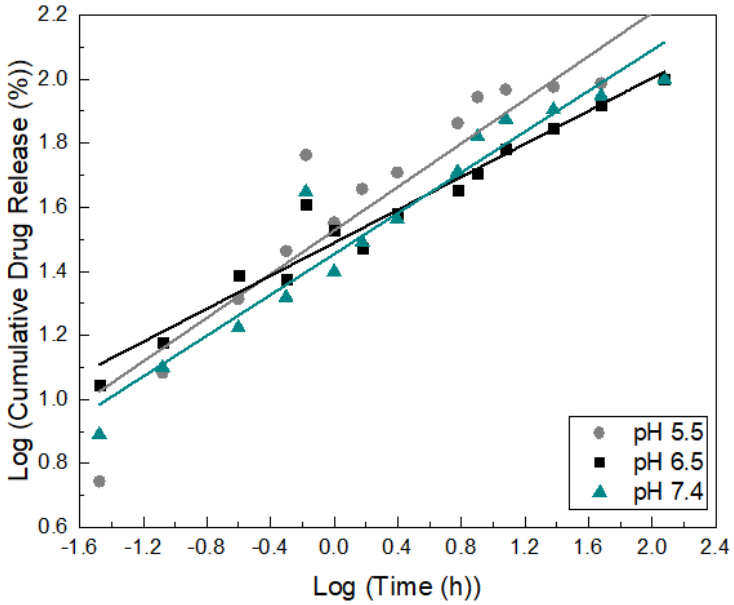

Figure 3.71: Korsmeyer-Peppas model representation for the release of daptomycin from Chi/PCL-PMMA-EUD-Dap films at pH values of 5.5, 6.5 and 7.4.

Table 3.13: Values of R^2 obtained for the linear fit of the several mathematical models that describe drug release profiles for Chi/PCL-PMMA-EUD-Dap.

	R^2 Value		
Model	**pH 5.5**	**pH 6.5**	**pH 7.4**
Zero Order	0.30632	0.6765	0.51344
First Order	0.14537	0.28691	0.39373
Higuchi	0.59868	0.90067	0.78888
Hixon-Crowell	0.20452	0.36526	0.49329
Korsmeyer-Peppas	0.84429	0.94965	0.92456

Again, calculating the value of n in order to obtain the kind of mechanism behind the drug release profile (Figure 6.35 in Appendix O) it is possible to conclude that the value of n is <0.5 for pH values of 6.5 and 7.4, and yet just above 0.5 for a pH value of 5.5 (Table 3.14). Thus, the mechanism is also Quasi-Fickian for the first two pH values, and yet, Fickian, or non-Fickian for a pH of 5.5. This indicates that for the films with the microspheres, at a lower pH, the drug release is affected by both diffusion and polymer swelling.

Table 3.14: Linear Fits obtained for the calculation of n value for Dap in Chi/PCL-PMMA-EUD-Dap films at pH values of 5.5, 6.5 and 7.4.

Release medium	**Linear Fit equation**
pH 5.5	Y = 0.5197 x + 1.6093
pH 6.5	Y= 0.26431 x + 1.4908
pH 7.4	Y= 0.35121 x + 1.46042

- **Chi/PCL-Van**

For Chi/PCL-Van films (Figure 3.72) the drug release shows to be more affected by the pH of the release medium. For all pH values 50 % of the drug is released within 1 and a half hours (Figure 6.36 in Appendix O). The same trend maintains itself for a drug release percentage of 90 % that occurs at 24 h for all pH values. This indicates that drug release of vancomycin from this film is not pH dependent. Additionally, similar concentrations of drug released are achieved for all pH values being of 6.85 ± 1.99 µg/mL, 29.70 ± 10.19 µg/mL, and 10.27 ± 1.94 µg/mL for a pH of 5.5, 6.5 and 7.4, respectively.

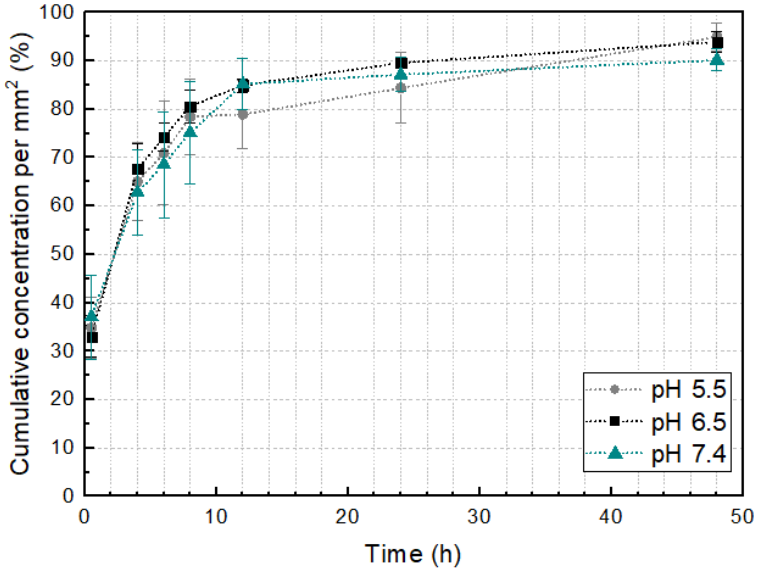

Figure 3.72: Cumulative vancomycin release from Chi/PCL-Van films plotted versus release time for the first 48 hours of drug release.

Comparing several release models (Figure 6.37 in Appendix O) it is possible to note that the release follows the Korsmeyer-Peppas (Figure 3.73) model since this model is the one that leads to a linear fit with a higher R^2 value (Table 3.15).

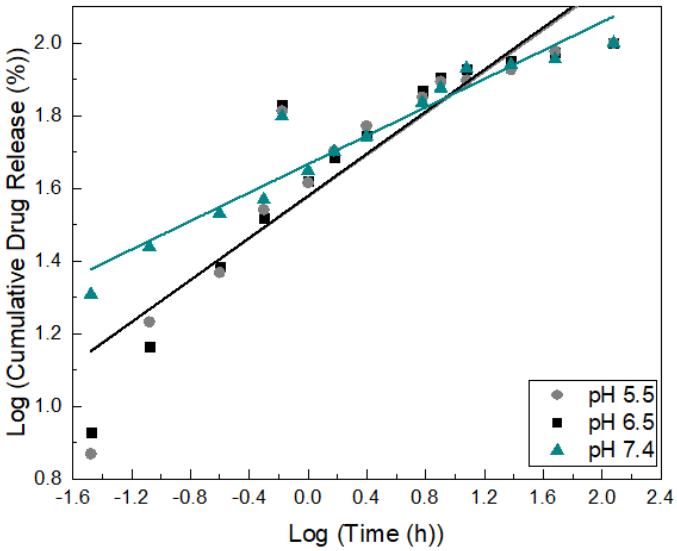

Figure 3.73: Korsmeyer-Peppas model representation for the release of vancomycin from Chi/PCL-Van films at pH values of 5.5, 6.5 and 7.4.

Table 3.15: Values of R2 obtained for the linear fit of the several mathematical models that describe drug release profiles for Chi/PCL-Van.

	R^2 Value		
Model	**pH 5.5**	**pH 6.5**	**pH 7.4**
Zero Order	0.35953	0.32639	0.41732
First Order	0.15478	0.15467	0.27008
Higuchi	0.62990	0.60076	0.69513
Hixon-Crowell	0.22195	0.21170	0.31899
Korsmeyer-Peppas	0.82198	0.83439	0.91429

Again, calculating the value of n in order to obtain the kind of mechanism behind the drug release profile (Figure 6.38 in Appendix O) it is possible to conclude that the value of n is <0.5 for all pH values (Table 3.16) and thus the mechanism is always Quasi-Fickian. This indicates that for the films loaded with freestanding vancomycin, the drug release is ruled by diffusion in the swollen matrix and solvent filled pores.

Table 3.16: Linear Fits obtained for the calculation of n value for Van in Chi/PCL-Van films at pH values of 5.5, 6.5 and 7.4.

Release medium	**Linear Fit equation**
pH 5.5	Y = 0.25901 x + 1.7794
pH 6.5	Y= 0.43279 x + 1.61402
pH 7.4	Y= 0.22212 x + 1.65421

- **Chi/PCL-PMMA-Van**

For Chi/PCL-Van films (Figure 3.74) the drug release shows to be more affected by the pH of the release medium. For a pH value of 5.5, 50 % of the drug is released within 2 and a half hours, and yet

for pH values of 6.5 and 7.4 the same only occurs after 4 h of drug release (Figure 6.39 in Appendix O). For a drug release of 90 % however, that occurs at 48 h for all pH values. This indicates that drug release of vancomycin from this film is only pH dependent in the burst release phase. Additionally, similar concentrations of drug released are achieved for all pH values being of 15.64 ± 4.00 µg/mL, 11.66 ± 1.76 µg/mL and 14.33 ± 1.36 µg/mL for a pH of 5.5, 6.5 and 7.4 respectively.

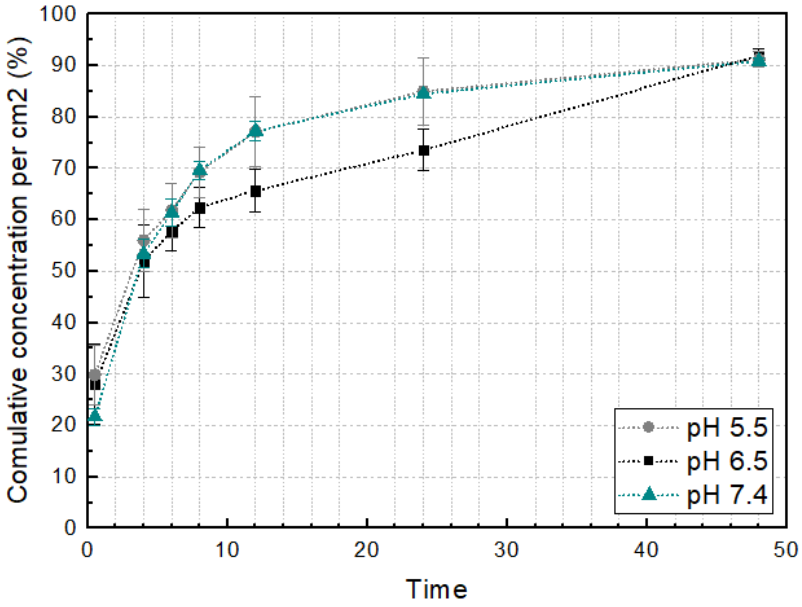

Figure 3.74: Cumulative vancomycin release from Chi/PCL-Van films plotted versus release time for the first 48 hours of drug release.

Comparing several release models (Figure 6.40 in Appendix O) it is possible to note that the release follows the Korsmeyer-Peppas (Figure 3.75) model since this model is the one that leads to a linear fit with a higher R^2 value (Table 3.17).

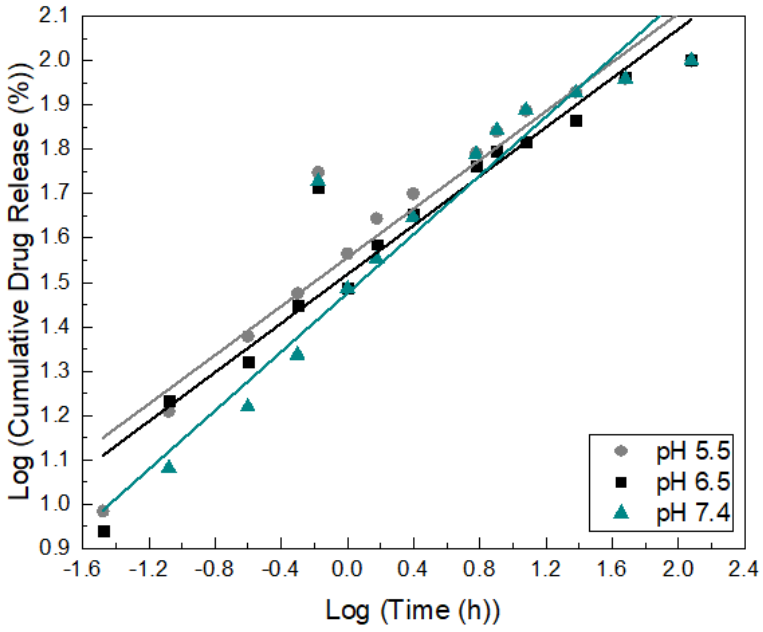

Figure 3.75: Korsmeyer-Peppas model representation for the release of vancomycin from Chi/PCL-Van films at pH values of 5.5, 6.5 and 7.4.

Table 3.17: Values of R2 obtained for the linear fit of the several mathematical models that describe drug release profiles for Chi/PCL-Van.

	R^2 Value		
Model	**pH 5.5**	**pH 6.5**	**pH 7.4**
Zero Order	0.44861	0.54697	0.44235
First Order	0.22828	0.27874	0.21808
Higuchi	0.72719	0.80285	0.72346
Hixon-Crowell	0.30194	0.36981	0.29382
Korsmeyer-Peppas	0.89497	0.90401	0.88698

Again, calculating the value of n in order to obtain the kind of mechanism behind the drug release profile (Figure 6.41 in Appendix O) it is possible to conclude that the value of n is < 0.5 for all pH values (Table 3.18) and thus the mechanism is always Quasi-Fickian. This indicates that for the films loaded with freestanding vancomycin, the drug release is ruled by diffusion in the swollen matrix and solvent filled pores.

Table 3.18: Linear Fits obtained for the calculation of n value for Van in Chi/PCL-Van films at pH values of 5.5, 6.5 and 7.4.

Release medium	**Linear Fit equation**
pH 5.5	Y= 0.38752 x + 1.61130
pH 6.5	Y= 0.34311 x + 1.54780
pH 7.4	Y= 0.44959 x + 1.52059

3.5.7 SEM

In the Chi/PCL-PMMA-Van films (Figure 3.76) it is possible to see the presence of microspheres in the surface of the film. Since the last layer is of PCL, which should not contain the spheres, we can conclude that the spheres from the chitosan solutions are being transferred to the PCL solution when the substrate is submerged on it.

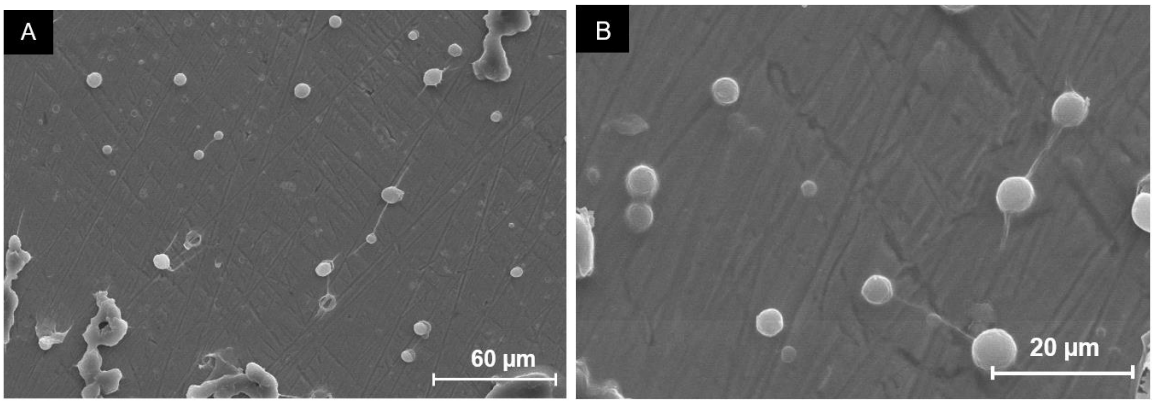

Figure 3.76: SEM micrograph of a Chi/PCL-PMMA-Van film at an ampliation of: A) 600 x and B) 2000 x.

It is possible to note lines correspondent to the mechanical abrasion performed in the metal, indicating that the treatment might affect the film's final rugosity.
The Chi/PCL-Van film (Figure 3.77) presents a smooth surface where, again, indentations from the treatment to the metal are present. It is possible to see some spheres in the film, showing a contamination of the surface occurred during the preparation of the sample for SEM analysis. Although some depressions can be observed in the film surface for a magnification of 600 x (Figure 3.77 A), the lack

of a large quantity of pores in the surface of the film indicates that the deposition of the final polymer layer is mostly homogeneous.

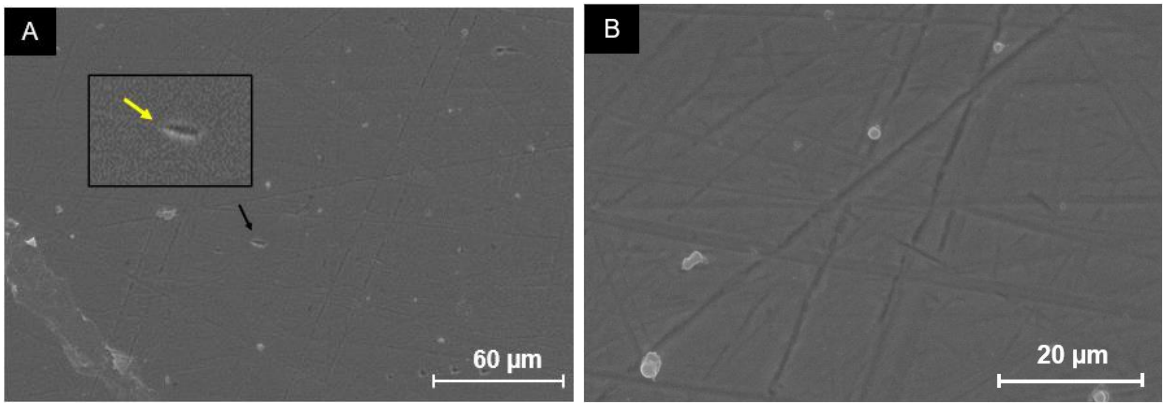

Figure 3.77: SEM micrograph of a Chi/ PCL -Van film at a magnification of A) 600 x and B) 2000 x with detail in an indentation in picture A.

The Chi/ PCL -PMMA-EUD-Dap films (Figure 3.78) show a very porous surface with uneven pores with a size of 1.38 ± 3.00 µm. No microspheres are present at the top of the film, indicating that if there are microspheres they are in the lower layers. The layer visible under the upmost one also presents porous, and there seems to be a sphere present in that layer (Figure 3.78 B denoted by a yellow arrow).

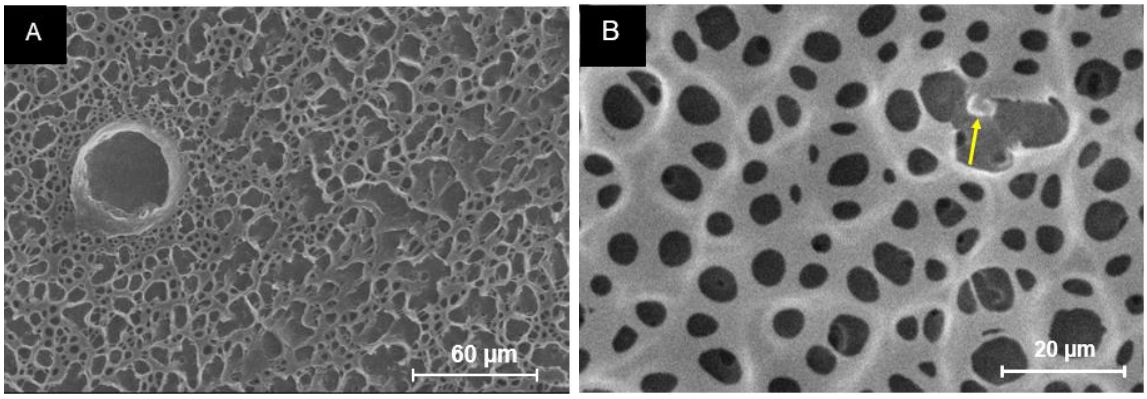

Figure 3.78: SEM micrograph of a Chi/ PCL -PMMA-EUD-Dap film at a magnification of A) 600 x and B) 2000 x with detail on a sphere in figure B by a yellow arrow.

In these films the lines from the metal treatment are not visible, indicating that perhaps the film is thicker or opaquer than the precious ones.
The Chi/PCL-Dap films (Figure 3.79) are also porous seeming to be however less so than the Chi/PCL-PMMA-EUD-Dap, indicating that the surface in the Dap loaded films is more homogenous than that of the films loaded with PMMA-EUD-Dap microspheres. The pores present also appear to be of similar size throughout the surface, with an average size of 0.94 ± 0.25 µm. In these images it is possible to note once again the lines from the metal treatment, just as it happened with the Van loaded films.

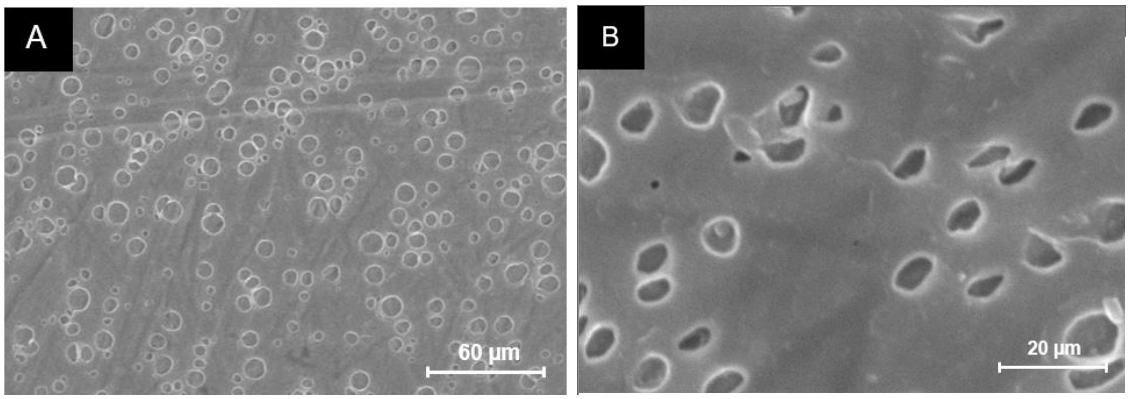

Figure 3.79: SEM micrograph of a Chi/ PCL-Dap film bilayers at a magnification of A) 600 x and B) 2000 x.

The unloaded Chi/pcl films (Figure 3.80) also show a porous surface with pores that are very much smaller than those found in the previous film. These pores are heterogenous with an average diameter of 2.56 ± 1.85 µm but appear to be more dispersed over the entire surface of the film than it happened with the Chi/PCL-Dap films.

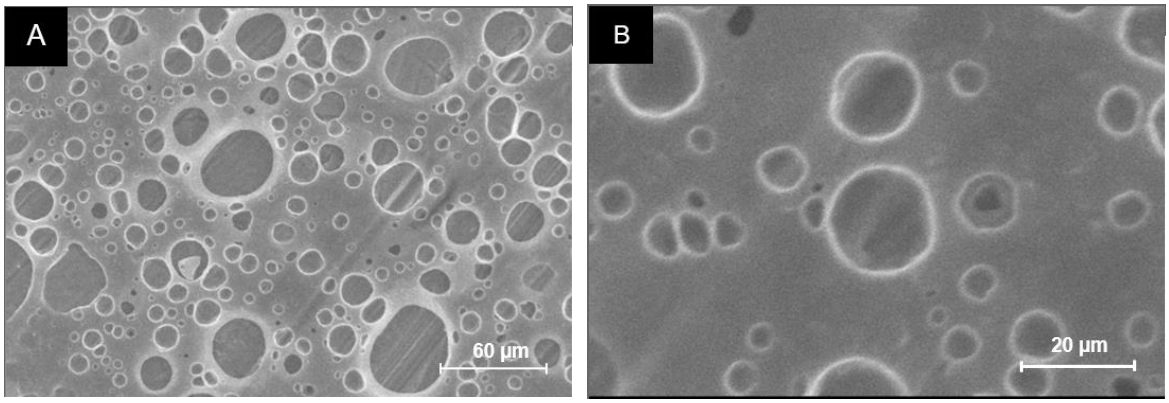

Figure 3.80: SEM micrograph of a Chi/ film with at a magnification of A) 600 x and B) 2000 x.

Reported formation of pores in films obtained by dip-coating indicate that the cause for their formation would be phase separation, in the cases of presented films. This phase separation occurs when a critical polymer or nonsolvent concentration is reached during solvent evaporation. When this happens, one phase of the phase-separated blends is removed when nonsolvent evaporates from the nonsolvent-containing phase[112]. Because no pores can be seen in Chi/PCL-Van or Chi/PCL-PMMA-Van films, it can be hypothesized that Van affects solvent evaporation from the chitosan layer.

4 Conclusions and future work

The main goal of this project was the development of novel polymeric coatings suitable for local controlled release of daptomycin and vancomycin from titanium and steel substrates using the dip-coating technique.
Towards that goal, films of 12 alternated layers of chitosan loaded with vancomycin and daptomycin loaded acrylic particles and loaded with daptomycin and vancomycin and PCL were successfully deposited in 316L-SS.

The work was split into several steps, including synthesis of daptomycin and vancomycin loaded particles, substrate treatment optimization and deposition of films. Chemical, structural, and morphological characterizations were also made to the produced microparticles and films.

Confirmation of successful production of microspheres was obtained via SEM. The loading of the spheres was confirmed via UV-Vis spectroscopy, with a encapsulation efficiency above 99% being obtained for PMMA-Van and PMMA-EUD-Dap spheres. Raman spectroscopy was also used to verify the presence of both drugs in the microspheres, confirming their presence, although not concluding on whether the drugs were inside or in the surface of the spheres.

As for the substrate treatment, three strategies were used: chemical etching, electrochemical etching, and mechanical abrasion. Using AFM it was possible to verify that the electrochemical etching produced rougher surfaces, and the mechanical abrasion and chemical etching produced surfaces of similar roughness. It was also possible to observe that the morphology of the erosion pattern caused by chemical and electrochemical etchings were similar and very different from the pattern obtained for mechanical abrasion.
From the film deposition, it was concluded that the mechanical abrasion treatment was the most appropriate, showing that the adhesion is more likely dependant in the morphology of the surface and not simply in the roughness of it.

Regarding the addition of both drugs and the several spheres into the films, by Raman spectroscopy it was possible to confirm the presence of the spheres and of vancomycin in the films, yet, the presence of daptomycin could not be ascertained by this spectroscopy.

Drug release studies were performed in the produced films, and the results demonstrated that none of the films showed a pH dependent drug release profile, with the drug release happening through diffusion even though swelling and degradation ratios indicated that the polymer in which the active compounds are encapsulated is pH responsive.

Acknowledging the problems faced during this work, much can be done to further study and understand these films:

I.	Further investigate different deposition parameters to produce more homogenous films;
II.	Improvement of the mechanical treatment, changing it from manual to machine-made to facilitate process reproducibility
III.	Study process alteration to improve pH response, such as crosslinking of the chitosan layers
IV	Study film surface characteristics, such as surface energy and rugosity

Biological studies including antimicrobial tests, bacterial and cell adhesion tests, and biocompatibility and bioactivity tests should also be done in order to determine if the produced films could be used in implants.
Silanization of Ti-6Al-4V were made using TEOS and APTES. Results indicate that Ti treated by immersion in APTES after a piranha passivation and Ti treated with TEOS vapor in argon atmosphere

without previous passivation in piranha solution result in Si deposition in the metal, indicating that these treatments are the most promising for film deposition.

5 Bibliography

[1] J. M. Schierholz and J. Beuth, "Implant infections : a haven for opportunistic bacteria," *J. Hosp. Infect.*, vol. 49, no. 2, pp. 87–93, 2001.

[2] E. T. J. Rochford *et al.*, "Infection burden and immunological responses are equivalent for polymeric and metallic implant materials in vitro and in a murine model of fracture-related infection," *J. Biomed. Res. B*, vol. 107, no. 4, pp. 1095–1106, 2018.

[3] F. Stuart B. Goodman, Zhenyu Yao, Michael Keeney, "The Future of Biologic Coatings for Orthopaedic Implants Stuart," *Biomaterials*, vol. 34, no. 13, pp. 3174–3183, 2013.

[4] I. Munaweera *et al.*, "Temperature-sensitive liposomal ciprofloxacin for the treatment of biofilm on infected metal implants using alternating magnetic fields," *Int. J. Hyperth.*, vol. 34, no. 2, pp. 189–200, 2018.

[5] M. Zilberman and J. J. Elsner, "Antibiotic-eluting medical devices for various applications," *J. Control. Release*, vol. 130, no. 3, pp. 202–215, 2008.

[6] S. K. Nandi, P. Mukherjee, S. Roy, B. Kundu, D. K. De, and D. Basu, "Local antibiotic delivery systems for the treatment of osteomyelitis - A review," *Mater. Sci. Eng. C*, vol. 29, no. 8, pp. 2478–2485, 2009.

[7] J. Li and D. J. Mooney, "Designing hydrogels for controlled drug delivery," *Nat. Publ. Gr.*, vol. 1, pp. 1–18, 2016.

[8] S. Garazzino *et al.*, "Ceftriaxone bone penetration in patients with septic non-union of the tibia," *Int. J. Infect. Dis.*, vol. 15, no. 6, pp. 793–805, 2011.

[9] C. R. Arciola and D. Campoccia, "Implant infections: adhesion, biofilm formation and immune evasion," *Nat. Rev. Microbiol.*, vol. 16, no. July, 2018.

[10] A. C. W. Farnsworth, E. M. Schott, A. M. Benvie, and R. A. Mooney, "Obesity/type 2 diabetes increases inflammation, periosteal reactive bone formation and osteolysis during Staphylococcus aureus implant-associated bone infection," *J. Orthop. Res.*, vol. 36, no. 6, pp. 1614–1623, 2018.

[11] A. Sousa, A. Carvalho, C. Pereira, E. Reis, and A. C. Santos, "Economic Impact of Prosthetic Joint Infection – an Evaluation Within the Portuguese National Health System," *J. Bone Jt. Infect.*, vol. 3, no. 4, pp. 197–202, 2018.

[12] R. Gupta and A. Kumar, "Bioactive materials for biomedical applications using sol-gel technology," *Biomed. Mater.*, vol. 3, no. 3, 2008.

[13] A. P. Gomes, J. F. Mano, J. A. Queiroz, and I. C. Gouveia, "Layer-by-layer deposition of antimicrobial polymers on cellulosic fibers: A new strategy to develop bioactive textiles," *Polym. Adv. Technol.*, vol. 24, no. 11, pp. 1005–1010, 2013.

[14] M. Cicuéndez, J. C. Doadrio, A. Hernández, M. T. Portolés, I. Izquierdo-Barba, and M. Vallet-Regí, "Multifunctional pH sensitive 3D scaffolds for treatment and prevention of bone infection," *Acta Biomater.*, vol. 65, pp. 450–461, 2018.

[15] B. Love, "Metallic Biomaterials," in *Biomaterials*, 1st ed., Elsevier Ltd, 2017, pp. 159–184.

[16] A. Bettencourt and A. J. Almeida, "Poly (methyl methacrylate) particulate carriers in drug delivery," *J. Microencapsul.*, vol. 29, no. 4, pp. 353–367, 2012.

[17] N. V. Majeti and M. N. V. R. Kumar, "A review of chitin and chitosan applications," *React. Funct. Polym.*, vol. 46, no. 2000, pp. 1–27, 2000.

[18] Laurence Mckeen, "Renewable Resource and Biodegradable Polymers," in *The Effect of Sterilization on Plastics and Elastomers*, 4th ed., J. Bayliss, Ed. Chennai, India: Elsevier Inc., 2012, pp. 305–317.

[19] D. Kahne, C. Leimkuhler, W. Lu, and C. Walsh, "Glycopeptide and lipoglycopeptide antibiotics," *Chem. Rev.*, vol. 105, no. 2, pp. 425–448, 2005.

[20] M. Bruniera, F.R. Ferreira, F.M. Saviolli, L.R.M Bacci, M.R. Feder, D. Da Luz Gonçalves Pedreira, "The use of vancomycin with its therapeutic and adverse effects : a review," *Eur. Rev. Med. Pharmacol. Sci.*, vol. 19, pp. 694–700, 2015.

[21] M. Bulwan, K. Wójcik, S. Zapotoczny, and M. Nowakowska, "Chitosan-based ultrathin films as antifouling, anticoagulant and antibacterial protective coatings," *J. Biomater. Sci. Polym. Ed.*,

vol. 23, no. 15, pp. 1963–1980, 2012.
[22] P. D. P. Lew and P. F. A. Waldvogel, “Osteomyelitis,” *Lancet*, vol. 364, no. 9431, pp. 369–379, 2004.
[23] S. Daghighi, J. Sjollema, H. C. Van Der Mei, H. J. Busscher, and E. T. J. Rochford, “Biomaterials Infection resistance of degradable versus non-degradable biomaterials : An assessment of the potential mechanisms,” *Biomaterials*, vol. 2013, pp. 1–5, 2013.
[24] A. Lamberet *et al.*, “Postoperative Spinal Implant Infections in Children,” *Pedriatic Infect. Dis. J.*, vol. 37, no. 6, pp. 511–513, 2018.
[25] I. P. Stefan Renvert, “Treatment of pathologic peri-implant pockets,” *Peridontology 2000*, vol. 76, pp. 180–190, 2018.
[26] S. Vasoo and M. Dudareva, “crossm Improving the Diagnosis of Orthopedic Implant-Associated Infections : Optimizing the Use of Tools Already in the Box,” *J. Clin. Microbiol.*, vol. 56, no. 12, pp. 10–14, 2018.
[27] S. A. Lopes, “A biodegradable PLGA – coating releasing DNase I to prevent bacterial adhesion and biofilm formation,” Universidade do Minho, 2015.
[28] L. G. Harris and R. G. Richards, “Staphylococci and implant surfaces : a review,” *Injury*, vol. 37, pp. 3–14, 2006.
[29] J. Barros *et al.*, “International Journal of Antimicrobial Agents Enterococcus faecalis and Escherichia coli isolates from orthopaedic implant-associated infections,” *Int. J. Antimicrob. Agents*, vol. 54, no. 3, pp. 329–337, 2019.
[30] N. J. Hickok, I. M. Shapiro, and A. F. Chen, “The Impact of Incorporating Antimicrobials into Implant Surfaces,” *J. Dent. Res.*, vol. 97, no. 1, pp. 14–22, 2018.
[31] P. C. Munasinghe and S. K. Khanal, “Biomass-derived syngas fermentation into biofuels,” *Biofuels*, vol. 101, no. 13, pp. 79–98, 2011.
[32] A. Roguska, A. Belcarz, J. Zalewska, and M. Holdynski, “Metal TiO 2 nanotube layers for the treatment of dental implant infections,” *Appl. Mater. Interfaces*, vol. 10, no. 11, pp. 17089–17099, 2018.
[33] A. S. Kranthi, T. S. S. Kumar, G. Perumal, and R. Sanghavi, “Progress in Organic Coatings Dual nano fi brous bioactive coating and antimicrobial surface treatment for infection resistant titanium implants,” *Prog. Org. Coatings*, vol. 121, no. October 2017, pp. 112–119, 2018.
[34] D. Inoue, T. Kabata, Y. Kajino, T. Shirai, and H. Tsuchiya, “Iodine-supported titanium implants have good antimicrobial attachment effects,” *J. Orthop. Sci.*, vol. 24, pp. 548–551, 2019.
[35] L. Tan *et al.*, “Rapid Biofilm Eradication on Bone Implants Using Red Phosphorus and Near-Infrared Light,” *Adv. Mater.*, vol. 30, no. 31, pp. 1–10, 2018.
[36] S. Lenoir, C. Pagnoulle, M. Galleni, P. Compe, and R. Je, “Polyolefin Matrixes with Permanent Antibacterial Activity : Preparation , Antibacterial Activity , and Action Mode of the Active Species 4000 Lie,” *Biomacromolecules*, vol. 7, no. 8, pp. 2291–2296, 2006.
[37] L. Cen, K. G. Neoh, and E. T. Kang, “Surface Functionalization Technique for Conferring Antibacterial Properties to Polymeric and Cellulosic Surfaces,” *Langmuir*, vol. 19, no. 14, pp. 10295–10303, 2003.
[38] S. T. Susmita Bose, “Calcium phosphate ceramic systems in growth factor and drugdelivery for bone tissue engineering: A review,” *Acta Biomater*, vol. 8, no. 4, pp. 1401–1421, 2012.
[39] M. Pfeiffer, E. Scholl, and B. S. Gmbh, “Comparative investigation of drug delivery of collagen implants saturated in antibiotic solutions and a sponge containing gentamicin,” *Biomaterials*, vol. 17, no. 17, pp. 1733–1738, 1996.
[40] H. Gollwitzer, K. Ibrahim, H. Meyer, W. Mittelmeier, R. Busch, and A. Stemberger, “Antibacterial poly (D , L -lactic acid) coating of medical implants using a biodegradable drug delivery technology,” *J. Antimicrob. Chemother.*, vol. 51, no. 3, pp. 585–591, 2003.
[41] J. L. Bourges *et al.*, “Intraocular implants for extended drug delivery : Therapeutic applications ☆,” *Adv. Drug Deliv. Rev.*, vol. 58, no. 11, pp. 1182–1202, 2006.
[42] K. Park, “The Controlled Drug Delivery Systems: Past Forward and Future Back,” *J. Control. Release*, 2014.
[43] A. Woischnig *et al.*, “Acrylic microparticles increase daptomycin intracellular and in vivo anti-biofilm activity against Staphylococcus aureus Laboratory of Infection Biology , Department of

Biomedicine , University and," *Int. J. Pharm.*, 2018.
[44] I. Santos, A. Bettencourt, B. Bétrisey, L. M. D. Gonçalves, A. Trampuz, and A. J. Almeida, "Improvement of the antibacterial activity of daptomycin-loaded polymeric microparticles by Eudragit RL 100 : An assessment by isothermal microcalorimetry," *Int. J. Pharm.*, vol. 485, no. 1–2, pp. 171–182, 2015.
[45] M. P. Ginebra, C. Canal, M. Espanol, D. Pastorino, and E. B. Montufar, "Calcium phosphate cements as drug delivery materials," *Adv. Drug Deliv. Rev.*, vol. 64, no. 12, pp. 1090–1110, 2012.
[46] B. Li, X. Liu, F. Meng, J. Chang, and C. Ding, "Preparation and antibacterial properties of plasma sprayed nano-titania/silver coatings," *Mater. Chem. Phys.*, vol. 118, no. 1, pp. 99–104, 2009.
[47] V. Stranak *et al.*, "Deposition of thin titanium-copper films with antimicrobial effect by advanced magnetron sputtering methods," *Mater. Sci. Eng. C*, vol. 31, no. 7, pp. 1512–1519, 2011.
[48] M. Catauro, F. Bollino, P. Veronesi, and G. Lamanna, "Influence of PCL on mechanical properties and bioactivity of ZrO 2-based hybrid coatings synthesized by sol-gel dip coating technique," *Mater. Sci. Eng. C*, vol. 39, no. 1, pp. 344–351, 2014.
[49] M. Catauro, F. Papale, and F. Bollino, "Characterization and biological properties of TiO2/PCL hybrid layers prepared via sol-gel dip coating for surface modification of titanium implants," *J. Non. Cryst. Solids*, vol. 415, pp. 9–15, 2015.
[50] D. Grosso and P. Marie, "How to exploit the full potential of the dip-coating process to better control film formation," *J. Mater. Chem.*, vol. 21, no. 17033, pp. 17033–17038, 2011.
[51] J. Puetz and M. A. Aegerter, "Dip Coatinng Technique," in *Sol-Gel Technologies for Glass Producers and Users*, 1st ed., M. Aegerter, Michel A., Mennig, Ed. New York: Springer US, 2004, pp. 37–48.
[52] C. J. Brinker, "Dip Coating," in *Chemical Solution Deposition of Functional Oxide Thin Films*, 1st ed., T. Schneller, R. Waser, M. Kosec, and D. Payne, Eds. Vienna: Springer-Verlag Wien, 2013, pp. 233–261.
[53] T. Li, J. Lee, T. Kobayshi, and H. Aoki, "Hydroxyapatite coating by dipping method, and bone bonding strength," *J. Mater. Sci. Mater. Med.*, vol. 7, no. 6, pp. 355–357, 1996.
[54] C. Hanyaloglu and B. Aksakal, "Bioceramic dip-coating on Ti – 6Al – 4V and 316L SS implant materials," *J. Mater. Sci. Mater. Med.*, vol. 19, no. 5, pp. 2097–2104, 2008.
[55] M. Khalid, M. Mujahid, A. N. Khan, and R. S. Rawat, "Dip Coating of Nano Hydroxyapatite on Titanium Alloy with Plasma Assisted g -Alumina Buffer Layer : A Novel Coating Approach," *J. Mater. Sci. Technol.*, vol. 29, no. 6, pp. 557–564, 2013.
[56] R. Du *et al.*, "Design and testing of hydrophobic core / hydrophilic shell nano / micro particles for drug-eluting stent coating," *NPG Asia Mater.*, vol. 10, pp. 642–658, 2018.
[57] H. Ai, S. A. Jones, and Y. M. Lvov, "Biomedical Applications of Electrostatic Layer-by-Layer Nano-Assembly of Polymers , Enzymes , and Nanoparticles," *Cell Biochem. Biophys.*, vol. 39, no. 1, pp. 23–43, 2003.
[58] M. L. Macdonald, R. E. Samuel, N. J. Shah, R. Padera, M. Yvette, and P. T. Hammond, "Tissue Integration of Growth Factor-Eluting Layer-by-Layer Polyelectrolyte Multilayer Coated Implants," *Biomaterials*, vol. 32, no. 5, pp. 1446–1453, 2012.
[59] K. C. Wood, J. Q. Boedicker, D. M. Lynn, and P. T. Hammond, "Tunable Drug Release from Hydrolytically Degradable Layer-by-Layer Thin Films," *Langmuir*, vol. 21, no. 10, pp. 1603–1609, 2005.
[60] T. Wei, Z. Tang, Q. Yu, and H. Chen, "Smart Antibacterial Surfaces with Switchable Bacteria-Killing and Bacteria-Releasing Capabilities," *Appl. Mater. Interfaces*, vol. 9, no. i, pp. 37511–37523, 2017.
[61] Q. Zeng, Y. Zhu, B. Yu, and Y. Sun, "Antimicrobial and Antifouling Polymeric Agents for Surface Functionalization of Medical Implants Antimicrobial and Antifouling Polymeric Agents for Surface Functionalization of Medical Implants," *Biomacromolecules*, 2018.
[62] R. K. Singh Raman and S. E. Harandi, "Resistance of Magnesium Alloys to Corrosion Fatigue for Biodegradable Implant Applications : Current Status and Challenges," *Materials (Basel).*, vol. 10, no. 1316, pp. 1–11, 2017.

[63] J. Walczak, F. Shahgaldi, and F. Heatley, “In vivo corrosion of 316L stainless-steel hip implants : morphology and elemental compositions of corrosion products,” *Biomaterials*, vol. 19, no. 1998, pp. 229–237, 1998.
[64] J. T. Capo, T. Kinchelow, K. Brooks, V. Tan, M. Manigrasso, and K. Francisco, “Biomechanical Stability of Four Fixation Constructs for Distal Radius Fractures,” *Am. Assoc. Hand Surg.*, vol. 4, pp. 272–278, 2009.
[65] U. Ali, K. Juhanni, B. Abd, and N. A. Buang, “A Review of the Properties and Applications of Poly (Methyl Methacrylate) (PMMA),” *Polym. Rev.*, vol. 19, no. 28, pp. 37–41, 2015.
[66] S. Ramakrishna, J. Mayer, E. Wintermantel, and K. W. Leong, “Biomedical applications of polymer-composite materials : a review,” *Compos. Sci. Technol.*, vol. 61, no. 9, pp. 1189–1224, 2001.
[67] L. Muzquiz-Ramos, EM and Guerrero-Chavez, V and Macias-Martinez, BI and Lopez-Badillo, CM and Garcia-Cerda, “Synthesis and characterization of maghemite nanoparticles for hyperthermia,” *Ceram. Int.*, vol. 41, no. 1, pp. 397–402, 2015.
[68] S. Luo, T. Jiang, Y. Yang, X. Yang, and J. Zhao, “Combination therapy with vancomycin-loaded calcium sulfate and vancomycin- loaded PMMA in the treatment of chronic osteomyelitis,” *BMC Musculoskelet. Disord.*, pp. 1–12, 2016.
[69] W. N. Ayre, J. C. Birchall, S. L. Evans, and S. P. Denyer, “A novel liposomal drug delivery system for PMMA bone cements,” *Soc. Biomater.*, vol. 104B, no. 8, pp. 1510–1524, 2015.
[70] P. I. Sealy, C. Nguyen, M. Tucci, H. Benghuzzi, and J. D. Cleary, “Delivery of Antifungal Agents Using Bioactive and Nonbioactive Bone Cements RESULTS :,” *Ann. Pharmacother.*, vol. 43, pp. 1606–1615, 2009.
[71] S. J. Kim *et al.*, “The Potential Role of Polymethyl Methacrylate as a New Packaging Material for the Implantable Medical Device in the Bladder,” *Biomed Res. Int.*, vol. 2015, pp. 1–8, 2015.
[72] J. Li, H. Wang, Q. Guo, C. Zhu, X. Zhu, and F. Han, “Multifunctional Coating to Simultaneously Encapsulate Drug and Prevent Infection of Radiopaque Agent,” *Int. J. Mol. Sci.*, vol. 20, no. 2055, pp. 1–17, 2019.
[73] J. Drobnik, I. Krucinska, A. Komisarczyk, S. Sporny, A. Szczepanowska, and J. Ciosek, “Effects of electrospun scaffolds of di-O-butyrylchitin and poly-(ε-caprolactone) on wound healing,” *Neuropept. Res.*, vol. 60, no. 3, pp. 162–171, 2017.
[74] K. L. Shantha, U. Bala, and P. Rao, “Tailor-made chitosans for drug delivery,” *Eur. Polym. J.*, vol. 31, no. 4, pp. 377–382, 1995.
[75] S. H. Kas, “Chitosan: properties, preparations and application to microparticulate systems,” *J. Microencapsul.*, vol. 14, no. 6, pp. 689–711, 1997.
[76] M. R. Leedy, H. J. Martin, P. A. Norowski, J. A. Jennings, W. O. Haggard, and J. D. Bumgardner, “Use of Chitosan as a Bioactive Implant Coating for Bone-Implant Applications,” *Adv. Polym. Sci.*, vol. 244, no. April, 2011.
[77] U. Edlund and A. Albertsson, “Degradable Polymer Microspheres for Controlled Drug Delivery,” *Adv. Polym. Sci.*, vol. 157, pp. 68–112, 2002.
[78] J. Xue *et al.*, “Drug loaded homogeneous electrospun PCL/gelatin hybrid nanofiber structures for anti-infective tissue regeneration membranes,” *Biomaterials*, vol. 35, no. 34, pp. 9395–9405, 2014.
[79] P. J. Stogios and A. Savchenko, “Molecular mechanisms of vancomycin resistance,” *Protein Sci.*, vol. 29, no. 3, pp. 654–669, 2020.
[80] M. Schäfer, T. R. Schneider, and G. M. Sheldrick, “Crystal structure of vancomycin,” *Structure*, vol. 4, no. 12, pp. 1509–1515, 1996.
[81] L. Mendez-vigo and D. A. K. Rice, “Daptomycin in bone and joint infections : a review of the literature,” *Arch. Orthop. Trauma Surg.*, vol. 129, pp. 1495–1504, 2009.
[82] J. N. Steenbergen, J. Alder, G. M. Thorne, and F. P. Tally, “Daptomycin: A lipopeptide antibiotic for the treatment of serious Gram-positive infections,” *J. Antimicrob. Chemother.*, vol. 55, no. 3, pp. 283–288, 2005.
[83] D. Jung, A. Rozek, M. Okon, and R. E. W. Hancock, “Structural Transitions as Determinants of the Action of the Calcium-Dependent Antibiotic Daptomycin,” *Chem. Biol.*, vol. 11, no. 7, pp. 949–957, 2004.
[84] K. L. Tedesco and M. J. Rybak, “Daptomycin,” *Pharmacotherapy*, vol. 24, no. 1, pp. 41–57,

2003.
[85] E. Łyczkowska-Widłak, P. Lochyński, and G. Nawrat, “Electrochemical polishing of austenitic stainless steels,” *Materials (Basel).*, vol. 13, no. 11, pp. 1–25, 2020.
[86] M. S. Hadi, S. N. Saud, E. Hamzah, and M. F. Mamat, “Hydrogen embrittlement of 316L stainless steels exposed in 1.0m hydrochloric acid solution,” *Ann. Chim. Sci. des Mater.*, vol. 43, no. 6, pp. 369–375, 2019.
[87] A. Lati, M. Imani, M. Taghi, and M. Daliri, “Electrochemical and chemical methods for improving surface characteristics of 316L stainless steel for biomedical applications,” *Surf. Coat. Technol.*, vol. 221, no. 2013, pp. 1–12, 2013.
[88] M. J. Booth, “Adaptive optical microscopy: The ongoing quest for a perfect image,” *Light Sci. Appl.*, vol. 3, no. November 2013, pp. 1–7, 2014.
[89] N. A. Geisse, “AFM and combined optical techniques,” *Mater. Today*, vol. 12, no. 7–8, pp. 40–45, 2009.
[90] M. Abd Mutalib, M. A. Rahman, M. H. D. Othman, A. F. Ismail, and J. Jaafar, *Scanning Electron Microscopy (SEM) and Energy-Dispersive X-Ray (EDX) Spectroscopy*. Elsevier B.V., 2017.
[91] M. A. De Moraes, C. F. Da Silva, and R. S. Vieira, *Biopolymer Membranes and Films: Health, Food, Environment, and Energy Applications*. Elsevier Science, 2020.
[92] A. M. Wokovich, S. Prodduturi, W. H. Doub, A. S. Hussain, and L. F. Buhse, “Transdermal drug delivery system (TDDS) adhesion as a critical safety, efficacy and quality attribute,” *Eur. J. Pharm. Biopharm.*, vol. 64, no. 1, pp. 1–8, 2006.
[93] C. D. Lee and E. Meng, “Mechanical properties of thin-film Parylene – metal – Parylene devices,” *Front. Med. Eng.*, vol. 1, no. September, pp. 1–14, 2015.
[94] K. M. Z. Hossain *et al.*, “Single Solvent-Based Film Casting Method for the Production of Porous Polymer Films,” *Macromol. Mater. Eng.*, vol. 303, no. 4, pp. 1–7, 2018.
[95] J. A. Jennings, “Controlling chitosan degradation properties in vitro and in vivo,” in *Chitosan Based Biomaterials: Volume 1: Fundamentals*, vol. 1, Elsevier, 2017, pp. 159–182.
[96] D. R. Rohindra, A. V Nand, and J. R. Khurma, “Swelling properties of chitosan hydrogels,” *South Pacific J. Nat. Sci.*, vol. 22, no. 1, pp. 32–35, 2004.
[97] A. Cüneyt Tas, “Synthesis of biomimetic Ca-hydroxyapatite powders at 37°C in synthetic body fluids,” *Biomaterials*, vol. 21, no. 14, pp. 1429–1438, 2000.
[98] B. Chatterjee, “Science and industry of electropolishing [Part 2),” *Galvanotechnik*, vol. 110, no. 2, pp. 255–262, 2019.
[99] C. C. Lin and C. C. Hu, “Electropolishing of 304 stainless steel: Surface roughness control using experimental design strategies and a summarized electropolishing model,” *Electrochim. Acta*, vol. 53, no. 8, pp. 3356–3363, 2008.
[100] M. Rezaee, L. C. Tsai, M. I. Haider, A. Yazdi, E. Sanatizadeh, and N. P. Salowitz, “Quantitative peel test for thin films/layers based on a coupled parametric and statistical study,” *Sci. Rep.*, vol. 9, no. 1, pp. 1–11, 2019.
[101] M. Bartnikowski, T. R. Dargaville, and D. W. Hutmacher, “Progress in Polymer Science Degradation mechanisms of polycaprolactone in the context of chemistry , geometry and environment,” vol. 96, pp. 1–20, 2019.
[102] A. Baranowska-Korczyc *et al.*, “Antimicrobial electrospun poly(ε-caprolactone) scaffolds for gingival fibroblast growth,” *RSC Adv.*, vol. 6, no. 24, pp. 19647–19656, 2016.
[103] A. Zając, J. Hanuza, M. Wandas, and L. Dymińska, “Determination of N-acetylation degree in chitosan using Raman spectroscopy,” *Spectrochim. Acta - Part A Mol. Biomol. Spectrosc.*, vol. 134, pp. 114–120, 2015.
[104] H. A. Willis, V. J. I. Zichy, and P. J. Hendra, “The laser-Raman and infra-red spectra of poly(methyl methacrylate),” *Polymer (Guildf).*, vol. 10, no. C, pp. 737–746, 1969.
[105] K. J. Thomas, M. Sheeba, V. P. N. Nampoori, C. P. G. Vallabhan, and P. Radhakrishnan, “Raman spectra of polymethyl methacrylate optical fibres excited by a 532 nm diode pumped solid state laser,” *J. Opt. A Pure Appl. Opt.*, vol. 10, no. 5, 2008.
[106] C. Assmann *et al.*, “Identification of vancomycin interaction with Enterococcus faecalis within 30 min of interaction time using Raman spectroscopy,” *Anal. Bioanal. Chem.*, vol. 407, no. 27, pp. 8343–8352, 2015.

[107] D. A. Gray and M. Wenzel, “More than a pore: A current perspective on the in vivo mode of action of the lipopeptide antibiotic daptomycin,” *Antibiotics*, vol. 9, no. 1, 2020.
[108] G. Zhu, X. Zhu, Q. Fan, and X. Wan, “Raman spectra of amino acids and their aqueous solutions,” *Spectrochim. Acta - Part A Mol. Biomol. Spectrosc.*, vol. 78, no. 3, pp. 1187–1195, 2011.
[109] H. Baishya, “Application of Mathematical Models in Drug Release Kinetics of Carbidopa and Levodopa ER Tablets,” *J. Dev. Drugs*, vol. 06, no. 02, pp. 1–8, 2017.
[110] C. Mircioiu *et al.*, “Mathematical modeling of release kinetics from supramolecular drug delivery systems,” *Pharmaceutics*, vol. 11, no. 3, 2019.
[111] C. Z. Bueno and Â. M. Moraes, “Influence of the incorporation of the antimicrobial agent polyhexamethylene biguanide on the properties of dense and porous chitosan-alginate membranes,” *Mater. Sci. Eng. C*, vol. 93, pp. 671–678, 2018.
[112] C. Y. Kuo, Y. Y. Chen, and S. Y. Lu, “A facile route to create surface porous polymer films via phase separation for antireflection applications,” *ACS Appl. Mater. Interfaces*, vol. 1, no. 1, pp. 72–75, 2009.

6 Appendixes

A. Absorbances and concentrations measured for EE and DL calculations

Table 6.1: Table representing the matrix of a well plate indicating the placement of the several samples for absorption measurements with solutions for calibration curves of yellow) Dap, purple) Van) with the respective concentrations of drug in each well (µg/mL), as well as the supernatant from the solutions of: blue) PMMA microspheres, red) PMMA-Van microspheres, green) PMMA-EUD microspheres, orange) PMMA-EUD-Dap microspheres and white) empty wells.

	1	2	3	4	5	6	7	8	9	10	11	12
A	1000	500	250	125	62.5	31.25	15.63	7.812	3.906	1.953	0.9766	0
B	1000	500	250	125	62.5	31.25	15.63	7.813	3.906	1.953	0.9766	0
C												
D												
E												
F												
G												
H												

Table 6.2: Absorbances measured at 230 nm for the supernatant after purification of all particle solutions obeying the matrix for sample distribution in a well plate described on table.

	1	**2**	**3**	**4**	**5**	**6**	**7**	**8**	**9**	**10**	**11**	**12**
A	3.14	3.38	3.33	2.29	1.21	0.77	0.45	0.29	0.21	0.20	0.17	0.10
B	3.50	3.50	3.50	3.50	2.08	1.13	0.67	0.40	0.25	0.21	0.16	0.11
C	3.50	3.50	3.50	3.50	3.50	3.50	2.35	2.37	2.38			
D	3.37	3.37	3.38	3.50	3.50	3.50	3.50	3.50	3.50			
E	1.64	1.54	1.56	1.53	1.61	1.58	2.67	3.50	2.06			
F	1.52	1.46	1.51	3.50	3.50	3.50	2.62	2.78	2.81			

Table 6.3: Absorbances measured at 260 nm for the supernatant after purification of all particle solutions obeying the matrix for sample distribution in a well plate described on table.

	1	**2**	**3**	**4**	**5**	**6**	**7**	**8**	**9**	**10**	**11**	**12**
A	3.45	3.28	2.01	0.88	0.46	0.30	0.19	0.13	0.11	0.12	0.11	0.07
B	2.78	1.16	0.68	0.44	0.24	0.17	0.15	0.11	0.09	0.11	0.09	0.08
C	2.06	1.83	1.92	2.80	2.85	2.91	1.24	1.25	1.29			
D	1.82	1.87	1.88	2.75	2.74	2.81	2.60	3.37	1.97			
E	0.74	0.74	0.75	0.72	0.76	0.74	0.95	1.29	0.73			
F	0.74	0.69	0.71	1.63	1.79	1.85	0.94	1.01	1.11			

Table 6.4: Absorbances measured at 280 nm for the supernatant after purification of all particle solutions obeying the matrix for sample distribution in a well plate described on table.

	1	**2**	**3**	**4**	**5**	**6**	**7**	**8**	**9**	**10**	**11**	**12**
A	3.50	2.14	1.23	0.55	0.30	0.21	0.14	0.10	0.09	0.10	0.10	0.07
B	3.50	2.02	1.15	0.70	0.36	0.23	0.17	0.12	0.09	0.10	0.08	0.07
C	1.67	1.47	1.55	2.96	3.20	3.21	1.04	1.05	1.08			
D	1.48	1.53	1.53	3.03	3.18	3.10	2.86	3.50	2.07			
E	0.65	0.64	0.64	0.62	0.65	0.64	0.68	0.93	0.53			
F	0.64	0.59	0.61	1.15	1.29	1.32	0.67	0.72	0.82			

Table 6.5: Absorbances measured at 365 nm for the supernatant after purification of all particle solutions obeying the matrix for sample distribution in a well plate described on table.

	1	**2**	**3**	**4**	**5**	**6**	**7**	**8**	**9**	**10**	**11**	**12**
A	2.566	1.579	0.942	0.429	0.24	0.165	0.118	0.083	0.078	0.084	0.077	0.058
B	0.111	0.065	0.057	0.07	0.055	0.06	0.063	0.055	0.054	0.073	0.053	0.059
C	0.73	0.642	0.67	0.781	0.783	0.816	0.447	0.453	0.469			
D	0.644	0.668	0.672	0.77	0.759	0.768	0.712	0.897	0.542			
E	0.286	0.279	0.283	0.269	0.289	0.279	0.443	0.618	0.348			
F	0.288	0.255	0.265	0.741	0.81	0.84	0.458	0.49	0.518			

Table 6.6: Concentrations measured at 230 nm for the supernatant after purification of all particle solutions obeying the matrix for sample distribution in a well plate described on table.

	1	**2**	**3**	**4**	**5**	**6**	**7**	**8**	**9**
C	0.170	0.170	0.170	0.170	0.171	0.170	0.139	0.139	0.140
D	0.081	0.081	0.081	0.081	0.081	0.081	0.081	0.081	0.081
E	0.081	0.079	0.079	0.079	0.080	0.080	0.098	0.113	0.088
F	0.079	0.079	0.080	0.114	0.114	0.114	0.099	0.102	0.103

Table 6.7: Concentrations measured at 260 nm for the supernatant after purification of all particle solutions obeying the matrix for sample distribution in a well plate described on table.

	1	**2**	**3**	**4**	**5**	**6**	**7**	**8**	**9**
C	0.028	0.028	0.028	0.029	0.029	0.029	0.027	0.027	0.027
D	0.028	0.028	0.028	0.029	0.029	0.029	0.029	0.029	0.028
E	0.028	0.028	0.028	0.028	0.029	0.028	0.030	0.032	0.028
F	0.028	0.028	0.028	0.034	0.035	0.036	0.030	0.030	0.031

Table 6.8: Concentrations measured at 280 nm for the supernatant after purification of all particle solutions obeying the matrix for sample distribution in a well plate described on table.

	1	**2**	**3**	**4**	**5**	**6**	**7**	**8**	**9**
C	0.040	0.040	0.040	0.045	0.046	0.046	0.038	0.038	0.038
D	0.040	0.040	0.040	0.046	0.046	0.046	0.045	0.048	0.042
E	0.036	0.036	0.036	0.036	0.036	0.036	0.036	0.037	0.036
F	0.036	0.036	0.036	0.038	0.039	0.039	0.036	0.037	0.037

Table 6.9: Concentrations measured at 365 nm for the supernatant after purification of all particle solutions obeying the matrix for sample distribution in a well plate described on table.

	1	**2**	**3**	**4**	**5**	**6**	**7**	**8**	**9**
E	0.011	0.011	0.011	0.011	0.011	0.011	0.012	0.012	0.012
F	0.011	0.011	0.011	0.013	0.013	0.013	0.012	0.012	0.012

B. Calibration curves obtained for DL and EE.

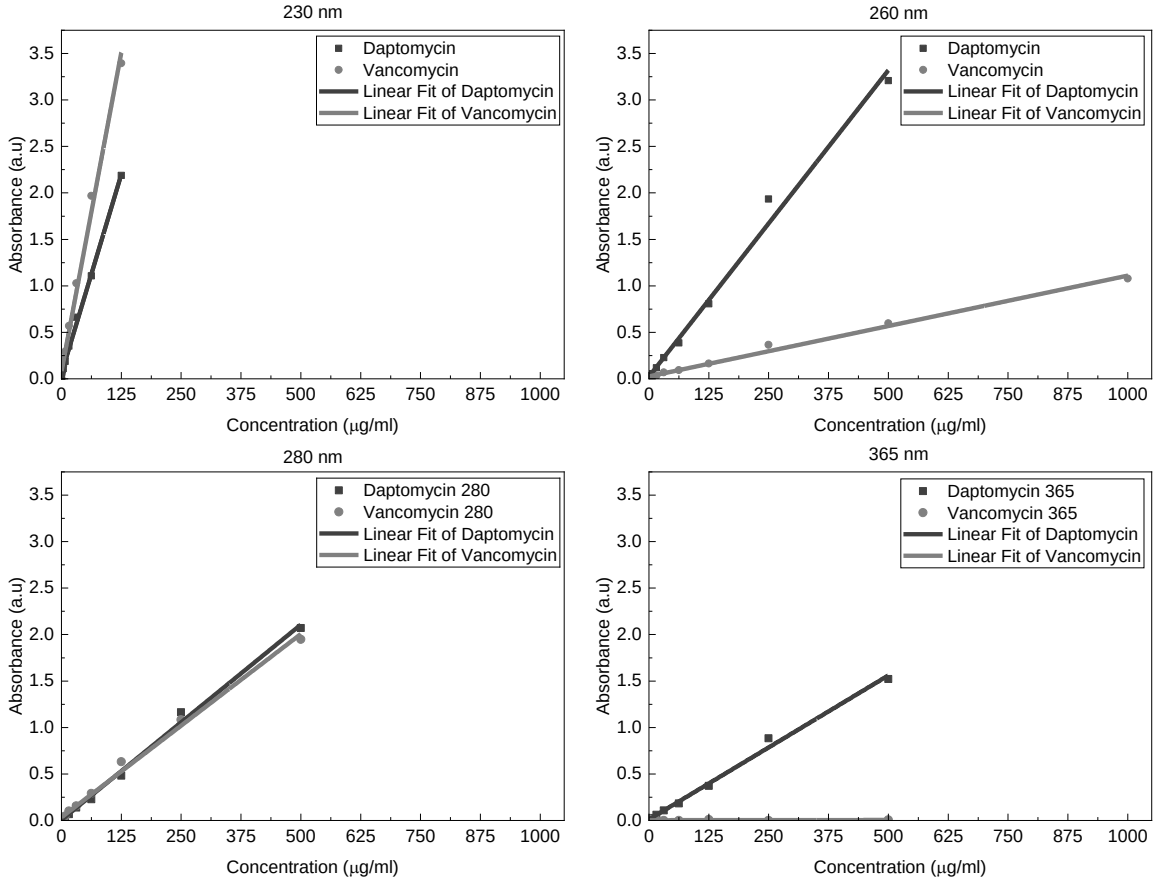

Figure 6.1: Calibration curves obtained for Dap (dark grey) and Van (light grey) at several wavelengths.

C. Histograms obtained for microsphere diameter

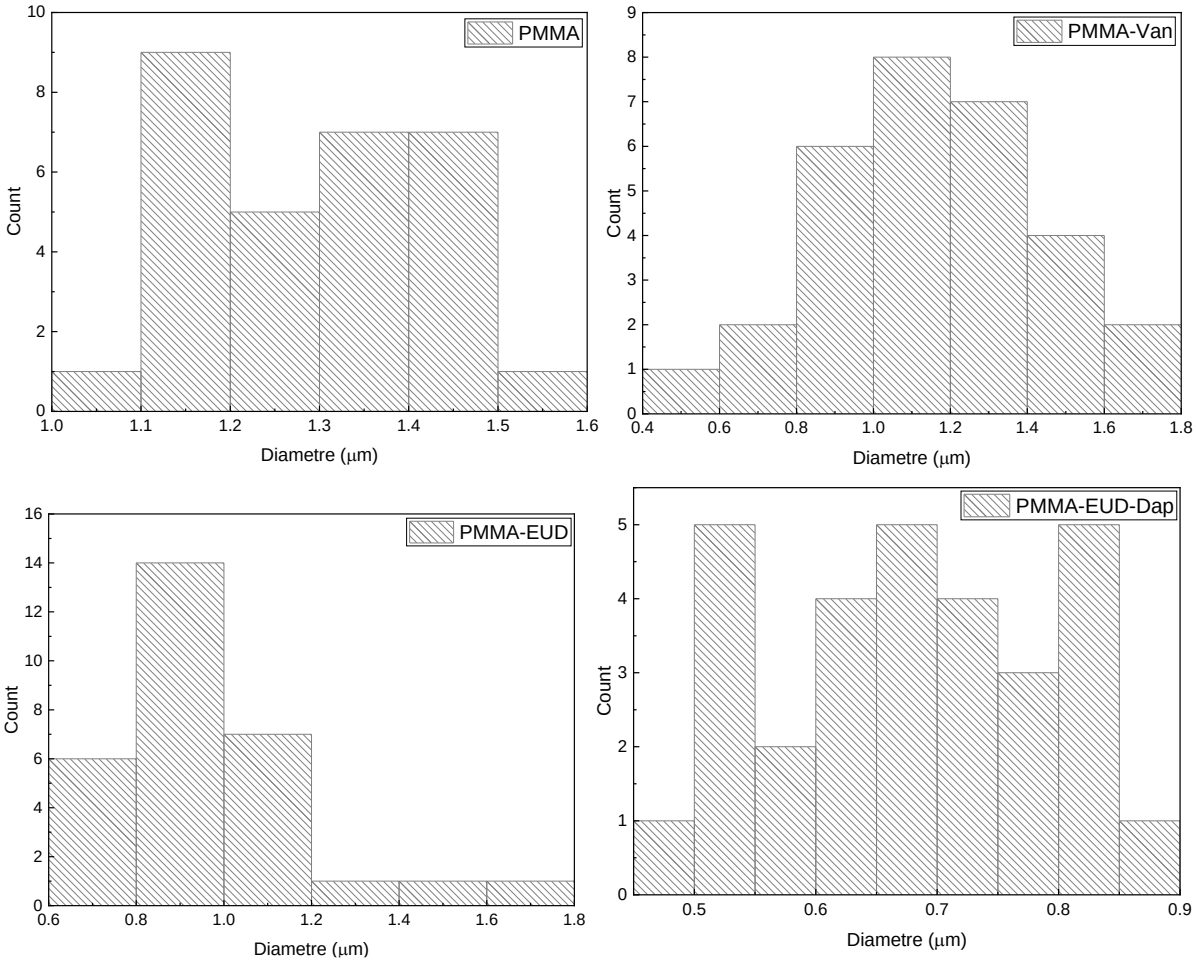

Figure 6.21: Histograms obtained for the average diameter values for PMMA, PMMA-EUD, PMMA-Van and PMMA-EUD-Dap spheres calculated using ImageJ software.

D. AFM 3D Maps

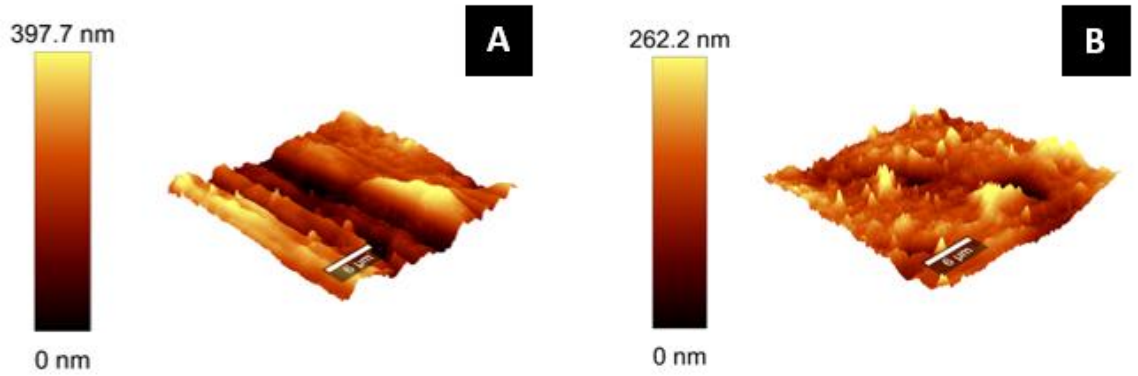

Figure 6.3: AFM images of a 316L-SS sample A) before and B) after an electropolishing step.

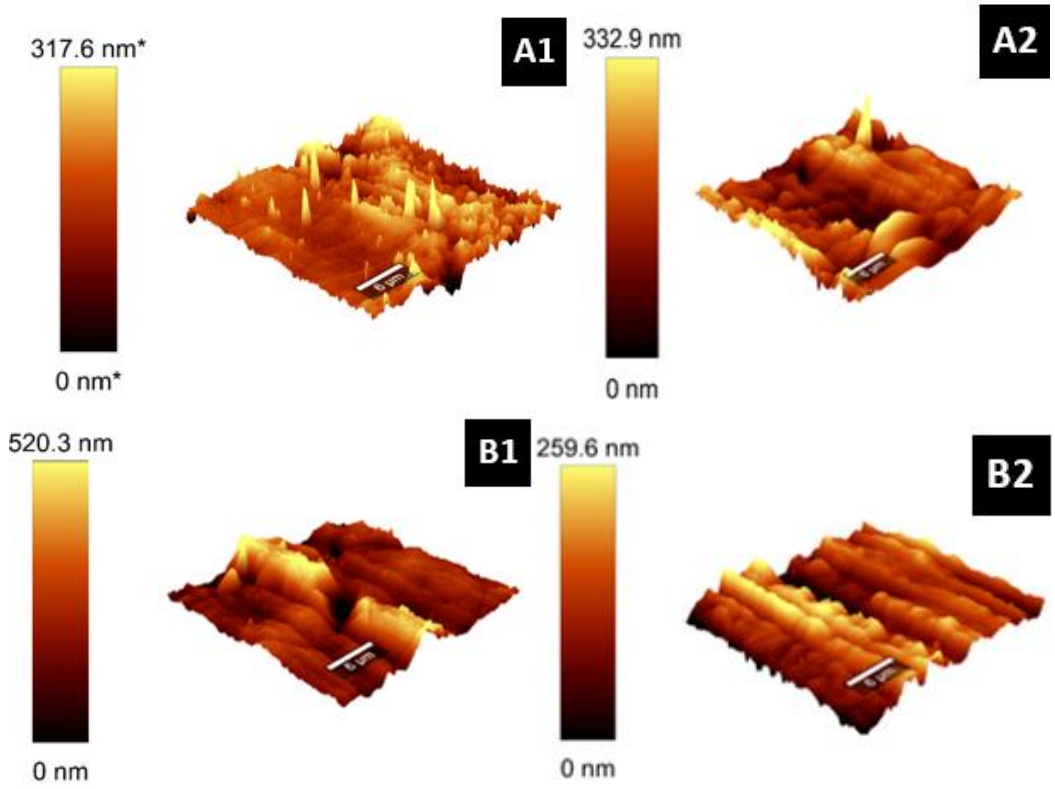
317.6 nm*
0 nm*
A1
332.9 nm
0 nm
A2
520.3 nm
0 nm
B1
259.6 nm
0 nm
B2

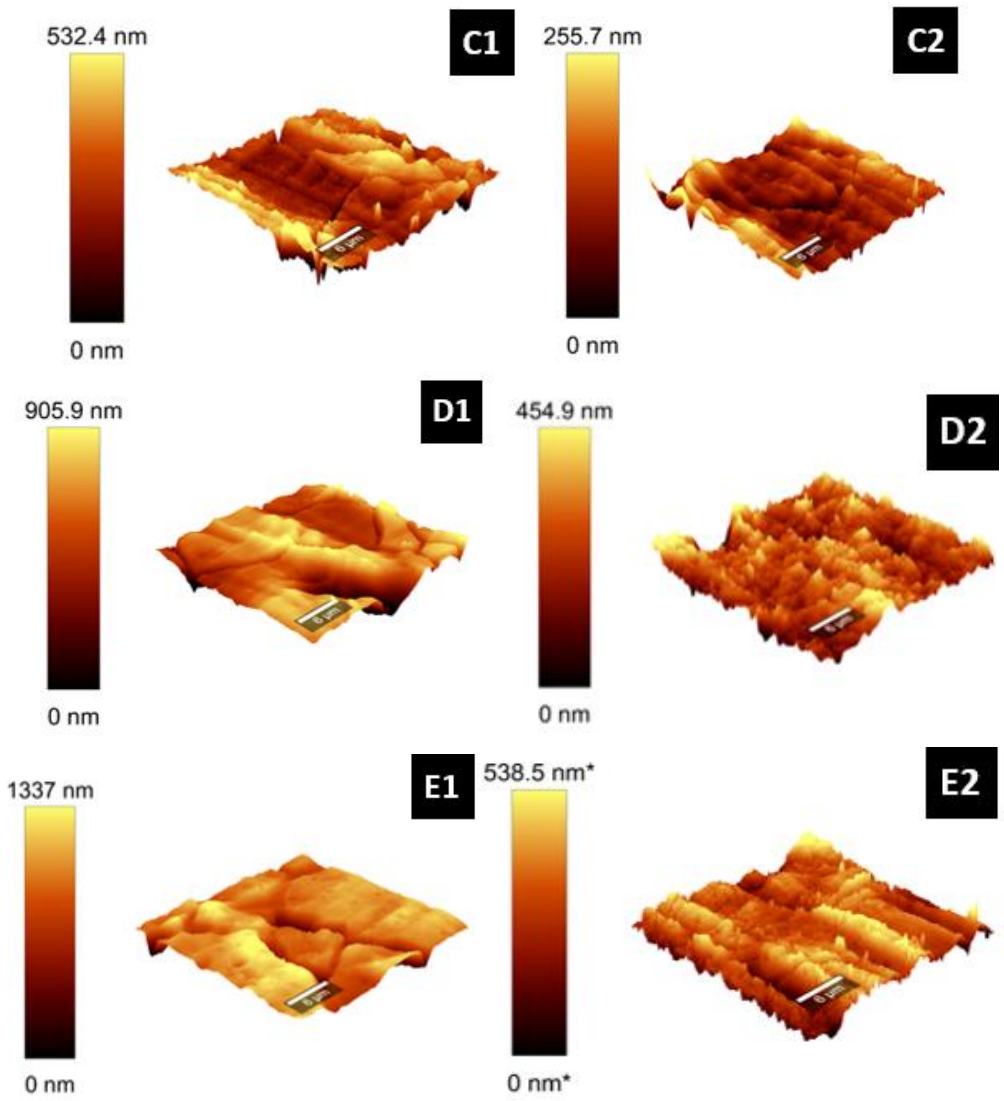

Figure 6.4: AFM 316L-SS immersed in HCl at concentrations of 1) 37 % v/v 2) 18.5 % v/v for a period of A) 30 min, B) 45 min, C) 1 h, D)1 h and 30 min, E) 2 h.

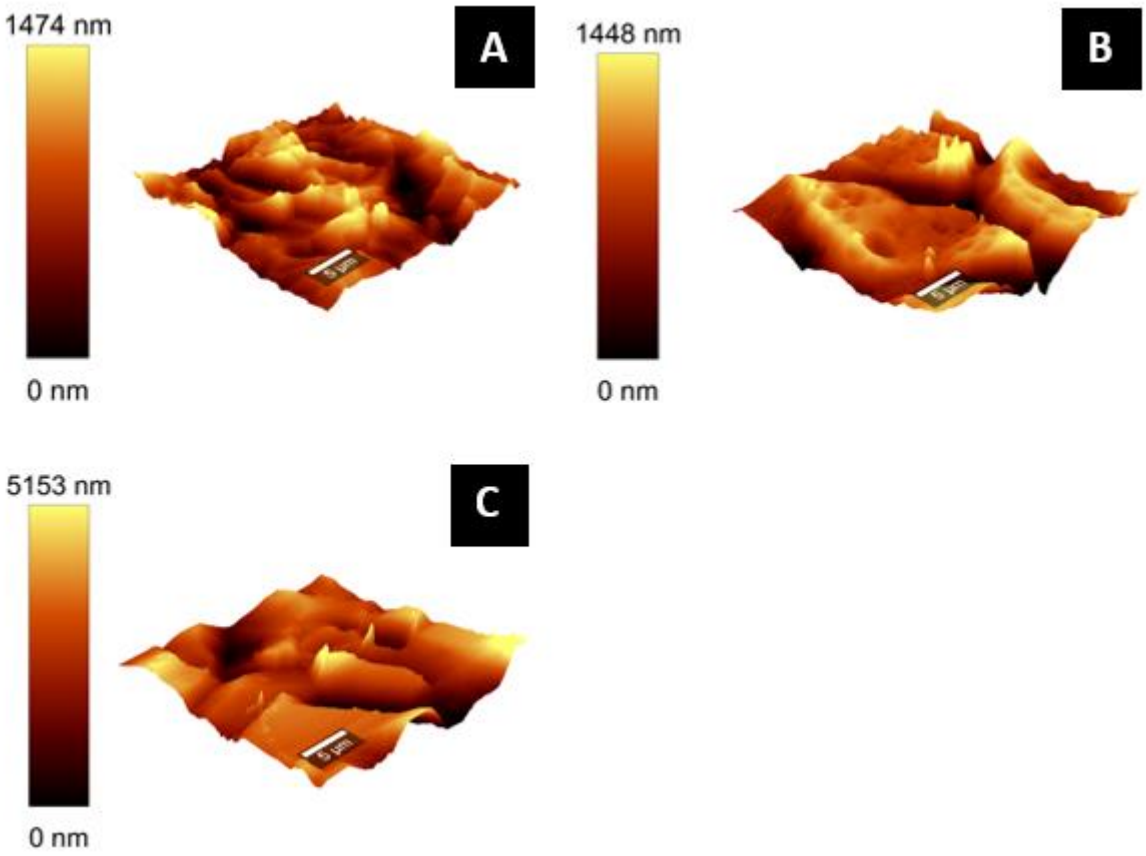

Figure 6.5: AFM 3D Maps obtained for 316L-SS treated by electrochemical etching with A) HCl, B) Piranha solution, C) H_2SO_4.

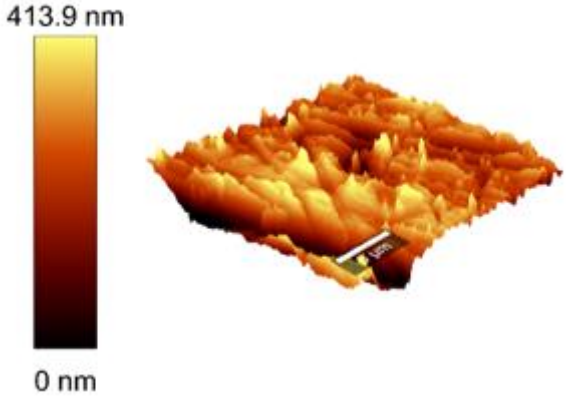

Figure 6.6: AFM 3D Maps obtained for 316L-SS treated by mechanical abrasion.

E. Histograms of the thickness obtained for 316L-SS treatments

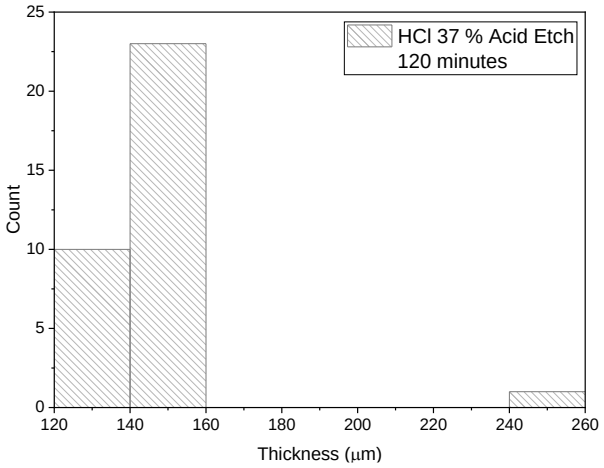

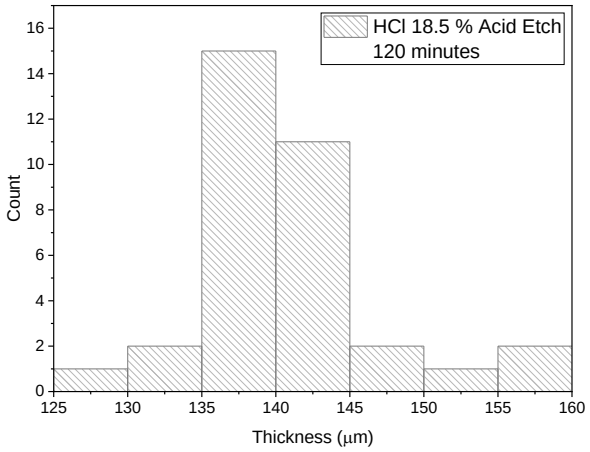

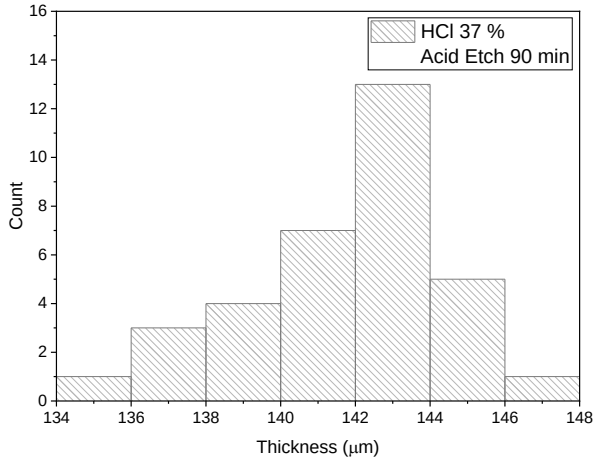

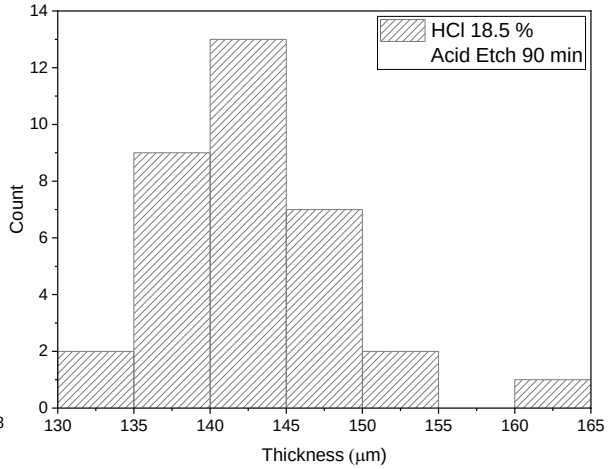

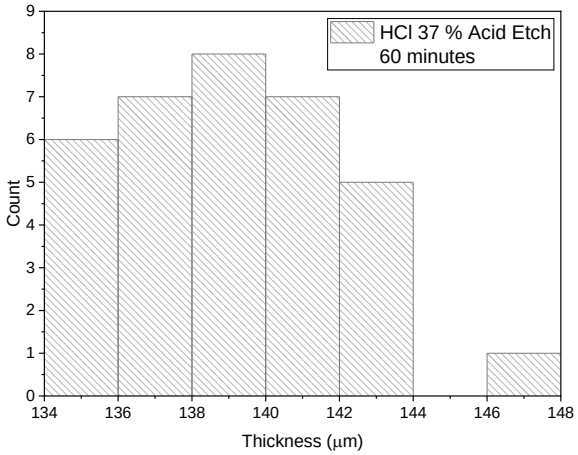

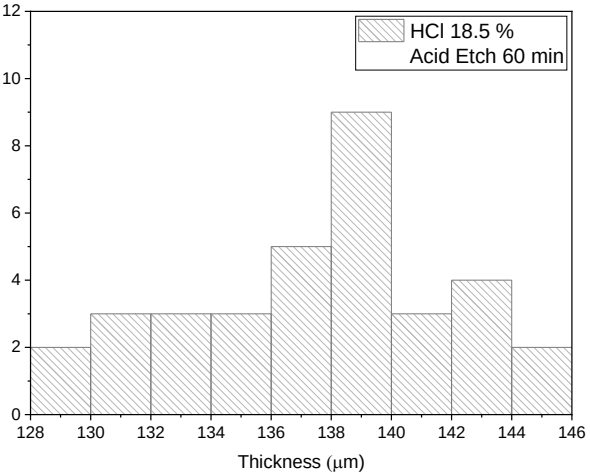

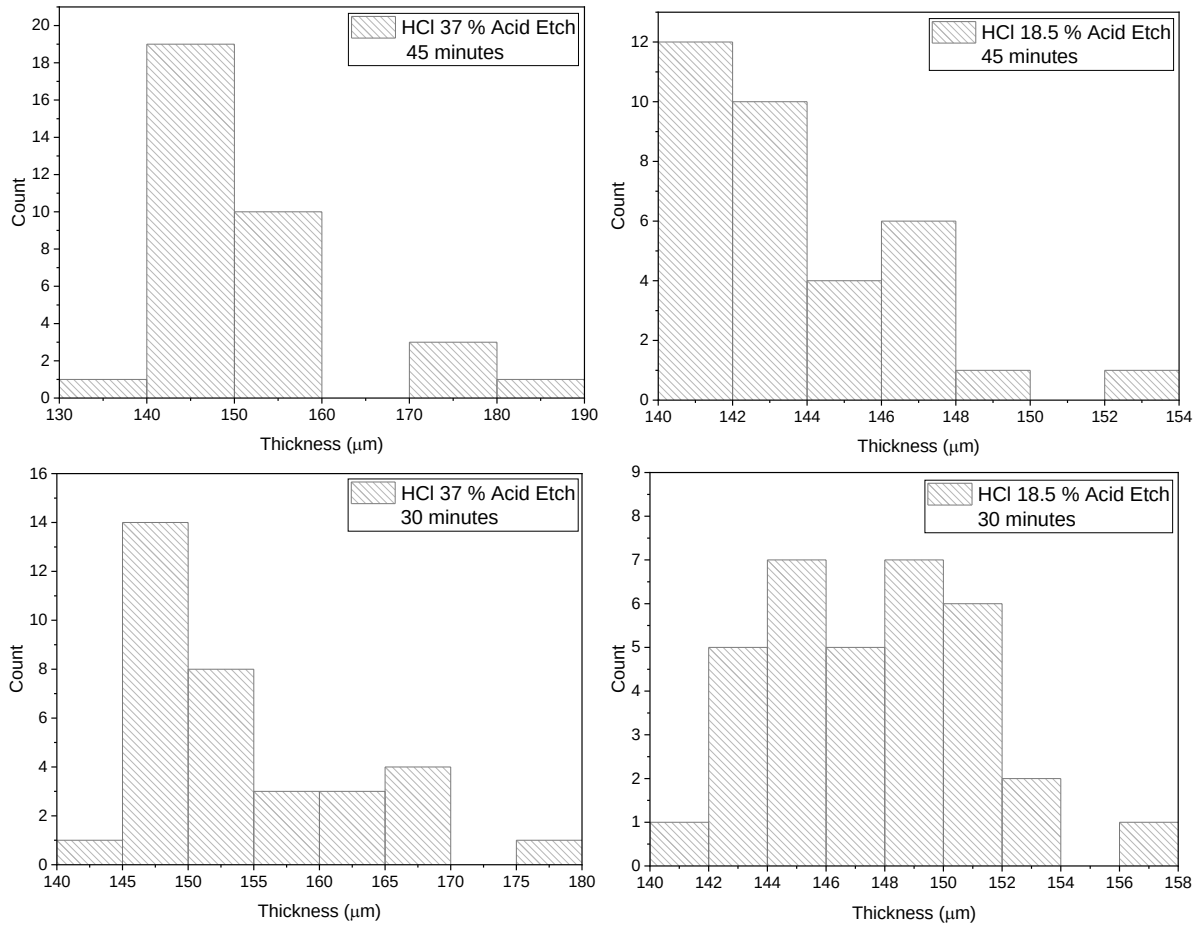

Figure 6.7: Histogram of the thickness values obtained for 316L-SS treated by acid etching with HCl.

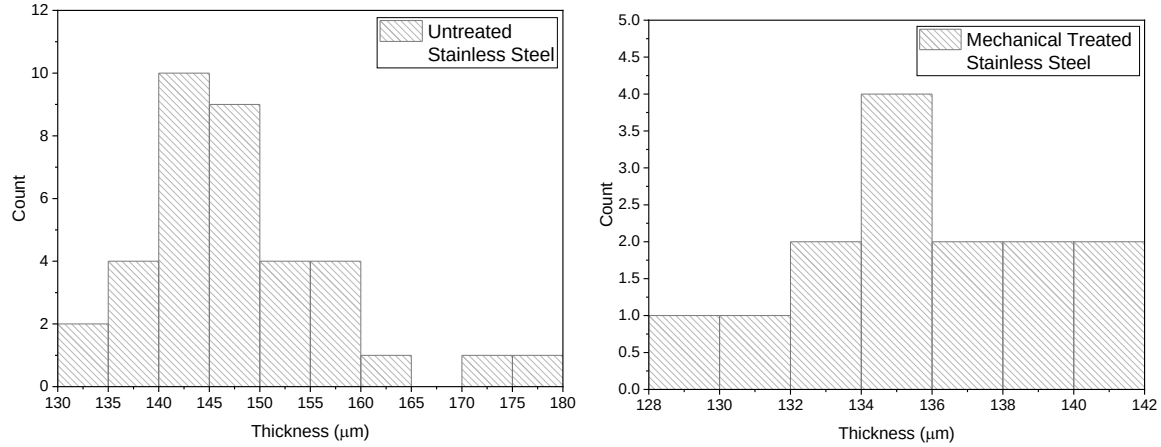

Figure 6.8: Histogram of the thickness values for untreated 316L-SS and 316L-SS treated by mechanical abrasion

F. SEM micrographs and EDS reports of Ti-6Al-4V after silanization.

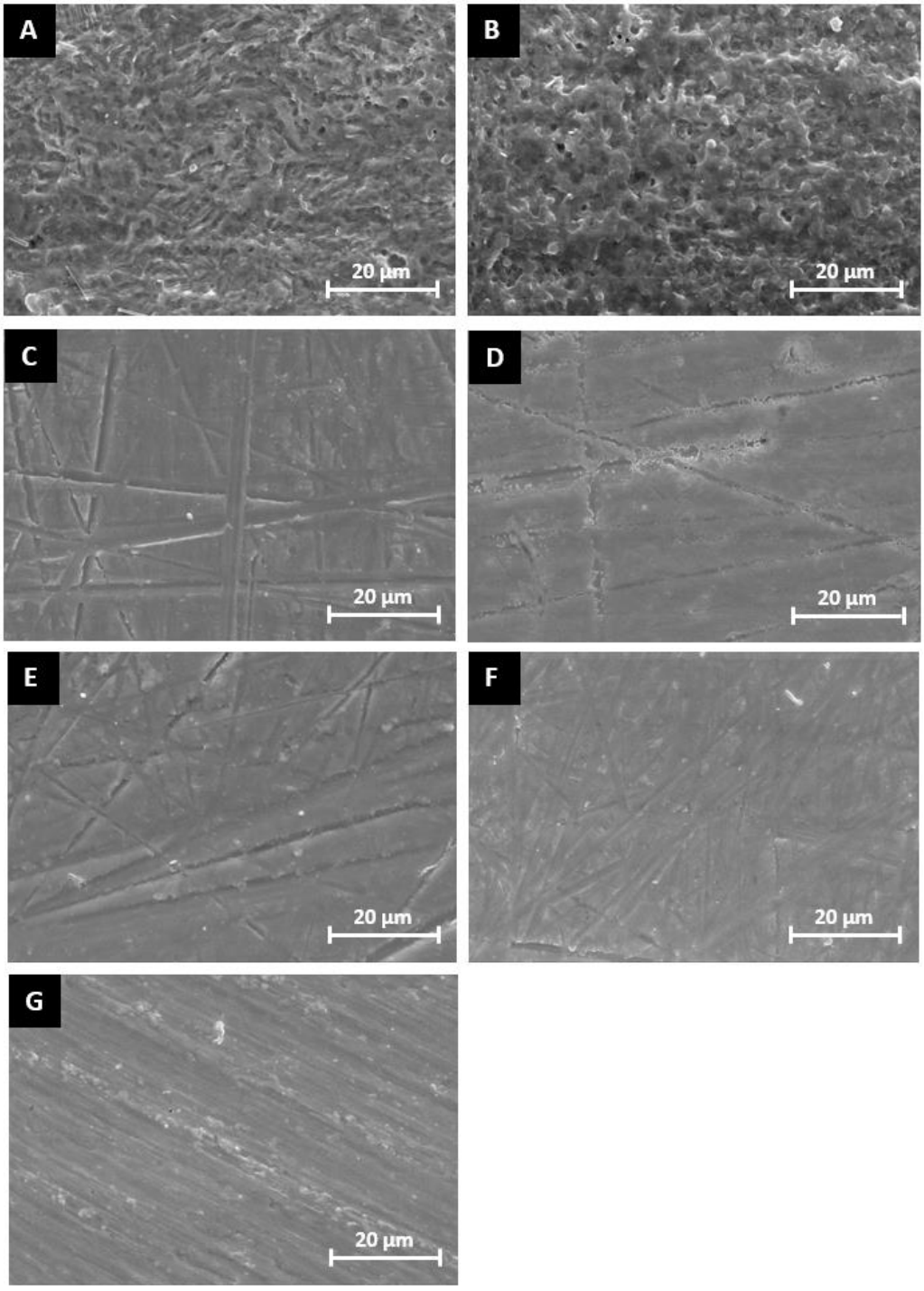

Figure 6.9: SEM micrographs of Ti surfaces after silanization process showing: A) Ti immersed in TEOS after passivation with piranha, B) Ti immersed in APTES after passivation with piranha, C) Ti immersed in APTES without passivation D) treated with TEOS vapour in Argon atmosphere, E) treated with TEOS vapour in normal atmosphere, F) treated with APTES vapour in Argon atmosphere and G) untreated Ti.

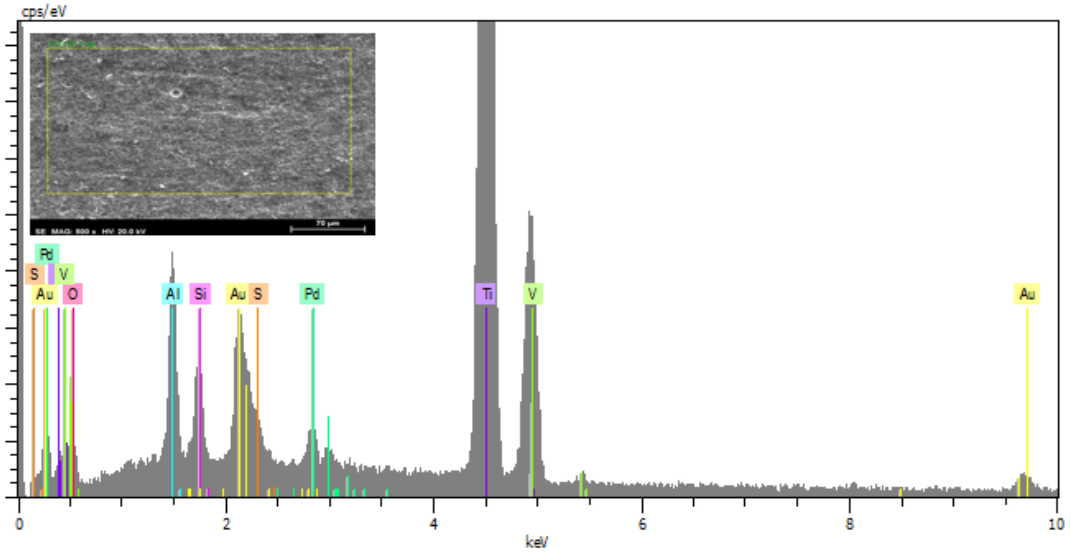

Figure 6.10: EDS report from Ti treated by immersion in APTES after a piranha passivation.

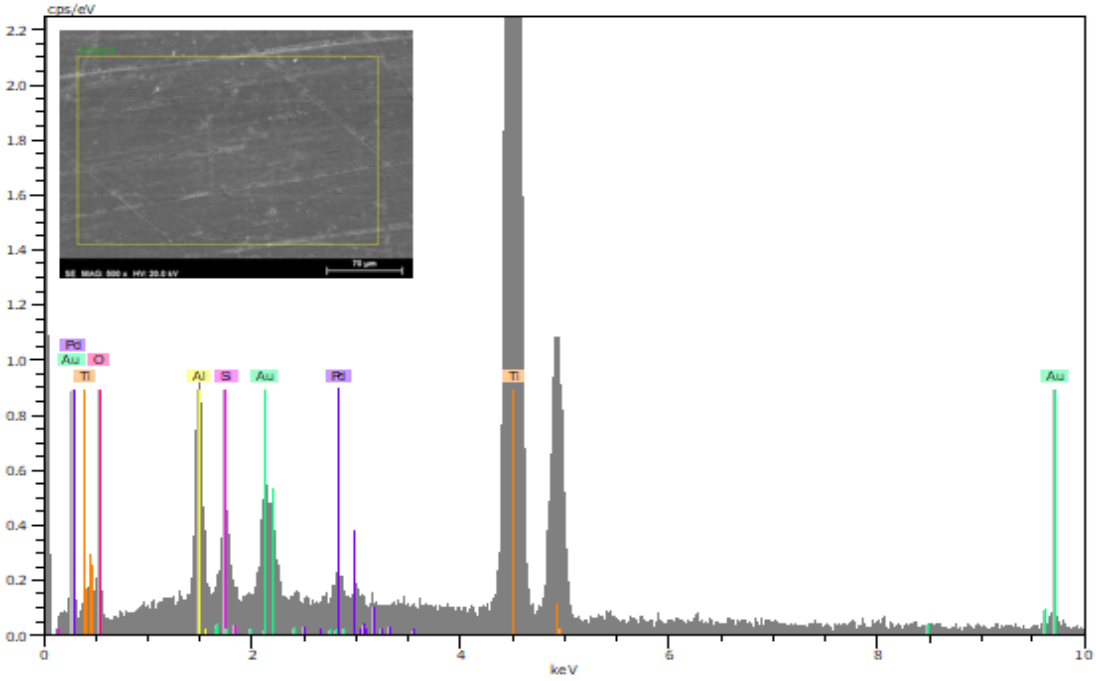

Figure 6.11: EDS report from Ti treated with TEOS vapour in Argon atmosphere without previous passivation in piranha solution.

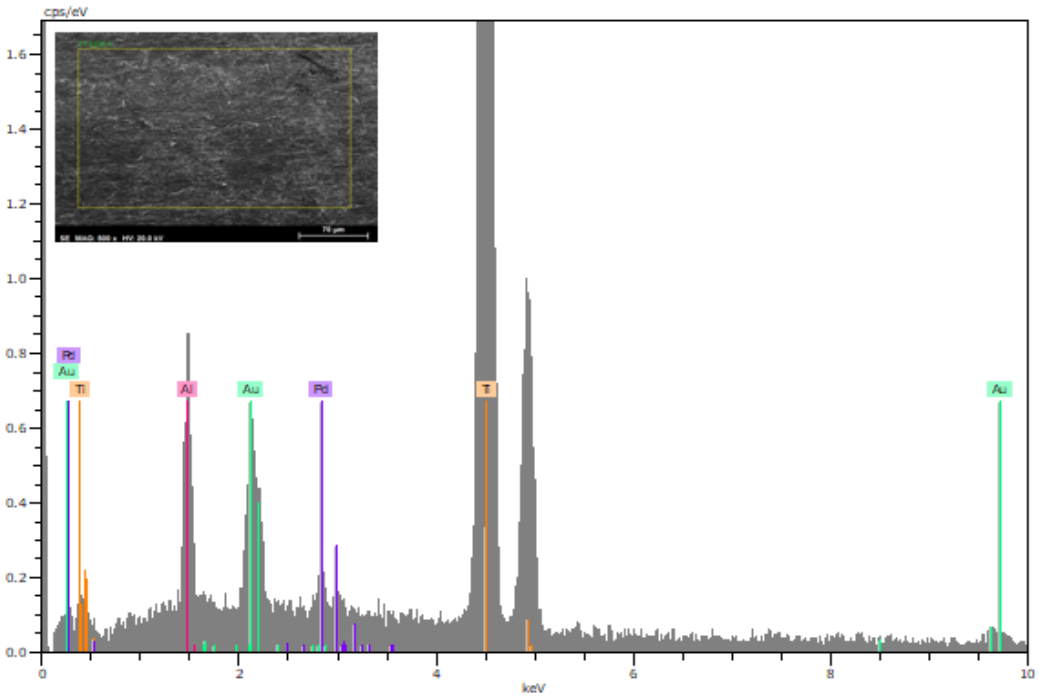

Figure 6.12: EDS report for Ti treated with immersion in TEOS after passivation in piranha solution.

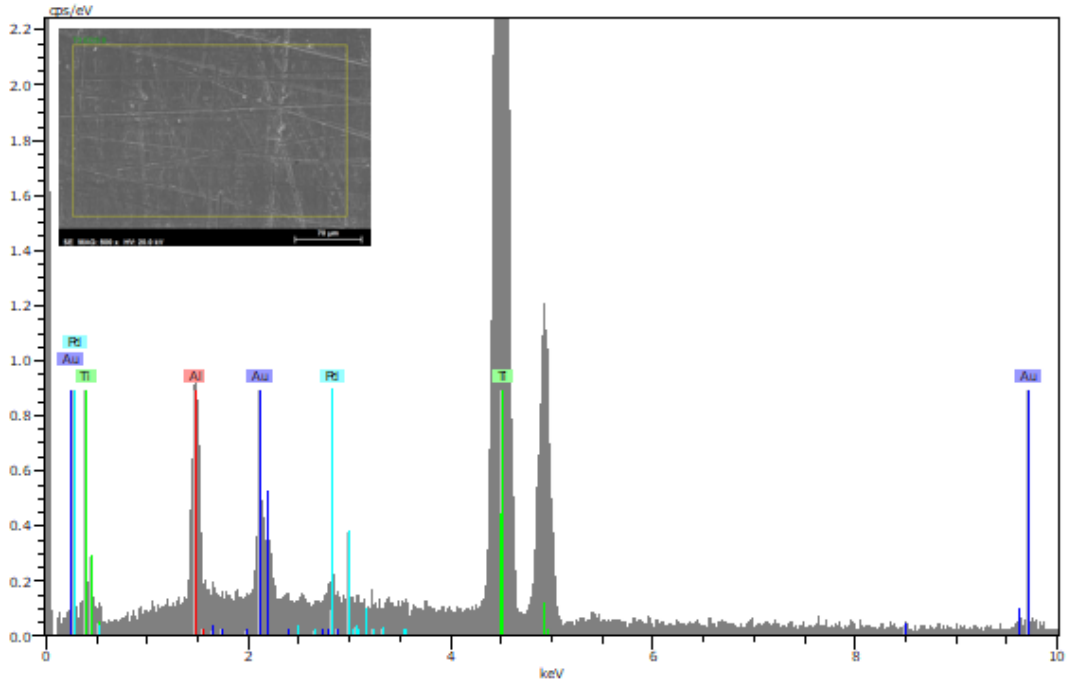

Figure 6.13: EDS report for Ti treated by immersion in TEOS after a passivation in piranha.

G. Parameters altered for film deposition studies

Table 6.10: List of parameters altered for PMMA in DCM film deposition studies on 316L-SS without a polishing step and respective adhesion evaluation in: green) full adhesion, yellow) detachment when submerged in water and red) detachment after drying.

HCl				Mechanical Abrasion				H_2SO_4			
Concentration	Dip Number	Crosslink	Adhesion	Concentration	Dip Number	Crosslink	Adhesion	Concentration	Dip Number	Crosslink	Adhesion
2.50 % wt/v	1	without		2.50 % wt/v	1	without		2.50 % wt/v	1	without	
		after				after				after	
	3	without			3	without			3	without	
		after				after				after	
		between				between				between	
	6	without			6	without			6	without	
		after				after				after	
		between				between				between	
n5 % wt/v	1	without		5 % wt/v	1	without		5 % wt/v	1	without	
		after				after				after	
	3	without			3	without			3	without	
		after				after				after	
		between				between				between	
	6	without			6	without			6	without	
		after				after				after	
		between				between				between	
20 % wt/v	3	without		20 % wt/v	3	without		20 % wt/v	3	without	
		after				after				after	
		between				between				between	
	6	without			6	without			6	without	
		after				after				after	
		between				between				between	

Table 6.11: List of parameters altered for PMMA in DMAc/Acetone film deposition studies on 316L-SS without a polishing step and respective adhesion: green) full adhesion, yellow) detachment when submerged in water and red) detachment after drying.

HCl				Mechanical Treatment				H_2SO_4 1:2			
Concentration	Dip Number	Crosslink	Adhesion	Concentration	Dip Number	Crosslink	Adhesion	Concentration	Dip Number	Crosslink	Adhesion
3 % wt/v	1	without		3 % wt/v	1	without		3 % wt/v	1	without	
		after				after				after	
	3	without			3	without			3	without	
		after				after				after	
		between				between				between	
	6	without			6	without			6	without	
		after				after				after	
		between				between				between	
6 % wt/v	1	without		6 % wt/v	1	without		6 % wt/v	1	without	
		after				after				after	
	3	without			3	without			3	without	
		after				after				after	
		between				between				between	
	6	without			6	without			6	without	
		after				after				after	
		between				between				between	
12 % wt/v	3	without		12 % wt/v	3	without		12 % wt/v	3	without	
		after				after				after	
		between				between				between	
	6	without			6	without			6	without	
		after				after				after	
		between				between				between	

Table 6.12: Parameters altered for the deposition of PMMA films with 1 layer.

Crosslinked	With Toluene	HCL	DCM DMAc/Acetone	**No Drug/ Free Drug/ Drug Loaded Spheres**
Non-Crosslinked				
Crosslinked	Without Toluene			
Non-Crosslinked				
Crosslinked	With Toluene	H_2SO_4		
Non-Crosslinked				
Crosslinked	Without Toluene			
Non-Crosslinked				
Crosslinked	With Toluene	Mec		
Non-Crosslinked				
Crosslinked	Without Toluene			
Non-Crosslinked				
Non-Crosslinked				

H. Thickness obtained during film optimization

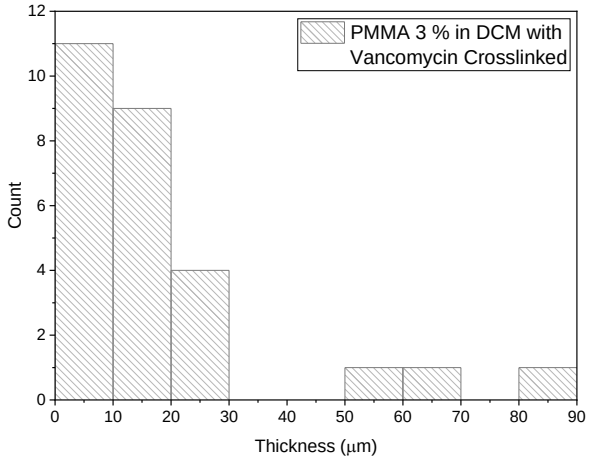

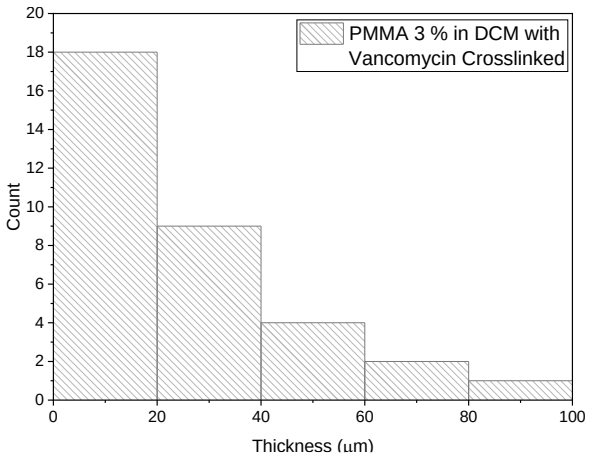

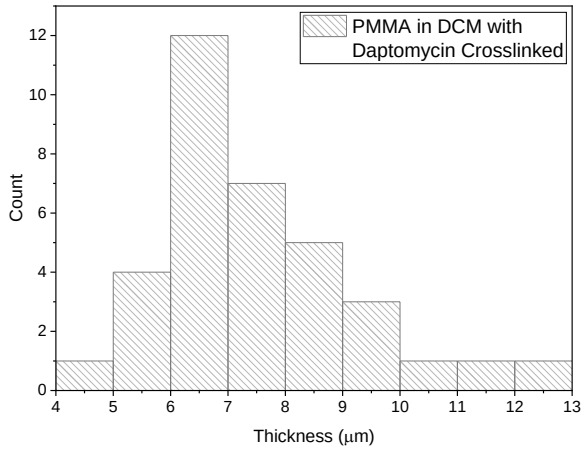

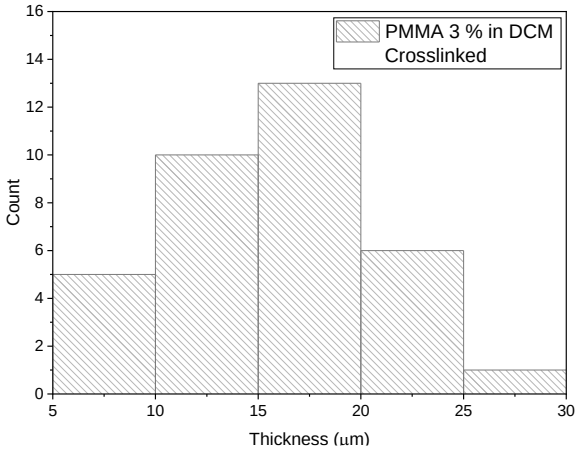

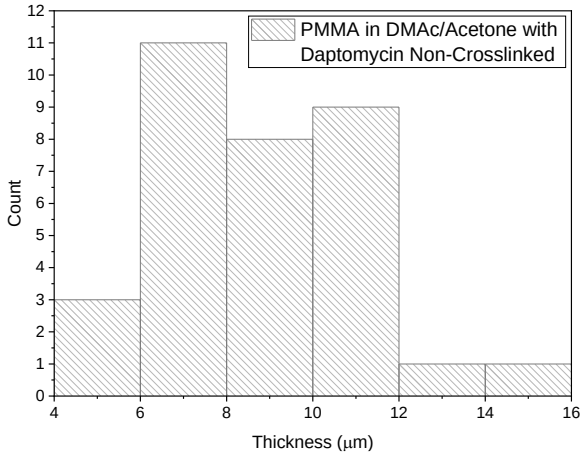

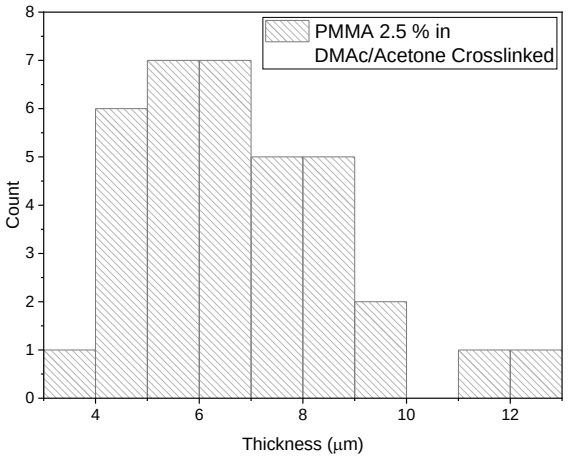

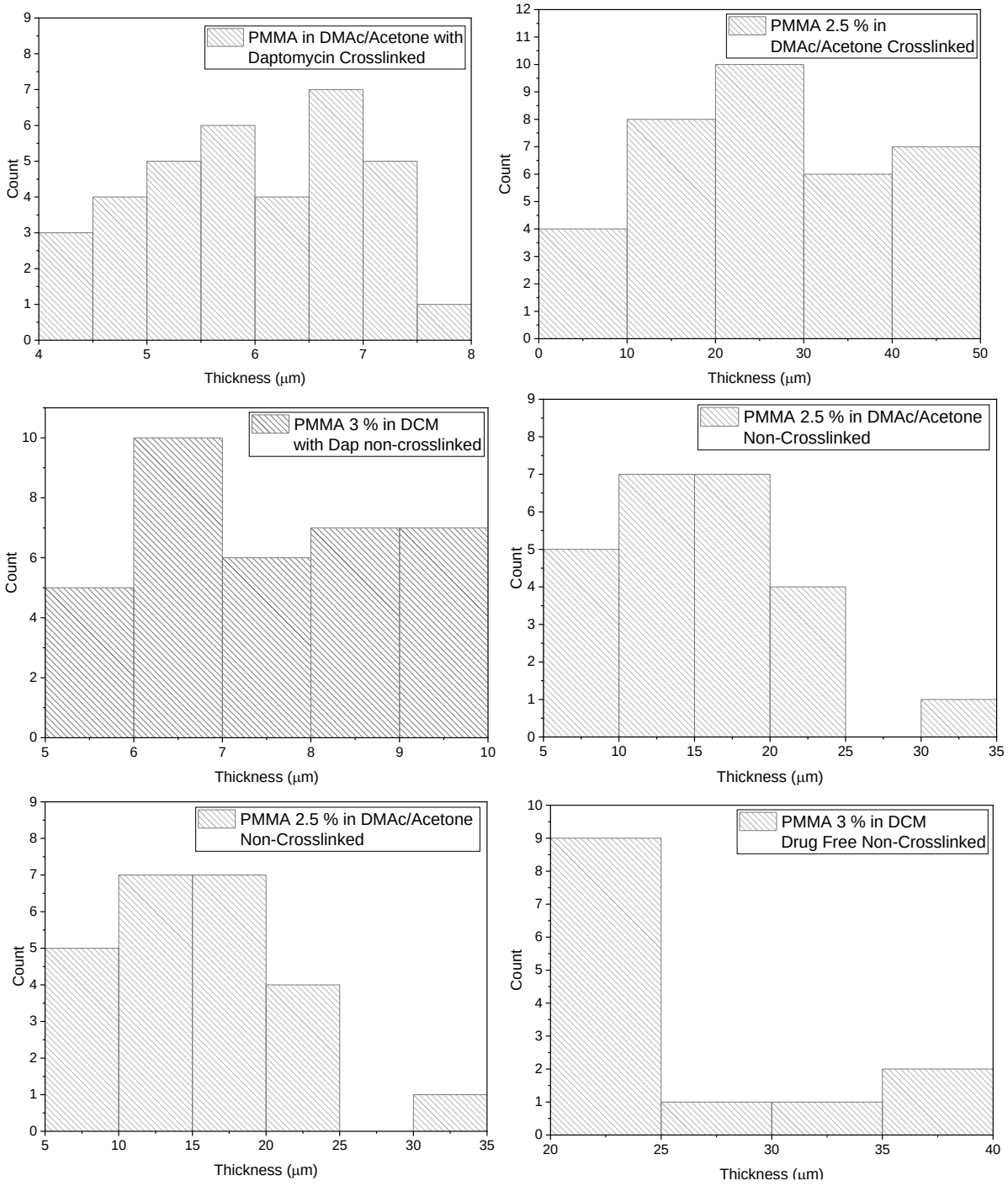

Figure 6.14: Histograms of the thicknesses obtained for PMMA films in DMAc/Acetone and DCM with dap, van, or no drug, crosslinked or non-crosslinked.

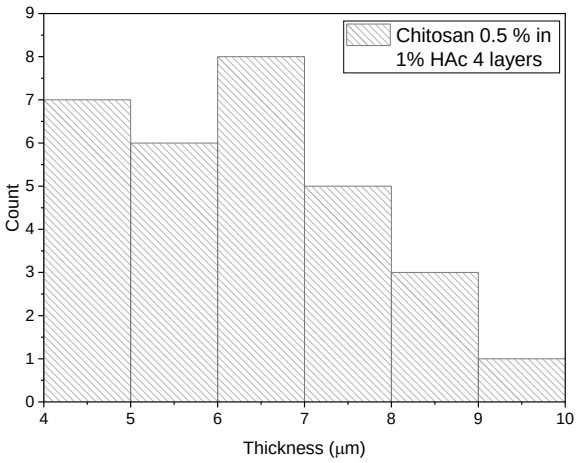
Chitosan 0.5 % in
1% HAc 4 layers
Count
Thickness (μm)

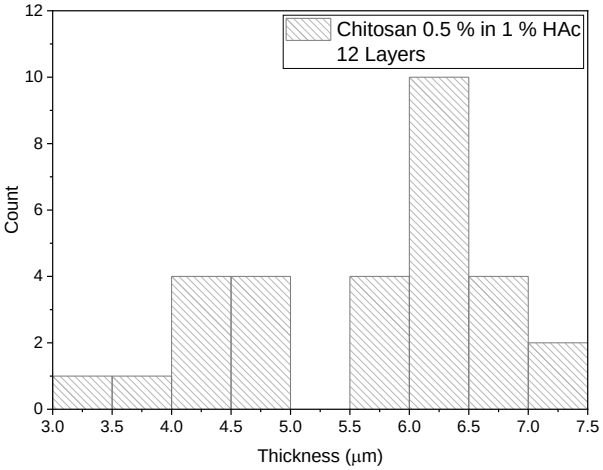
Chitosan 0.5 % in 1 % HAc
12 Layers
Count
Thickness (μm)

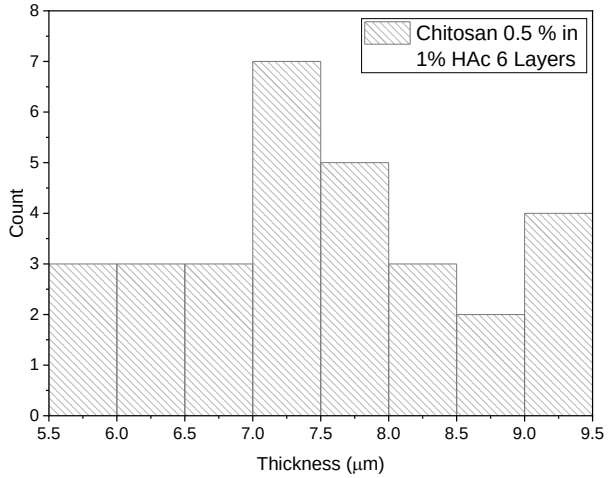
Chitosan 0.5 % in
1% HAc 6 Layers
Count
Thickness (μm)

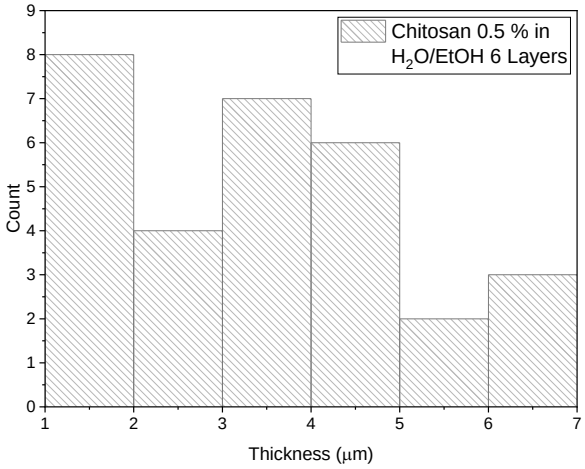
Chitosan 0.5 % in
H2O/EtOH 6 Layers
Count
Thickness (μm)

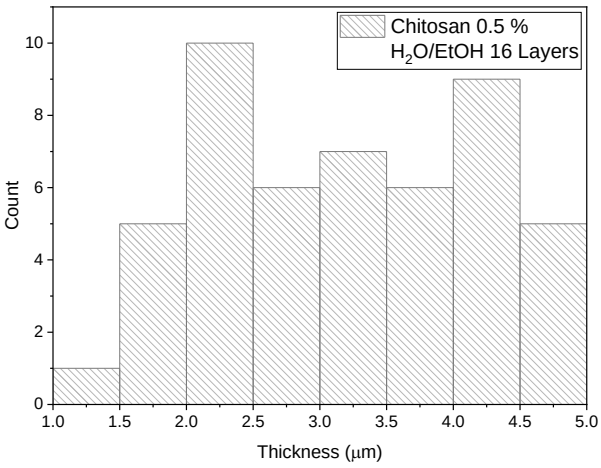
Chitosan 0.5 %
H2O/EtOH 16 Layers
Count
Thickness (μm)

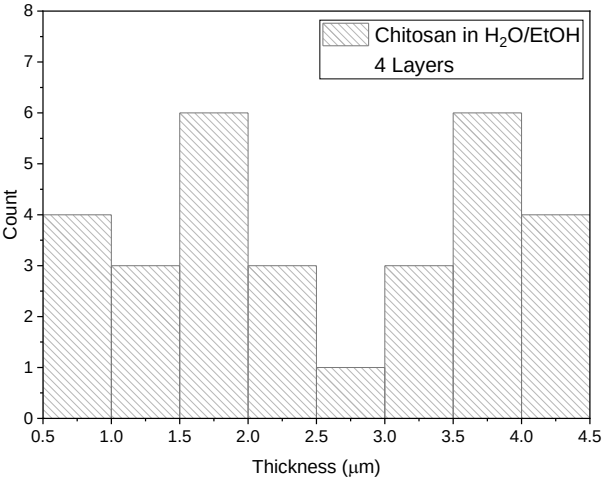
Chitosan in H2O/EtOH
4 Layers
Count
Thickness (μm)

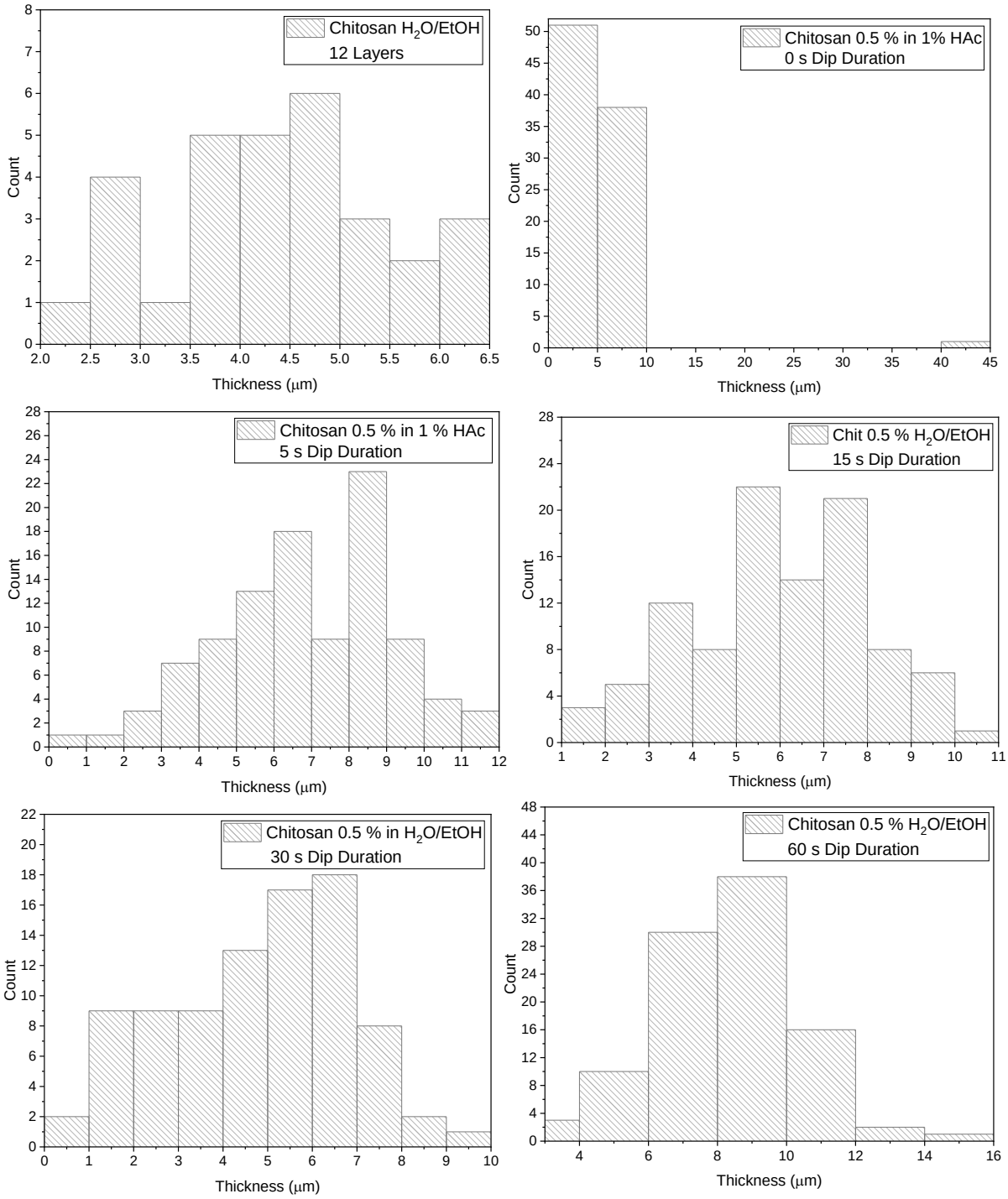

Figure 6.15: Histogram of the thickness values obtained for chitosan films of several layers in HAc 1% v/v and in HAc 1 % v/v + ethanol.

I. Electrophoretic deposition

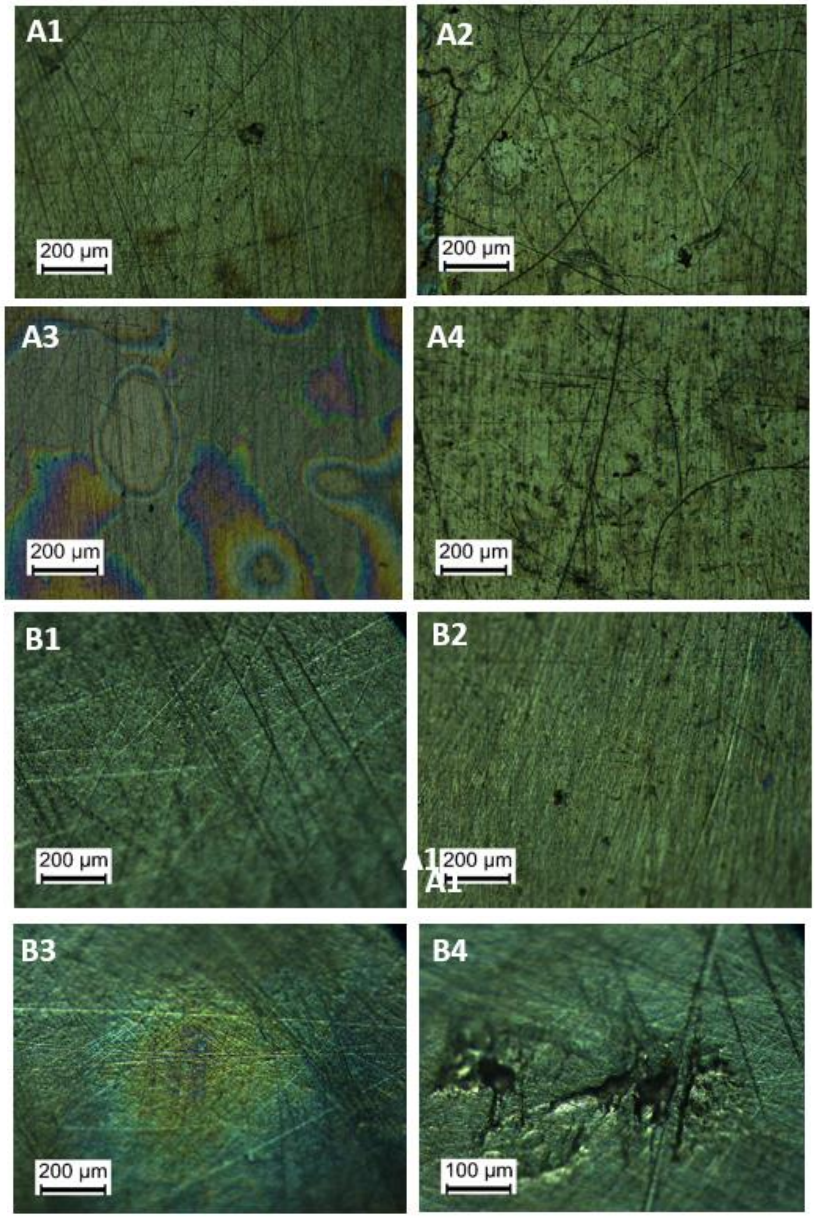

Figure 6.16: Optical microscope images of the substrates with a chitosan film deposited for A) 10 minutes at 4 mA and B) 5 minutes at 4 mA showing 1) deposited film and 2) metal with no film, 3) birefringence and 4) pitting in the film covered area.

J. Peel-off Curves obtained during film optimization

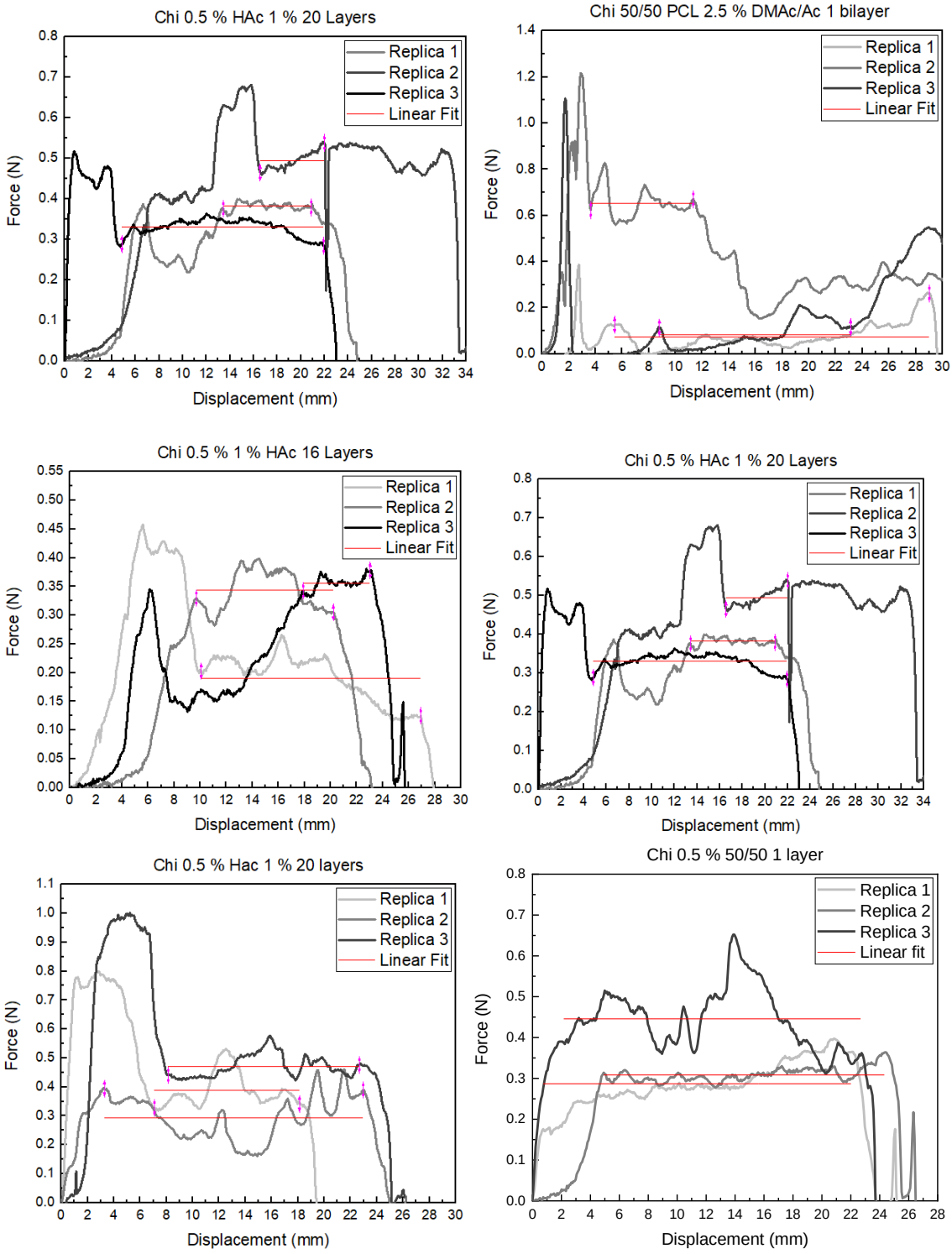

Figure 6.17: Peel-off curves obtained for film optimization of chitosan.

K. Thickness obtained for optimized films

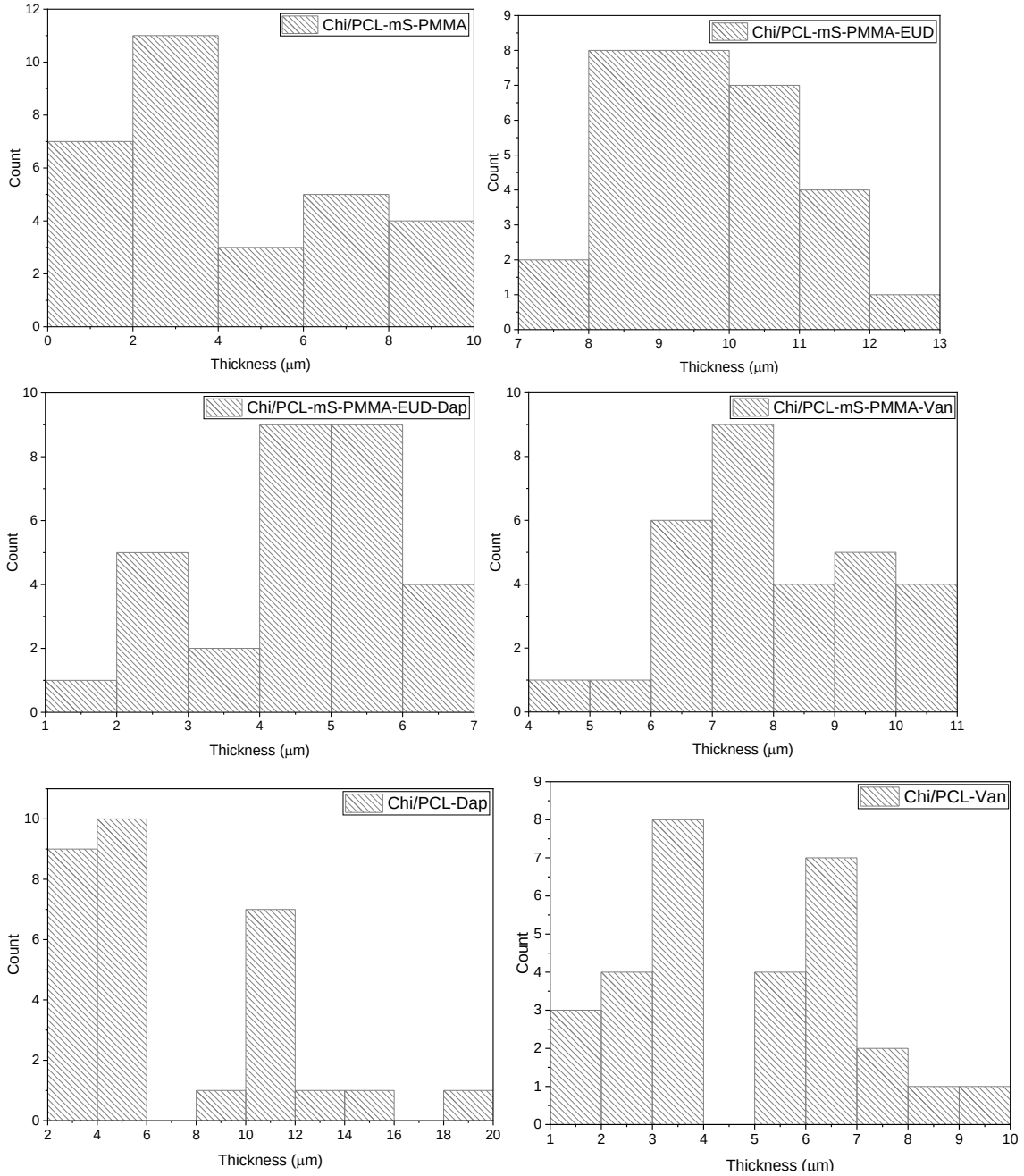

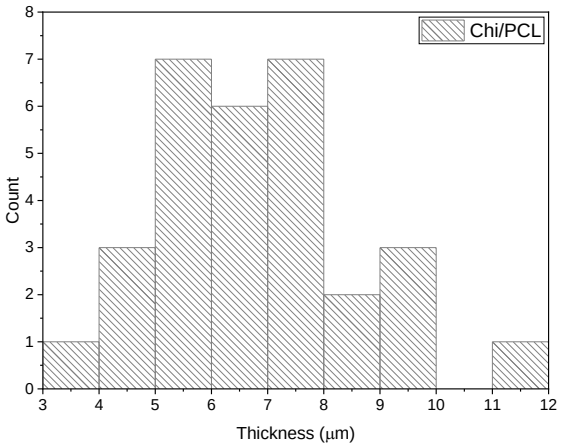

Figure 6.18: Histograms of the thickness values obtained for optimized films.

L. Peel-Off curves obtained for optimized films

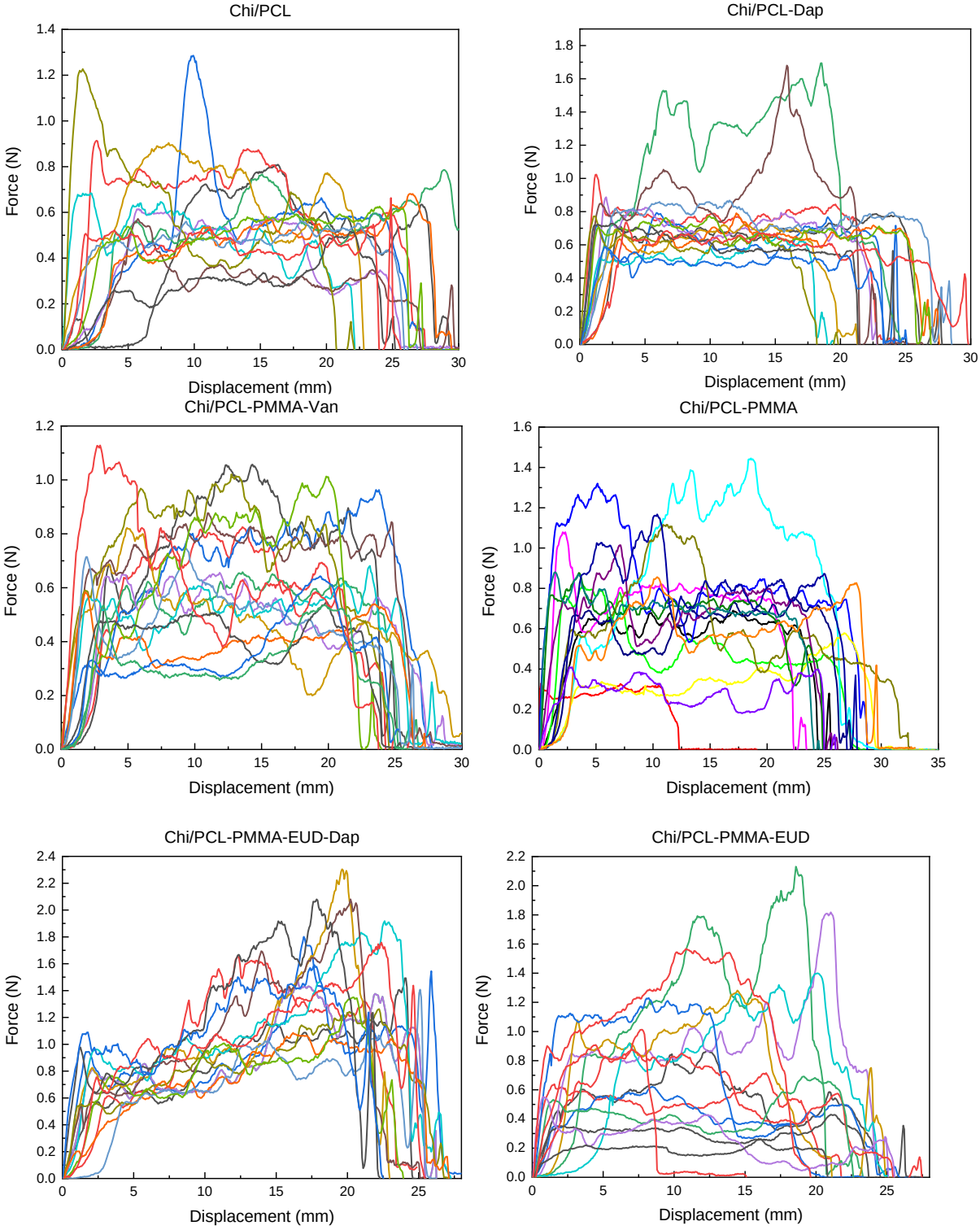

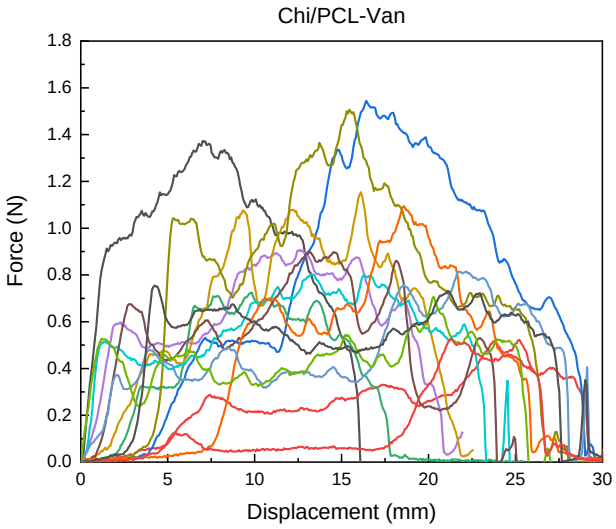

Figure 6.19: Pee-Off curves obtained for the several replicas of the optimized films.

Table 6.13: Interception values of the linear fits obtained for optimized films and 316L-SS treated by mechanical abrasion.

Replica	Chi/PCL	Chi/PCL-Dap	Chi/PCL-Van	Chi/PCL-PMMA-EUD-Dap	Chi/PCL-PMMA-EUD	Chi/PCL-PMMA-Van	Chi/PCL-PMMA	316L-SS mechanical abrasion
1	0.531	0.766	0.980	1.076	1.017	0.797	0.286	0.354
2	0.487	0.693	0.749	1.377	0.574	0.708	0.463	0.363
3	0.556	0.849	0.501	0.740	1.375	0.874	0.750	0.313
4	0.484	0.710	0.749	1.220	0.463	0.586	0.622	0.310
5	0.462	1.382	0.446	1.226	0.939	0.529	0.322	0.370
6	0.273	1.006	0.585	0.844	0.540	0.572	0.777	0.286
7	0.546	0.668	0.453	0.973	0.858	0.527	0.478	0.273
8	0.764	0.611	0.697	0.746	1.252	0.761	1.218	0.311
9	0.681	0.558	1.126	1.006	0.850	0.869	0.720	0.408
10	0.564	0.627	0.844	0.983	0.192	0.867	0.623	0.288
11	0.824	0.637	0.904	0.629	0.240	0.477	0.720	0.411
12	0.544	0.713	0.258	0.795	1.125	0.395	0.691	0.499
13	0.586	0.791	0.663	1.725	0.797	0.284	0.786	0.310
14	0.546	0.674	0.685	0.916	0.306	0.296	0.692	0.357
15	0.764	0.675	0.508	1.438	0.366	0.473	0.619	0.374

M. Degradation and swelling ratio of Chi and PCL Films

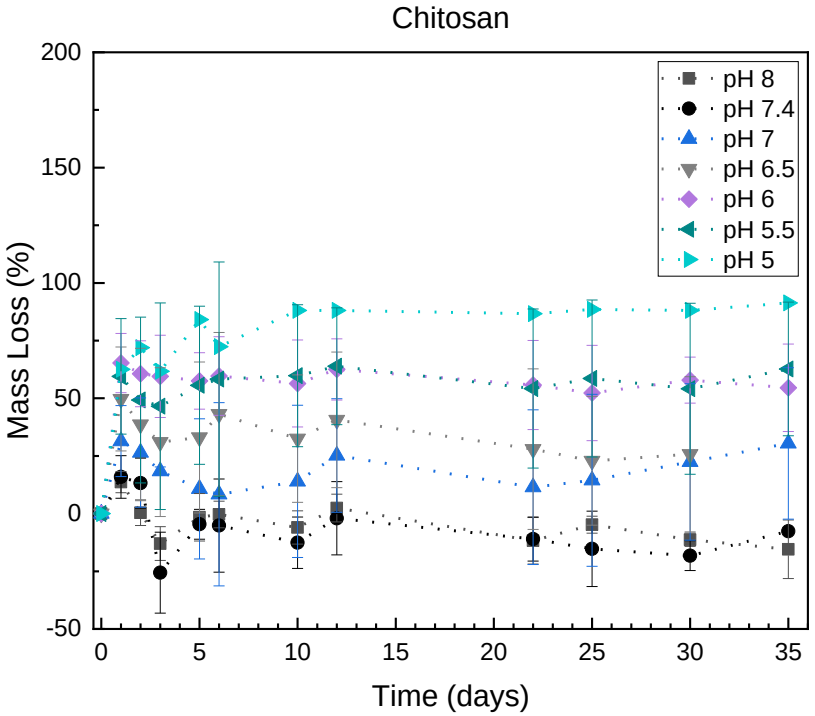

Figure 6.20: Degradation of chitosan films at pH values between 5 and 8.

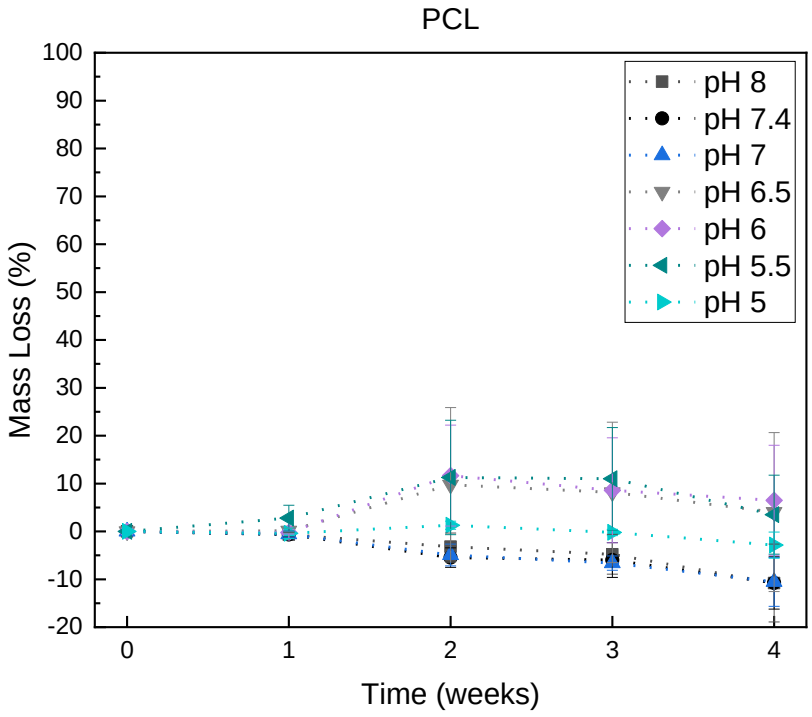

Figure 6.21: Degradation of PCL films at pH values between 5 and 8.

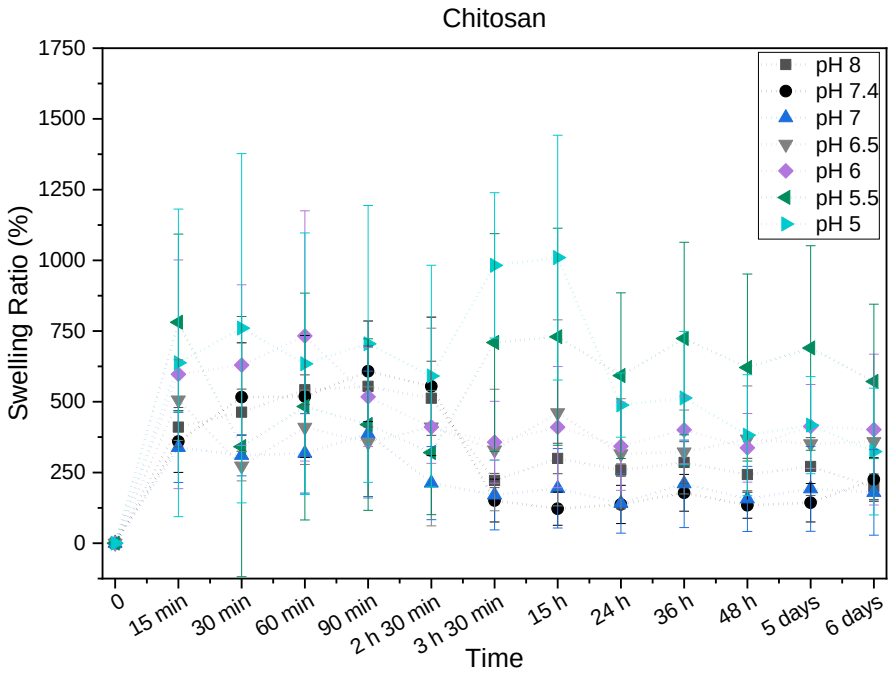

Figure 6.22: Swelling ratio of chitosan films at pH values between 5 and 8.

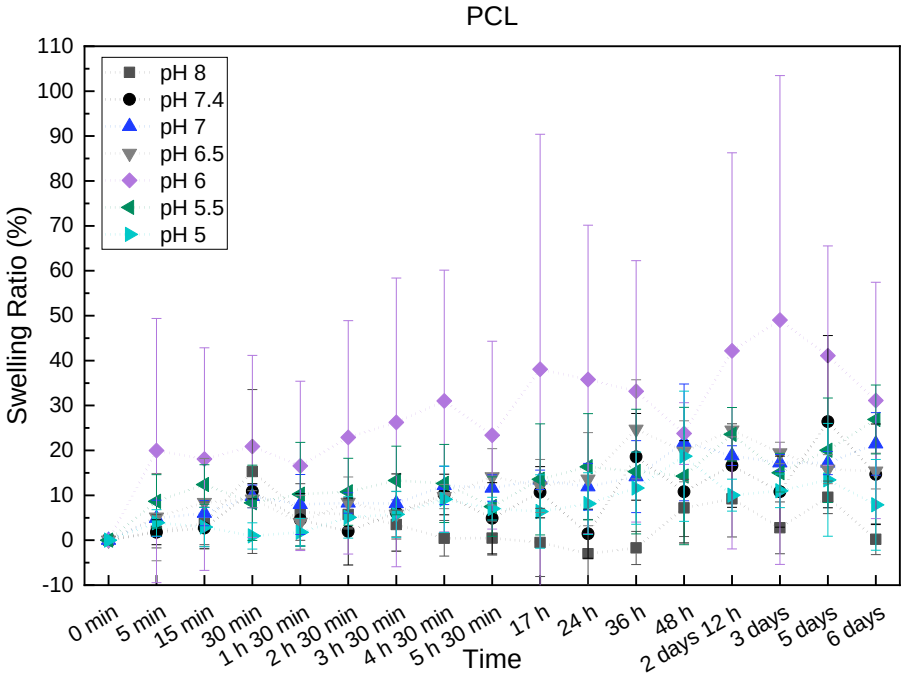

Figure 6.23: Swelling ratio of PCL films at pH values between 5 and 8.

N. Raman

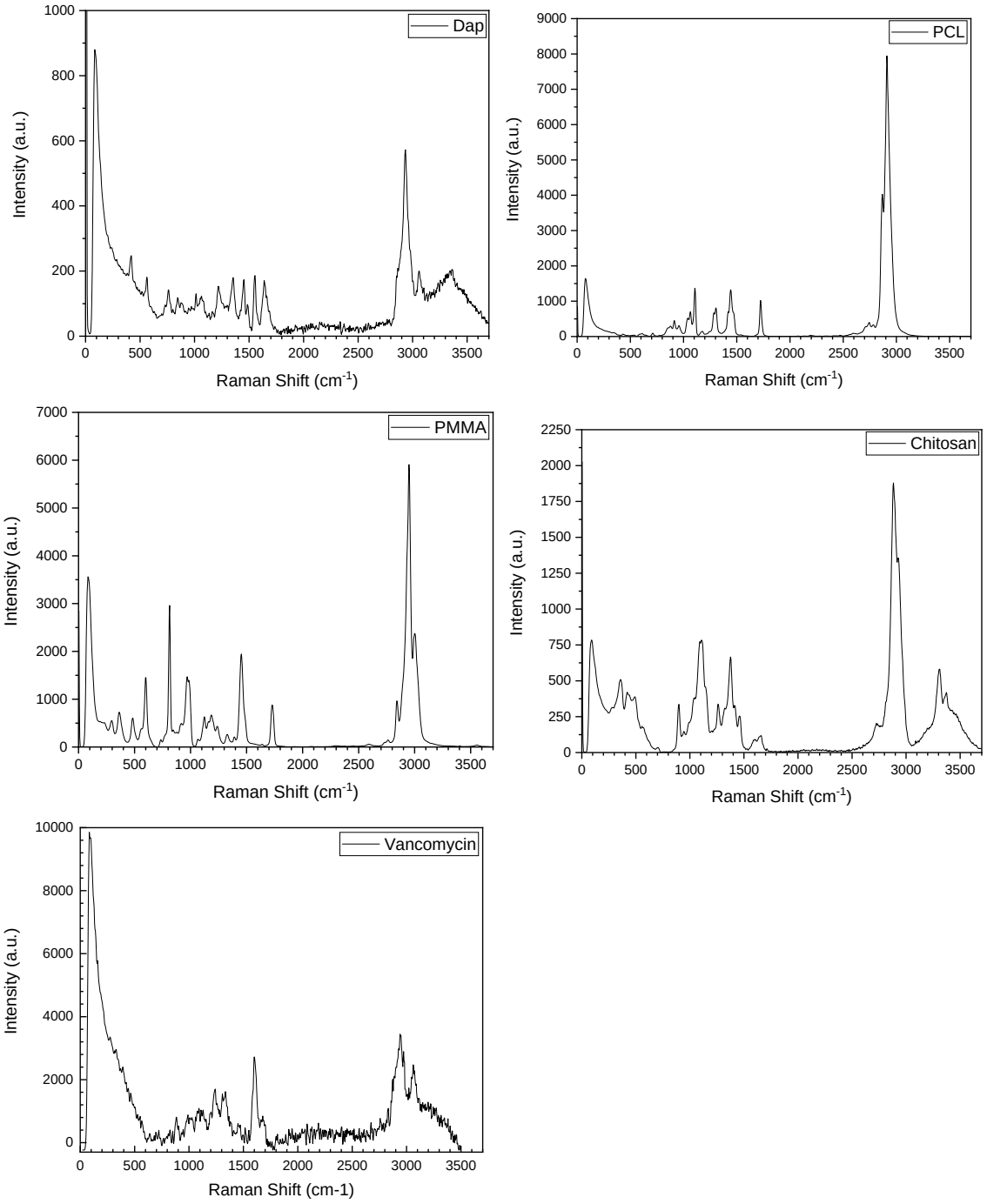

Figure 6.24: Raman spectra of the several compounds used for film deposition.

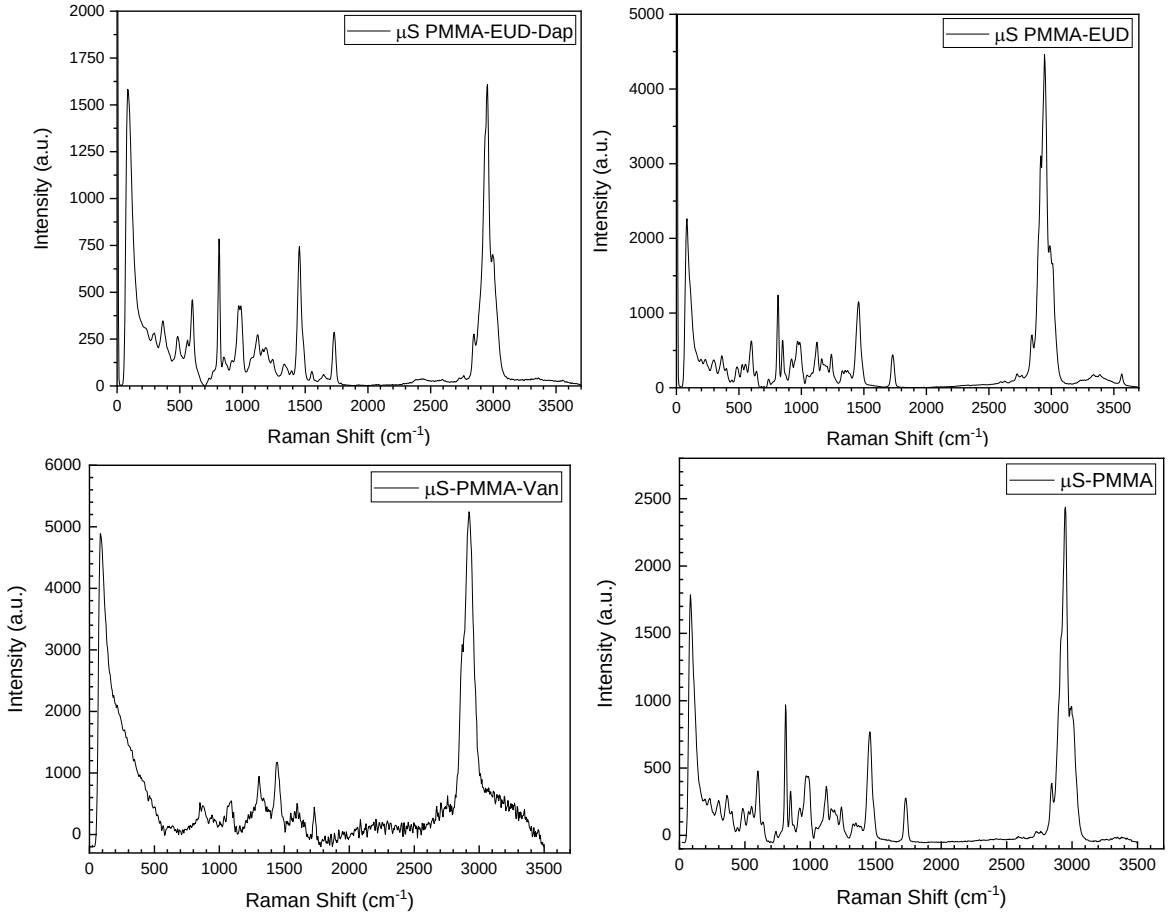

Figure 6.25: Raman spectrum of the microspheres (μS) produced.

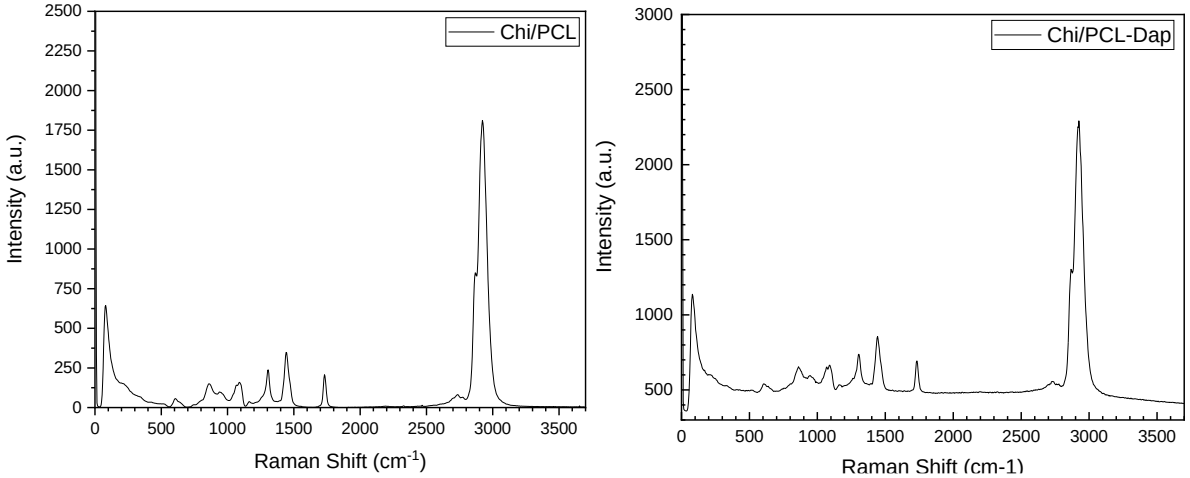

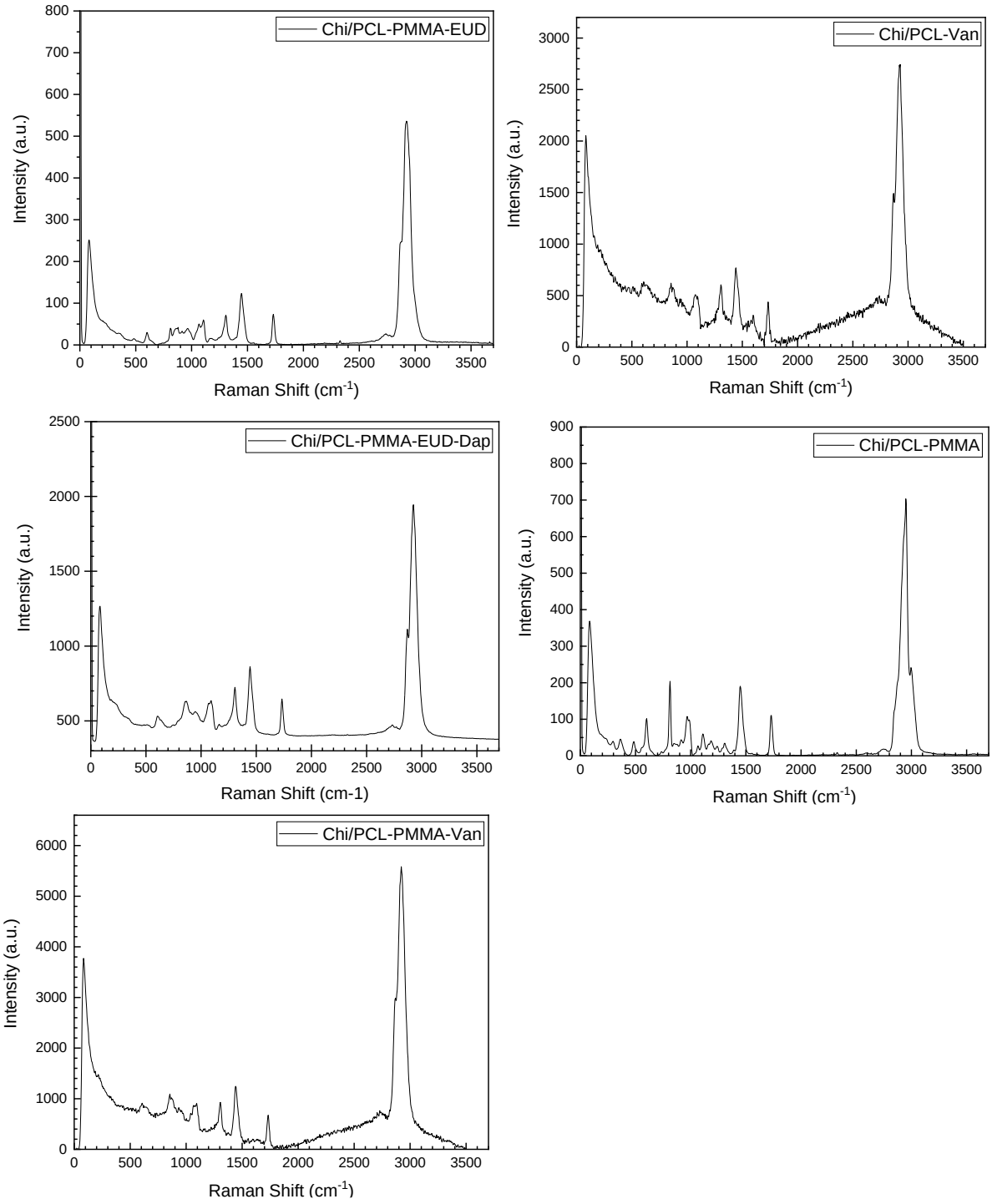

Figure 6.26: Raman Spectra obtained for the several optimized films.

Table 6.14: Peak assignment for Raman spectra of PCL, PMMA, Chi, Van and Dap showing the experimental and literature peaks, and the correpondant vibrational mode.

Component	**Peak in spectrum (cm^{-1})**	**Peak in literature (cm^{-1})**	**Vibrational mode**
PCL	878	865 (broad)	
	913	913	ν(C–COO)
	1063, 1106	1003-1110	skeletal stretching
	1302	1270-1320	ω(CH_2)
	1441	1405-1470	δ(CH_2)
	2910	2800-3200	υ(CH)
Several narrow peaks at 913 cm^{-1}, 1003–1110 cm^{-1}, 1270– 1320 cm^{-1}, 1405–1470 cm^{-1} (d) and 2800– 3200 cm^{-1} refer to the crystalline fraction and the broad peak at 865 cm*1 indicates the amorphous phase.			
Chitosan	358, 420.0	357,424,444	γ(OH) + γ(ϕ)
	489	493	δ(CO-NH) + δ(C-CH_3)
	558	566	γ(NH) + γ(C=O) + ω(CH_3)
	1037	1044	ρ(CH_3) + δ(CH) + δ(OH)
	1106, 1156	1093, 1114	ν(C-O-C) + ν(ϕ) + ν(C-OH) + ν(C-CH_2) + δ(CH) + ρ(CH_2) + CH_3
	1261	1263	δ(OH…O) + ν(C-C) + ν(C-O) + δ(CH) + ρ(CH_2)
	1318	1325	ν(CN) + δ(CH)
	1376	1377	δ(CH_2) + δ(CH) + δ(OH) + ν(ϕ)
	1461	1458	δ(CH) + ω(CH_2) + δ(OH)
	1603	1591	δ(NH_2)
	1657	1654	ν(CO)
	2883.6	2885	ν(CH_2)
	3311.6, 3373.3	3308, 3362	ν(OH) HB
PMMA	296.7	304	δ(C-C-C)
	362.2	370	ν_s(C–COO) + δs(O-C=O)
	481.7	487	ν_6(C–COO)
	601.2	602	ν(C–COO), ν_s(C–C–O)
	813.3	818	ν_s(C–O-C)
	971.4	967	α–CH_3 rock
	1125.6	1125	ν(C-C) skeletal mode
	1187.3	1188	ν_a(C–O-C)
	1453.3	1456	δ_a (C–H) of α-CH_3, δ_a(C–H) of O–CH_3
	1730	1736	ν(C=O) of (C–COO)
	2841	2848	Combination band involving O–CH3
	2949	2957	ν_s(C–H) of O–CH_3 with ν_s(C–H) of α-CH_3 and ν_a(CH_2)
	3003.2	3001	ν_a (C–H) of O–CH_3, ν_a (C–H) of α-CH_3
Vancomycin	990	993	ν(C-C) skeletal mode
	1242	1232	ν (C-N) of amide III
	1334	1328	δ(C-H) of CH_2 and CH_3
	1602	1610	ν(C=O) of amide I
	1678	1682	ν(C=C)

Daptomycin	420	399, 418	Arginine, Threonine
	562	533, 564	Arginine, Threonine
	759	749, 779, 742, 774	Aspartic Acid, Aspartic Acid, Threonine, Threonine
	844	852	Alanine
	1013	1021, 1010	Alanine, Serine
	1063	1083, 1084, 1045	Arginine, Aspartic Acid, Threonine
	1218	1199, 1220	Arginine, Serine
	1353	1361, 1364, 1338, 1362, 1341	Alanine, Arginine, Aspartic Acid
	1433	1423, 1443, 1426, 1419, 1442	Arginine, Arginine, Aspartic Acid, Threonine, Glycine
	1553	1568, 1548	Glycine, Threonine
	1638	1630, 1621, 1651	Serine, Threonine, Threonine

ν_a **- asymmetric stretching mode;** ν_s **- symmetric stretching mode (same for δ).** Φ**-pyranoid ring;** ν **- stretching;** δ**- in-plane bending vibrations;** ω,γ **- out-of plane bending;** HB**, hydrogen bond**

O. Drug Release

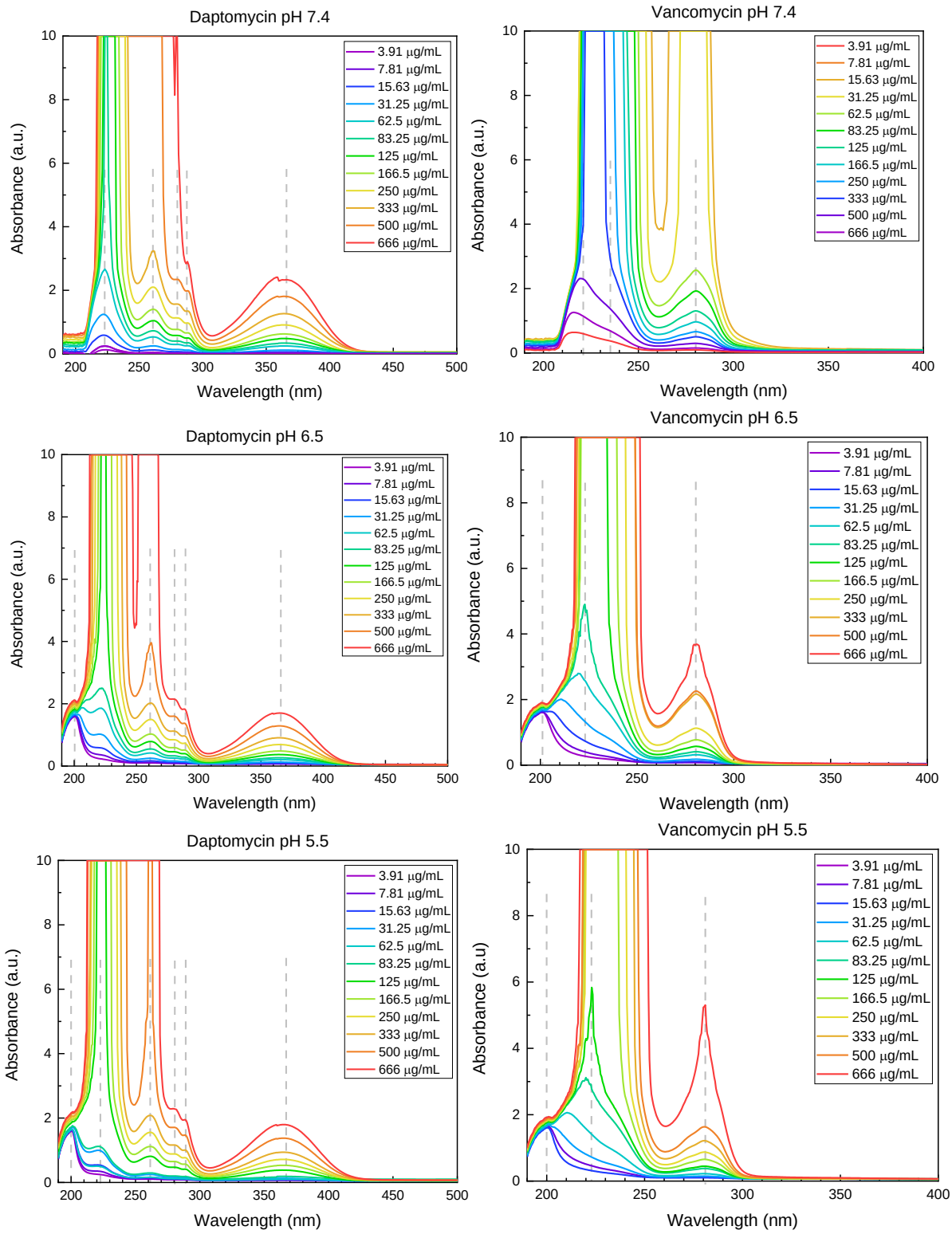

Figure 6.27: UV-Vis spectra obtained for Van and Dap calibration curves at pH values of 5.5, 6.5 and 7.4.

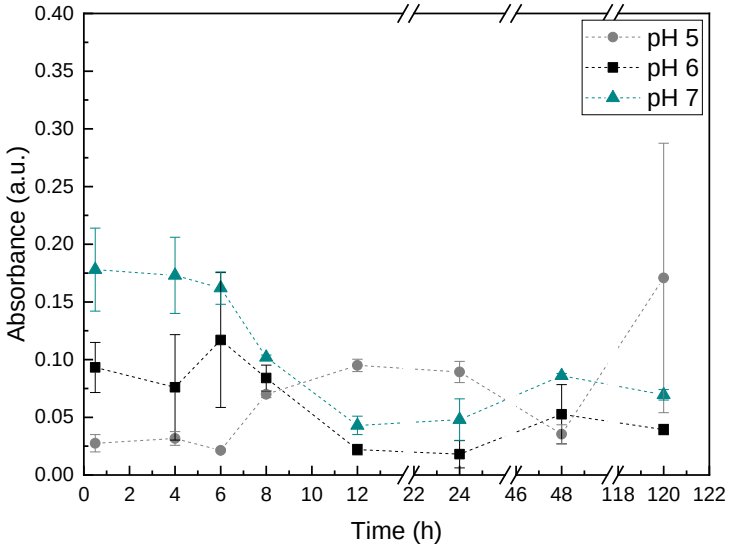

Figure 6.28: Absorbances measured for Chi/PCL films at 280 nm.

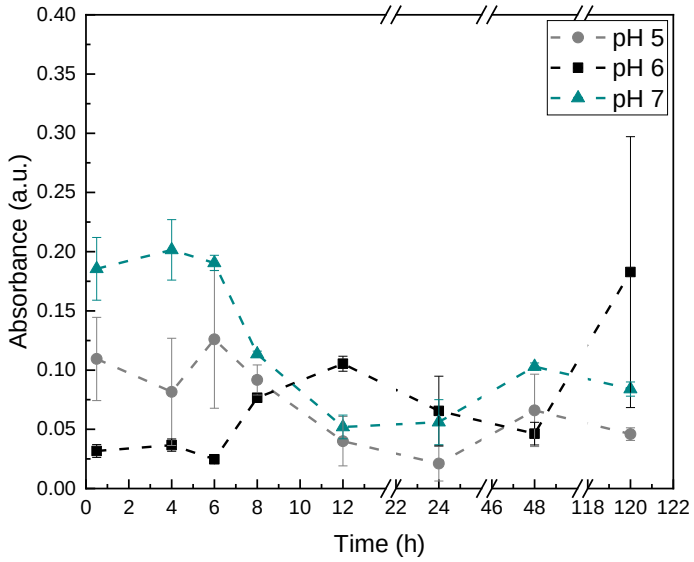

Figure 6.29: Absorbances measured for Chi/PCL films at 262 nm.

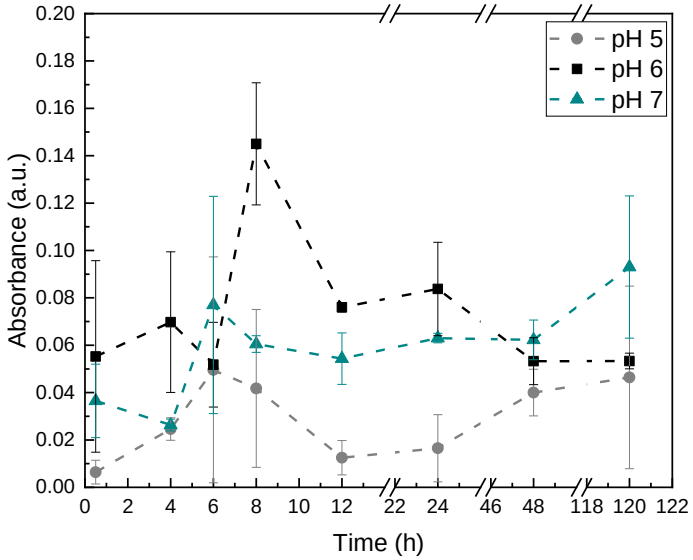

Figure 6.30: Absorbances measured for Chi/PCL-PMMA films at 280 nm.

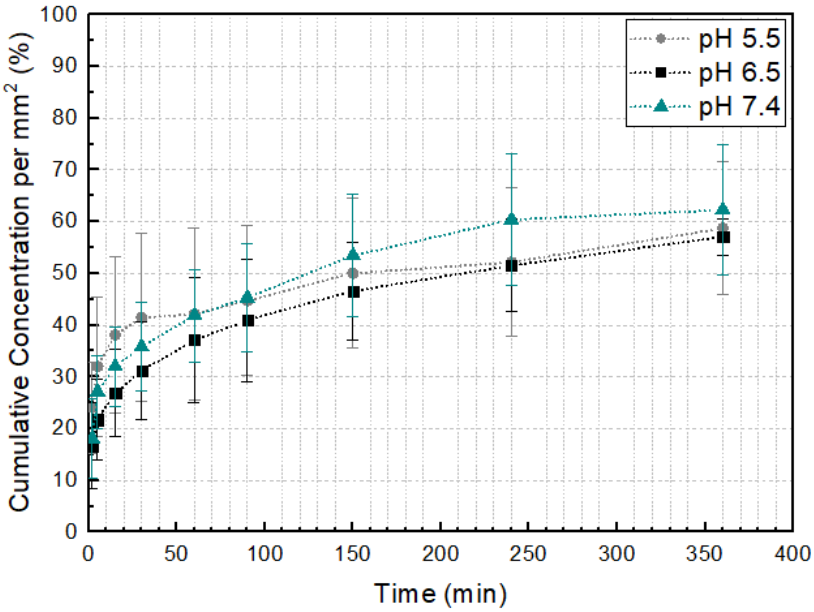

Figure 6.31: Plot of the cumulative daptomycin release from Chi/PCL-PMMA-EUD-Dap films vs. release time for the first 6 hours of drug release.

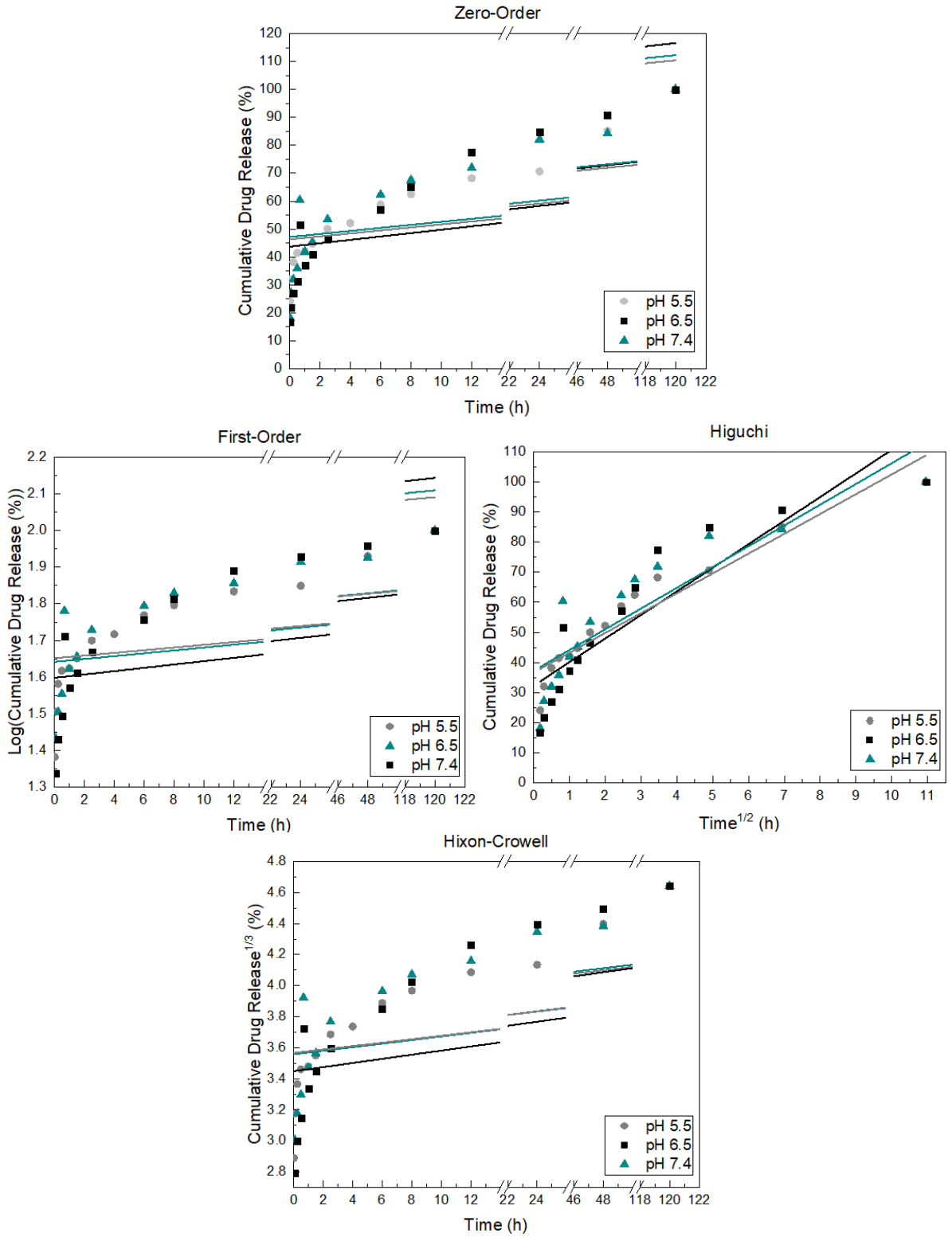

Figure 6.32: Comparison of drug release to mathematical models for Chi/PCL-Dap films.

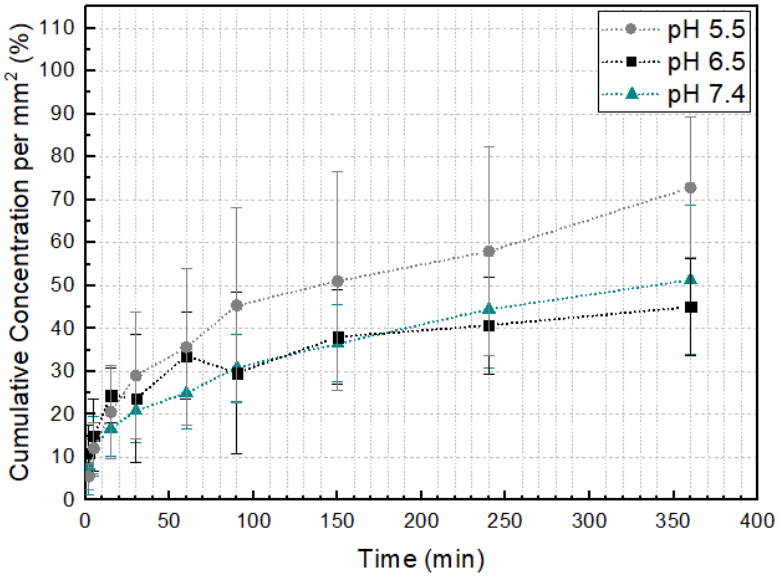

Figure 6.33: Plot of the cumulative daptomycin release from Chi/PCL-PMMA-EUD-Dap films vs. release time for the first 6 hours of drug release.

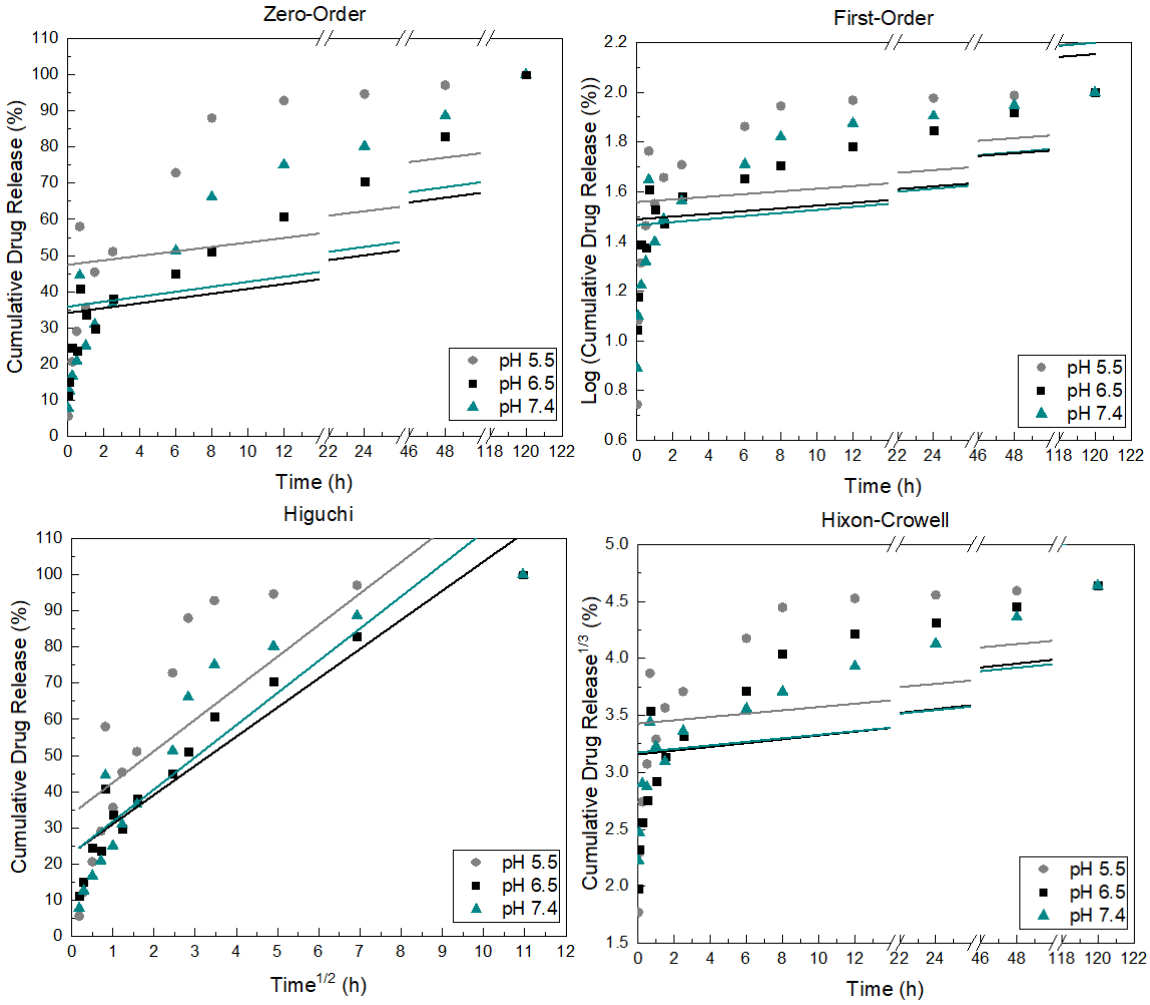

Figure 6.34: Comparison of drug release to mathematical models for Chi/PCL-PMMA-EUD-Dap films.

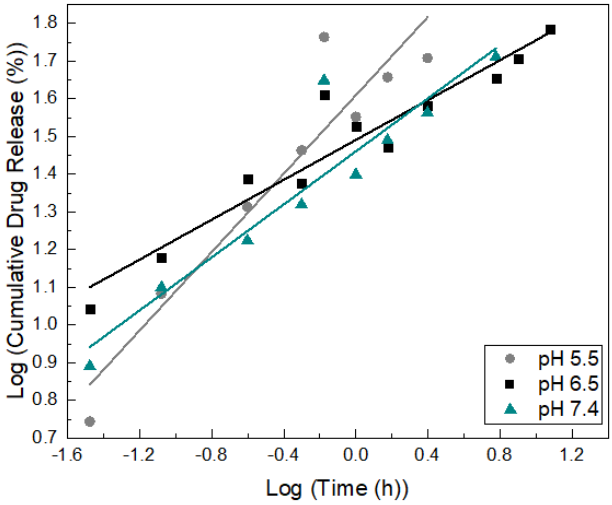

Figure 6.35: Korsmeyer-Peppas representation for a cumulative drug release < 60 % for the calculation of the value of n for Chi/PCL-PMMA-EUD-Dap films.

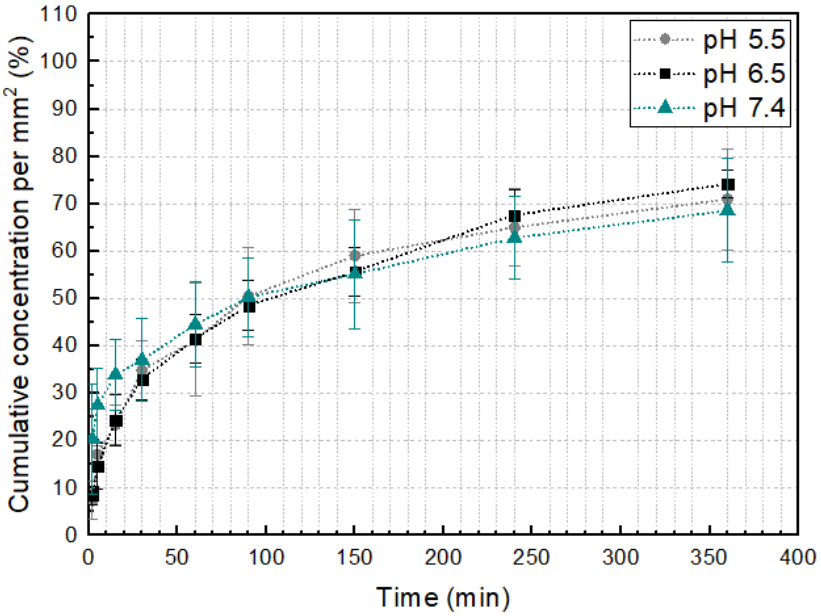

Figure 6.36: Cumulative vancomycin release from Chi/PCL-Van films vs. release time for the first 6 hours of drug release.

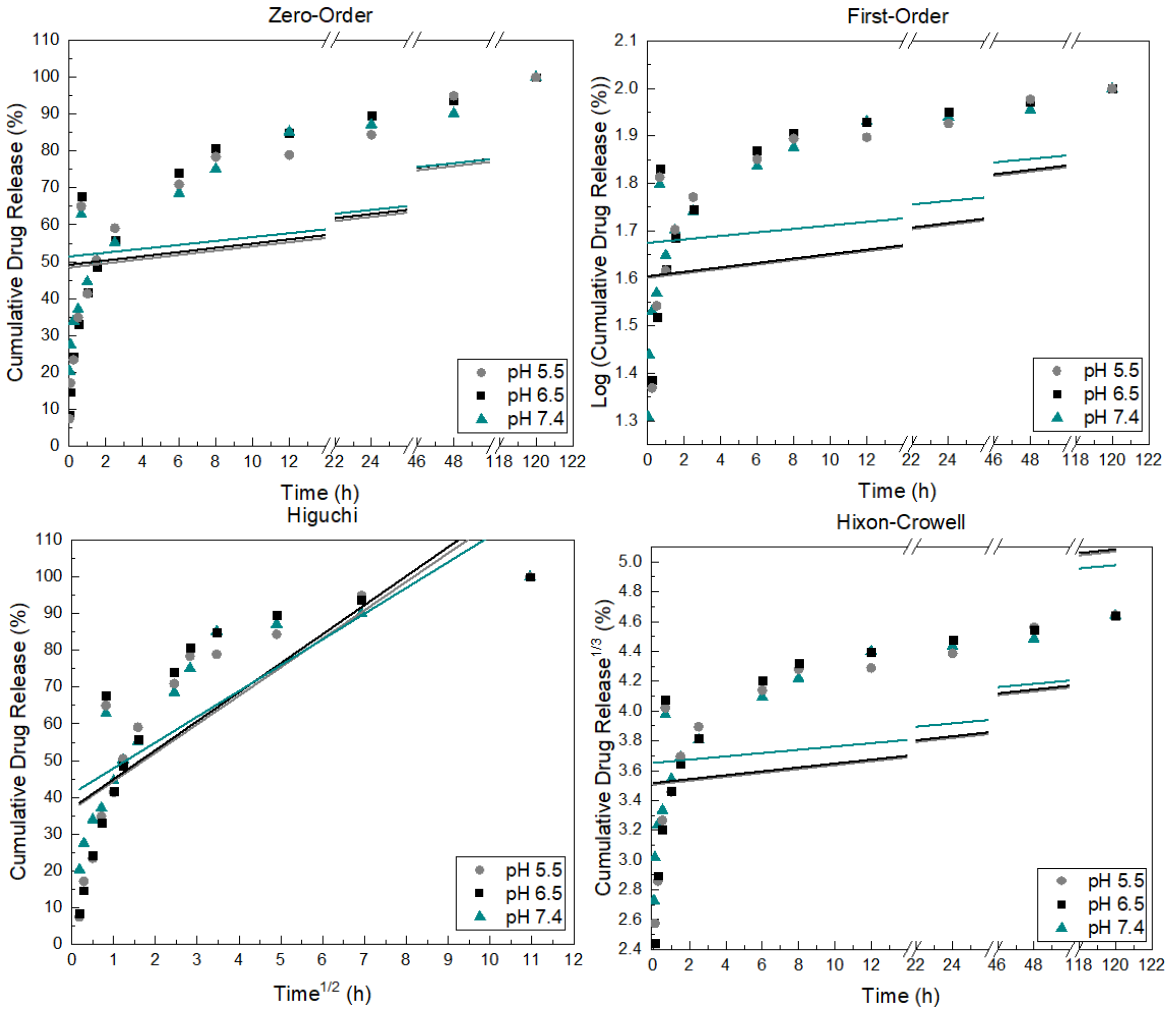

Figure 6.37: Comparison of drug release to mathematical models for Chi/PCL-Van films.

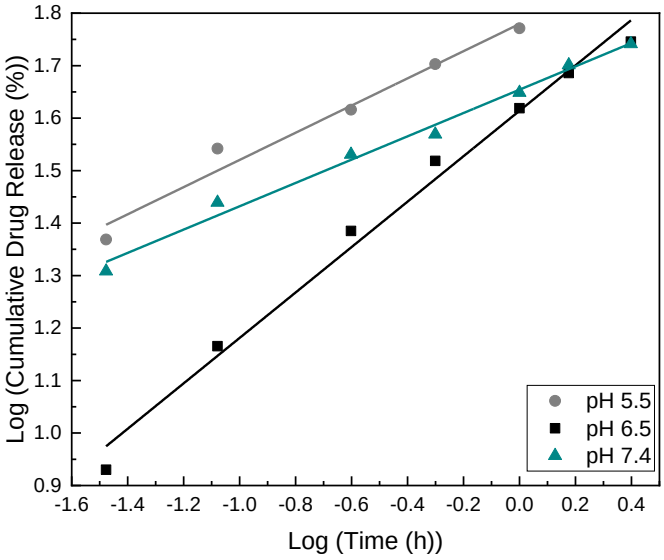

Figure 6.38: Korsmeyer-Peppas representation for a cumulative drug release < 60 % for the calculation of the value of n for Chi/PCL-Van films.

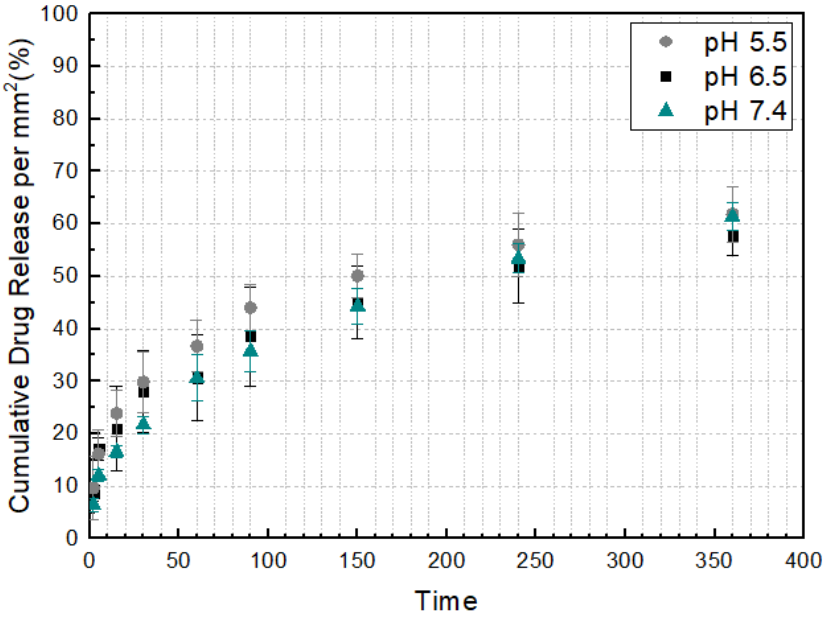

Figure 6.39: Cumulative vancomycin release from Chi/PCL-PMMA-Van films vs. release time for the first 6 hours of drug release.

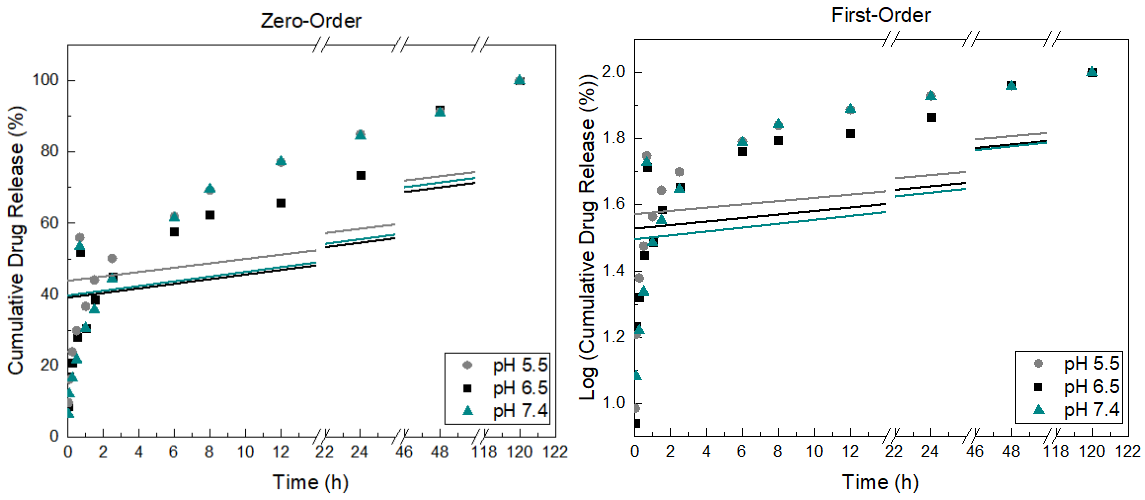

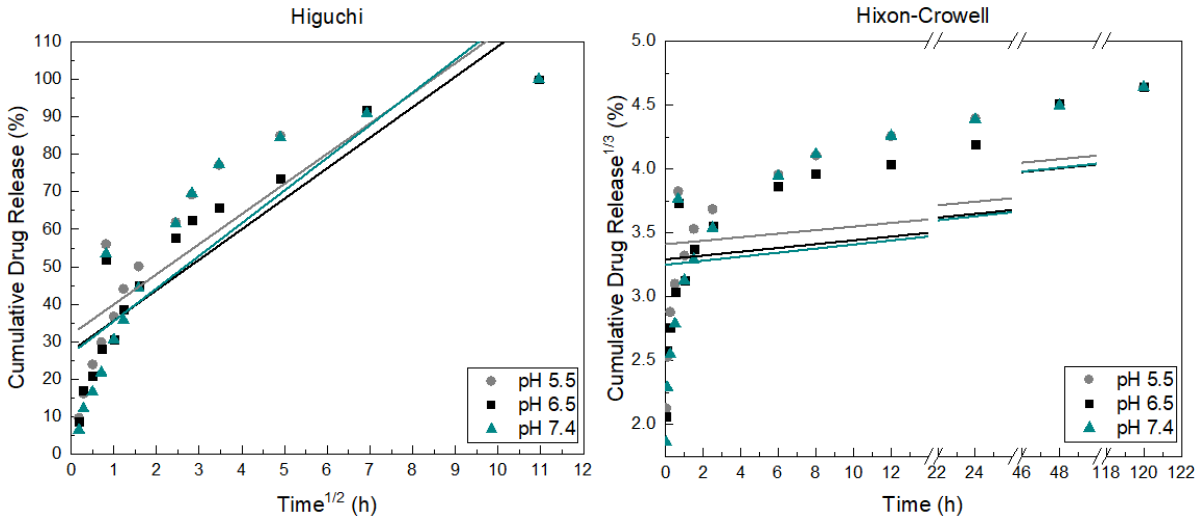

Figure 6.40: Comparison of drug release to mathematical models for Chi/PCL-PMMA-Van films.

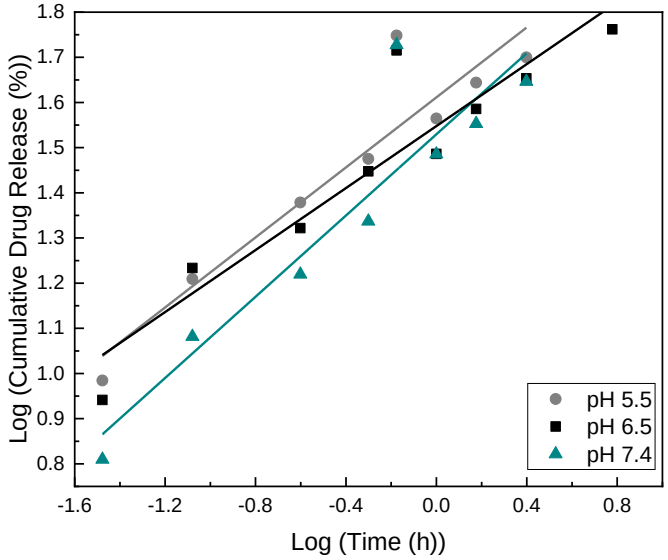

Figure 6.41: Korsmeyer-Peppas representation for a cumulative drug release < 60 % for the calculation of the value of n for Chi/PCL-PMMA Van films.